



Dissertation von Markus Thürkow

AIR QUALITY IN GERMANY

SOURCE ATTRIBUTION OF
MAJOR AIR POLLUTANTS
IN GERMANY THROUGH
CHEMISTRY TRANSPORT
MODELLING

zur Erlangung des Grades eines
Doktors der Naturwissenschaften
am Fachbereich Geowissenschaften
der Freien Universität Berlin

Freie Universität



Berlin

Air quality in Germany

Source attribution of major air pollutants in Germany through chemistry transport modelling

Dissertation

zur Erlangung des Grades
eines Doktors der Naturwissenschaften
am Fachbereich Geowissenschaften
der Freien Universität Berlin

vorgelegt von

Markus Thürkow

Berlin 2024

Erstgutachter: **Prof. Dr. Martijn Schaap**
Zweitgutachter: **Prof. Dr. Uwe Ulbrich**

Tag der Disputation: **14.11.2024**

© **Markus Thürkow, 2024**

*Dissertation submitted to the
Department of Earth Sciences, Freie Universität Berlin*

All rights reserved. No part of this publication may be reproduced or transmitted, in any form or by any means, without permission.

Preface

This thesis is submitted in fulfillment of the requirements for the degree of Doctor rerum naturalium (Dr. rer. nat.) to the Department of Earth Sciences of the Freie Universität Berlin. The research presented here was conducted at the Freie Universität Berlin, under the supervision of Prof. Dr. Martijn Schaap and Prof. Dr. Tim Butler and was mainly funded by the German Environmental Agency (UBA) and the Federal Ministry for Digital and Transport (BMDV) through grant Nr. 3716 51 203 0 (PM-Ost), 19F2065 (S-VELD) and 3720 51 201 0 (OzonEval). The thesis is a collection of four research articles published in international and peer-reviewed journals. The papers are preceded by an introductory chapter that relates them to each other and provides background information and motivation for the work. One of the papers is joint work with Joscha Pültz. I am the lead author of the three remaining papers.

Markus Thürkow
Berlin, 2024

Scientific Publications

This work is based on the following publications:

Paper I

Thürkow, M. and Banzhaf, S. and Butler, T. and Pültz, J. and Schaap, M. “ [Source attribution of nitrogen oxides across Germany: Comparing the labelling approach and brute force technique with LOTOS-EUROS](#) ”. In: *Atmospheric Environment*. Volume 292, Pages 119412 (January 2023), ISSN 1352-2310, DOI: [10.1016/j.atmosenv.2022.119412](https://doi.org/10.1016/j.atmosenv.2022.119412), URL <https://www.sciencedirect.com/science/article/pii/S1352231022004770>.

Paper II

Pültz, J. and Banzhaf, S. and Thürkow, M. and Kranenburg, R. and Schaap, M. “ [Source attribution of particulate matter in Berlin](#) ”. In: *Atmospheric Environment*. Volume 292, Pages 119416 (January 2023), ISSN 1352-2310, DOI: [10.1016/j.atmosenv.2022.119416](https://doi.org/10.1016/j.atmosenv.2022.119416), URL <https://www.sciencedirect.com/science/article/pii/S1352231022004812>.

Paper III

Thürkow, M. and Kirchner, I. and Kranenburg, K. and Timmermans, R.M.A. and Schaap, M. “ [A multi-meteorological comparison for episodes of PM₁₀ concentrations in the Berlin agglomeration area in Germany with the LOTOS-EUROS CTM](#) ”. In: *Atmospheric Environment*. Volume 244, Pages 117946 (January 2021), ISSN 1352-2310, DOI: [10.1016/j.atmosenv.2020.117946](https://doi.org/10.1016/j.atmosenv.2020.117946), URL <https://www.sciencedirect.com/science/article/pii/S1352231020306804>.

Paper IV

Thürkow, M. and Schaap, M. and Kranenburg, R. and Pfäfflin, F. and Neunhäuserer, L. and Wolke, R. and Heinold, B. and Stoll, J. and Lupaşcu, A. and Nordmann, S. and Minkos, A. and Butler, T. “ [Dynamic evaluation of modeled ozone concentrations in Germany with four regional chemistry transport models](#) ”. In: *Science of The Total Environment*. Volume 906, Pages 167665 (January 2024), ISSN 0048-9697, DOI: [10.1016/j.scitotenv.2023.167665](https://doi.org/10.1016/j.scitotenv.2023.167665), URL <https://www.sciencedirect.com/science/article/pii/S0048969723062927>.

Contents

Preface	i
Scientific Publications	iii
Contents	v
List of Figures	vii
List of Tables	ix
1 Summary and Zusammenfassung	1
1.1 Summary	1
1.2 Zusammenfassung	3
2 Overview of thesis	5
3 Introduction	7
3.1 Ambient air pollution in Germany	7
3.2 Air pollutants	11
3.3 Monitoring air quality on the national (German) level . . .	16
3.4 Air quality modeling at the regional scale	17
3.5 Evaluation of chemistry transport models	25
3.6 Remaining challenges	26
4 Research aims	29
5 Summary of included papers	31
5.1 Source attribution of nitrogen oxides across Germany: Comparing the labelling approach and brute force technique with LOTOS-EUROS	31
5.2 Source attribution of particulate matter in Berlin	32
5.3 A multi-meteorological comparison for episodes of PM ₁₀ concentrations in the Berlin agglomeration area in Germany with the LOTOS-EUROS CTM	33
5.4 Dynamic evaluation of modeled ozone concentrations in Germany with four regional chemical transport models . . .	35
6 Synthesis	37
7 Outlook and future perspectives	45

Presentation of research publications	48
I Source attribution of nitrogen oxides across Germany: Comparing the labelling approach and brute force technique with LOTOS-EUROS	49
I.1 Introduction	51
I.2 Methodology	53
I.3 Results	58
I.4 Discussion and conclusion	71
I.5 Appendix	74
II Source attribution of particulate matter in Berlin	81
II.1 Introduction	83
II.2 Methodology	85
II.3 Results	89
II.4 Discussion and conclusion	101
III A multi-meteorological comparison for episodes of PM₁₀ concentrations in the Berlin agglomeration area in Germany with the LOTOS-EUROS CTM	105
III.1 Introduction	107
III.2 Methodology	108
III.3 Results	117
III.4 Discussion and conclusions	131
IV Dynamic evaluation of modeled ozone concentrations in Germany with four regional chemistry transport models	135
IV.1 Introduction	137
IV.2 Description of models and experimental design	139
IV.3 Results and discussions	146
IV.4 Summary and conclusion	162
IV.5 Appendix - figures	165
IV.6 Appendix - statistical indicators	166
References	169
Curriculum vitae	211
Danksagung	217
Selbstständigkeitserklärung	221

List of Figures

2.1	Overview of research publications included	6
3.1	Trend of PM ₁₀ emissions in Germany	8
3.2	Trend of NO _X emissions in Germany	8
3.3	Emission trend of selected air pollutants in Germany	9
3.4	Years of life lost per 100.000 inhabitants attributable to air pollution in European countries, 2015	10
3.5	Global population-weighted PM _{2.5} composition	11
3.6	Timeseries of daily PM ₁₀ mass and contributions	12
3.7	Air quality monitoring network	16
3.8	Air pollution pathways	18
3.9	Illustrative summary of a chemistry transport modelling exercise	19
3.10	Illustrative summary of the labeling/ tagging approach	20
3.11	Illustrative summary of the brute force approach	21
3.12	Workflow of emission modeling	23
3.13	A framework for evaluating regional-scale photochemical modeling systems	26
I.1	Domain configuration of the model area	54
I.2	Yearly averaged labelled contributions for NO ₂	59
I.3	Time series of labelled contributions and potential impacts	60
I.4	Labelled Explained Mass and Sector Explained Mass	61
I.5	Comparison of Sector- and Labelled Explained Mass	62
I.6	Time series of Sector- minus Labelled Explained Mass	63
I.7	Exemplary relation for NO, NO ₂ , NO _X and O ₃	64
I.8	Comparison (temporal) of pot. impacts and lab. contributions	65
I.9	Comparison (spatial) of pot. impacts and lab. contributions	66
I.10	Labelled contributions and potential impacts per station type	67
I.11	Consistency ratio for impacts and potential impacts	68
I.12	Additive behavior of potential impacts	69
II.1	Domain configuration of the model area	86
II.2	Incremental Lenschow approach for observed data	90
II.3	PM ₁₀ and PM _{2.5} timeseries (urban background) for 2016-2018	91
II.4	Mass concentration for PM ₁₀ as function of wind direction	91
II.5	Berlin source apportionment for PM _{2.5}	93
II.6	Linear regression of modelled PM _{2.5} concentration in Berlin	94
II.7	Timeseries of the PM _{2.5} and coarse mode urban increments	95
II.8	Sectorial contributions/ increments for PM ₁₀ , PM _{2.5} and PM _{CO}	96
II.9	Regional contributions/ increments for PM ₁₀ , PM _{2.5} and PM _{CO}	97

List of Figures

III.1	Domain configuration of the model area	109
III.2	Time series for PM and meteorological parameters	110
III.3	Wind- and temperature profiles	118
III.4	Time series of mixing layer height	119
III.5	Modelled PM for sensitivity runs	121
III.6	PM in relation to mixing layer height	124
III.7	Maps for observed and modelled PM	125
III.8	Diurnal and weekly cycles for PM	126
III.9	Time series of chemical composition for PM	130
III.10	Comparison for modelled and observed nitrate and sulfate	131
IV.1	Annual averaged MDA8 O ₃	147
IV.2	Annual averaged NO ₂	148
IV.3	Time series of the MDA8 O ₃ (station average)	150
IV.4	Uncertainty of modeled MDA8 O ₃	151
IV.5	Time series of the MDA8 O ₃ (example sites)	152
IV.6	Day of the week ozone concentration	153
IV.7	Day of the week nitrogen dioxide concentration	154
IV.8	Statistics for ozone and nitrogen dioxide	155
IV.9	Air quality model benchmarking for ozone and nitrogen dioxide	156
IV.10	Ozone concentration in relation to temperature and humidity	160
IV.11	Graphical abstract	165
IV.12	Ozone concentration in relation to temperature (urban/ rural)	168

List of Tables

I.1	List of source categories investigated	56
I.2	List of model simulations	56
I.3	Ratio between added and individually reduced source sectors . .	74
I.4	RMSE of PI_X and labelled contributions for NO_2	74
I.5	Mean values and std-dev. of labelled contributions for NO_2 . . .	75
I.6	Statistics of BASE simulation, LEM and SEM for NO	76
I.7	Same as in Table I.6, but for NO_2	77
I.8	Same as in Table I.6, but for NO_X	78
I.9	Mean values and std-dev. of Potential Impacts (PI_{20}) for NO_2 .	79
II.1	List of emission sources investigated	88
II.2	List of measurement sites	89
II.3	Model performance statistics	92
II.4	Mean labelled concentrations	100
III.1	Planetary boundary layer parameterizations	112
III.2	Overview of model simulations	114
III.3	PM-statistics for January 2016	122
III.4	PM-statistics for December 2016 to February 2017	128
IV.1	Model-description (part 1)	142
IV.2	Model-description (part 2)	143
IV.3	Breakdown of the GNFR sector F	144
IV.4	Height distribution of area sources for GRETA	144
IV.5	Threshold exceedance events for ozone	157
IV.6	Dependence of ozone concentration on temperature	161

Chapter 1

Summary and Zusammenfassung

1.1 Summary

Political regulations are an efficient instrument to reduce emissions, but developing mitigation strategies require information on the source contributions. Informations on local traffic emissions are usually available, but the contribution to the regional background is often missing. CTMs are widely used to assess the air pollution and support policy decisions. This study focuses on improving the quantification of the source contribution to the concentration levels of PM, NO₂ and O₃ in Germany.

A source apportionment was performed to identify the most important sources for NO_x in Germany and Berlin. Contributions to NO_x were calculated using the labeling system in LOTOS-EUROS. Most important contributions to NO₂ are road transport (~45 %), non-road transport (~24 %), energy & industry (~20 %) and households (~10 %). The impact of emission reduction was calculated using the brute force technique. Main differences between potential impacts (upscaling the impact to 100 %) and contributions were observed for ozone-limiting conditions. At night and in winter, the non-linear photochemical reaction between source sectors is often hampered and no regime change in the titration of O₃ takes place. In the urban background, the sum of the potential impacts from each source sector overestimates the unperturbed baseline concentration for NO by about 50 % on annual average. For rural background sites, the overestimation is roughly 10 % lower. Larger overestimation was observed for hourly time series and small-sized source categories. For NO₂, the attributed concentration from the brute force simulation is about 5 % lower close to emission sources than that of the labeling system. For larger cities, differences between the two calculations are about -15 %. The differences between both techniques increase with smaller NO_x reduction. A 25 % reduction in NO_x emissions was identified as the limit for application of the brute force technique.

As prior research studies show similar deficiencies for PM, the source attribution for PM was performed using the labeling system. Combustion processes from residential heating (~30 %), industry & energy production (~19 %) and road-transport (~12 %) are the most important sources in Berlin. Agriculture and the boundary contribute about 12 % and about 14 % respectively on annual average. The remaining contribution is explained by natural emissions. Domestic sources from Berlin (~25 %) and Germany (~24 %) explain about a half to the annual average concentration. About 33 % originate from transboundary transport. The rest can be attributed to natural sources. For PM episodes in winter up to a third of the PM concentration originates from sources in neighboring countries further east. Seasonal variations were caused by emissions

1. Summary and Zusammenfassung

from residential heating and energy production, most important in winter. Agriculture is a large source of PM in spring and summer. Households (~53 %) and road-transport (~17 %) contribute most to the urban increment in Berlin. Road transport explains about 22 % of coarse material in urban background sites. Previous research studies show larger traffic contributions of up to a factor of 4 in summer. Incomplete reporting of non-exhaust emissions from road traffic and land management activities may partly explain the underestimation.

Model simulations with COSMO-CLM were performed to downscale meteorological reanalysis from ECMWF to the national scale for Germany and were used for the first time as input data in LOTOS-EUROS. This paves the way for forthcoming modeling in Germany and to incorporate meteorological forecasts from DWD. The study shows improved statistics for meteorological conditions in Germany with COSMO-CLM compared to the lower resolved ECMWF forecasts. Simulations with the dynamic mixed-layer set-up show too high mixing from the planetary boundary layer to higher model layers in LOTOS-EUROS. Different turbulence parameterizations were used in COSMO-CLM, but show no clear indication to improve the mixing in LOTOS-EUROS. The pollutants stay closer to the surface when a larger number of vertical layers is used. The refined vertical layering improves the modeling with LOTOS-EUROS for Berlin and lowers the bias in the urban background, especially for cold and stagnating weather conditions in winter. Ammonium and nitrate responded most sensitive to the higher resolved vertical layering and show increased concentrations.

Modeling of O₃ with LOTOS-EUROS for Germany was evaluated with three other CTMs in a national scale multi model inter-comparison. The individual models often show lower model-measurement agreement and a lower statistical skill than the ensemble mean of all models, especially at night and for high ozone levels. A dynamic model evaluation was designed that compares modeled and observed concentration regimes for temperature and humidity. Room for improvement was identified to reproduce the O₃ sensitivity to temperature, where a large spread was observed between the models. LOTOS-EUROS captures the regional build-up and removal of O₃ for day-to-day and season-to-season variations, but underestimates the O₃ sensitivity to temperature. Different sensitivities of O₃ to temperature between rural and urban background sites and spring and summer are captured with LOTOS-EUROS.

Detailing the emission inventories at national level, the integration of resuspended coarse material as an additional source and the use of the high resolved vertical layering are recommended for future modeling with LOTOS-EUROS. Contributions from the labeling system must be the first guess for emission reduction scenarios using the brute-force technique. The calculation of potential impacts must be avoided for NO and for small-sized emission categories. The implementation of the labeling system for O₃ will allow to account for the contributions of O₃ in Germany with LOTOS-EUROS. The dynamic evaluation must be expanded to longer timeframes and to other pollutants.

1.2 Zusammenfassung

Politische Regelungen sind ein wirksames Instrument zur Reduktion von Emissionen. Die Entwicklung von Strategien zur Minderung von Emissionen erfordert Informationen zum Beitrag einzelner Quellen. Informationen über lokale Verkehrsemissionen sind in der Regel verfügbar, aber der Beitrag zum regionalen Hintergrund ist häufig unbekannt. CTMs werden häufig zur Bewertung der Luftqualität und als Stütze für politische Entscheidungen eingesetzt. Im Rahmen dieser Arbeit wird die Berechnung der Quellenbeiträge zur Gesamtkonzentration von PM, NO₂ und O₃ in Deutschland verbessert.

Um die wichtigsten Quellen für NO_x in Deutschland zu ermitteln, wurde eine Quellenzuordnung durchgeführt. Die Beiträge für NO_x wurden mit dem Kennzeichnungssystem in LOTOS-EUROS berechnet. Die wichtigsten Beiträge zu NO₂ sind der Straßenverkehr (~45 %), der nicht straßengebundene Verkehr (~24 %), die Energiewirtschaft und der industrielle Sektor (~20 %) sowie die Beheizung von Wohngebäuden (~10 %). Die Auswirkungen einer Emissionsreduktion wurden mit der Brute-Force-Technik ermittelt. Die größten Unterschiede zwischen den potenziellen Einwirkungen (Skalierung der Auswirkung auf 100 %) und den Beiträgen wurden für ozonbegrenzende Bedingungen festgestellt. Nachts und im Winter ist die nichtlineare Photochemie zwischen den Quellensektoren gehemmt und es findet kein Regimewechsel in der Titration von O₃ statt. Im städtischen Hintergrund ist die Summe der potenziellen Einwirkungen jedes Quellensektors für NO im Jahresdurchschnitt etwa 50 % größer als die Konzentration der ungestörten Simulation. Für Stundenwerte und kleine Quellenkategorien ist eine größere Abweichung festzustellen. Im ländlichen Hintergrund ist die Überschätzung etwa 10 % geringer. Für NO₂ ist die Summe der potentiellen Einwirkungen in der Nähe von Emissionen etwa 5 % niedriger als die Basissimulation. In Großstädten betragen die Unterschiede etwa -15 %. Mit geringerer NO_x-Reduktion nehmen die Abweichungen zwischen den beiden Verfahren zu. Die Grenze der Anwendbarkeit des Brute-Force-Verfahrens liegt bei einer 25-prozentigen Reduktion der NO_x-Emissionen.

Die Quellenzuordnung für PM wurde mit dem Kennzeichnungssystem vorgenommen. Private Haushalte (~30 %), die Industrie & Energieerzeugung (~19 %) und der Straßenverkehr (~12 %) sind wichtige Quellen in Berlin. Der Anteil der Landwirtschaft und des Grenzbeitrags beträgt ~12 % und ~14 %. Natürliche Emissionen erklären den Rest. Emissionen in Berlin (~25 %) und Deutschland (~24 %) tragen zur Hälfte der Konzentration im Jahresdurchschnitt bei. Etwa 33 % sind dem Ferntransport zuzuschreiben. Der übrige Anteil ist auf natürliche Quellen zurückzuführen. Emissionen aus östlich gelegenen Nachbarländern tragen im Winter ein Drittel zur Konzentration in Berlin bei. Saisonale Schwankungen sind auf Emissionen aus der Energieerzeugung und der Beheizung von Wohngebäuden zurückzuführen, die überwiegend im Winter anfallen. Im Frühjahr und Sommer trägt die Landwirtschaft wesentlich zur Konzentration bei. Der Straßenverkehr (~17 %) und die Beheizung von Wohngebäuden (~53 %) zeigen größere Beiträge im Stadtgebiet von Berlin und sind im Umland geringer. Der Straßenverkehr hat einen Anteil von etwa 22 % am Grobmaterial im städtischen

1. Summary and Zusammenfassung

Hintergrund. Frühere Studien haben einen bis zu 4-fach größeren Beitrag des Verkehrs im Sommer festgestellt. Die Unterschätzung lässt sich zum Teil durch eine lückenhafte Berichterstattung von nicht abgasbedingten Emissionen aus dem Straßenverkehr und der Bewirtschaftung von landwirtschaftlichen Flächen erklären.

In dieser Studie wurden erstmalig meteorologische Daten aus COSMO-CLM als Antrieb für die Simulation mit LOTOS-EUROS verwendet. Die Reanalyse des ECMWF wurde mit COSMO-CLM auf die nationale Skala für Deutschland skaliert. Dies eröffnet die Möglichkeit in einer zukünftigen Modellierung, die meteorologischen Vorhersagen des DWD einzubeziehen. Die Simulation mit COSMO-CLM erfasst die meteorologischen Bedingungen in Deutschland besser als die niedriger aufgelöste ECMWF-Vorhersage. In LOTOS-EUROS wird standardmäßig von einer gut durchmischten Grenzschicht ausgegangen. Die Durchmischung von der planetaren Grenzschicht in höhere Modellschichten ist dabei oft zu stark ausgeprägt. Verschiedene Turbulenzparametrisierungen wurden in COSMO-CLM verwendet, zeigten aber keinen klaren Hinweis auf eine Verbesserung der Durchmischung in LOTOS-EUROS. Wenn eine höhere Anzahl von vertikalen Schichten verwendet wird, verbleiben die Schadstoffe näher an der Oberfläche. Dies reduziert den Modellfehler im städtischen Hintergrund für Berlin, insbesondere bei kalten und stagnierenden Wetterlagen im Winter. Ammoniak und Nitrat reagieren am empfindlichsten auf die höher aufgelöste vertikale Schichtung und zeigen erhöhte Konzentrationen.

Die Modellierung von O_3 mit LOTOS-EUROS in Deutschland wurde im Rahmen eines nationalen Multimodellvergleichs mit drei weiteren CTMs bewertet. Die einzelnen Modelle zeigen häufig eine geringere Übereinstimmung zwischen der modellierten Konzentration und den Messwerten und verfügen über eine schlechtere Statistik als das Ensemble-Mittel aller Modelle, insbesondere in der Nacht und bei hohen Ozonwerten. Die tägliche und jahreszeitliche Variation in der Produktion und dem Abbau von O_3 wird mit LOTOS-EUROS erfasst. Eine neue Methodik wurde zur Bewertung der Modelle entwickelt, bei der die modellierten und beobachteten Konzentrationen gegenüber der Temperatur und der Luftfeuchtigkeit betrachtet werden. Die Empfindlichkeit von O_3 gegenüber der Temperatur wird von den Modellen sehr unterschiedlich abgebildet und mit LOTOS-EUROS unterschätzt. Die unterschiedliche Empfindlichkeit von O_3 gegenüber der Temperatur zwischen dem ländlichen und städtischen Hintergrund sowie zwischen Frühling und Sommer wird meist erfasst.

Für die zukünftige Modellierung mit LOTOS-EUROS wird empfohlen, eine hochauflösende vertikale Schichtung zu verwenden, die nationalen Emissionsinventare zu erweitern und grobes, wieder aufgewirbeltes Material als zusätzliche Quelle einzubeziehen. Mit dem Kennzeichnungssystem berechnete Beiträge müssen als erste Schätzung für Emissionsminderungsszenarien verwendet werden. Die Berechnung der potenziellen Einwirkung muss für NO und kleine Emissionskategorien vermieden werden. Um auch Beiträge für O_3 mit LOTOS-EUROS berechnen zu können, muss ein Kennzeichnungssystem für O_3 implementiert werden. Die Evaluation der modellierten Konzentration gegenüber meteorologischer Variablen bedarf längere Zeiträume und weitere Schadstoffe.

Chapter 2

Overview of thesis

The presented dissertation consists of 7 chapters, followed by four separate research articles and is summarized in [Chapter 1](#). [Chapter 3](#) introduces main air quality concerns for Europe and Germany ([Section 3.1](#)) and provides information on air pollutants examined in this research study ([Section 3.2](#)). [Chapter 3](#) further summarizes monitoring standards for air pollution ([Section 3.3](#)). The chapter also outlines modeling aspects for air pollution reanalysis and forecast purposes using chemistry transport models (CTMs), detailing the main processes in CTMs and its input data needed and gives an overview for emission source attribution techniques ([Section 3.4](#)). The subsequent [Chapter 4](#) provides the main research questions that will be addressed in this thesis. [Chapter 5](#) briefly summarizes the four research publications that are contributing to this dissertation. All four scientific articles have already been published. [Paper I](#) focuses on the comparison of different source attribution techniques. Contributions of emission source sectors and regions for NO_x and PM were calculated in [Paper I](#) and [Paper II](#) for Germany and Berlin. Model improvements for the LOTOS-EUROS CTM are addressed in [Paper III](#). [Paper IV](#) presents a multi-model evaluation assessment with different CTMs. The main findings from the four publications are discussed in [Chapter 6](#). Finally, [Chapter 7](#) gives an outlook and future perspectives that may be of interest for upcoming research activities.

2. Overview of thesis



Figure 2.1: Overview of research publications included.

Chapter 3

Introduction

3.1 Ambient air pollution in Germany

Ambient air pollution has become a serious challenge to human wellbeing since the start of the industrialization and globalization in the twentieth century (e.g., Fang et al., 2013; Krotkov et al., 2016; Ventriglio et al., 2021). Exposure to air pollution is thought to be one of the major drivers of human diseases worldwide with (long-term) exposure reported to be one of the leading environmental health risk factors including premature death (e.g., Gurjar et al., 2010; Anderson et al., 2012; Burnett et al., 2018). Although the human organism is not capable of distinguishing between clean- and toxic air simply from smell or taste of the surrounding conditions, air pollutants may cause local damages, for example allergic reactions, after entering the human body via respiratory pathways (e.g., D'Amato et al., 2002). Particles with a diameter less than 2.5 μm , are of particular interest as they can enter the cardiovascular system and may damage the heart or brain (e.g., Calderón-Garcidueñas et al., 2007; Arias-Pérez et al., 2020; Daiber et al., 2020). In addition to exposure to particles, gaseous air pollutants may also cause negative impacts on human health (e.g., Chen et al., 2007; Kampa and Castanas, 2008). Long term exposure to nitrogen oxides has been proven to lead to an increased mortality, also at very low levels (e.g., Per et al., 2004; Raaschou-Nielsen et al., 2012; Beelen et al., 2014; Fischer et al., 2015). Long-term exposure to high ozone concentrations have been found to be carcinogenic (e.g., Dabass et al., 2014). Especially, older (e.g., Lepeule et al., 2014) and very young people (e.g., Gauderman et al., 2004; Pujol et al., 2016) as well as persons with medical diseases (e.g., Pope, 2000) are vulnerable to short term and long-term exposure to high concentrations of air pollutants.

Political regulations have been put in place to lower man-made (anthropogenic) emissions and to protect human health (e.g., Schöpp et al., 2003; Vestreng et al., 2007; Jafari et al., 2021). Since the industrialization, several guidelines have been established at international and national level. (Negative) environmental impacts on the human being and ecosystems have been tackled for example by the Clean Air For Europe Directive 2008/50/EC (CAFE, EC, 2008) and the Gothenburg Protocol by UNECE. The first legislation to be officially established in law was the Clean Air Act (CAA), an agreement passed by the Parliament of the United Kingdom in 1956. The act was triggered by a severe smog event in London, caused by exhaust smoke from industrial activities, residential heating and traffic, that costed thousands of people their lives (e.g., Wilkins, 1954; Bell and Davis, 2001). Currently, clean air policy in Europe is based on three pillars. The first addresses emission standards for various emission sources like as the traffic- (e.g., Berg, 2003; Vestreng et al., 2009; Favre

3. Introduction

Staub (PM10)-Emissionen nach Quellkategorien

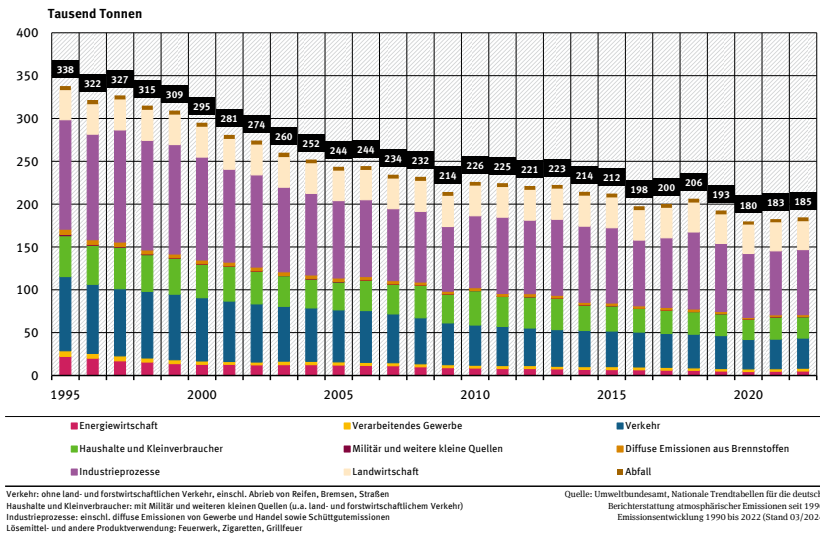


Figure 3.1: Trend of PM₁₀ emissions in Germany. Source: German Environment Agency (UBA, 27/03/2024).

Stickstoffoxid (NO_x, gerechnet als NO₂)-Emissionen nach Quellkategorien

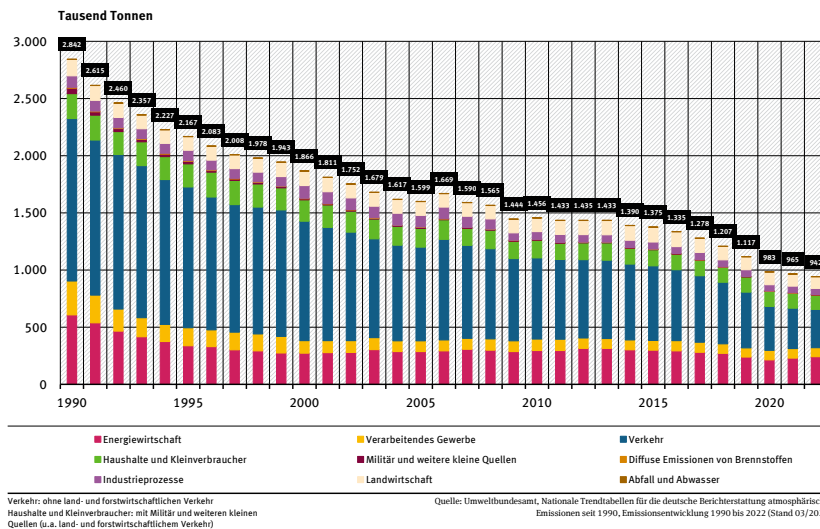


Figure 3.2: Trend of NO_x emissions in Germany. Source: German Environment Agency (UBA, 27/03/2024).

Emissionen ausgewählter Luftschadstoffe

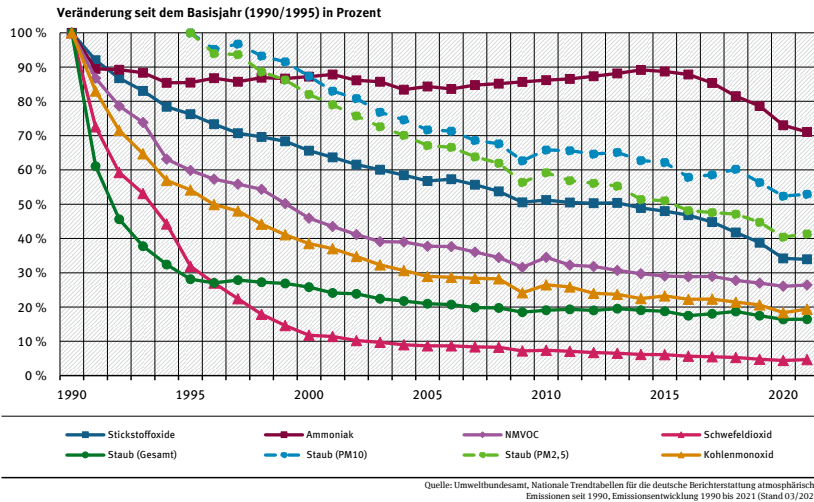


Figure 3.3: Emissions of selected air pollutants. Source: German Environment Agency (UBA, 01/06/2023).

et al., 2016), industry- (e.g., Bergqvist et al., 2015; Sardar, 2015) or agricultural sector (e.g., Giannakis et al., 2019; Silveira et al., 2023). The second aims to reduce national emissions in total through the National Emission reduction Commitments (NEC) Directive (2016/2284/EU). The third pillar includes the limit and target values set by the European legislation to protect the whole population and minimize the long-term exposure to near-surface air pollutants (EC, 2008). Exceedances of the target- and the limit values are still a challenging issue in Europe (e.g., Guerreiro et al., 2014; Gozzi et al., 2017). In particular, close to large agglomeration areas and urban centers the ambient air pollution often shows high concentrations exceeding the limit values or WHO guidelines (e.g., Annesi-Maesano, 2017; Viana et al., 2020).

Emission inventories provided by the Federal Environment Agency (UBA, 2019) and several scientific research activities (e.g., Zimmermann et al., 2003; Mayer et al., 2008) report decreasing trends for German air pollutant emissions over the last three decades (see Figure 3.1, Figure 3.2 and Figure 3.3), which is consistent with national monitoring data. Technical improvements, for example on power plants, have significantly reduced emissions from industrial and commercial sources in western European countries and the US (e.g., Vestreng et al., 2007; Rafaj et al., 2015; Crippa et al., 2016). The application of catalytic converters and particle filters in the road transport sector (e.g., Gerard and Lave, 2005; Twigg, 2011) and the use of alternative fuels in the energy sector (liquid or gas compared to solid) and house holds were important for the success of the mitigation efforts (e.g., Hossain and Davies, 2013; Sangeeta et al., 2014; Yilmaz and Atmanli, 2017). However, the rate of change is strongly dependent

3. Introduction

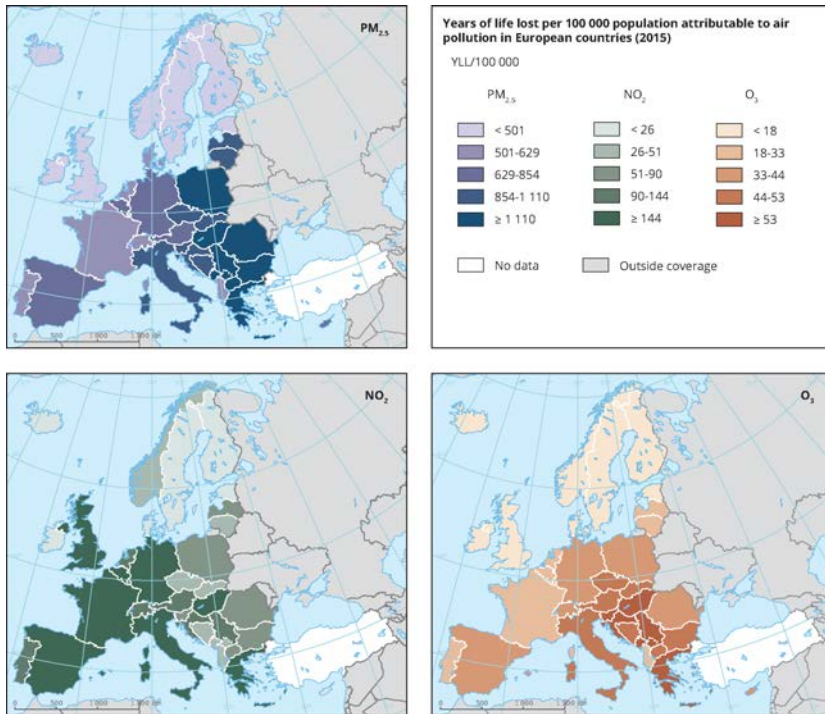


Figure 3.4: The maps show the number of years of life lost per country attributable to air pollution (PM_{2.5} left, NO₂ center and O₃ right). Source: [EEA, 2018b](#).

on the emission sector and time frame being considered, as for example ammonia emissions, that are mainly related to agricultural activities, show a positive trend between 2005 and 2015 (e.g., [Wagner et al., 2017](#); [UBA, 2019](#)).

Despite the declining trends for most pollutants, millions of people are still exposed to concentrations above the WHO guidelines for particulate matter and nitrogen dioxide (e.g., [WHO, 2005](#)). Hence, exposure to these priority pollutants remains a major health concern (see [Figure 3.4](#)). The European Environment Agency reports that each year in Germany, about 60,000 and 13,100 people prematurely pass away due to exposure to fine particulate matter and nitrogen dioxide, respectively ([EEA, 2018a](#)). Although trends are negative, the daily limit values for particulate matter are still exceeded close to traffic sites, near to industrial locations or in large (urban) agglomerations (e.g., [LFU, 2018](#); [SenStadt, 2019](#); [UBA, 2019](#)). The same holds for the annual limit value for NO₂ that is often exceeded in densely populated regions, such as the Rhine-Main area and near to busy roads in Germany ([UBA, 2019](#)). Alongside particulate matter and nitrogen oxides, ambient ozone levels in Germany persist as a critical disease burden (e.g., [Krug et al., 2019](#); [Krug et al., 2020](#)).

The following subsection briefly summarizes the most important information on particulate matter, nitrogen oxides and ozone.

3.2 Air pollutants

3.2.1 Particulate matter

Particulate matter (PM) includes a wide range of particles suspended in the air, ranging in size from a few nanometers to tens of micrometers (Seinfeld and Pandis, 2006). In general, two size groups within PM are commonly distinguished: coarse- (PM_{10}) and fine- ($PM_{2.5}$) particulate matter. PM_{10} refers to particles with a diameter less than or equal to 10 μm in diameter and $PM_{2.5}$ which is defined as all particles with a diameter less than or equal to 2.5 μm . Owing to its lower size and a corresponding lower sedimentation velocity, $PM_{2.5}$ has a longer lifetime in the atmosphere than the coarse mode. $PM_{2.5}$ often is further divided into the Aitken mode (also ultrafine particles: 0.005 to 0.1 μm) and the accumulation mode (0.1 to 1 μm) (Seinfeld and Pandis, 2006). However, the contribution of ultrafine particles to the total PM mass is negligible.

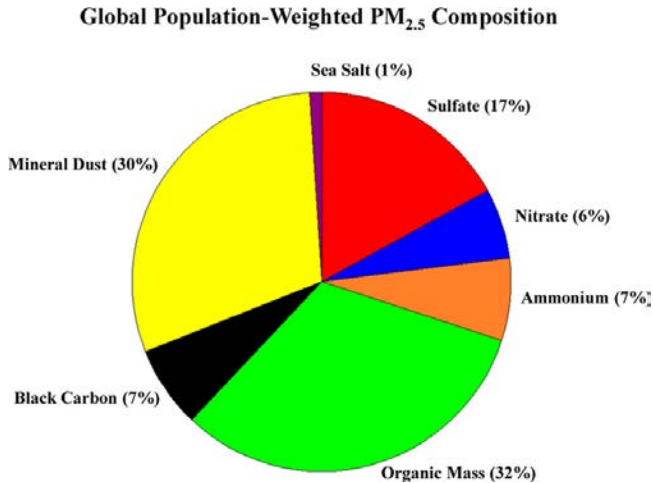


Figure 3.5: Global population-weighted $PM_{2.5}$ composition. Source: Philip et al., 2014.

The origin and sources for PM widely vary in space and time (e.g., Putaud et al., 2004; Querol et al., 2004). PM can be solid, liquid as well a combination of both and either be released by primary (local) emission sources or formed by secondary processes via gas-to-particle conversion in the atmosphere (e.g., Zhang et al., 2015). In terms of chemical composition, sulfate (SO_4), nitrate (NO_3) and ammonium (NH_4), a number of trace metals (e.g. Si, Al, Ca, K, Fe, and Ti), elemental (EC) and organic carbon (OC), along with sodium (Na) and chloride (Cl) are major compounds (e.g., Schaap et al., 2010). Secondary formed particulate organic aerosol (SOA) formed by precursor gasses represents a further component of PM (see also Figure 3.5). The chemical composition of PM at a given location and time strongly depends on the synoptic meteorological condition (e.g., Lenschow et al., 2001; Mues et al., 2012; Fuzzi et al., 2015). Long-range transport of secondary aerosols that have their origin in combustion

3. Introduction

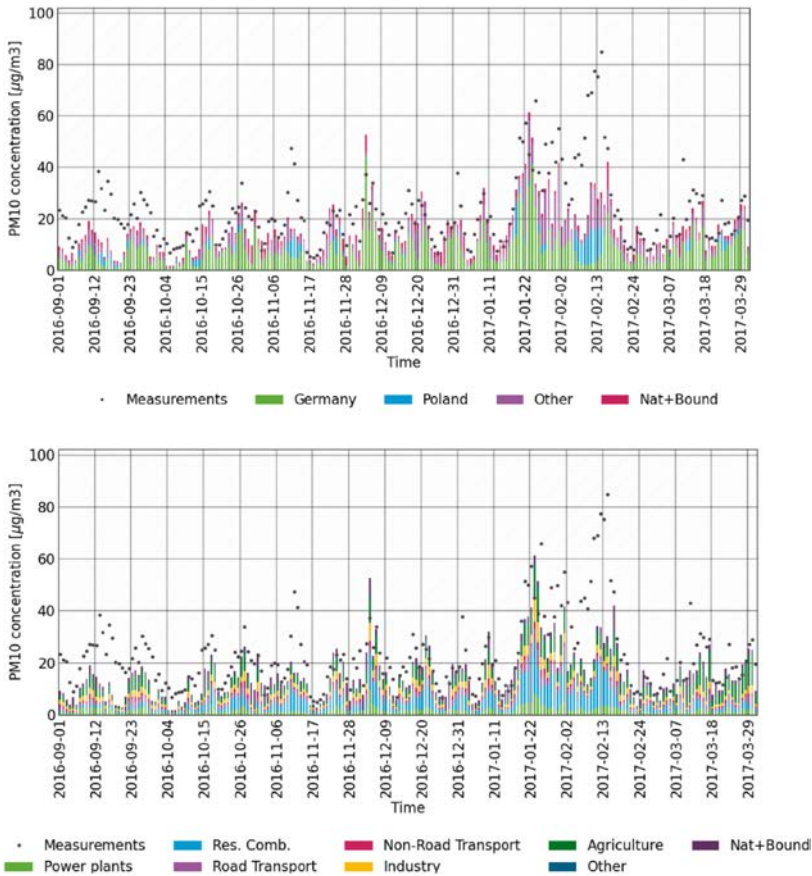


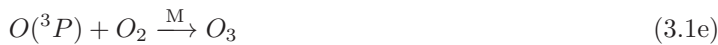
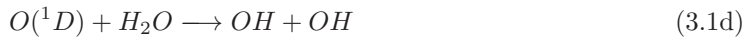
Figure 3.6: Timeseries of daily PM₁₀ mass at Melpitz, regional contributions from different regions (top plot, Germany, Poland and other countries) and contributions from different source sectors (bottom plot). Source: Timmermans et al., 2022.

processes (e.g. ammonium nitrate and sulfate) can significantly contribute to PM concentrations in the rural background in Germany (e.g., van Pinxteren et al., 2019). The regional background contribution is often the major contribution in urban agglomerations (e.g., Beekmann et al., 2015 and Figure 3.6). LOTOS-EUROS shows high accuracy modelling the regional background in Berlin for PM and that most peak concentrations were captured. Intense PM episodes are triggered by a combination of local or regional build-up of pollution (e.g., Banzhaf et al., 2013) and often occur during cold winter episodes for stagnant conditions. The results in figure Figure 3.6 clearly illustrate that the understanding and modelling for some of these PM episodes (e.g. dominant long-range transport or stagnant conditions) needs to be improved. Mixing is difficult to model and the mass concentration is often underestimated by the simulations in winter. In summer, modelled PM concentrations are typically lower than observed when resuspension of coarser material prevails.

3.2.2 Ozone and nitrogen oxides

The ozone formation and degradation in the troposphere involves continuous non-linear chemical reactions in the presence of sunlight ($h\nu$) (Seinfeld and Pandis, 2006). Both volatile organic compounds (VOCs) emitted from anthropogenic and biogenic sources, and nitrogen monoxide (NO) and nitrogen dioxide (NO_2), also referred to as nitrogen oxides (NO_x), are the primary ozone precursors. The main reaction pathways leading to production and removal of O_3 and NO_x are explained below.

The initial step in the formation of ozone is actually its destruction through photo-dissociation at daytime. When ozone is photolyzed, reactive oxygen ($\text{O}({}^1\text{D})$), oxygen in the ground state ($\text{O}({}^3\text{P})$), and molecular oxygen (O_2) are released (Eq. 3.1a and 3.1b). Through collision with molecular-oxygen (O_2) or nitrogen (N_2) (both M) energy is taken away from the reactive oxygen and it falls back to oxygen in the ground state (Eq. 3.1c). Reactive oxygen is very short-lived. In the troposphere the ratio for reactive oxygen to oxygen in the ground state is about 1:9. In a few percent (1-3 %) of the collisions the reaction of reactive oxygen with water vapor (H_2O) produces two hydroxyl radicals (Eq. 3.1d). All ground state oxygen recombines to ozone (Eq. 3.1e). Note that Eq. 3.1a to Eq. 3.1e do not result in a net loss or net production of ozone, as O_3 is neither destroyed nor formed (balanced destruction and production: null cycle).



At the same time, photolysis of nitrogen dioxide forms NO and more oxygen in the ground state (Eq. 3.2a). Ozone further rapidly reacts with nitrogen monoxide to form NO_2 and molecular oxygen (Eq. 3.2b). The overall duration of the reaction cycle between NO and NO_2 during daytime is on a time scale of a minute and a photo-stationary state can be observed between NO, NO_2 and O_3 , limiting ozone levels in the troposphere (null cycle following Eq. 3.2a, Eq. 3.2b and Eq. 3.1e (Leighton, 1961).



A large fraction of the NO_x is emitted primarily as nitrogen monoxide. However, nitrogen oxides were also formed at oxidation involving organic and molecular nitrogen (Eq. 3.3a) or during combustion processes at high temperatures, in which the molecular oxygen thermolyzes (Eq. 3.3b) and the reactive oxygen reacts with the molecular nitrogen to produce NO (Eq. 3.3c).

3. Introduction

The nighttime chemistry totally differs compared to daytime. At night, in the absence of light the NO_2 photolysis ceases and the ozone concentration declines when continuing emissions of NO titrate ozone away leading to increase NO_2 at night (Eq. 3.2b). When the ozone level is fully removed, the NO_2 concentration will only further increase by primary emitted NO_2 , and the concentration of NO starts to build up due to primary emissions. Hence, for effective buildup of NO , first all ozone needs to be reacted away in this case.



The chemical production and loss of ozone in the troposphere is initiated by the hydroxyl radical (OH). OH is a highly reactive radical species and often referred to as the "detergent of the atmosphere". For many trace species it is the primary removal mechanism. Because of competition among the reactants, it depends on chance and reaction probability which OH reaction takes place. The OH radical plays a key role during daytime and does not react with O_2 or N_2 (both illustrated as M in the chemical reactions). Its primary production in the troposphere stems from O_3 photolysis in humid air (Eq. 3.1a and Eq. 3.1d).

Oxidation of VOCs, including alkenes, aromatics and oxygenated organic species, by OH produces peroxy radicals (RO_X and HO_X). Depending on the fate of the peroxy radicals, their oxidation can lead to net production or net destruction of O_3 . It applies that all reaction pathways of RO_X and HO_X that produces NO_2 enhances the O_3 formation following Eq. 3.2a and Eq. 3.1e. Further secondary reactions of peroxy radicals can also remove O_3 from the atmosphere. The most important peroxy radicals that boost O_3 production or O_3 degradation are the hydroperoxy radical (HO_2) and the methyl peroxy radical (CH_3O_2 ; RO_2) from BVOC.

HO_2 is produced by oxidation with carbon monoxide (CO) (Eq. 3.4a) and O_3 (Eq. 3.4b). Further reaction with NO regenerates OH and forms NO_2 (Eq. 3.5a) which promotes the O_3 formation.



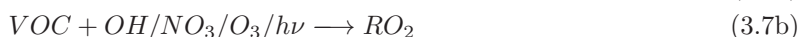
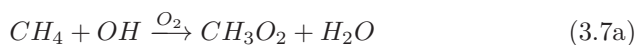
The reaction of HO_2 and OH produces water vapour (Eq. 3.5b) and indirectly removes O_3 from the atmosphere (Eq. 3.1d). Another termination reaction of O_3 is the interconversion between HO_2 and OH (Eq. 3.4b) and (Eq. 3.5c).



Hydrogen peroxide (H_2O_2), produced by two HO_2 radicals (Eq. 3.5d), can act as sink of ozone when removed through deposition. Nitric acid (HNO_3) formed by reaction of OH with NO_2 (Eq. 3.6a) acts as a sink for OH and NO_2 when deposited, limiting the recycling of OH and NO_2 .



CH_3O_2 (RO_2) is formed by oxidation of CH_4 (Eq. 3.7b). For non-methane VOCs (NMVOCs), there are many other reaction pathways to form RO_2 when they are oxidised (simplified in Eq. 3.7a). RO_2 has similar properties to HO_2 and can lead to production or destruction of O_3 . As for the CO oxidation, the fate of RO_2 is important and depends on the prevailing NO_X conditions (not shown here).



In summary, the ozone production efficiency of NO_X can vary considerably depending on the location and the timing of the NO_X emissions. Most of the chemical processes involved in the titration of ozone take place near the sources. Away from the direct surrounding of the sources, when VOCs are present, NO_X plays a crucial role and facilitates the ozone formation. As a function of the ratio between the VOC and NO_X concentration, the OH radical either preferentially reacts with VOCs (high VOC, low NO_X) or the reaction with NO_2 (low VOC, high NO_X) will dominate. The complex non-linear relationship illustrates that NO_X , VOCs and O_3 should always be considered simultaneously. In the NO_X -sensitive regime (also NO_X -limited), there is a higher probability that peroxy radicals will react with other radicals to produce NO_2 rather than NO is converted to NO_2 by Eq. 3.2b. Increasing VOC emissions barely affect the ozone level. The ozone concentrations in the VOC-sensitive regime (also NO_X -saturated) are generally affected by VOC emissions. Higher VOC emissions more likely form NO_2 from NO by peroxy radicals, causing a higher O_3 concentration. Higher NO_X values only has little affect on the O_3 production. The ozone production is maximized at the turning point of both regimes, characterized by O_3 production sensitive to both VOC and NO_X levels (namely the VOC-and- NO_X sensitive regime). As this thesis mainly focuses on Germany and it's urban areas with high NO_X emissions, the VOC-sensitive regime is often prevailing.

Enhanced levels of O_3 can be found downwind from areas with large emissions of nitrogen oxides. NO_X ($NO + NO_2$) concentrations show a seasonal cycle with larger levels in winter than in summer due to less favorable mixing conditions and larger anthropogenic emissions in winter. The amplitude of the seasonal variability is largest for nitrogen monoxide, as a buildup of NO occurs normally under conditions with shallow boundary layers, stagnant weather, and low background ozone levels. A growing planetary boundary layer normally leads to a higher ground-level ozone concentration when ozone from the free troposphere or reservoir layers is entrained. The latter are predominant during the spring and summer season.

3.3 Monitoring air quality on the national (German) level

Air quality control implies the need of a long-term monitoring program in which the air pollution level is continuously observed (e.g., Panteliadis et al., 2014; Shaddick and Zidek, 2014; Sullivan et al., 2018). In Germany, the Federal Environment Agency (UBA) is responsible for monitoring the trend of the air pollution level (UBA, 2019). The monitoring network of UBA provides measurements in so-called clean air environments, far away from large agglomerations and big cities (UBA, 2019). Measuring the pollution load far away from (local) anthropogenic emission sources, allows to monitor the air quality of air masses that have been transported from remote areas, that for Germany can be part of the neighboring country (e.g., van Pinxteren et al., 2017; van Pinxteren et al., 2019; Timmermans et al., 2020). The measuring sites are evenly distributed over Germany and include distinct geographical locations near the coast, at high altitudes or close to remote areas, for example Zingst or the Zugspitze (UBA, 2019). In addition to the monitoring network of UBA, each of the 16 German federal states are responsible to provide information on the air quality near major emission sources, such as urban agglomerations, industrial power plants, and busy roads (UBA, 2019). Measured concentrations from the federal state monitoring networks become also available and are submitted to UBA for each site and air pollutant separately (UBA, 2019). The Berliner Luftgüte-Messnetz (BLUME, SenStadt (2019)) is one example, that covers the capital of Berlin and thus the largest metropolitan area of Germany. All ground-based observations from the monitoring (station) networks are further classified by certain criteria for their station type (traffic, industrial or background), their

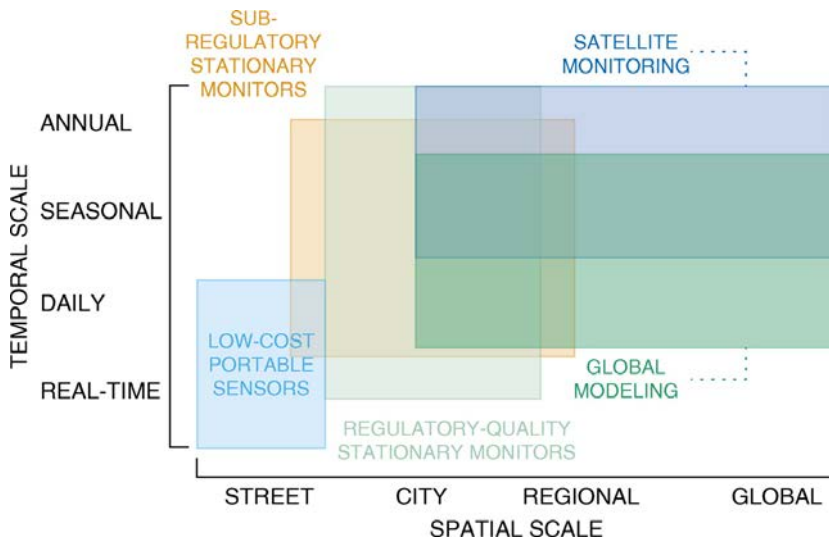


Figure 3.7: Illustrative summary of air pollution monitoring technologies by effective spatial and temporal scales. Source: Cromar et al., 2019.

location (urban, suburban or rural) and characterization of their area under consideration (traffic, residential, commercial, agriculture, industrial, nature, a combination of these or unknown).

The observed air quality is assessed and reviewed against threshold- and limit values defined in the Bundesimmissionsschutzgesetz (BImSchG) and set by the European guidelines (EC, 2008), to decide whether mitigation actions are required. In-situ monitoring networks are usually designed to enable the evaluation of designed mitigation policies (e.g., Guerreiro et al., 2014). Nevertheless, despite harmonization efforts, station measurements usually suffer from several sources of uncertainties hampering the estimation of the spatial and the temporal distribution (e.g., Zhan et al., 2018). Monitoring stations are often not homogeneously distributed across the region of interest (e.g., Castro and Pires, 2019). For example, the European monitoring station network has a much higher density in northwestern Europe than in the southeastern part (e.g., Schaap et al., 2013). Different monitoring networks adopt different calibration and siting strategies hampering comparability. A range of different measuring instruments can be in use in different networks, even within single countries and federal state authorities (e.g., Kasstele and Velders, 2006; Borrego et al., 2016; Dinoi et al., 2017). Hence, it is common practice to obtain the evolution of air pollution concentrations with additional numerical model simulations or using different instruments, such as satellite observations, to capture the entire spatial and temporal scale (see Figure 3.7).

3.4 Air quality modeling at the regional scale

Chemistry transport models (CTMs) are widely used in the scientific community to assess the ambient air pollution at the regional and national scale (e.g., Kukkonen et al., 2012; Conti et al., 2017; Sharma et al., 2017; Baklanov and Zhang, 2020). Often referred to as air quality models (AQMs), such model applications deliver a consistent picture over large domains (e.g., Mar et al., 2016; Weger et al., 2018; Lin et al., 2020), but can also help to provide information on the chemical composition and dispersion of emissions for local scale research activities (e.g., Timmermans et al., 2013; Amato et al., 2016; Kuik et al., 2018). CTMs have a wide application-range and can be used to provide information on source regions and sectors, contributing to the ambient air pollution in the rural and urban background or even from (mega)-cities (e.g., Beekmann et al., 2015; Timmermans et al., 2017; Pommier et al., 2020). AQMs can also be used to simulate the air quality in the tropospheric boundary layer for long periods (e.g., Pierce et al., 2010; Colette et al., 2017) and to produce decadal reanalysis datasets (e.g., Flemming et al., 2017; Inness et al., 2019). Chemistry transport models are central for political and economic policy-making in the context of air pollution control planning (e.g., SenStadt, 2019; UBA, 2019). The EMEP model ("European Monitoring and Evaluation Programme", <https://www.emep.int/>) and the GAINS (Greenhouse Gas - Air Pollution Interactions and Synergies) model system (Amann et al., 2011) are

3. Introduction

pivotal for mitigation strategy developments from the European commission. Examples of other regional CTMs are the Dutch LOTOS-EUROS (Manders et al., 2017), the German REM-CALGRID (Stern, 2003) and the French CHIMERE (Mailler et al., 2017) models, to name a few. These models are often used to benchmark the EMEP model. In short, developing an efficient policy to reduce air pollution concentrations, requires a deep understanding of their emission sources, mass transport, chemical reaction products and removal in the form of an AQM.

3.4.1 Main processes in CTMs and input data needed

CTM s aim to represent a digital version of reality. In a mathematical sense a CTM combined many process descriptions to represent chemical reactions (e.g., formation, depletion, removal processes), emissions, transport of air pollutants in the atmosphere and deposition of air pollutants as good as possible (see Figure 3.8). For running a CTM, extensive input datasets are required to perform forecasts or source attribution with regional CTMs. In the following, a short overview of the main processes in CTMs and its input data needed is presented and illustrated in Figure 3.9.

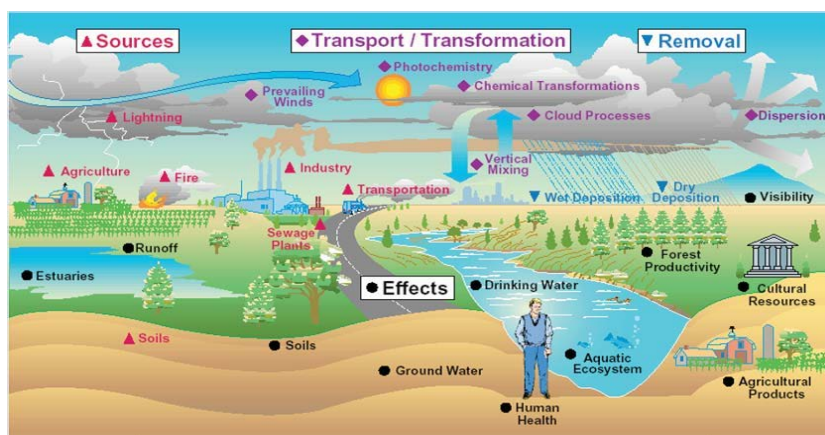


Figure 3.8: The interrelationships among pollutants, sources, transport and transformation pathways, and environmental effects. Source: EPA, 2008.

3.4.2 The LOTOS-EUROS chemistry transport model

In this thesis, the LOTOS-EUROS model serves as the central model system. The LOTOS-EUROS model has been used for many years to investigate air quality with focus on the European domain and has already proven its reliability in several international comparative studies (e.g., Vautard et al., 2007; Bessagnet et al., 2016). In the presented research activities, the LOTOS-EUROS model has been applied to address several research questions on source apportionment

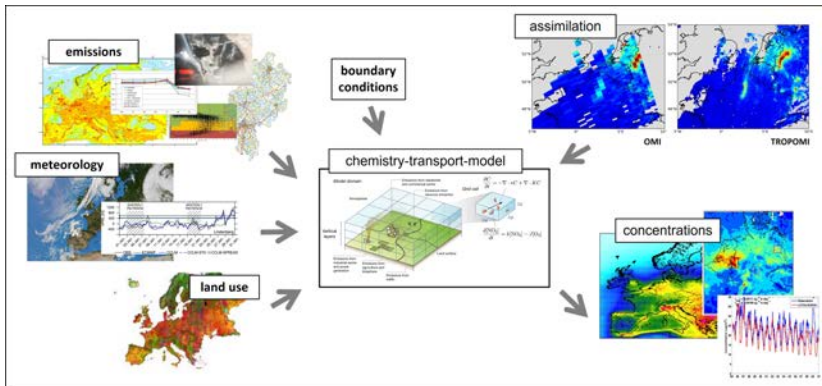


Figure 3.9: Illustrative summary of input data needed to perform a chemistry transport model simulation. Source: own illustration.

of nitrogen dioxide and particulate matter. Furthermore, we participated with this model in a model intercomparison exercise.

LOTOS-EUROS (Manders et al., 2017) is a state-of-the-art CTM that can be used for process studies (e.g., Curier et al., 2014; Mues et al., 2014) as well as for air quality applications (e.g., Hendriks et al., 2013; Timmermans et al., 2017; Escudero et al., 2019). The model is widely used in scientific research activities, but has also been part of regulatory efforts to control the ambient air pollution, for example in Germany (e.g., SenStadt, 2019; UBA, 2019). Launched as an open-source model system, LOTOS-EUROS has been developed continuously in collaboration with partners at TNO (Netherlands Organisation for Applied Scientific Research), FUB (Freie Universität Berlin), RIVM (National Institute for Public Health and the Environment) and KNMI (Royal Netherlands Meteorological Institute) to meet the most recent scientific standards. LOTOS-EUROS is part of the CAMS (Copernicus Atmosphere Monitoring Service) ensemble system, providing operational forecasts and analyses for Europe (Marécal et al., 2015). Furthermore, the model is applied to provide source apportionment information for European cities. For a more comprehensive description of LOTOS-EUROS, we refer to the curriculum vitae and the supporting material therein (Manders et al., 2017).

3.4.3 Identify and apportion of air pollution to different sources

Apart from statistical data analysis of observations or receptor modeling, CTMs are commonly used to perform source attribution studies (e.g., Belis et al., 2020). Depending on the quality of the emission inventory and the process description, a detailed analysis of the contributions of different source regions and source sectors can be performed throughout the study areas and period.

Two main methods can be distinguished for source allocation purposes using a CTM application. First, the labeling approach (e.g., Kranenburg et al., 2013)

3. Introduction

or the tagging method (e.g., Lupaşcu and Butler, 2019), that allows to track concentrations of selected source sectors or regions. Second, the brute force technique calculates the impact of different emission reduction simulations, from which the source contributions are being deduced (e.g., Thunis et al., 2020).

Currently there is an ongoing debate on the applicability and comparability of these techniques. Previous research activities for PM showed the importance to account for different outcomes of both source attribution techniques. It is a well-known feature that both approaches give equivalent results for inert compounds. However, nonlinear chemical effects can lead to significantly different contributions, especially when emission reduction strengths have been used outside its limits of applicability (e.g., Clappier et al., 2017; Thunis et al., 2019; Thunis et al., 2020). Information on the comparability of both techniques is missing for nitrogen oxides. The LOTOS-EUROS model with its labeling routine is well suited to compare these techniques.

The LOTOS-EUROS CTM includes a labeling system, that can track the source contributions to air pollution for primary, inert aerosol- and chemically active tracers through the chemically conserved reduced or oxidized C, S or N atoms (Manders et al., 2017). The labeling module has been implemented and validated by Kranenburg et al. (2013) and has been used already in several scientific research activities (e.g., Hendriks et al., 2013; Timmermans et al., 2017; Pommier et al., 2020; Timmermans et al., 2022; Schaap et al., 2023).

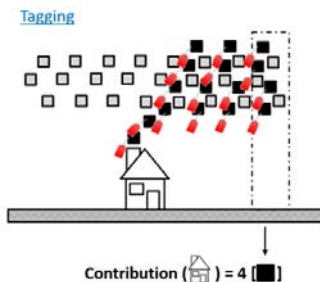


Figure 3.10: Illustrative example of the labeling/ tagging approach for residential emissions (black symbols) that mix with the background pollution (grey symbols) and lead to a given pollutant concentration downwind of the source (dashed rectangle). Contributions are obtained by tagging (red tags on the figure) the emission precursors. Source: Clappier et al., 2022.

The brute force (model) approach can be performed with every model and focuses on the impact of emission reductions. This implies at least two model simulations with different emission configurations need to be performed. In this context, model runs are often referred to as the baseline and the emission reduction simulation. The impact is derived from the difference between the emission reduction simulation and the baseline model configuration. As different emission reduction fractions X can be used, several investigations are possible. Upscaling impacts by multiplying with $100/X$, determines potential impacts that refer to the contribution of the source under investigation (e.g., Thunis et al., 2020).

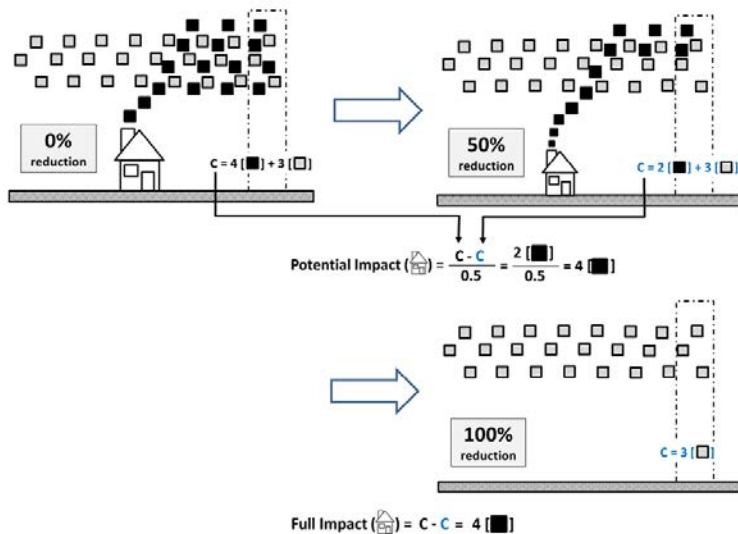


Figure 3.11: Illustrative summary of the brute force approach for residential emissions (black squares) that mix with the background pollution (grey squares) and lead to a given concentration downwind of the source (right dashed rectangle). When the source is reduced by 50 % (right top), two out of the four black squares remain together with the background while for a full reduction, only the background remains (right bottom). Potential impacts correspond to the change of mass (projected to 100 %) that results from the reduction or elimination of the emission source, i.e. the difference between the downwind concentrations, with and without the source emissions, scaled by the percentage reduction: four black squares in this example. Source: Clappier et al., 2022.

3.4.3.1 Emissions and emission inventories

Sources of air pollutants are manifold, which often leads to a simplified allocation and grouping of the individual emissions under investigation into source (sector) families. One primary distinction is made between emissions from natural sources (e.g., Novak and Pierce, 1993; Simpson et al., 1999; Heinold et al., 2011) and anthropogenic emissions of pollutants caused by human activities (e.g., Vestreng et al., 2007; Granier et al., 2011; Masiol and Harrison, 2014).

Among natural emissions, one finds for example forest fires (e.g., Wiedinmyer et al., 2011; Kaiser et al., 2012), pollen (e.g., Zhang et al., 2014), sea salt (e.g., Monahan, 1986; Mårtensson et al., 2003; Tsyro et al., 2011) or mineral dust (e.g., Schaap et al., 2009). The intensity of natural sources normally vary a lot, depending on meteorological conditions. Forest fires occur during particular periods of the year in dry areas and emit a significant portion of dust and ash, as well as toxic gasses into the atmosphere and are often deduced from satellite imagery. Saharan dust and sea salt are natural emission sources that are extensively often observed as long-range contributions worldwide. Both sources are normally integrated in CTMs using process based routines, which are sensitive to wind speed conditions and soil properties in case of (desert) dust.

3. Introduction

Anthropogenic emissions are predominantly related to combustion processes, for example at large industrial facilities (such as firing of wood or coal for electricity production, e.g., [Beirle et al. \(2019\)](#)), household- (e.g., residential fireplaces and stoves, e.g., [van der Gon et al. \(2015\)](#)) or small-scale incinerators (e.g., waste incineration, e.g., [Wiedinmyer et al. \(2014\)](#)) that lead to the emissions of particulate matter, nitrogen oxides, organic compounds and many other pollutants. The transport sector (road, air and shipping) emits a large fraction of emissions through fossil fuel combustion (e.g., [Rexeis and Hausberger, 2009](#); [Vestreng et al., 2009](#)). In addition, emissions from road transport also contribute a considerable amount of resuspended soil material (e.g., [Harrison et al., 2012](#); [Gulia et al., 2019](#); [Valotto et al., 2019](#)), as well as small amounts of brake (e.g., [Garg et al., 2000](#); [Grigoratos and Martini, 2015](#); [Hagino et al., 2016](#)) and tire wear (e.g., [Räisänen et al., 2005](#); [Dahl et al., 2006](#); [Gustafsson et al., 2009](#)). Agricultural production is a sector in which emissions take place without large fossil fuel combustion. Livestock excreta (e.g., [López-Aizpún et al., 2020](#)), fertilizer incorporation (e.g., [Linguist et al., 2012](#)), and crop management (e.g., [Cooter et al., 2012](#)) cause highly variable seasonal emissions that are a source of ammonia, PM and NO_x.

Above-mentioned anthropogenic emission sources, along with those of many other activities, must be reported on a mandatory basis by all state authorities in Europe in accordance with the international regulations of the UNECE air pollution convention (<https://unece.org/>). These submissions include national totals of emissions per year. The reported inventories follow guidelines and a naming convention called the Gridded Nomenclature For Reporting (GNFR).

For Europe, the anthropogenic PM and trace gas emission inventory of the Copernicus Atmosphere Monitoring Service (CAMS) is widely used (e.g., [Kuenen et al., 2014](#); [Granier et al., 2019](#); [Kuenen et al., 2022](#)), whereas in non-European regions the emission inventory EDGAR is generally applied (e.g., [Crippa et al., 2018](#)). Through CAMS the reported time series of the annual emissions by the member states serve as input for European simulation activities as discussed in [Section 3.4](#).

The national emission totals for each year, need to be distributed using proxy maps for area sources and (real) emission information for point sources using fitting parameters (e.g., [Kuenen et al., 2014](#); [Mues et al., 2014](#); [Guevara et al., 2021](#); [Kuenen et al., 2022](#)). This involves special attention to different emission source sectors, as each emission source sector and region has its own local characteristics. As previously mentioned, agricultural emissions, for example, may be caused by animal farming or be a result of land management activities (e.g., [Cooter et al., 2012](#); [Linguist et al., 2012](#); [López-Aizpún et al., 2020](#)). As a result, agricultural emissions can be emitted from both, small and/ or large farms, as well as over large agricultural used fields. For this reason, the spatial distribution of the emissions is realized by means of point and area sources that are separated between their source categories (e.g., [Kuenen et al., 2014](#); [Kuenen et al., 2022](#)). For all available point sources, the different emission heights are assigned as well. The altitude of emissions can largely affect the dispersion of the concentration level in the subsequent model simulation and is of particular

relevance for tall stacks commonly found in the industrial and energy sector (e.g., [Beirle et al., 2019](#)). The spatial re-/ gridding of emissions in Germany is calculated using the UBA-GRETA tooling ([Schneider et al., 2016](#)).

When using the emissions for chemistry transport modeling, they need to be distributed in time by adding source specific time profiles (e.g., [Guevara et al., 2021](#)). The application of time factors ranges between simple assumptions using static time profiles to more complex/ dynamic approaches. Static time profiles normally make use of weekly-, daily- and hourly- time cycles that can capture the annual emission trend in a combined manner. More sophisticated emission inventories normally make use of hourly varying time profiles for the entire year. Such hourly emission timings are often derived from additional and/ or combined products, like sociodemographic factors and climatological conditions (e.g., [Mues et al., 2014](#); [Hendriks et al., 2016](#); [Guevara et al., 2021](#)). Activity information from traffic counts can for example be correlated to meteorological conditions to account for the cold-start effect in a diesel-engine car and further improve the model performance in winter time (e.g., [Yusuf and Inambao, 2019](#)). Emission inventories, such as CAMS, are regularly published to include recent submissions, also updating the past periods of time (e.g., [Kuenen et al., 2014](#); [Kuenen et al., 2022](#)). [Figure 3.12](#) shows a typical workflow with spatial and temporal allocation of emissions for use in a CTM.

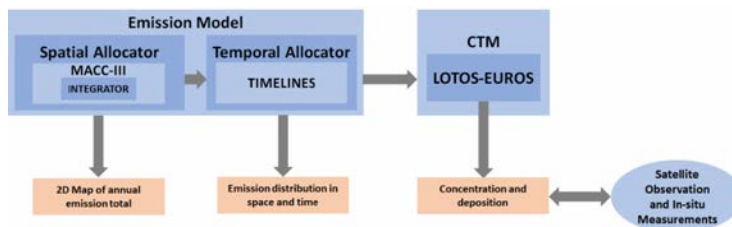


Figure 3.12: A simplified scheme of the workflow in a typical emission model, involving the development of spatial and temporal allocators as well as verification with measurement data. Source: [Ge et al., 2020](#).

3.4.3.2 Meteorological input data

To simulate the chemical transformations and transport of air pollutants, the information on the meteorological condition is obviously required. Meteorological weather forecast simulations or reanalysis data are commonly being used for this purpose, e.g. those provided by the European Centre of Medium Range and Weather Forecast (ECMWF) ([Flemming et al., 2009](#)). To account for special meteorological conditions one can make use of meteorological products that have a higher spatial, temporal and/ or vertical resolution. An additional advantage is that one controls the output of the meteorological model and one can optimize these for the CTM application. For Germany meteorological information's are provided by the German weather service (DWD, [Reinert et al. \(2016a\)](#)).

3. Introduction

The use or implementation of meteorological forcing data, differs in form of online and offline coupled CTMs (e.g., Grell, 2004; Grell and Baklanov, 2011). For offline coupled model simulations, the meteorological input data is provided as previously obtained from the meteorological forecasts and needs to be available throughout the entire model domain, but remains unchanged (e.g., Im et al., 2015a; Im et al., 2015b). For online coupled CTMs, the meteorological fields are computed simultaneously to the chemical dispersion (e.g., Im et al., 2015b), which allows to take feedbacks between the atmospheric composition and the meteorology into account. LOTOS-EUROS and REM-CALGRID, are examples for offline coupled model systems. Two examples for online coupled CTMs are the WRF-Chem (Grell et al., 2005; Fast et al., 2006) and the COSMO-MUSCAT (Wolke et al., 2012) models.

3.4.3.3 Dispersion and chemistry

In LOTOS-EUROS, all transport and transformation processes such as advection (Walcek, 2000), hydrolysis of N_2O_5 (Schaap et al., 2004), cloud chemistry (Banzhaf et al., 2012), gas-phase chemistry (Whitten et al., 1980), aerosol chemistry (Fountoukis and Nenes, 2007), or dry (Zhang et al., 2001; Van Zanten et al., 2010; Kruit et al., 2012) and wet deposition (Banzhaf et al., 2012) are performed on a horizontal Eulerian grid and terrain following coordinates, solved by a numerical balancing of the air-mass using an analytical equation. Eulerian models balance the air mass between two fixed neighboring grid boxes and are per definition mass-conserving (Collett and Oduyemi, 1997). The mass balancing is performed for each single model time step and for all grid points during the model runtime. With respect to the needs, the required application and/ or the demand on computing capabilities, the spatial and temporal resolution of the model simulation can be chosen as desired. Given this fixed resolution of the computational grid, the spatial resolution of the final product (the mass concentration of the air pollutant) will be fixed as well. This can affect the simulation of emissions close to point sources, as pollutants emitted from high stack sources have to be extrapolated to a larger area that corresponds to the grid dimension. Note, grid models do not represent local conditions but urban and regional scales.

3.4.3.4 Chemical boundary conditions, nesting and other input data

The models also require information on the background concentrations outside of the region covered by the model domain itself, which is relevant to capture the transport of air pollutants from remote areas. Chemical boundary conditions are most commonly obtained from global model simulations (e.g., Inness et al., 2019). For high resolution model applications focussing on a particular region or country, a grid refinement using a single CTM is frequently used (e.g., Schaap et al., 2015). In this context, a model simulation with coarse resolution serves as boundary condition for a model simulation that offers a more refined grid but smaller domain size. This method is known as nesting and can

be performed easily as often as needed with a several number of different nests (e.g., Schaap et al., 2015).

Apart from the emissions and the meteorology, there are a number of other key inputs required to perform a regional CTM simulation. Datasets for land use, vegetation and soil types are required to model (semi-n) natural emissions as well as the dry deposition during the model simulation (e.g., Köble and Seufert, 2001; China and James, 2012; EEA, 2021; Luttkus et al., 2022).

3.4.3.5 Deposition of air pollutants

The removal of air pollutants from the atmosphere to the surface (soil, water or vegetation) is expressed by the term of deposition, with the total deposition being divided into the dry, wet and occult part. Dry deposition refers to adsorption of gaseous compounds and sedimentation of particles at the surface (e.g., Zhang et al., 2001; Van Zanten et al., 2010; Kruit et al., 2012). For the deposition a high correlation can be observed to the (local) meteorological conditions (e.g., Kavassalis and Murphy, 2017). The importance of the dry deposition for individual compounds depends strongly on the compound reactivity and water solubility. The deposition of substances by precipitation is referred to as wet deposition (e.g., Theobald et al., 2019). The wet deposition correlates to the mass concentration of the material that is washed out by rainfall and rainfall-intensity of the precipitation, or even the cloud properties, such as the droplet size or the liquid water content (e.g., Banzhaf et al., 2012). The removal through cloud and/ or fog droplets is called occult deposition (e.g., Kalina et al., 2002; Hůnová et al., 2022). The occult deposition flux depends on the concentration of the chemical compounds within the cloud/ fog droplets and the water flux to the surface. This process is only important in mountainous regions and is normally neglected in CTMs.

3.5 Evaluation of chemistry transport models

The quality of chemistry transport model simulations is most commonly assessed by quantifying the model error in a paired comparison to (in-situ or remote sensed) observations. For this purpose, a simple and straightforward operational evaluation is often performed using statistical indicators (e.g., Dennis et al., 2010). Typical statistical measures may include the correlation coefficient, the mean bias and the root mean squared error. In FAIRMODE (Forum for AIR quality MODELing in Europe, <https://fairmode.jrc.ec.europa.eu/>) more detailed information and examples are presented to perform an advanced operational evaluation using different modelling quality objectives and modelling performance criteria for air pollution applications. However, the ability of the model to capture the impact of variable meteorological conditions and/ or emissions is often not well diagnosed with the operational evaluation. Here, the diagnostic and dynamic evaluation can help to assess the model uncertainty within a broader perspective (e.g., Dennis et al., 2010; Lecœur and Seigneur, 2013; Henneman et al., 2017). The dynamic evaluation allows for the quality assessment of model simulations,

3. Introduction

based on the analysis of concentrations and their sensitivity to different input data, such as meteorology and/ or emissions. While the operational evaluation compares the absolute modelled concentration levels to observations, the dynamic evaluation is based on the comparison of the modelled and observed concentration differences (e.g., Dennis et al., 2010; Lecœur and Seigneur, 2013). Shortcomings in model parameterisations can further be identified using the diagnostic evaluation (e.g., Dennis et al., 2010; Henneman et al., 2017). Diagnostic evaluation often includes the comparison of process parameterisation results against detailed observations. For example, recent evaluation of the dry deposition process description elucidated that the observed sensitivity of the dry deposition velocity to relative humidity is not captured by the parametrisation of this process (Wintjen et al., 2022). Inter-comparison studies also assist the evaluation of chemistry transport models, can help to identify shortcomings in their process implementation and foster the exchange of best practices. Multi-model (ensemble) inter-comparison studies are often used to pinpoint differences for each model or different configurations in use. Figure 3.13 summarizes the mentioned evaluation techniques.

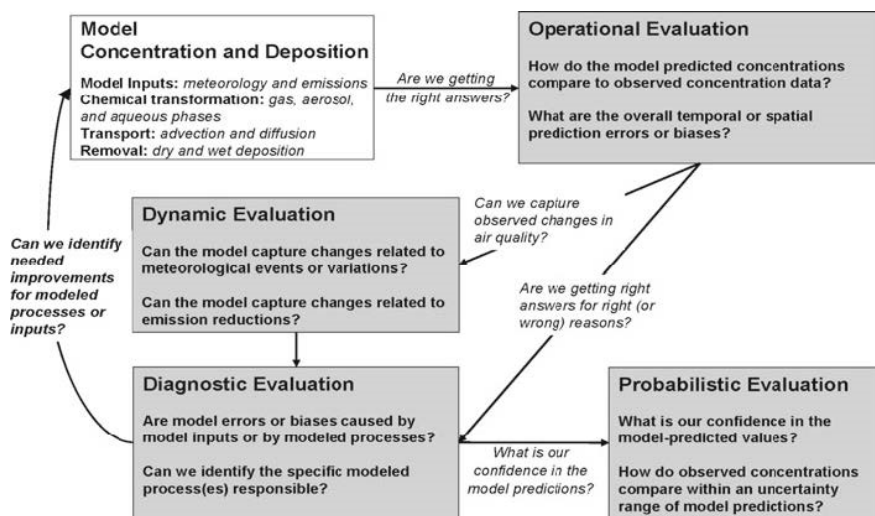


Figure 3.13: A framework for evaluating regional-scale photochemical modeling systems. Source: Dennis et al., 2010.

3.6 Remaining challenges

Despite the progress made in regulating anthropogenic emissions to reduce air pollution and to understand their impact on human health knowledge gaps remain. Some will be shown and discussed in the following section.

Nowadays, most research activities focus on a single pollutant or a single source to assess the impact on human health due to emission control. Incomplete

information is available for air quality regulations lowering the emissions from several pollutants and sources to estimate their long-term exposure. A lack of information exists when regulations far away from central site measurement stations taking place. More information on current and future contributions from source regions and sectors are needed to properly understand the whole picture of atmospheric chemistry and to link them with health. Limited information is available e.g. on non-exhaust emissions. The attribution of emission sources is difficult to obtain and strongly relies on the quality of the model. CTMs are complex systems and the model based source attribution technique can vary from model to model. Different techniques applied for source attribution purposes can yield to different outcome. The results from source attribution activities needs to be regularly assessed by comparing to observations and between models. Comparisons for PM and ozone show large uncertainties between the techniques. A comparison for NO₂ has not yet been performed. Non-modelled concentrations when comparing to observations cannot be apportioned and make further investigations necessary to improve the performance of CTMs. Modelled biases can often be linked to meteorological sensitive processes or not complete emission inventories used. In winter, CTMs hardly capture peak concentrations for PM and NO₂ when stagnant conditions prevail. In summer, CTMs to some extent underestimate PM concentrations during drought periods when coarse material is resuspended.

More research is needed to address the mentioned knowledge gaps and to gain a larger expertise on how to manage them within an appropriate future policy, e.g. to implement new guidelines.

Chapter 4

Research aims

Chemistry transport models (CTMs) are essential to assess the exposure to air pollution (Section 3.4) and to develop mitigation strategies. The overall goal being addressed in this thesis is:

"To improve our ability to quantify the source contributions to concentration levels of priority pollutants in Germany through regional scale modelling"

Below I detail the specific research questions that were addressed.

It has already been shown that the source attribution and the calculation of contributions with the labeling and the brute-force approach can lead to different results for PM, especially when the brute-force approach has not been performed within the specified application range. For nitrogen oxides ($\text{NO}_X = \text{NO} + \text{NO}_2$) such a comparison was not available and the following research question results:

1. To what extent are source contributions derived from the labeling approach comparable to the potential impacts from the brute force technique for NO_X ?

A good model skill in comparison to observations is essential for research and policy support applications. In this context, the evaluation of modeled concentrations and the further development of model process descriptions to capture the sensitivity of modeled concentrations to meteorology and emissions are of decisive importance. The following research questions are addressed:

2. In how far is the LOTOS-EUROS CTM able to reproduce the observed variability in the concentrations of PM, NO_2 and O_3 in Germany?
3. In how far can we improve the model performance through detailing the vertical resolution and applying alternative boundary layer schemes?

The emission source sectors and regions explaining the PM and NO_2 levels at a given location and time can be manifold, but their contributions should be understood when cost effective mitigation actions are formulated in the framework of policy advice. In this context, the research question is:

4. What are the most relevant source sectors and regions of PM and NO_2 in the rural and urban background of Germany and its capital Berlin?

In Germany, a large scientific community offers the opportunity to employ hindcasts and forecasts for air pollution. The research groups often use chemistry

4. Research aims

transport models different to LOTOS-EUROS. As comparisons between the models applied in Germany are rare, the (German) exposure to air pollution and the (modeled) sensitivity of concentrations to meteorological conditions should also be studied in a multi-model ensemble assessment, leading to the following research question:

5. Can we identify model specific and general shortcomings in emission and process descriptions to be tackled in future research?

To address these research questions in the presented study, a variety of CTM simulations has been performed and evaluated for Germany and the Berlin agglomeration area. The analysis of different process implementations and several sensitivity (model) simulations have been used to improve the modeling quality for the air pollutants PM, NO₂ and O₃. The applied models and methodologies have been introduced and their outcome with discussions and conclusions have been described in more detail in the papers [I](#) to [IV](#) and were presented in the following.

Chapter 5

Summary of included papers

5.1 Source attribution of nitrogen oxides across Germany: Comparing the labelling approach and brute force technique with LOTOS-EUROS

In [Paper I](#), air quality model simulations were performed to quantify source sector contributions to the background concentration of NO, NO₂ and NO_x in Germany. The four main emission source sectors road transport, non-road transport, energy & industry and household were tracked. All remaining emissions were combined in one category, named others. The sector contributions were calculated, first using the labeling approach implemented in the LOTOS-EUROS model and second by applying emission reduction simulations (hereafter referred to as the brute force technique). In addition, the brute force technique has been compared with the labeling approach. Systematic differences have already been observed between the two source attribution methods in previous research activities, for particulate matter (e.g., [Clappier et al., 2017](#); [Carnevale et al., 2018](#); [Thunis et al., 2019](#); [Thunis et al., 2020](#)) or for ozone (e.g., [Mertens et al., 2018](#); [Butler et al., 2020](#)). Here, non-linear chemical processes have been identified to be the main limiting factors related to most of the observed differences. However, no information could yet be provided for nitrogen oxides and no study was available comparing both methods head-to-head.

The source attribution of emission reduction simulations for nitrogen oxides is found to be largely limited to non-linearity triggered by photochemical reactions between different emission source sectors. The results of the exercise show that attributed concentrations of NO from sector wise NO_x emission reductions show larger contributions of NO than the labeling. For NO₂, the attributed concentrations from the brute force method were on average lower in the urban background and larger in the surrounding rural background than the labeling approach. Brute force sensitivity simulations that were performed with variable NO_x emission reductions are strongly affected by (the lack of) regime changes in the titration of ozone, most notably present at ozone-limiting conditions during nocturnal winter months and close to emission source regions in or near urban areas. When upscaling the simulated impacts (the concentration difference to the baseline without emission reduction) to 100 %, the concentration level differs from the baseline concentration. By implication, inconsistencies between the brute force technique and the labeling approach become larger for smaller emission reductions, for shorter time scales and when small-sized emission source sectors are investigated.

Lessons learned from the comparative study reinforces the appropriate selection of the source attribution method for nitrogen oxides and

supports the Forum for AIR quality MODeling in Europe (FAIRMODE, <https://fairmode.jrc.ec.europa.eu/>) for assessing future mitigation strategies. It has been stated that the application of emission reduction simulations is potentially not the most suitable option to estimate source sector contributions to NO. However, both methods are suitable for the source attribution of NO₂, as the observed differences between both techniques are considerably smaller than the model bias compared to the observations. Nevertheless, it is also recommended to avoid the brute-force technique for NO₂ when small-sized emission source sectors are examined.

As the labeling approach has several practical advantages but is limited for the mitigation purpose, air quality planning should be addressed by combining both methodologies. Source sector contributions that have been performed with a labeling approach, can e.g., yield as an initial ranking for the follow up emission reduction sensitivity analysis and provide additional information.

5.2 Source attribution of particulate matter in Berlin

Exposure to PM (coarse: PM₁₀ and fine: PM_{2.5}) is one of the primary environmental health concerns for large conurbations in Europe, such as Berlin (e.g., Boldo et al., 2006; Brook et al., 2010; Costa et al., 2014). Here, an in-depth understanding in terms of the source regions and -sectors for the origin of PM is required, using comprehensive monitoring and modeling frameworks, to ensure that mitigation strategies are effectively realized (e.g., Belis et al., 2020; Pandolfi et al., 2020).

In Paper II, a source attribution of PM has been performed for Berlin, Germany, that can be used as a first step towards defining source categories of brute force model simulations for follow up mitigation assessments. For this purpose, model simulations were conducted for a (3 year-) period from 2016 to 2018 with the LOTOS-EUROS CTM applying the labeling module (Kranenburg et al., 2013). Sectoral and regional contributions for PM₁₀ and PM_{2.5} in Berlin mainly agree with previous findings. Emissions from households and industry & power contribute most to the mean modeled urban background PM_{2.5} concentration and sum up to about 50 %. The source attribution for PM₁₀ is (on average) similar to PM_{2.5}. However, for PM₁₀ the relative shares for natural sources are higher. The regional source attribution has shown that domestic contributions exceed those of the transboundary transports to Berlin. However, about one third of the PM concentration can still be attributed to neighboring countries, such as Poland and the Czech Republic, in particular during wintertime episodes.

The evaluation of the modeled coarse material (difference between PM₁₀ and PM_{2.5}) and the urban increment of the coarse mode was another focus of this study. Quality assessment of the LOTOS-EUROS CTM against the UBA monitoring network has shown an underestimation for modeled PM concentrations. On average, the study shows better agreement between model and measurements for fine material than for the coarse mode, which results in a

A multi-meteorological comparison for episodes of PM₁₀ concentrations in the Berlin agglomeration area in Germany with the LOTOS-EUROS CTM

too low modeled coarse mode fraction. Here, the study discussed the reduced capability of the LOTOS-EUROS CTM to simulate PM during stagnating (cold) weather conditions in Berlin that are related to the vertical mixing and presents the possibility for recent model improvements, which has been presented in paper [Paper III](#).

Following [Lenschow et al. \(2001\)](#), the contributions of source sectors and regions have also been used to calculate gradients between the urban and the rural background (urban increment), to provide information in terms of possible reasons for the model shortcomings. Normally, a large part of enhanced coarse mode in large conurbations can be explained by (road) resuspension that is a predominant emission source during (warm and dry) summer episodes. Results of the presented study also show that the urban increments for PM can be attributed to traffic as well as to household emissions. However, the simulated (total) coarse mode urban increment is underestimated by a factor of ~4 compared to those derived from the observations. It is suggested that the missing mass of the coarse mode (increment) can partly be explained by too low modeled traffic contributions, which are by a large part related to (road) resuspension processes that currently are not covered by the model. To further improve the modeling quality more attention is needed on estimates of resuspension processes for national scale emission inventories from e.g., traffic and land management activities.

The study also highlights examples for future scientific research perspectives. A side-by-side comparison of receptor model results with those presented here may reveal further limitations of the LOTOS-EUROS model. A dynamic model evaluation can be used with focus on source contributions. This can help to identify the modeled sensitivity to meteorological parameters such as the temperature for different source regions and sectors. A (road) resuspension emission scheme with sufficient spatial and temporal variability should be implemented in CTMs or in emission inventories as well.

5.3 A multi-meteorological comparison for episodes of PM₁₀ concentrations in the Berlin agglomeration area in Germany with the LOTOS-EUROS CTM

In Germany, high concentrations of particulate matter (PM) are often associated with cold stagnant weather conditions, especially during wintertime ([UBA, 2019](#)). Exceedances of the daily limit value for PM in East-Germany are also highly correlated to air pollution transport from neighboring countries ([van Pinxteren et al., 2019](#); [Timmermans et al., 2020](#)). In [Paper III](#), model simulations with the LOTOS-EUROS CTM have been performed to investigate the spatial distribution and the temporal evolution for PM in the German subdomain. The study showed how well the LOTOS-EUROS model performs during cold stagnant weather situations and compares different weather conditions, meteorological forcing data and modeling set-ups.

In this study, the CTM simulations have been performed with differing

meteorological input datasets. The operational set-up of the LOTOS-EUROS CTM is driven by meteorological forecasts from the European Centre for Medium-Range Weather Forecasts (ECMWF, [Flemming et al., 2009](#)). For the first time, the LOTOS-EUROS model was also driven with meteorological input data from the regional climate model COSMO-CLM (Consortium for Small-Scale Modelling-Climate Limited-area Modelling, [Doms et al. \(2011\)](#); [Doms and Baldauf \(2018\)](#)). ERA-Interim reanalysis ([Dee et al., 2011](#)) of the ECMWF was dynamically downscaled by the regional climate model COSMO-CLM. In addition, the turbulence scheme of the planetary boundary layer meteorology has been studied in COSMO-CLM using different parameterizations and has been used as input to LOTOS-EUROS in test case simulations.

Two set-ups of the LOTOS-EUROS model, that differ in their vertical resolution, have been used to study the mixing in the planetary boundary layer. The operational system of the LOTOS-EUROS model, using a well-mixed boundary layer concept ([Manders et al., 2017](#)), has been used as reference set-up. However, investigations for ozone have already shown a better performance in capturing the vertical transport phenomena during summer in southern Europe when using a larger number of layers ([Escudero et al., 2019](#)). Following the results from [Escudero et al. \(2019\)](#), the multi-layer approach has also been introduced and used to investigate the impact in reproducing the surface concentrations for PM during wintertime in the eastern part of Germany.

All simulations were conducted for past periods where observational data were available and the model output could be compared to the observed state. The sensitivity of PM to different meteorological conditions has been evaluated by comparing each concentration sensitivity (modeled and measured) to the driving meteorological input data. The comparative study showed that the mixed layer model set-up, used in the operational version, on average indicates too high mixing from the ground surface to higher model layers and led to an underestimation of observed PM concentrations in the eastern part of Germany. Here, the planetary boundary layer height serves as the main limiting factor to determine the mixing. However, the meteorology modeled in the planetary boundary layer using COSMO-CLM showed a better agreement to the radiosonde measurements compared to the ECMWF forecasts. Thus, changing the meteorological input data, from the coarser resolved ECMWF forecasts to the higher resolved reanalysis product from COSMO-CLM, improved the air pollution simulations with LOTOS-EUROS. Nevertheless, the investigation of different mixing-parameterization schemes in COSMO-CLM did not further improve the model performance. Results of the higher vertical model resolution contributes to a better agreement with the measurements. The higher vertical resolution keeps the PM concentration closer to the surface, especially during colder months and close to areas with high emission sources.

The study substantiates the findings by [Escudero et al. \(2019\)](#) that a higher resolved vertical layering along with a horizontal grid refinement improves the model skill of the LOTOS-EUROS model. Following the results shown for PM, it has been recommended not to make use anymore of the mixed-layer approach for air pollution modeling in the LOTOS-EUROS CTM. The study gave advice

to adopt the operational model system within the Copernicus Operational Model System (CAMS, [Marécal et al. \(2015\)](#)) and to use the multi-layering model version as the standard approach.

5.4 Dynamic evaluation of modeled ozone concentrations in Germany with four regional chemical transport models

Air pollution fore- and hindcasts with CTMs remain challenging and need to be performed with as much as high accuracy (e.g., [Bessagnet et al., 2016](#); [Colette et al., 2017](#); [Galmarini et al., 2017](#)). Modeled concentrations often lack correlation to the regional buildup of ozone to the general synoptic state and several meteorological parameters such as the temperature, the moisture and/or the solar radiation (e.g., [Otero et al., 2016](#); [Otero et al., 2018](#)). In Paper II, the quality of modeled ambient ozone concentrations has been assessed and evaluated with four CTMs using a multi-model intercomparison, for the first time, on a national scale for Germany.

Two offline- (LOTOS-EUROS, [Manders et al. \(2017\)](#) & REM-CALGRID, [Stern \(2003\)](#)) and two online coupled (COSMO-MUSCAT, [Wolke et al. \(2012\)](#) & WRF-Chem, [Grell et al. \(2005\)](#); [Fast et al. \(2006\)](#)) CTMs have been employed in the context of this study. All model simulations have been conducted for the period of 2019 with as far as possible harmonized emissions (CAMS-REG, [Kuenen et al. \(2022\)](#) & GRETA, [Schneider et al. \(2016\)](#)), meteorological input data (DWD, [Reinert et al. \(2016a\)](#)), boundary conditions (CAMS/EAC4, [Inness et al. \(2019\)](#)), model domains (Europe & Germany) and resolutions ($7\times 8\text{ km}^2$ & $2\times 2\text{ km}^2$) using a standardized experimental design, that is defined by an intercomparison protocol.

The quality of the model results have been assessed within an operational (model) evaluation that follows (standard) statistical indicators such as the root mean squared error, mean bias, correlation coefficient and index of agreement when compared with observations. Air quality modeling benchmarking indicators provided by the FAIRMODE initiative has been calculated to support the quality assessment ([Janssen and Thunis, 2022](#)). The study focused on the evaluation of the whole (model) ensemble and verifies possible benefits when using a poor man's ensemble, that applies the mean from all four models. Variations between the models (within this ensemble) were pointed out and were used to indicate future directions for model improvements. A recommendation whether one model performs better or worse for a specific application or in general was not the aim of this study and, hence, no recommendations are given. In addition, a dynamic (model) evaluation has been designed to investigate the sensitivity to the temperature and the humidity. The evaluation of the ensemble has been applied for urban and rural sites as well as for three periods of the year separately and to assess ozone processes in different precursor regimes. The MDA8 for ozone has been used as the most important parameter for the quality assessment presented. All models were also scored on their rate to predict exceedances of the $120\text{ }\mu\text{g m}^{-3}$ EU long-term target value for MDA8 O₃.

5. Summary of included papers

Most of the model simulations satisfy the modeling quality objectives and criteria set by the FAIRMODE initiative. The models show larger model-measurement agreement in rural areas compared to the urban background and for springtime than for summertime. All models lack performance forecasting threshold exceedances for MDA8 O₃ above 120 µg m⁻³ and when simulating ozone concentrations at night. For MDA8 O₃ > 120 µg m⁻³ high values for missed alarms and false alarms have been calculated. In particular, for a specific period in springtime the models missed the exceedances that could be linked to deficiencies in the representation of background ozone, including long-range transport. Too low ozone concentrations at night are likely related to difficulties in simulating the stable nocturnal boundary layer. The (four model) ensemble further confirms room for improvement when using an ensemble mean, providing a better model-measurement agreement than applying individual models.

The observed sensitivity of ozone to temperature and humidity is (on average) captured by the model ensemble. In general, both, (1) the lower photochemical production in springtime compared to summertime as well as (2) the lower temperature sensitivity during spring and the higher sensitivity in summer in the urban background are captured by the models. Despite this good representation, the individual models show a large spread in the modeled ozone sensitivities. During the summer season the models show an overestimation in the simulated ozone concentrations with a too low modeled ozone sensitivity to temperature. This can be linked to a systematic overestimation of "mid-range" ozone concentrations that are predominant at moderate temperatures.

As the sensitivity of ozone to temperature also depends on the NO_x/BVOC ratio the study recommends a further diagnostic evaluation of temperature sensitive processes in the models and their model descriptions, such as for biogenic and anthropogenic emissions or the dry deposition. It was also recommended to make use of longer periods in a follow up multi-model intercomparison assessment, to generalize the results of the operational and dynamic (model) evaluation for longer timeframes.

Chapter 6

Synthesis

The focus of this study pertained **"to improve our ability to quantify the source contributions to concentration levels of priority pollutants in Germany through regional scale modeling"**. Air quality model simulations were performed for different temporal and spatial scales. Particulate matter, nitrogen oxides and ozone were specified as the primary pollutants for the analysis. The following section summarizes the most important results of this study, discusses potential reasons for model biases and addresses the research questions mentioned in [Chapter 4](#):

"To what extent are contributions derived from the labeling approach comparable to the potential impacts from the brute force technique for NO_x?"

This study presents an important and a pioneer comparison of potential impacts calculated from brute force model simulations with source contributions identified using the labeling technique for background nitrogen oxide levels. The study shows that O₃ limiting conditions at night during the winter season and the lack of regime changes in the titration of O₃, triggered by non-linearity of the photo-chemical equilibrium (e.g., [Leighton, 1961](#); [Kwok et al., 2015](#)), can cause considerable differences between the two techniques for NO and NO₂. Similar to previous findings for PM and O₃ (e.g., [Mertens et al., 2018](#); [Thunis et al., 2020](#)), the study shows that the sum of potential impacts for NO and NO₂ can differ from the unperturbed baseline simulation. The results presented in this study contributed to the latest version of the FAIRMODE guidance document to support air quality management practices on source apportionment ([Clappier et al., 2022](#)).

For NO₂ the sum of potential impacts is lower in the urban background and larger for rural background sites than the baseline concentration of the labeling simulation. This can be explained by the fact that emission sources in urban regions often vary on a small scale and non-linear chemical regimes occur more frequent (e.g., [Verstraeten et al., 2018](#)). For NO₂, differences were observed of about ±5 % on annual average. Daily or even hourly time series show even larger differences than the annual average. For larger cities differences for NO₂ were observed of about -15 %.

O₃ is titrated away during the build-up of NO under high NO_x conditions and thus NO levels are lowered more than proportionally with respect to NO_x emission reductions. This means that the uncertainty in estimates for potential impacts increases with smaller reduction fractions of NO_x. The emission reduction fraction of 25 % was identified as a limit to perform brute force model

simulations for NO. For PM larger differences are common with increasing emission reductions (e.g., Carnevale et al., 2018; Thunis et al., 2020). For a 20 % emission reduction fraction, an overestimation for urban (~53 %) and rural (~40 %) background sites were observed for NO. Note that these differences vary from region to region (~25 %). The titration of O₃ can vary between different source sectors leading to larger non-linearity (e.g., Belis et al., 2020). The study shows larger differences for small-sized emission sectors under investigation than for large-sized sector categories for NO.

For NO₂ the model bias is typically a factor of 2 when compared to measurements (e.g., Kuik et al., 2018). In this case one can interpret the results of both source attribution techniques as similar. For NO it is recommended to make use of the labeling technique to calculate contributions of emission source sectors and regions, but to avoid the brute force technique to calculate potential impacts owing to the aforementioned shortcomings. This is of particular relevance for single sectors that have a small contribution. Brute force model simulations are more beneficial for policy advice when emission reduction scenarios needed to be performed (e.g., Thunis et al., 2020). Previous studies already showed that the labeling approach is not always a suitable method to derive the impact of an emission reduction (e.g., Clappier et al., 2017). Contributions calculated with the labeling technique are most informative when used as a first guess for the subsequent emission mitigation assessment. As shown by Butler et al. (2020) for O₃, a combined assessment, using the labeling technique and the brute force approach, provide an even more complete insight that none of the two methods can address alone.

"In how far is the LOTOS-EUROS CTM able to reproduce the observed variability in the concentrations of PM, NO₂ and O₃ in Germany?"

The concentration for PM, modeled with LOTOS-EUROS, show good agreement to the observations in the regional background for Berlin and its surroundings. The temporal variability of PM is fairly represented by the simulations throughout the year. For urban background sites the model simulations show a distinct underestimation compared to the observations. This underestimation is even larger for PM episodes. LOTOS-EUROS represents about 55 % (75 %) in summer (winter) of the observed urban background concentration in Berlin. The underestimation for urban background sites is in agreement with previous research studies using LOTOS-EUROS (e.g., Hendriks et al., 2013; Manders et al., 2017) or other models (e.g., Bessagnet et al., 2016). This study shows that LOTOS-EUROS simulates a lower urban increment (~4 $\mu\text{g m}^{-3}$) than observed (~7 $\mu\text{g m}^{-3}$) for Berlin. The lowest model-measurement agreement for Berlin was observed for coarse material (PM₁₀-PM_{2.5}) and the urban increment. LOTOS-EUROS only covers 1/4 of the observed (3 $\mu\text{g m}^{-3}$) coarse mode urban increment in summer. Larger particles often originate from resuspended road dust (e.g., Amato et al., 2009; Denby et al., 2013) or from urban land management activities. Following van Pinxteren et al. (2019)

emissions of coarse material can have a large effect on Berlin and partly can explain the model bias in the course mode. Exceedances of the daily limit value for PM can often be identified for prolonged (cold) stagnating episodes in winter close to emission sources, e.g. in populated (urban) areas and near busy roads (e.g., [van Pinxteren et al., 2019](#); [Timmermans et al., 2022](#)). LOTOS-EUROS hardly captures these winter PM episodes in Berlin. The study concludes that vertical mixing in LOTOS-EUROS during these episodes is not well simulated.

Largest NO₂ levels in Germany were modeled close to high populated urban agglomerations (e.g., the Rhine area) and in large city centers like in Munich or Berlin. LOTOS-EUROS is well suited to model large scale patterns in the regional background for nitrogen oxides but needs improvement to account for the variability in the urban background. The model simulations are in agreement to observations for NO and NO₂ in the rural background. In the urban background LOTOS-EUROS shows an underestimation for NO₂ and an even larger bias for NO. Largest disagreement between modeled and monitored nitrogen oxide levels for urban background sites were observed during the morning and afternoon traffic rush hour peaks. The urban increment for NO₂ and NO is often modeled too low. This can partly be related to an underestimation of NO_x emissions in inventories for the urban background (e.g., [Kuik et al., 2018](#)).

Nitrogen oxides further promote the build-up of O₃. Low O₃ levels were modeled near NO_x source regions, while high O₃ concentrations are present away from the source areas. Simulations with LOTOS-EUROS show a lower O₃ concentration in spring than for summer. This is related to larger local photo-chemical production during the summer month. LOTOS-EUROS well captures the observed differences between urban background sites and the rural background. Rural background sites were better captured than urban background sites, but on average too high values were observed for both site classes (~6 µg m⁻³). The same holds for spring compared to summer. At night, the simulation shows overestimation and remain a major challenge in the modeling of O₃ with LOTOS-EUROS. The overestimation at night can be attributed to difficulties in simulating the vertical mixing of the stable nocturnal boundary layer. O₃ levels for high (peak) concentrations during prolonged episodes, e.g. exceedances of the MDA8 O₃ > 120 µg m⁻³, are not always captured with LOTOS-EUROS and show room for improvement. All modeling objectives and criteria set by the FAIRMODE initiative are satisfied for LOTOS-EUROS. From the operational model evaluation one can conclude that LOTOS-EUROS is well suited to address the air quality for O₃ in Germany.

"In how far can we improve the model performance through detailing the vertical resolution and applying alternative boundary layer schemes?"

For the first time LOTOS-EUROS was driven with model simulations of the regional climate model COSMO-CLM. The use of COSMO-CLM for simulations with LOTOS-EUROS provides an important guidance for mitigation assessments at national (German) level. Weather forecasts performed at the Ger-

man Weather Service using COSMO-CLM and ICON can now easily be applied LOTOS-EUROS. COSMO-CLM was used to downscale meteorological reanalysis from ECMWF for Germany and Berlin. The COSMO-CLM simulations have a higher horizontal and vertical resolution than the meteorological input data from ECMWF. The study shows a better representation of the meteorological condition in the planetary boundary layer (PBL) simulated with COSMO-CLM than for the ECMWF product. Largest changes were observed for the mixing layer height (MLH). The study shows lowered concentrations in the rural background and higher PM levels for urban sites when the horizontal resolution is increased and meteorological input from COSMO-CLM is used. But similar to previous results for ECMWF from [Schaap et al. \(2015\)](#), the LOTOS-EUROS simulations driven with the higher resolved COSMO-CLM meteorology show no clear indication for improvements in Berlin. The underestimation in the urban background and the urban increment deficit remains. This shows room for improvement in detailing the emission inventories at national level, for example previously shown for condensable material in residential wood combustion (e.g, [van der Gon et al., 2015](#)).

The reduced capability to simulate the urban background concentration for PM and NO₂ with LOTOS-EUROS can to a small extent be attributed to vertical mixing. Sensitivity simulations were performed to understand the vertical mixing in LOTOS-EUROS. The study shows that the vertical mixing in numerical weather prediction models is uncertain and their use in CTMs is challenging. Different turbulence parameterization schemes used in COSMO-CLM and to model the MLH do not have a huge impact on simulations with LOTOS-EUROS. Modeled PM values for Berlin vary between $\sim 0.5 \mu\text{g m}^{-3}$ when using the different model realizations. Thus the MLH is not the most limiting factor affecting the vertical mixing in LOTOS-EUROS.

Larger impact was observed for the model layer structure used in LOTOS-EUROS. The dynamic mixed-layer model set-up in LOTOS-EUROS assumes a well-mixed PBL with 5 vertical model layers. Simulations with the dynamic mixed-layer approach show too large mixing from the surface to higher model layers. This leads to a lower modeled concentration than observed for winter PM episodes in Berlin.

The study presents and evaluates an alternative modeling strategy for vertical mixing in LOTOS-EUROS. This approach, referred to as the multi-layer model set-up, negates the assumption of a well-mixed PBL and uses a larger number of model layers. Model layers in the multi-layer set-up follow the vertical layering of the driving meteorological model. The vertical transport phenomena can thus be better captured. The higher vertical resolution is crucial in areas with higher emissions. For stagnating conditions in winter the concentration in high polluted regions mainly remain below 1000 m even when emitted from high stack sources. Model simulations with higher vertical grid resolution show lower dilution and keep the pollutants closer to the surface than when modeled with the dynamic mixed-layer approach. The study shows a reduced model bias in the urban background for Berlin, when the simulations were performed with the multi-layer model version of LOTOS-EUROS. This can mainly be related

to redistribution and increase in nitrate and ammonium concentrations. For regions with lower concentration and when the lower tropospheric layer is well mixed, e.g. in warmer month, the multi-layer model set-up performs similar to the dynamic mixed-layer model version. A model evaluation assessment in Spain for O₃ shows similar results (Escudero et al., 2019). It is recommended not to apply the dynamic mixed-layer set-up anymore. Instead, the higher resolved vertical layering must be used for future research activities with LOTOS-EUROS.

"What are the most relevant source sectors and regions of PM and NO₂ for Germany and its capital Berlin?"

The attribution of emitting sectors and regions along with the calculation of contributions using the labeling system in LOTOS-EUROS allows to draw conclusions on main culprits and to give advice for further mitigation efforts. As part of this research, the most important emission source regions and sectors for PM and NO₂ were identified in Germany and Berlin.

Contributions from household (~30 %) and industry & power (~19 %) are the most dominating emission sectors for PM in Berlin. Traffic (~12 %), agriculture (~12 %) and the boundary (~14 %) contribute the other half. The remaining contribution is explained by a rest term, for example from natural emissions. For PM₁₀ this term shows a slightly larger contribution compared to PM_{2.5}. The source sector contributions for PM₁₀ and PM_{2.5} can differ with meteorological conditions and between PM episodes, but the relative contributions are similar. Most distinct differences for relative contributions of PM₁₀ and PM_{2.5} were observed between the winter and the summer season. The study confirms previous results for transboundary contributions of neighboring countries further east, especially for wintertime PM episodes. Domestic contributions exceed the transboundary transport to larger cities like Berlin. About 49 % of the total concentration in Berlin can be attributed to sources in Berlin itself (~25 %) and to emissions in Germany (~24 %). About 33 % originate from transboundary transport. One third of the transboundary transport has its origin in Poland and the Czech Republic. The urban increment of Berlin is mainly composed of households (~53 %) and traffic (~17 %). Most of the rest can be attributed to agriculture and natural sources, which show a negative urban increment. Mineral dust, emitted as resuspended particle from road traffic and from agriculture, contribute about 22 % to the coarse mode urban increment for Berlin during the summer season. Previous studies suggest that this contribution is too low by a factor of 4. The e-mobility will further intensify in the coming years and may raise the high relevance of re-emitted particles from the road transport sector. Despite, no political regulations are yet in place for non-exhaust emissions and their risk assessment.

For NO₂, emissions from the road transport sector are the most important source on annual, weekly and daily time scales and show contributions of about 45 % in Germany. The S-VELD project adjoined to this thesis shows that, given the current composition of the German vehicle fleet, the majority of the traffic emissions are caused by light duty vehicles (S-VELD, 2022). The largest share

of the traffic concentration for NO_2 is attributable to emissions originating from highways, followed by sources in urban and rural environments (S-VELD, 2022). Interestingly, the highway contributions of NO_2 that were transported into the urban background exceed the traffic-generated concentration of the inner-city area itself (S-VELD, 2022). This can be related to an insufficient representation of emissions in the urban background for major cities like Berlin. The Rhine Valley, the coastal regions and the Kiel-Hamburg channel are mainly affected by emissions from non-road transport (e.g., shipping emissions) and shows typical contributions to NO_2 of about 24 %. Emissions from the industry and the energy sector (e.g., originating from point sources, like industrial power plants) contribute about 20 % to the total NO_2 concentration in Germany, mainly located in the Ruhr area and Brandenburg. Domestic incomplete combustion processes (e.g., residential heating) can affect the environment. The impact of residential heating is limited at local level and particularly affects areas with a high population density. Combustion from households contributes about 10 % to the total NO_2 concentration in Germany on annual average. In the northern part of Germany and in the vicinity of the alpine region, emissions from agriculture play an important role, especially in spring. Owing to the short lifetime of NO_2 , the transboundary contributions of European countries for NO_2 are limited and were only observed on annual average at the German border.

In this study no source attribution was performed for O_3 . The implementation of a source attribution system for LOTOS-EUROS is still ongoing. In a joint UBA project with RIFS Potsdam and TNO the source apportionment technique was implemented similar to the “Toast” module in WRF-Chem and is currently under evaluation (e.g., Schaap et al., 2023). The implementation will help to quantify the origin of simulated O_3 for Germany with LOTOS-EUROS. Previous studies show that long-range transport of ozone is of high relevance for European countries (e.g., Lupaşcu et al., 2022). About 1/3 of the regional ozone concentration is produced by oxidation of methane in remote areas and further transported into Europe (e.g., Butler et al., 2020). The remaining part is locally produced at the given location. The local production of ozone is highest in spring, while the contribution of long-range transport is larger in summer (e.g., HTAP, 2010). High ozone concentrations and exceedances of limit values can primarily be attributed to the photo-chemical build-up of ozone as a result of precursor emissions in the regional background (e.g., Lupaşcu and Butler, 2019).

"Can we identify shortcomings in emission and process understanding to be tackled in future research?"

The systematic underestimation of the urban background concentration and the urban increment for PM and NO_2 can partly be related to an underestimation of urban emissions. The study by Kuik et al. (2018) supports this hypothesis and concludes that a low model bias in the urban increment for NO_2 in Berlin can be attributed to the prescribed emission inventory. The annual emission totals are generally well captured and spatial redistribution of the emissions can be used to reduce the model bias. Improving the emission profiles further

allow to compensate the timing in the model simulations for concentrations in the morning and afternoon traffic rush hour peaks (e.g., [Mues et al., 2014](#)). Redistributing the emissions in time can reduce the model biases, often observed with static time profiles, on weekend and at night (e.g., [Mues et al., 2014](#)).

The study shows low affect of different vertical mixing descriptions used in LOTOS-EUROS for warm and dry periods in summer. It was concluded that the model bias for coarse material during these periods is partly related to emission inventories at national level that show underestimation of PM in the urban background. This study shows that seasonal variations for resuspended material can make up to a factor of 4 in Berlin.

Resuspension from road traffic and from agriculture land management activities are an important source for coarse material (e.g., [van Pinxteren et al., 2019](#)). Most research findings point to large uncertainties on the spatial distribution for road dust resuspension (e.g., [Padoan and Amato, 2018](#)) and show lower contributions in rural areas compared to densely populated regions (e.g., [Gon et al., 2010](#)). Higher dust levels in urban environments were mentioned as one of the potential explanations ([Schaap et al., 2009](#)). In Southern Europe the resuspension of course material can be expected as higher than in Central Europe (e.g., [Denby et al., 2018](#)). The Mediterranean region is usually drier compared to Northern Europe and shows higher values for coarse material. Recent studies show large seasonal variation induced by different weather conditions for resuspension of road dust (e.g., [Denby et al., 2013](#); [Padoan and Amato, 2018](#)). In some northern European cities, studded tires and road gritting are used in winter or spring. This leads to a seasonal variation with high peaks and spatial differences for non-exhaust emissions of up to 90 % (e.g., [Omstedt et al., 2005](#); [Kupiainen et al., 2020](#)).

The same applies to resuspended material from agriculture land management activities. Manure and harvesting activities contribute as source for coarse material and show high fraction in late summer. Ongoing research point to large uncertainties for different crop types and show large variations from year to year, depending on the weather condition.

Resuspension of road dust and from land management activities is not yet reported in emission inventories. Emission factors from traffic resuspension that account for seasonal variations are scarce in Europe and are not necessarily applicable to sites beyond their origin (e.g., [Amato et al., 2011](#); [Denby et al., 2018](#)). Reliable estimates for emission factors that can cope with different geographical areas in Europe and capture the variation in time, on seasonal, daily and hourly time scales can improve the model results (e.g., [Padoan and Amato, 2018](#)). The observed non-exhaust emission factors often not differentiate between primary emissions, like as tire or break wear and the secondary source from resuspended material (e.g., [van der Gon et al., 2018](#)). This can result in a double counting for emissions in inventories when a breakdown of non-exhaust emissions is used (e.g., [Pulles and Heslinga, 2007](#)).

In LOTOS-EUROS, modeling the resuspension of coarser material from traffic is incorporated using a simple emission factor per mileage driven (e.g, [Schaap et al., 2009](#)). The emission factor is separated for each grid-cell by vehicle

type (light and heavy traffic) and road category (urban, rural and highways). Rain affects road surface moisture and lowers the subsequent resuspension by wet deposition (e.g., [Padoan and Amato, 2018](#)). This is simply approximated by an on/ off approach based on the precipitation availability in LOTOS-EUROS. Different climate conditions are covered using a simple approximation in LOTOS-EUROS. A linear scaling of the emission factor is applied using annual averaged soil moisture levels to account for the spatial distribution ([Schaap et al., 2009](#)). But modeling seasonal variations for resuspended material are not yet covered. This implies that the dust reservoir remains constant over time.

The modeling of O_3 using CTMs in Germany still remains challenging. For the first time, a high resolution multi-model inter-comparison study was performed at national level for Germany. The study takes into account four regional CTMs that are commonly applied in Germany. The results strengthened conclusions from former research activities that a model ensemble mean often shows higher model-measurement agreement and larger statistical skill than what can be achieved with a single model simulation (e.g., [Galmarini et al., 2017](#); [Jonson et al., 2018](#)). The study further assessed the regional build-up of O_3 and its sensitivity to meteorological parameters such as temperature and humidity. A dynamic model evaluation was designed that classify the modeled O_3 for observed discrete concentration regimes. It was concluded that the sensitivity of O_3 to different meteorological conditions need more attention. The study shows that CTMs lack correlation to the synoptic state and differ in the modeled dynamic response to temperature and humidity for O_3 . LOTOS-EUROS well captures the differences observed between site classes (urban/ rural) and between the seasonal variation (spring/ summer) for the ozone sensitivity to temperature and to humidity. Despite the well reproduced seasonal variations, the model simulations with LOTOS-EUROS underestimate the O_3 sensitivity to temperature on annual average.

Chapter 7

Outlook and future perspectives

Below research directions are introduced which interest me and may be of interest for upcoming applications using LOTOS-EUROS.

Regular model inter-comparison activities can improve the model quality for air pollution reanalysis and forecasts. Similar to the CAMS ensemble prediction system for Europe, multi-model inter-comparison studies must be periodically promoted at national level in the future. The ensemble used in a model inter-comparison, usually use more than one CTM or is realized for different parameterizations of the same model. Thus, for an multi-model evaluation assessment, the input datasets like emissions and meteorology must be standardized. This promotes the collaboration within the CTM community and new model developments can be addressed regularly and undergo a scientific review process within the scientific community.

Multi-model inter-comparison studies must be introduced more often for Germany. This can promote the development of an air pollution prediction system that make use of CTMs at national (German) level. A joint working group must be installed to outline a first action plan and to coordinate this program at regular time intervals. As part of this program, working groups and other models can be added in the future. High-resolution meteorological forecasts are consistently performed by DWD and can be used in the proposed ensemble system for Germany. Emissions at national level for Germany can be provided by UBA.

The proposed air quality prediction service for Germany must be designed to provide information from different applications, for several state authorities and for large cities. At FUB, an air quality prediction system is currently under development for Berlin. The forecasting system will use LOTOS-EUROS and will be driven by DWD forecasts. This application may serve as example to support the program.

Surface observations and satellite retrieval data, used for assimilation into CTMs, can strengthen the forecast skill. It is recommended to design a satellite-based data assimilation that considers each emission source sector individually and is performed on annual, monthly and - with newer instruments - daily and hourly time frames to ensure optimum results.

Source attribution activities can provide additional information for main emission sources. TNO offers the possibility with its TOPAS system to track and calculate the most important sources for European and German cities (<https://topasdata.tno.nl>). The near-real time application for individual federal states and cities can provide even more details when the source regions and source sectors will be customized to the respective target area and the requirements of the corresponding administration.

7. Outlook and future perspectives

To warrant the huge effort when using the source attribution technique for near-real time application or even in forecast mode, the contributions must be carefully evaluated for each source sector and for all pollutants. This requires new monitoring campaigns that take into account measurements for different compounds. Apart from ground based measurements, receptor modeling studies and satellite information must be considered as independent datasets to support the evaluation. This can help to evaluate the new implementation of the labeling technique for O₃ in LOTOS-EUROS. Further, it is recommended to compare the result from this source apportionment with emission reduction simulations. Shortcomings in the emission inventories and in the model parameterization, that were observed and tackled by different groups in Germany, can easily be compared in a standardized way as part of this program.

Detailing the spatial and temporal information of emission inventories in the urban background and the use of additional sources that are not yet covered will provide a more complete picture and must be envisaged to reduce the model biases. Static time profiles are normally used as first guess for new emission sources introduced, but must be replaced by time-resolving profiles. For example, temperature-dependent time profiles for road traffic emissions can reduce the model bias for urban agglomerations in cold winter periods (e.g., [S-VELD, 2022](#)). A further subdivision of source sectors on the national scale can support the application for source attribution.

Resuspension of mineral dust from road traffic and from agriculture land management activities was identified to partly explain deficiencies in the modeling of coarse material for PM with LOTOS-EUROS. The current understanding of resuspension from both sources is still limited. The modeling of resuspension from road transport in LOTOS-EUROS is parameterized by simple emission factors and can benefit from a further differentiation of the vehicle fleet. The implementation of time-dependent recovery rates as shown by [Amato et al. \(2012\)](#) can further improve the model simulation with LOTOS-EUROS. Time-dependent soil moisture levels must be implemented to account for different weather conditions. Resuspension from agriculture land management activities must be prescribed as additional source in emission inventories. Future studies must focus on measurements of resuspended coarse material from both sources. The measurements must consider different regions, periods and the chemical compounds the coarse material is composed of. This can help to evaluate the models and to estimate emission factors.

The study identifies deficiencies in the modeling of the O₃ sensitivity to temperature with LOTOS-EUROS. Longer time frames must be examined for different regions and periods to confirm and precise the findings from this study. The ratio of NO_x and BVOC can affect the correlation of O₃ to temperature (e.g., [Otero et al., 2021](#)), but the uncertainty related to BVOC emissions is still large (e.g., [Im et al., 2015b](#)). The investigation of the precursor emissions can provide more insights and offers the opportunity to improve the process description in LOTOS-EUROS. The dynamic response to meteorology must further be assessed for other pollutants, like PM, and for separate source sectors. This can help to understand and to explain the observed non-modeled mass.

Presentation of research publications

Source attribution of nitrogen oxides across Germany: Comparing the labelling approach and brute force technique with LOTOS-EUROS

M. Thürkow¹, S. Banzhaf¹, T. Butler^{1,3}, J. Pültz¹ and M. Schaap^{1,2}

Published in Atmospheric Environment, Volume 292, January 2023, 119412, ISSN: 1352-2310, DOI: 10.1016/j.atmosenv.2022.119412, URL: <https://www.sciencedirect.com/science/article/pii/S1352231022004770>

This publication is licensed under a <https://creativecommons.org/licenses/by/4.0/>.

Contents

I.1	Introduction	51
I.2	Methodology	53
I.3	Results	58
I.4	Discussion and conclusion	71
I.5	Appendix	74

Highlights

- Two techniques for source attribution of nitrogen oxides were successfully applied.
- Upscaling the impacts of scenarios under- or overexplains the total concentrations.
- Differences between methodologies are largest for smaller emission source sectors.
- Applying the brute force technique to single sectors for NO should be avoided.

Abstract

Millions of people are exposed to enhanced levels of nitrogen dioxide in urbanized areas, leading to severe health effects. Moreover, nitrogen oxides contribute to the formation of ozone and particulate matter, and as such have wider health related impacts. A substantial reduction of nitrogen oxides may offer considerable health benefits for the human society. As a first step, this requires a detailed understanding of source sector contributions to nitrogen oxide levels. Whereas many regions have information on the local (traffic) contributions, the source contributions to the rural and urban background levels are commonly not available. In this study we compared and evaluated the results of two source attribution techniques to quantify the contribution of 5 source sectors to background nitrogen oxide levels across Germany. The results of a labelling technique were compared to brute force simulations with variable emission reduction percentages. The labelled NO₂ source contributions of the main sectors averaged for all urban background stations are road transport (45±5 %), non-road transport (24±6 %), energy & industry (20±3 %), households (10±6 %), and the remaining source sectors (1±1 %). For the brute force technique, the explained mass differs from the unperturbed baseline concentration after scaling the impact of each sensitivity simulation to 100 %. The attributed concentration of NO₂ is lower in urban background areas (-3±5 %) and larger in the rural background (4±6 %) than that of the labelling. Largest deviations up to -15 % are calculated for the major cities along the Rhine and Main. The annual average overestimation for NO is about 53±24 % for urban and 40±26 % for rural background sites based on a 20 % reduction of emissions. On shorter time scales the differences are larger. These deviations are caused by (the lack of) regime changes in the titration of ozone, most notably present at ozone-limiting conditions during nocturnal winter periods. As a consequence, the differences between the methodologies are larger for smaller emission reduction percentages applied in the brute force technique. Similarly, for small-sized emission source sectors larger deviations were found compared to large-sized sector categories. Hence, applying the brute force technique for the source attribution for a single sector should be avoided as there is no way to verify for consistency and quantify the error for the sector and total explained contribution. We recommend applying the labelling approach to estimate sector contributions in forthcoming studies for nitrogen oxides.

Keywords: *source attribution, labelling, brute force, chemistry transport model, nitrogen oxides*

Author affiliation:

¹Institute of Meteorology, Freie Universität Berlin, Carl-Heinrich-Becker-Weg 6-10, 12165, Berlin, Germany

²TNO, Department Climate Air and Sustainability, Princetonlaan 6, 3584 CB, Utrecht, the Netherlands

³IASS, Institute for Advanced Sustainability Studies, Berliner Strasse 130, 14467, Potsdam, Germany

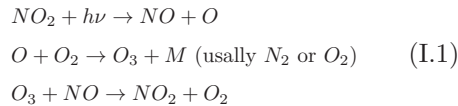
I.1 Introduction

Poor air quality is one of the key challenges of the 21st century facing the environmental community (Lim et al., 2012). Nitrogen oxides ($\text{NO}_x = \text{NO} + \text{NO}_2$) belong to the main pollutants causing a range of negative effects on human wellbeing. Numerous studies have confirmed that exposure to nitrogen dioxide (NO_2) leads to increased mortality (Raaschou-Nielsen et al., 2012; Beelen et al., 2014; Fischer et al., 2015). In Germany, exposure to NO_2 is a major health concern with an estimated annual number of 13,100 premature deaths (EEA, 2018a). In addition, nitrogen oxides contribute to the formation of ozone (O_3) and particulate matter (PM), and as such are relevant to wider health implications (Kampa and Castanas, 2008). Additionally, nitrogen oxides contribute to acidification and eutrophication of soils and water bodies and, consequently, to a loss of biodiversity in terrestrial and aquatic ecosystems (Fowler et al., 2013). Exceedances of limit values usually only occur in high populated areas near busy roads. The annual limit value of $40 \mu\text{g m}^{-3}$ for NO_2 as introduced by the European Ambient Air Quality Directive (EC, 2008) is currently exceeded by about 39 % at German traffic sites (UBA, 2019). The hourly mean limit value of $200 \mu\text{g m}^{-3}$ for NO_2 has not been exceeded in Germany recently (UBA, 2019).

Major emission sources and formation processes of nitrogen oxides are well documented. Anthropogenic emissions of nitrogen monoxide (NO) mostly form at high temperatures during (incomplete) combustion processes, such as from traffic, shipping, energy

production, or residential combustion (Vestreng et al., 2009; Granier et al., 2011). In addition, smaller emission sources derive from agricultural soils, lightning and geogenic sources (Fowler et al., 2013). In the presence of ozone, NO is oxidized to NO_2 . As such, near their sources NO emissions disturb the photochemical equilibrium of the Leighton cycle (Leighton, 1961; Finlayson-Pitts and Pitts, 2000) and cause a titration of ozone levels (Eq. I.1).

Leighton cycle:



Occasionally, an excess of fresh NO may titrate all ozone away and a build-up of NO occurs. Such events occur mostly under low ventilation conditions during winter in high emission areas such as urban centers (Leighton, 1961; Finlayson-Pitts and Pitts, 2000). In presence of ozone, NO_2 can be oxidized to nitric acid in several hours with subsequent particulate nitrate formation in presence of ammonia or sea salt (Schaap et al., 2004).

To further improve the ambient air quality it is important to know the extent to which the different anthropogenic activities contribute to the NO_2 exposure (Belis et al., 2020). Source attribution is a process of tracing pollution levels back to its origin. Increments between roadside and urban background stations and/or urban street canyon modelling are often used to quantify local contributions, with the limitation that no source attribution for the urban background is obtained (Thunis et al., 2018). Hence, a source

I. Source attribution of nitrogen oxides across Germany: Comparing the labelling approach and brute force technique with LOTOS-EUROS

attribution of background levels is commonly not available for city, municipal and state authorities. Rural and urban background levels can be assessed using chemical transport model (CTM) simulations, which are applied in an increasing number of studies (SenStadt, 2019; UBA, 2019). When applying CTMs for source attribution two main methods can be considered: (1) source apportionment approaches, also known as the labelling (Kranenburg et al., 2013) or tagging technique (Wagstrom et al., 2008; Wang et al., 2009; Butler et al., 2018), based on the calculation of a mass concentration and (2) brute force algorithms which are based on sensitivity simulations perturbing the emission input data (Clappier et al., 2017; Thunis et al., 2019). As both methods differ intrinsically, their target quantities can be distinguished as contributions (labelling) and impacts (brute force) (Clappier et al., 2017). Numerous studies assessed the source attribution for particulate matter or ozone, either applying the labelling approach (Hendriks et al., 2013; Schaap et al., 2013; Curier et al., 2014; Banzhaf et al., 2015; Timmermans et al., 2017; Lupaşcu and Butler, 2019; Timmermans et al., 2020) or the brute force technique (Amann et al., 2011; Dingenen et al., 2018; Huang et al., 2018; Thunis et al., 2018). Although the application of the labelling technique to nitrogen oxides has implicitly been performed in these studies, they have hardly been the main focus and comparing the labelling and brute force techniques has received little attention.

Several studies indicate that the brute force technique tends to fail for the determination of contributions (Kwok et al., 2015), which can be related to indirect effects such as oxidant-

limited reaction processes (Koo et al., 2009). In case of non-linear relations, the estimated total impact from sensitivity simulations may not correspond to the total mass concentration of the base simulation (Koo et al., 2009). Large inconsistencies have been reported for ozone by e.g. Mertens et al. (2018), who showed that ozone source attribution using a perturbation approach could differ by up to a factor of 4 compared with a tagging approach. Butler et al. (2020) combined both perturbation and tagging approaches for ozone to show that the ozone production efficiency of precursors from unperturbed emission sectors increased to partially compensate for reduced emissions of ozone precursors by a given sector. In case of nitrogen oxides, non-linear behavior can be expected with respect to photochemistry and ozone titration effects (Leighton, 1961; Finlayson-Pitts and Pitts, 2000), which are highly sensitive to meteorological conditions (Munir, 2016). Hence, as there is no standardized method and/or definition available on how to conduct source attribution studies for background nitrogen oxide levels, we aim to compare the results of the labelling and brute force approach in this study.

This study aims to answer the following research questions: (1) To what extent are contributions by the brute force technique and the labelling approach comparable to each other for the source attribution of nitrogen oxides? (2) Does the application of sensitivity simulations reveal non-linear impacts in the concentration with respect to varying nitrogen oxide emission reduction levels? (3) Up to what application range are sensitivity simulations suitable to determine contri-

butions for nitrogen oxide source attribution purposes? To answer these research questions, we conducted a source attribution study for Germany by performing air pollution simulations using the LOTOS-EUROS CTM for January 1st to December 31st, 2018. In [Section I.2](#) we describe the labelling and brute force approach taken in this study as well as the approach for comparison. In [Section I.3](#) the results are provided in terms of distributions and station typology across Germany. Finally, the results are discussed and put in broader perspective in [Section I.4](#).

I.2 Methodology

Below, we first provide a description of the LOTOS-EUROS CTM and the model set-up. Next, we introduce the labelling and brute force concepts, which have been applied to evaluate their ability for source attribution purposes of nitrogen oxides. The last subsection details the methodology used to evaluate the differences between the methods.

I.2.1 Chemical transport modelling

For this study, the LOTOS-EUROS chemical transport model (CTM) version 2.2 was employed. The model has a long application history in Europe ([Manders et al., 2017](#)) and is part of the regional ensemble of the Copernicus Atmospheric Monitoring Service (CAMS). Within CAMS the model is applied operationally to provide air quality forecasts and analyses for the European region ([Marécal et al., 2015](#)), including particulate matter source attribution information using

a labelling approach ([Pommier et al., 2020](#)). Air quality simulations with the LOTOS-EUROS CTM are performed on an Eulerian grid of variable resolution in the horizontal and terrain following coordinates in the vertical ([Manders et al., 2017](#)), with horizontal advected air pollutants calculated according to a monotonic advection scheme developed by [Walcek \(2000\)](#). The gas-phase chemistry is described by the TNO CBM-IV scheme, a modified implementation based on the scheme by [Whitten et al. \(1980\)](#). Aerosol chemistry related processes are handled by the thermodynamic equilibrium module ISORROPIA-II ([Fountoukis and Nenes, 2007](#)), while the cloud chemistry sulfate formation is explicitly treated according to the algorithm developed by [Banzhaf et al. \(2012\)](#). To handle dry deposition within gas phase, the DEPAC module (DEPosition of Acidifying Compounds) is applied ([Van Zanten et al., 2010](#); [Kruit et al., 2012](#)), with the derivation of particles following the scheme of [Zhang et al. \(2001\)](#). The wet deposition is solved as described in the study of [Banzhaf et al. \(2012\)](#). More detailed information with full process descriptions and implementation examples of the LOTOS-EUROS CTM, are provided by [Manders et al. \(2017\)](#) and references therein.

The model simulations, covering Europe and the target area of Germany, were conducted by applying a one-way nesting approach ([Figure I.1](#)). The outer domain with a horizontal grid resolution of 0.5° longitude to 0.25° latitude ($\sim 28 \times 32 \text{ km}^2$) was used to encompass the impacts of long-range transport on air quality in Germany and extends from 22°W - 44°E to 31°N - 69°N . The inner domain (0.125° longitude \times 0.0625° latitude,

I. Source attribution of nitrogen oxides across Germany: Comparing the labelling approach and brute force technique with LOTOS-EUROS

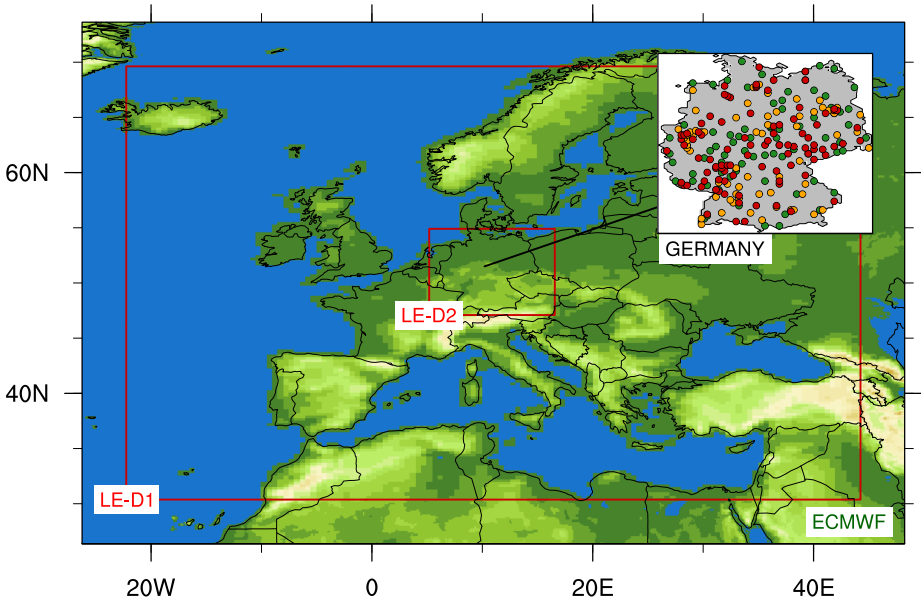


Figure I.1: Domain configuration of the model area. Two zooming domains are used for the LOTOS-EUROS CTM simulations (red). Meteorological input data are provided by the ECMWF model (green). The investigation area of Germany is highlighted on the right-hand side with dots indicating the German monitoring sites (urban background: red, sub-urban background: orange and rural background: green).

$\sim 7 \times 8 \text{ km}^2$) focuses on Germany, and covers parts of the neighboring countries, e.g. the Netherlands, Belgium, Luxembourg, and Poland. To determine the vertical layering of the model system, we used a dynamic mixed layer approach (Manders et al., 2017). Following the operational set-up of the LOTOS-EUROS, meteorological input data of the IFS (Integrated Forecasting System) is provided by the ECMWF (Flemming et al., 2009). We performed model simulations for the period of January 1st to December 31st, 2018, plus one month of spin-up time.

For Germany, the official reported anthropogenic emission inventory, gridded using the GRETA (Gridding Emission Tool for ArcGIS, Schneider et al. (2016)) system, was applied. The CAMS emissions developed

by the TNO for 2015 (CAMS-RWC-SNAP78_2015), were taken for the rest of Europe. Time profiles for individual source sectors represent the temporal variation, which break down the annual emission totals based on monthly, daily, and hourly scaling factors. Temporal variability for residential combustion emissions was considered using a heating degree days approach to allow for different heating demands depending on meteorological conditions following Mues et al. (2014). Except for road transport, we used 97 % for NO and 3 % for NO₂ for the direct emissions. For road transport the direct NO₂ emission percentage was set to 20 %, which is in agreement with recent studies (Kimbrough et al., 2017; Richmond-Bryant et al., 2017). Information on wild fire emissions were taken from

the CAMS fire product (Kaiser et al., 2012). C-IFS (Integrated Forecasting System including Chemistry, Marécal et al. (2015)) distributions were used as input for chemical boundary conditions for the European domain.

1.2.2 Simulation strategy for source attribution

The LOTOS-EUROS CTM contains a labelling module for source attribution, to determine the origin of particulate matter compounds and their related precursors (Kranenburg et al., 2013). A pre-defined number of emission sectors or regions can be given a label which are traced during the model simulation of the LOTOS-EUROS CTM. Through the preserved atoms (C, S and reduced and oxidized N) the contributions of the separate sources are tracked for chemically active tracers. In addition to the determination of the concentration change, the contribution of each labelled category to each tracer is tracked in each process description. The categories can be configured flexibly, for instance by regions, sectors, or combinations thereof. For a detailed description of the source attribution used in the LOTOS-EUROS CTM we refer to Kranenburg et al. (2013). Applications to particulate matter and its precursor can be found in previous studies (Schaap et al., 2013; Curier et al., 2014; Banzhaf et al., 2015; Hendriks et al., 2016; Timmermans et al., 2017). In this study we focus on the source attribution of background concentrations of nitrogen oxides in terms of source sectors. To compare the source attribution methodologies, we used a limited set of 5 labels including the 4 main source sectors and the remaining other sectors combined.

Table I.1 contains detailed information on the available emission sources and the associated labels used in this study. The labelling system requires to label all sources of nitrogen oxides within the domain and therefore the contribution of natural sources and boundary conditions were tracked as well.

An alternative method used for deriving source attribution information is provided by the brute force technique. We make use of the terminology of contributions and potential impacts $PI_{S,X}$ as introduced by Thunis et al. (2020) to distinguish between the applied methods for source attribution. The brute force technique determines the impact $I_{S,X}$ of a emission reduction in source sector S in comparison to a baseline concentration ($I_{S,X} = \Delta C_{S,X} = C_{S,X} - C_{REF}$). When using a brute force approach, the selected emission source sectors and/or regions are reduced by a percentage X. Using a linearity assumption, the impact is converted into the potential impact $PI_{S,X}$, by scaling it to 100 % by applying the multiplication factor $100/X$ (Eq. I.2). In this study we applied the brute force technique to NO_X emissions using 8 reduction percentages ranging from $X = 5, \dots, 100$ % (hereafter indicated as RED_5, \dots, RED_{100}). All reduction percentages were applied to each of the 5 source categories to investigate the sensitivity to the size of the emission reduction applied (Table I.2). Furthermore, a set of sensitivity simulations were performed, in which emissions of all source sectors were reduced simultaneously to investigate additivity. We will use the term combined simulations when further referring to these scenarios ($COMB_5, \dots, COMB_{100}$). Sensitivity simulations with individually reduced emission sectors are just referred

I. Source attribution of nitrogen oxides across Germany: Comparing the labelling approach and brute force technique with LOTOS-EUROS

Table I.1: Source categories considered in this study.

Source Category	Source Composition
Road Transport	Gasoline, diesel, and LPG/gas powered light and heavy-duty vehicles, motorcycles, mopeds.
Non-Road Transport	Mobile sources excluding road-traffic such as aviation, rail, shipping, inland waterways and mobile machinery from agriculture and manufacturing industries.
Energy & Industries	Power plants for coal, liquid fuels, gas or solid biomass and associated combustion processes. Combustion in the industrial sector covering the production of iron and steel, pulp and paper or cement manufacturing as well as the chemical industry.
Households	Combustion processes of coal, gas, solid biomass, and liquid fuels of private households and small businesses.
Others	All other source sectors are combined into this category i.e., production processes for coal, oil, gas and flaring and emissions from the agricultural sector.

Table I.2: Overview of performed model simulations.

	Description of model set-up
BASE	Reference simulation without emission reduction and source attribution to compare with sensitivity simulations.
LA	Source attribution with labelled source sectors defined in Table I.1 applying the labelling approach.
RED _X	Emission sensitivity simulations performed individually for each source category (Table I.1) according to the specific reduction level (X = 5, 10, 20, 25, 35, 50, 75, 100 %) for NO _X .
COMB _X	Emission sensitivity simulations performed for all source categories simultaneously (Table I.1) according to the specific reduction level (X = 5, 10, 20, 25, 35, 50, 75, 100 %) for NO _X .

to as sector reduction simulations. All in all, the number of annual simulations totals 49 on both domains: the baseline, 40 RED_X and 8 COMB_X simulations.

Potential Impact:

$$PI_{S,X} = I_{S,X} * \frac{100}{X} \quad (I.2)$$

I.2.3 Metrics to evaluate the source attribution

To evaluate the source attribution for nitrogen oxides (NO₂, NO and NO_X), the labelled contributions and potential impacts were compared to each other by quantifying absolute and relative differences. NO_X concentrations are provided in the mass equivalent of NO₂. In addition, a linear regression model is used to compare the labelled contributions with potential impacts for each individual source sector. As statisti-

cal indicator, we calculated the root mean squared error (RMSE, Eq. I.3). Besides the evaluation of spatial distributions, the modelling results were sampled for the background sites of the German monitoring network (UBA; www.uba.de). We chose to select the monitoring sites with a 99 % data availability. In total, 235 observation sites were included (Figure I.1). All monitoring sites were further clustered into their sub-categories of urban- (94), suburban- (66) and rural-background (75) stations. The site classification is used as an indicator to discriminate between more and less polluted areas in Germany. Observations at traffic and industrial locations were neglected as we are focusing on the background concentrations and as the resolution of chemistry transport models are not representative for conditions close to large sources.

To allow for a deeper insight and to diagnose the behavior of the brute force methodology, we deduce the degree of the non-linearity using the sensitivity simulations as suggested by Thunis et al. (2019). For non-linear systems a 10 % emission reduction may yield a smaller or larger relative impact in the pollutant concentration. Moreover, a subsequent 10 % reduction may not have the same impact as the first 10 % reduction. Hence, the potential impacts for a sector may vary with the emission reduction percentage applied. In a linear regime they would be equal. Furthermore, the sum of the potential impacts of all sectors may not correspond to the modelled concentration in the baseline simulation. A proportionality analysis has been carried out to assess the degree of non-linearity in the responses to the emission reductions. Here, we defined an indicator

based on the ratio between the impact $I_{S,X}$ / potential impact $PI_{S,X}$ of a given reduction level X (RED_X) and the impact $I_{S,20}$ / potential impact $PI_{S,20}$ of the 20 % reduction scenario (RED_{20}), hereafter referred to as the consistency ratio for impacts $CR_{I_{S,X}}$ and potential impacts $CR_{PI_{S,X}}$ (Eq. I.4). By this, differences between individual reduction levels for impacts and potential impacts are highlighted. To illustrate, in an ideal case, the consistency ratio for the impact ($CR_{I_{S,X}}$) of a linear/proportional relation would result in $CR_{I_{S,X}} = X/20$. The consistency ratio for potential impacts (CRPI) would be equal to 1 for each reduction level. We decided to define a 20 % reduction level to be used as reference criterion here, to be in line with the EMEP (European Monitoring and Evaluation Programme) and SHERPA (Screening for High Emission Reduction Potentials on Air quality) approach where 15 % and 20 % emission scenarios are applied, respectively. Applying the consistency ratio one can easily indicate the linear response to different emission reductions. With a proportional behavior, a linear regime can be assumed, and the impacts would be scalable. When the response to the emission reduction would be lower/larger than X, the consistency ratio would yield in a less/ more than proportional reduction with respect to the emission reduction of X and one cannot perform a linear scaling of the impacts.

In addition, we determined the additivity to provide further evidence of non-linear responses (Thunis et al., 2019). The concentration derived by accumulating all potential impacts $PI_{S,X}$ of the sector reduction simulations for a given reduction level X we refer to as the Sector Explained Mass SEM_X (Eq.

I. Source attribution of nitrogen oxides across Germany: Comparing the labelling approach and brute force technique with LOTOS-EUROS

I.5). The potential impact derived from the combined simulations (COMB_X) are referred to as the Combined Explained Mass CEM_X. By comparing the SEM_X and the CEM_X you proof additivity. Additivity is assured when the SEM_X equals the CEM_X. Inconsistencies that become present in this context are defined as lack of additivity. In that case, the Sector Explained Mass will not reflect the total mass of the baseline simulation (Thunis et al., 2020). We also introduced the acronym of the Labelled Explained Mass LEM, which is defined as the accumulated sum of all source sector contributions derived by the labelling simulation. The LEM is used when comparing the results side-by-side with respect to the SEM_X.

Root Mean Squared Error:

$$RMSE_{S,X} = \sqrt{\frac{1}{N} \sum_{i=1}^n (PI_{S,X} - LA_S)^2} \quad (I.3)$$

Consistency Ratio for Impact and Potential Impact:

$$CRI_{S,X} = \frac{I_{S,X}}{I_{S,20}}; CRPI_{S,X} = \frac{PI_{S,X}}{PI_{S,20}} \quad (I.4)$$

Sector Explained Mass:

$$SEM_X = \sum_S PI_X \quad (I.5)$$

I.3 Results

I.3.1 Source attribution using the labelling approach

In this section, we present the sectoral source attribution of background concentrations for nitrogen oxides across Germany obtained using the labelling approach. In Germany,

the largest emissions and associated concentrations for nitrogen oxides are found in major transportation corridors, industrialized areas (e.g. the Ruhr region) and urbanized agglomerations (e.g. Berlin, Munich, Hamburg) as shown in Figure I.2 & Figure I.4. Annual mean (urban) background concentration above $20 \mu\text{g m}^{-3}$ are only modelled for these large cities. Under normal conditions, the emitted NO is readily converted to NO₂ explaining that most of the NO_X is present in the form of NO₂. For the buildup of NO first all ozone needs to be reacted away. Hence, the enhanced levels of NO are more clearly related to the areas with the largest emissions of nitrogen oxides i.e. the largest cities and transport corridors.

The concentration patterns for NO₂ can be further explained using the source attribution as provided in Figure I.2. The largest absolute and relative shares for road transport are modelled in the urban background of cities and along the highway network. The larger relative share in rural background in southern Germany as compared to northern Germany is explained by the absence of large emissions from industry and other transportation modes. The non-road transport contributions maximize in the Rhine Valley, the coastal regions and around the Kiel-Hamburg channel and are mainly explained by shipping emissions. Agricultural emissions (incorporated in others) contribute most to the total concentration in rural areas in northern Germany and near to the German Alps. Also, the relative contribution of households shows a striking gradient between northern and southern Germany. This can be explained with the spatial allocation for emissions

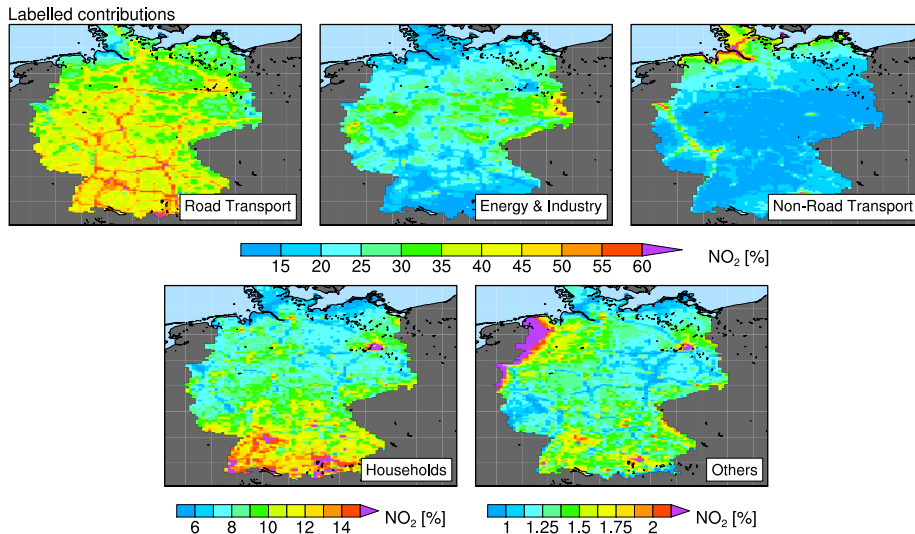


Figure I.2: Source attribution by the labelling approach (LA) across Germany for January to December 2018 shown as yearly average. Contributions of NO_2 are shown as relative share with respect to the absolute baseline concentration.

across Germany. The accessibility to wood and number of (wood) stoves in southern parts of the country is larger than in the north. The larger emission density causes the north/ south gradient. Although the absolute contribution of the industry and energy sector is largest in the Ruhr area, the relative contribution from this sector is notably larger in central and especially eastern Germany. The latter is explained by a number of larger power plants and industrial sites in this sparsely populated region.

In Figure I.3 the time series of modelled daily mean background concentrations and their sector contributions for 2018 are shown for NO_x , NO_2 and NO . The time series represent the average across all rural, suburban, and urban background observation sites (depicted in Figure I.1) and show a seasonal cycle with larger concentrations in winter than in summer due to less favorable

mixing conditions and larger anthropogenic emissions in winter. The amplitude of the seasonal variability is largest for nitrogen monoxide, as a buildup of NO occurs normally under conditions with shallow boundary layers, stagnant weather, and low background ozone levels.

As expected, the largest contributions are calculated for road transport followed by non-road transport, energy & industry, households, and the smallest contribution for other emission source sectors (Figure I.3). For Figure I.3 and all statistics presented below the average across all background observation sites distinguishing their station type was used. In the urban background, relative contributions from road transport (URBG: 45 ± 5 %, RUBG: 42 ± 5 %) and households (URBG: 10 ± 6 %, RUBG: 9 ± 5 %) are on average slightly larger compared to those in rural background areas, while

I. Source attribution of nitrogen oxides across Germany: Comparing the labelling approach and brute force technique with LOTOS-EUROS

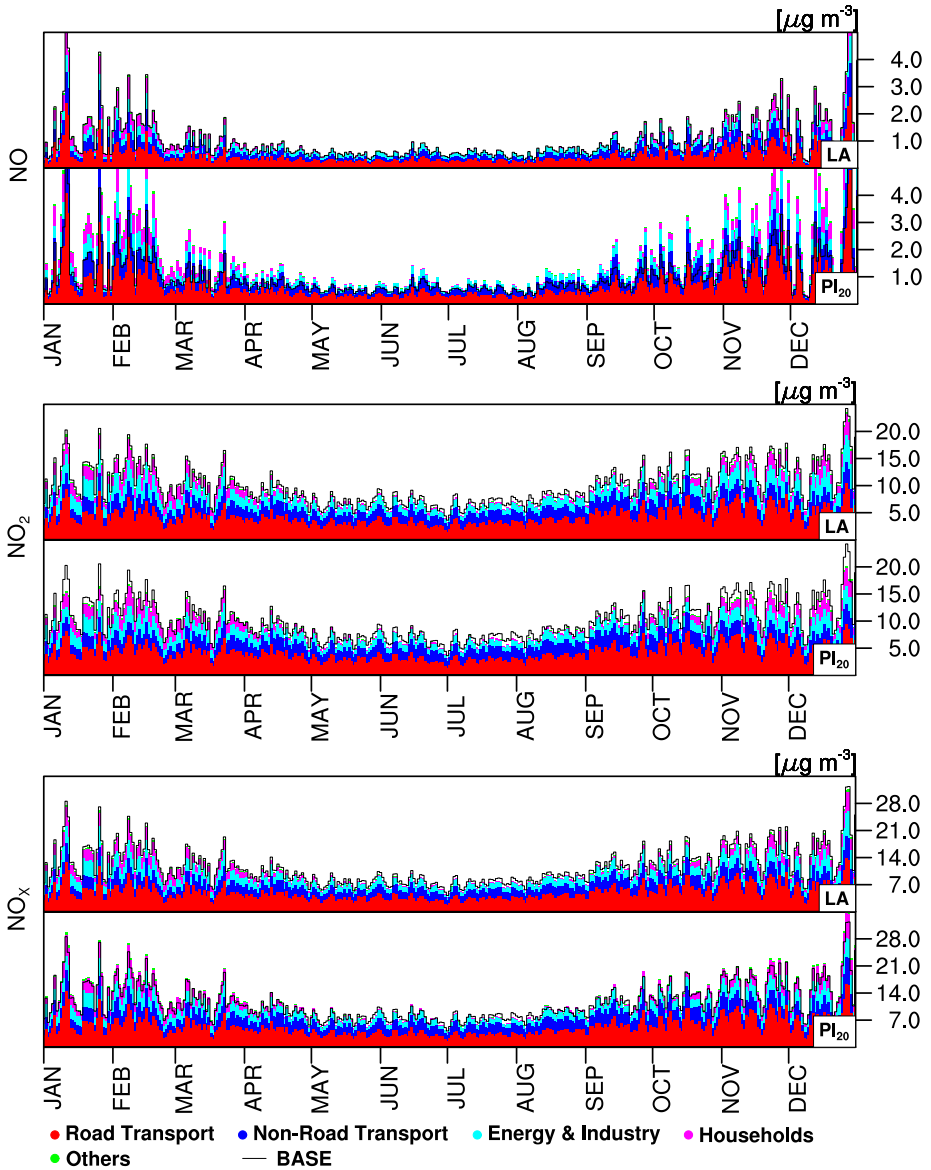


Figure I.3: Labelled contributions (LA) and potential impacts of a 20 % NO_x reduction (PI₂₀) across Germany for January to December 2018 shown as daily average. Contributions and potential impacts of NO (top), NO₂ (center) and NO_x (bottom) have been averaged over space across all German observation types.

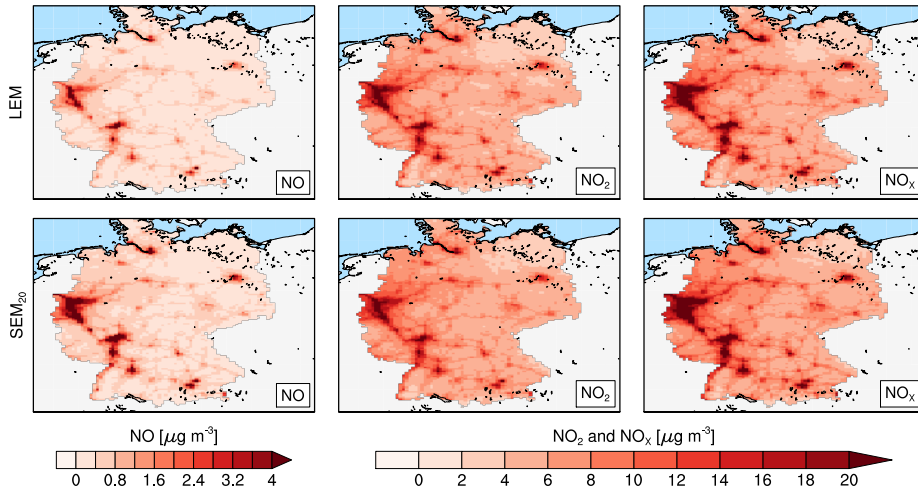


Figure I.4: Mass concentration of the Labelled Explained Mass (LEM, top) and Sector Explained Mass for the NO_x reduction level of 20 % (SEM₂₀, bottom). From left to right: NO, NO₂ and NO_x.

in rural background areas contributions from energy & industrial sources (URBG: $20\pm 3\%$, RUBG: $23\pm 4\%$) and non-road transport (URBG: $24\pm 6\%$, RUBG: $25\pm 7\%$) are slightly more pronounced (Figure I.2 & see Table I.5). Contributions from households (DJF: $16\pm 4\%$, JJA: $4\pm 1\%$) as well as of energy & industry (DJF: $24\pm 3\%$, JJA: $19\pm 2\%$) show maximum values in winter, which can be related to additional energy demand and subsequent combustion emissions during the heating period (Figure I.3 & see Table I.5).

I.3.2 Comparison of the 5-sector total attributed background concentration

We illustrate the behavior of source attribution results from the brute force simulations using the RED₂₀ scenarios. Figure I.4 shows the spatial distribution of the summed potential impact of all five sectors, the SEM₂₀, in comparison to the

labelling result. The absolute and relative differences in the annual average are shown in Figure I.5. The SEM₂₀ for NO shows large systematic deviations to the labelled source attribution results. The attributed total NO background concentration is tens of percent larger than with the labelling, showing largest deviations in the source regions. Both absolute and relative differences increase with shorter distance to the urban background. On annual average, the overestimation is about $53\pm 24\%$ for urban and $40\pm 26\%$ for rural background sites, respectively (see Table I.6). Note that the attributed SEM₂₀ also largely overestimates the station averaged total modelled NO background concentration of the baseline by about $46\pm 25\%$ (see Table I.6). Relative deviations for NO₂ and NO_x are considerably smaller than for NO (see Table I.7 & Table I.8). The SEM₂₀ of NO₂ is lower than attributed concentrations of the labelling in urban background areas

I. Source attribution of nitrogen oxides across Germany: Comparing the labelling approach and brute force technique with LOTOS-EUROS

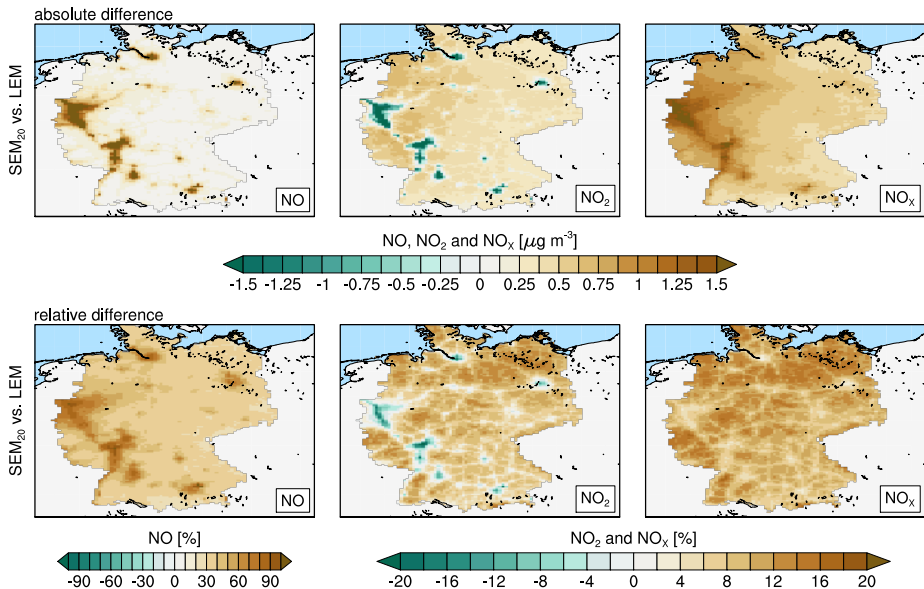


Figure I.5: Absolute (top) and relative (bottom) differences between Sector Explained Mass for NO_X reduction level of 20 % (SEM₂₀) and the Labelled Explained Mass (LEM). From left to right: NO, NO₂ and NO_X.

(-3 ± 5 %), with largest deviations in the cities along the Rhine and Main. In the rural background the difference changes sign systematic, indicating that the SEM₂₀ attributes a (4 ± 6 %) larger concentration than the labelling approach. For NO_X the differences are positive everywhere, with up to 6 ± 5 % on station average. In the urban background, the relative difference is closer to zero which was expected as NO_X is not as sensitive to the titration regimes as its constituents (see Table I.8).

In Figure I.6 the time series for the SEM₂₀ minus the LEM are provided, showing the average across all background observation sites. The levels of the station average themselves for the SEM₂₀ and LEM can be read from Figure I.3. Inspection of the daily time series learns that the SEM₂₀ for NO is equal or (substantially) larger than the LEM throughout the year.

For monthly values, averaged over all station locations, the SEM₂₀ overestimates the NO concentration up to 75 ± 18 % (see Table I.7). Deviations between the techniques are more prevalent in winter (DJF: 69 ± 26 %) than during the summer season (JJA: 31 ± 16 %). In contrast, the SEM₂₀ of NO₂ can be larger or smaller throughout the year compared to the labelling. The underestimation occurs during periods with stagnation and thus the highest NO₂ levels (see explanation and example below). As mentioned above, the results for NO_X show mostly an overestimation in comparison to the labelling results. The absolute differences follow the seasonal cycle of NO_X itself. Note that on average urban background stations show larger deviations than rural ones for all compounds (see Table I.5 to Table I.8).

The different behavior for NO and

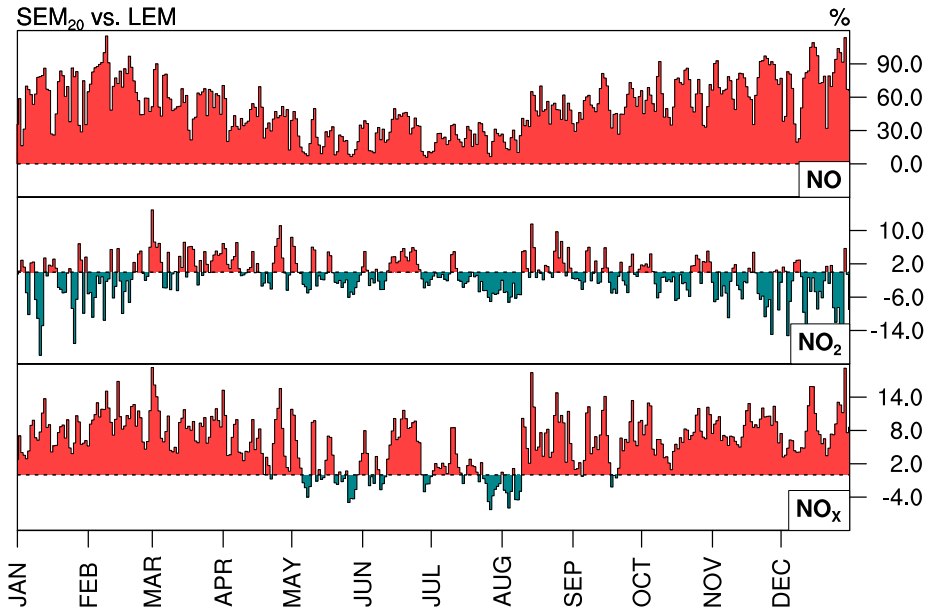


Figure I.6: Sector Explained Mass from NO_x reduction level 20 % (SEM₂₀) minus the Labelled Explained Mass (LEM) across Germany for January to December 2018. The mass concentrations of NO (top), NO₂ (center) and NO_x (bottom) have been averaged over all German background observation sites (rural, sub-urban, and urban).

NO₂ concerning the deviations between SEM and LEM can be explained by the occurrence of ozone limiting titration conditions (Figure I.7). The oxidation of NO is normally not limited during daytime. However, the ground level ozone background concentration decreases fast during stable conditions occurring when fresh NO titrates the ozone. When the ozone is fully removed, NO₂ levels will only increase further by primary NO₂, whereas NO starts to build up due to continuing emissions. In Figure I.7 this process is illustrated for four days in January 2018. During the first hours of two days of stagnant conditions (see the planetary boundary layer height in Figure I.7) the ozone is titrated away, after which a build-up of both NO and NO₂ occurs. For NO the background

concentrations increase from near zero to exceed those of NO₂ with concentrations above 100 $\mu\text{g m}^{-3}$ in the peak at the 11th. After the weather changes the situation turns back to instable, mixed conditions with near-zero NO levels. This feature occurs frequently in winter when a limited amount of ozone is available caused by lower photochemical production of ozone and shallow boundary layers. A too large SEM₂₀ with respect to the LEM and baseline for NO simply occurs as for each sensitivity simulation it has been assumed to start from 100 % emissions in the brute force approach. When the system stays in the regime with zero ozone the reduction in NO₂ is limited to the direct emission. In contrast, the NO levels are lowered more than proportional to the NO_x emission

I. Source attribution of nitrogen oxides across Germany: Comparing the labelling approach and brute force technique with LOTOS-EUROS

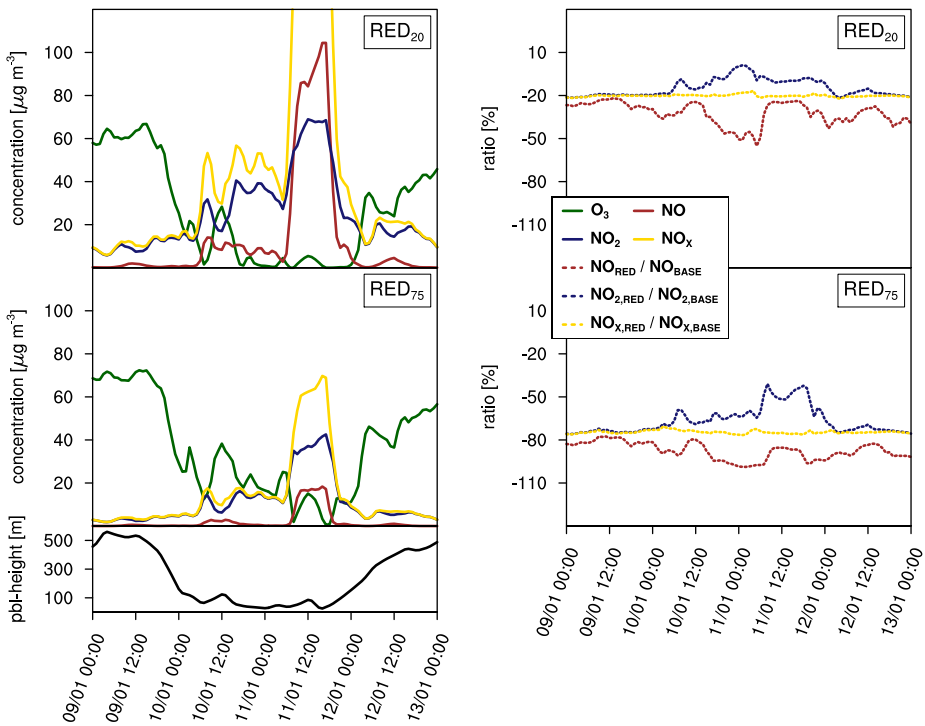


Figure I.7: Relation for NO, NO₂, NO_x and O₃ indicated for an urban background site in Berlin (capital of Germany) for 4 winter days in 2018.

change (Figure I.7). Starting from the baseline for each reduction simulation means that this non-proportionality effect is incorporated in each individual brute force reduction simulation. With smaller NO_x emission reductions, the likelihood of leaving the range where all ozone is completely titrated away is much smaller than for large emission reductions. Hence, the SEM_x for NO will be larger when smaller reduction percentages are applied. During these conditions the reasoning for NO₂ is the other way around, whereas NO_x in the source regions responds consistently with the emission reduction.

A further effect when applying reduction simulations is related to the lifetime of NO_x. In the presence of

NO during the night, the oxidation pathways of NO₂ to nitric acid do not take place. As it takes longer to titrate all ozone away with lowered NO_x emissions, the duration in which this ozone limiting conditions are present is reduced in the reduction simulations. Hence, this allows ozone to oxidize NO₂ through heterogeneous chemistry and thus the lifetime of the NO₂ and NO_x can be slightly reduced. This effect is more important in the less polluted regions and leads to lower transport from source regions to more remote areas and thus a sign change for NO₂ in the rural areas.

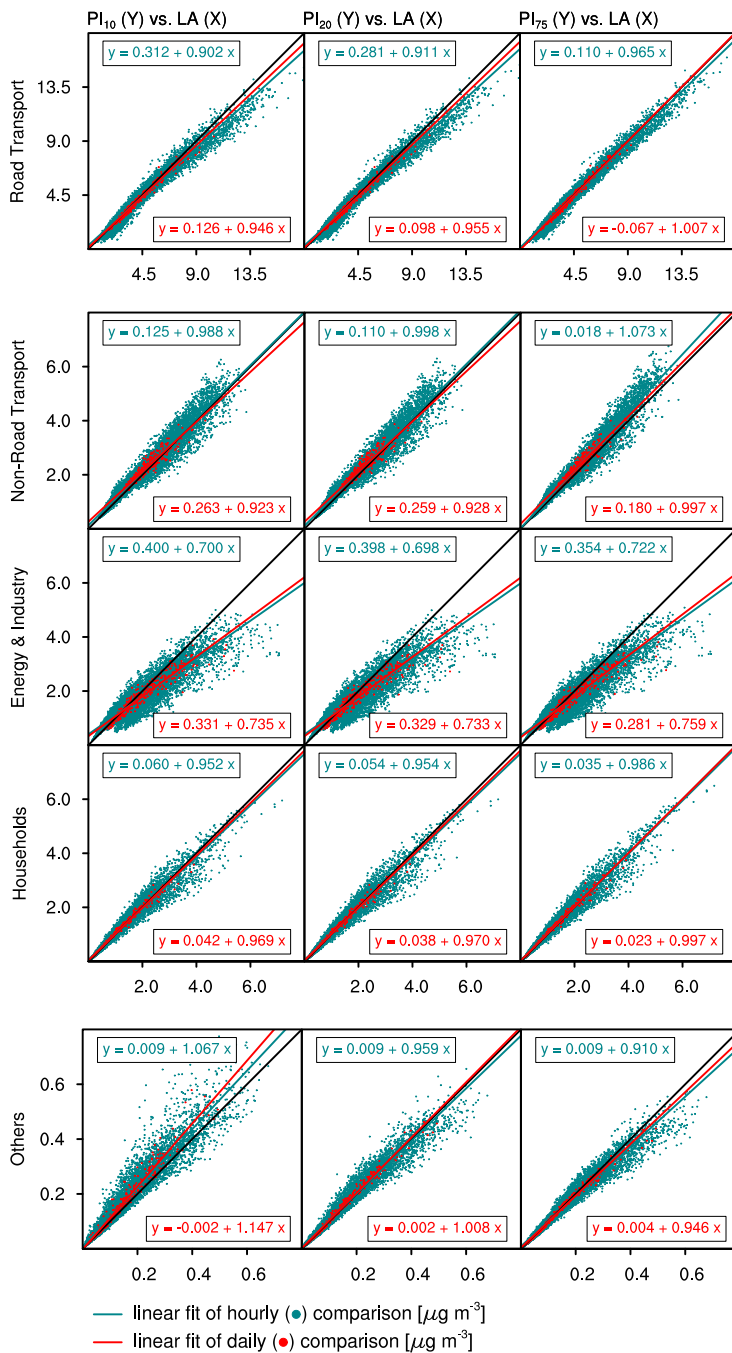


Figure I.8: Differences of potential impacts from NO_x reduction levels 10, 20, and 75 % (PI₁₀, PI₂₀, and PI₇₅; y-axis) compared to labelled contributions (LA; x-axis) across Germany for January to December 2018. The mass concentration of NO₂ has been averaged over space.

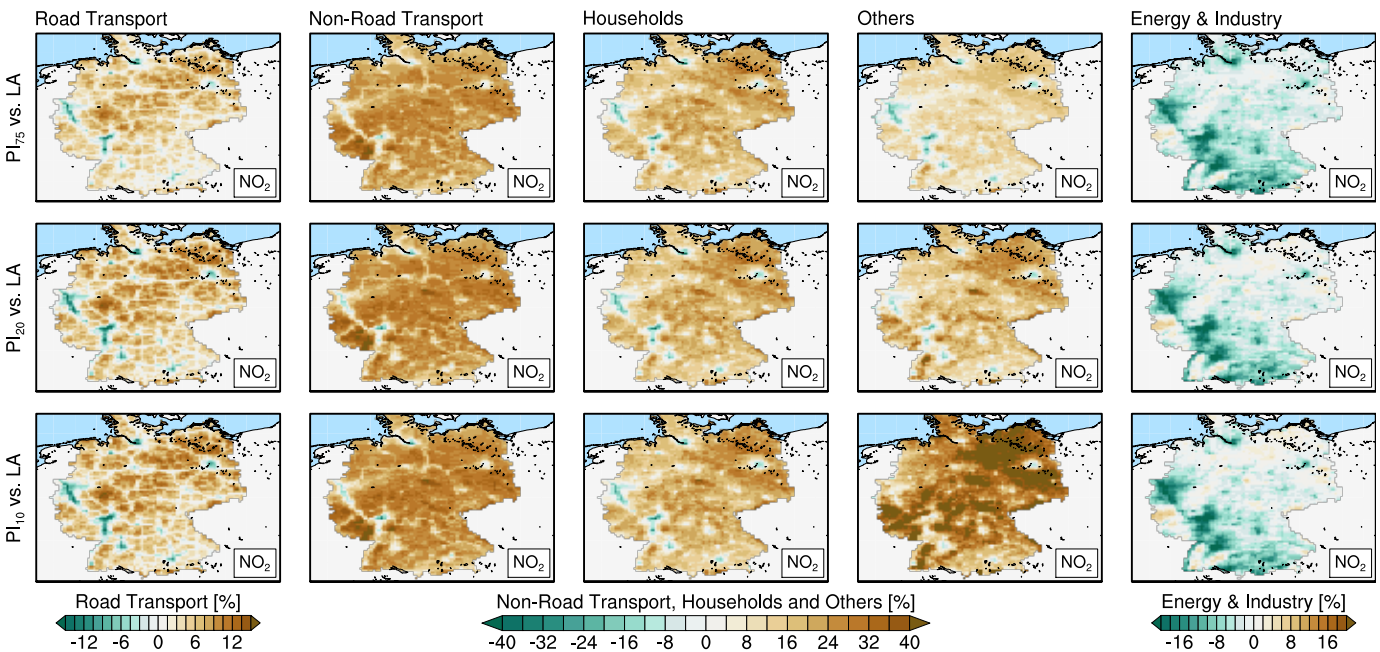


Figure I.9: Same as in Figure I.8 with relative differences and averaged in time.

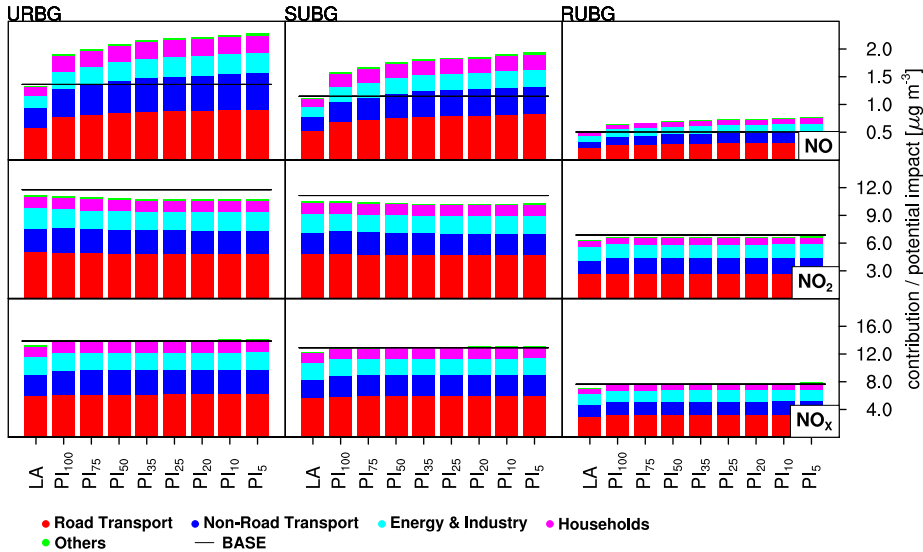


Figure I.10: Labelled contributions (LA) and potential impacts of NO_x reduction levels from 5 to 100 % (PI_5 , ..., PI_{100}) across Germany for January to December 2018. Three station types have been investigated and are presented from left to right (urban background: URBG, sub-urban background: SUBG, and rural background: RUBG). The mass concentration of NO (top), NO_2 (center) and NO_x (bottom) have been averaged over time and space.

I.3.3 Comparison of contributions and potential impacts for source sectors

In this section we compare the attribution to the individual sectors and add the dependency of the reduction percentage applied. Although the annual and monthly average share of NO_2 across the country is in close agreement for both methodologies (see Table I.5 & Table I.9), the deviations show spatial and temporal variability. Figure I.8 compares daily and hourly averages of potential impacts (PI_X) with labelled contributions (LA) for all source sectors and for reduction fractions of $X = 10, 20$ and 75% using a regression analysis for NO_2 . From the comparison one sees that differences between potential impacts and labelled contri-

butions are smaller for daily averaged values compared to hourly estimates. All source sectors show lower RMSE's for daily averaged values, when comparing the potential impacts with the labelled contributions. For example, the RMSE for road transport on an hourly basis is 0.52 compared to 0.24 on a daily basis for the 20 % reduction scenario (see Table I.4). Moreover, we notice a closer agreement between potential impacts and labelled contributions for the largest source sectors.

The spatial distribution for potential impacts and labelled contributions is compared in Figure I.9 using annual averages. In Figure I.9 the same source sectors and reduction levels are shown as used in Figure I.8. For road transport (URBG: $44 \pm 5\%$, RUBG: $40 \pm 5\%$), non-road transport (URBG: $25 \pm 7\%$, RUBG: $28 \pm 8\%$), households

I. Source attribution of nitrogen oxides across Germany: Comparing the labelling approach and brute force technique with LOTOS-EUROS

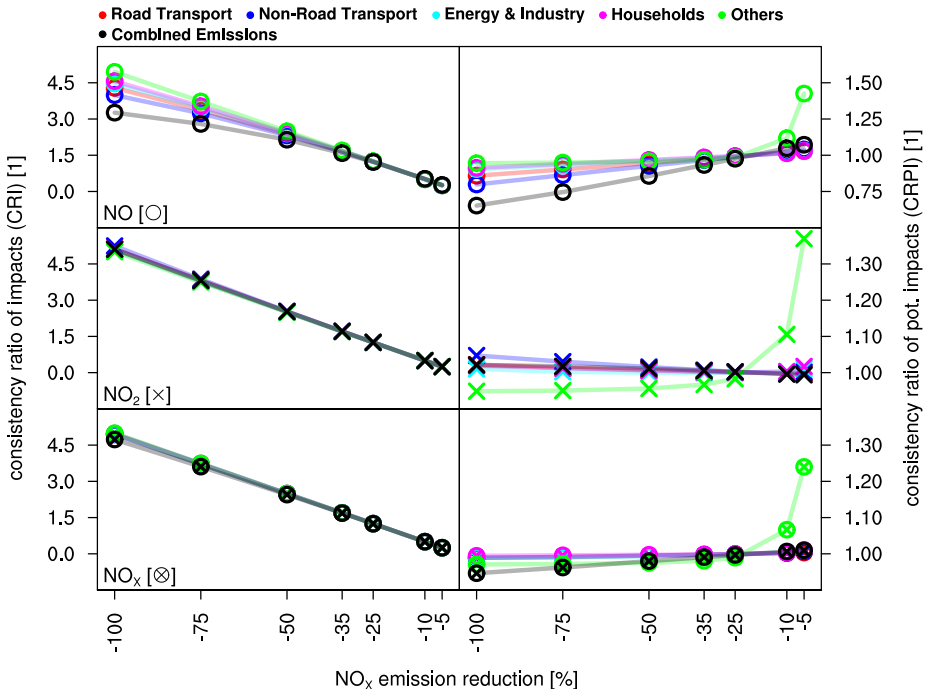


Figure I.11: Consistency ratios for impacts (left) and potential impacts (right) for NO (top), NO₂ (mid) and NO_x (bottom). Sector and combined reduction simulations for 5 to 100 % are divided by different colors.

(URBG: 10 ± 6 %, RUBG: 9 ± 6 %), and the remaining sources (URBG/ RUBG: 1 ± 1 %) the patterns follow the picture described for the SEM₂₀ above, with almost lower/ larger potential impacts in urban/ rural background areas compared to labelled contributions for NO₂ (see Table I.5 & Table I.9). The relative difference for non-road transport is larger as a large fraction of the emissions is emitted during nighttime in comparison to the other sectors. The sector with a deviating behavior is the energy & industry sector (URBG: 18 ± 3 %, RUBG: 22 ± 4 %). Overall differences for small reduction fractions become larger for road transport, non-road transport and households, whereas differences for energy

& industry increases with larger reduction fraction (Figure I.8 and Figure I.9). The different behavior of the power sector is attributed to the impact on ozone above the surface layer. This can be explained with contrasting interactions when emitting from the ground level or from high-stack sources. Emission reductions may enhance the ozone above the urban and industrialized areas which induces a small compensation effect through conversion of NO to NO₂ from the other sources when mixed towards the ground.

Figure I.10 summarizes mentioned above findings for annual mean potential impacts (PI_X) for all reduction levels as function of station categories and indicates that deviations between the

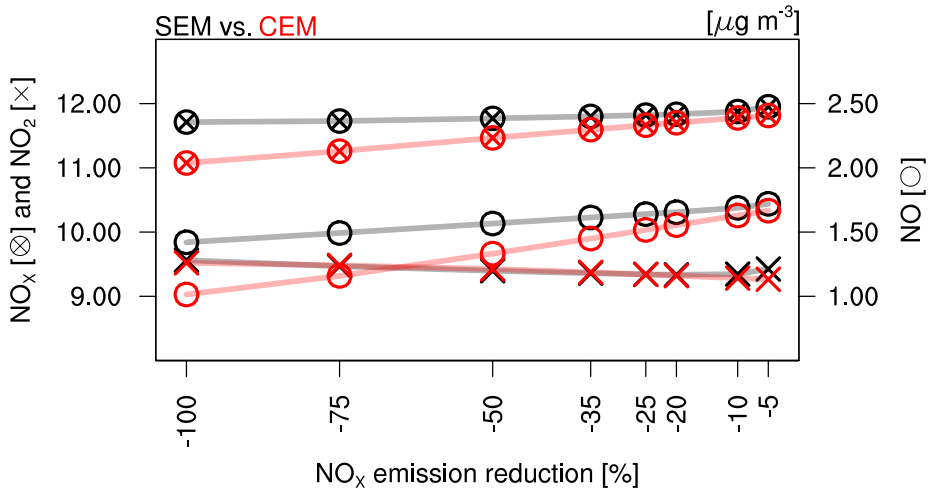


Figure I.12: Additive behavior of the source attribution for the brute force technique, of NO_x reduction levels from 5 to 100 %, across Germany for January to December 2018. Potential Impacts of combined emission reduction simulations (CEM) are shown in red, with potential impacts of added and individually reduced source sectors are represented in black (SEM).

SEM_X and the LEM are sensitive to the chosen emission reduction fraction and increase for smaller reduction levels X. For example, the SEM₅ deviates on average $-7\pm 5\%$ from the baseline for NO₂ at urban background stations, whereas the relative difference for the SEM₂₀ is $-8\pm 5\%$. The differences are smaller for rural background conditions where the SEM₅ deviates on average $-3\pm 8\%$. The results for NO indicate a deviation of $54\pm 26\%$ for SEM₅ in comparison to $48\pm 25\%$ for SEM₂₀. The differences between urban and rural background environments are related to the frequency of ozone limiting titration regimes as already described in Section I.3.2.

I.3.4 Non-linearity and additivity of the brute force results

In this section we illustrate the response to different emission reductions using the consistency ratio of

impacts (CRI) and potential impacts (CRPI) as already introduced and explained in the methodology section. Figure I.11 shows the CRI (left) and CRPI (right) for all emission reduction levels for NO (top), NO₂ (mid) and NO_x (bottom). Here, a linear regime can be assumed when the CRI shows a proportional behavior. In that case, the impacts are scalable and the CRPI for each emission reduction fraction would be 1. When the CRI shows a less or more than proportional reduction (with respect to the emission fraction of X), the linear scaling of the impacts differs from 1 for the CRPI.

The CRI indicates that reduced NO_x emissions do not lead to a proportional reduction of the NO concentration amount for the German background (Figure I.11, top left). This indicates that NO_x emission reductions of level X lead to a NO response larger than X. Largest differences to a proportional reduction can be seen for the

I. Source attribution of nitrogen oxides across Germany: Comparing the labelling approach and brute force technique with LOTOS-EUROS

combined reduction scenario and for the non-road transport source sector of about 35 % and 20 % respectively, which can be seen by the offset from the ideal case ($X/20$). The remaining source sectors (others) show the most linear relation with differences to the ideal case of about 1.5 % as the regime change does hardly occur. The CRI for NO_2 and NO_X shows an almost proportional behavior, as the errors for certain changes are small. For example, the difference to a proportional emission reduction between 5 and 50 percent is within 1.5 % for both compounds and within 5 % between 5 and 100 percent reduction. Overall, the proportionality of the CRI is reduced with higher emission reductions of NO_X for all compounds.

The proportionality for consistency ratios of potential impacts CRPI are decreasing with higher reduction levels, similar to the CRI (Figure I.11, right) as shown by their offset to 1. When only considering the 4 main source sectors, the largest differences for NO are evident for non-road transport (20 %) and lowest for households (9 %). Even larger deviations are obvious for the combined reduction scenario (35 %). For NO_2 and total NO_X , the CRPI reveals an almost proportional behavior with differences within 2-5 % each. By considering the CRPI for remaining sources (others), considerably larger differences can be seen for NO (43 %), NO_2 (37 %) and NO_X (24 %), respectively. This can be explained by the linear scaling to 100 % to estimate the potential impact of each source sector and indicates that small-sized emission categories are related to larger differences due to increased non-linearities as they remain more often in the titration regime.

To further highlight the non-linear interaction of emission reductions to nitrogen oxides, we performed an additivity analysis. Figure I.12 shows the Sector Explained Mass (SEM, in black) and Combined Explained Mass (CEM, in red) of NO, NO_2 and total NO_X . The results suggest that on average for NO_2 additivity is present within 2 % (see Table I.3). This correlates to the proportional concentration response to the NO_X emission reduction, which was shown for NO_2 . A lack of additivity can be seen for NO, where the additivity is reduced with higher reduction levels. Here, additivity can only be assumed for reduction levels up to about -25 %. For larger reduction percentages, differences of up to 40 % can be seen between the SEM_X and the CEM_X (see Table I.3). Reducing the emissions of a single sector by 50 or 100 % implies one leaves the regime in several sector reduction simulations, which is not the case with small reductions. Hence, the emission reduction to leave the regime counted several times at large reduction percentages. In the combined reduction simulations, all NO_X is removed and in the individual simulations only a part of total NO_X is diminished. Based on this, in the combined simulations more impact of the overall chemistry change (e.g. NO_X dependent ozone formation in summer) can be seen as an additional effect. For NO_X , the largest deviations between the SEM_X and CEM_X can be seen for higher reduction scenarios. However, as the averaged deviation between the SEM_{100} and CEM_{100} is overall small with about 5.8 %, additivity can be assumed for NO_X (see Table I.3).

I.4 Discussion and conclusion

In this study we compared the source attribution from the brute force and the labelling methods for nitrogen oxides. We successfully enhanced the understanding of limitations due to non-linearity triggered by the photochemical equilibrium of the Leighton cycle (Leighton, 1961; Finlayson-Pitts and Pitts, 2000). As summarized in previous studies, these non-linear chemical processes are the main limiting factors for different source attribution approaches for different compounds. Our study advances these findings by adding a source attribution evaluation for background levels of nitrogen oxides. Lessons learned from this study might be beneficial to support the joint FAIRMODE (Forum for AIR quality MODEling in Europe) initiative for assessing the source attribution, developing strategies to explain the observed contributions in urban, suburban and rural background locations of nitrogen oxides as a first starting point for further mitigation purposes.

It is well known that NO levels are lowered more than proportionally with respect to NO_x emission reductions. This is explained by the situation that NO levels build up under high NO_x conditions when ozone has been removed by titration. Hence, a 10 % reduction of NO_x has a larger effect on NO than subsequent 10 % reductions while the chemical regime is still ozone titrating. Whereas emission reduction simulations can explore the impacts of the emission change on NO levels, upscaling the impacts towards 100 % (to estimate contributions) leads

to systematically larger levels of attributed NO compared to the labelling approach. The resulting deviations between the explained mass of the brute force approach and the labelled results become larger when smaller emission reduction fractions are applied, which is in contrast to findings obtained from studies for particulate matter (Clappier et al., 2017; Carnevale et al., 2018; Thunis et al., 2019; Thunis et al., 2020). Moreover, a source attribution for a single sector, based on emission reduction simulations and a baseline should be avoided as there is no way to verify for consistency and the approach will largely overestimate the sector explained mass. In the study we showed station-based differences on annual average, which vary about 46 ± 25 % from the baseline and a lack of additivity for NO of up to 40 %. Thus, we conclude that the application of brute force simulations is potentially not the most suitable option for performing a source attribution in a consistent manner to estimate contributions of specific sources for NO.

Kwok et al. (2015) already indicates that the non-linear nature of ozone limits the applicability of potential impacts for NO₂. We agree that the source attribution of NO and NO₂ is affected by the non-linear photochemical equilibrium for ozone and nitrogen oxides and therefore can be perturbed, especially during nocturnal winter periods. It should be noted that model simulations with low emission reduction levels (<25 %) can be performed to reduce deviations caused by ozone-limiting conditions as additivity and linearity can be assumed to a certain degree. However, our study shows that larger deviations can be seen when small-sized emission source sectors are

I. Source attribution of nitrogen oxides across Germany: Comparing the labelling approach and brute force technique with LOTOS-EUROS

perturbed compared to large-sized sector categories. This implies that separating out more source sectors (and thus smaller sized ones), investigations may encounter larger problems due to the non-linearities induced by the titration regimes. This result is comparable to [Belis et al. \(2020\)](#), in which the authors indicate that the brute force technique fails to reflect the impact of varying emission levels in a specific source sector with related chemical reaction processes on any other sector. In addition, inconsistencies between the brute force technique and the baseline are increased in urban background regions, near emission sources. This is in agreement with [Verstraeten et al. \(2018\)](#), who emphasized that small-scale uncertainties become more relevant in urban areas, due to non-linear chemical phenomena. As these are the regions where limit values are exceeded and health effects are greatest, it is unfortunate that the inconsistency is most pronounced here. Still, since for NO₂ linearity and additivity can be assumed and the differences between potential impacts and labelled sector contributions are relatively small (<15 %), the brute force technique is an appropriate method to be used to estimate the contributions of the main sectors for NO₂. These differences are considerably smaller than typical systematic underestimations of CTMs to the observed ambient total NO₂ concentration, which can be in the order of a factor of 2 (e.g. [Schaap et al., 2015](#); [Kuik et al., 2018](#)). However, when small-sized emission sectors are under investigation, we recommend avoiding the upscaling of sensitivity simulations for NO₂.

The use of a labelling approach has several practical advantages as

the internal consistency is enforced by design and computational burden and chances of errors are lower ([Wagstrom et al., 2008](#); [Kranenburg et al., 2013](#)). In addition, the flexibility for defining the labels is large, including the contributions of natural and boundary conditions ([Carnevale et al., 2018](#)). Comparative studies carried out by [Thunis et al. \(2019\)](#) and [Clappier et al. \(2017\)](#) indicate that the labelling approach may not always be an appropriate method to derive the impact of emission reduction options for mitigation purposes. They state that non-linear chemical mechanisms, in particular indirect processes, cannot be modelled and a linear scaling of the simulated mass or share for the source sectors cannot be performed for varying emission levels. In the same vein, the emission changes induced by mitigation options often differ substantially from the idealized reduction scenarios of the brute force method. Hence, explicit simulations of dedicated mitigation packages must be performed in any case.

For air quality planning, an initial quantification of the impact of emission reductions as well as the contribution for different source sectors are of decisive interest but each approach has its own limitation. Hence, we suggest combining both. We recommend conducting brute force sensitivity simulations based on the ranking of source contributions obtained from a labelling approach and to define this as the best practice for the air pollution management of nitrogen oxides for source attribution purposes. The studies by [Mertens et al. \(2018\)](#) and [Butler et al. \(2020\)](#) already indicate that for ozone, a combination of the perturbation and the tagging approaches can yield com-

plementary information that neither approach can deliver on its own. As by definition combined simulations would be additive and able to represent indirect processes as well as the natural and boundary contribution could be separated out, this would widen the scope of advice to mitigate air-pollution. However further analysis is needed to gain a deeper understanding of the interactions of such combined concepts.

CRedit authorship contribution statement. **M. Thürkow:** Conceptualization, Methodology, Software, Validation, Formal analysis, Investigation, Resources, Data curation, Writing - original draft, Writing - review & editing, Visualization. **S. Banzhaf:** Writing - review & editing. **T. Butler:** Writing - review & editing. **J. Pültz:** Conceptualization, Methodology, Software, Resources, Writing - review & editing. **M. Schaap:** Conceptualization, Methodology, Writing - review & editing, Supervision, Project administration, Funding acquisition.

Declaration of competing interest.

The authors declare that they have no known competing financial interests or personal relationships that could have appeared to influence the work reported in this paper.

Acknowledgment. This research was funded by the Federal Ministry of Transport and Digital Infrastructure (BMVI) within the framework of the mFUND research initiative (grant no. 19F2065). The authors would like to thank the HPC Service of ZEDAT, Freie Universität Berlin, for computing time (Bennett et al., 2020).

Data availability. Data will be made available on request.

I. Source attribution of nitrogen oxides across Germany: Comparing the labelling approach and brute force technique with LOTOS-EUROS

I.5 Appendix

Table I.3: Ratio [%] between added and individually reduced source sectors (SEM_X) with respect to potential impacts of combined emission reduction simulations (CEM). For all reduction levels listed in Table I.2.

	NO	NO ₂	NO _x
SEM ₅ /CEM	3.18	1.72	1.15
SEM ₁₀ /CEM	3.66	0.68	0.84
SEM ₂₀ /CEM	6.47	0.15	1.12
SEM ₂₅ /CEM	8.14	0.02	1.34
SEM ₃₅ /CEM	11.30	-0.14	1.78
SEM ₅₀ /CEM	17.61	-0.29	2.64
SEM ₇₅ /CEM	28.80	-0.15	4.17
SEM ₁₀₀ /CEM	40.08	0.44	5.75

Table I.4: RMSE of PI_X and labelled contributions for NO₂.

Sectors	Scenario	Hourly	Daily
Road Transport	PI ₁₀	0.52	0.24
	PI ₂₀	0.49	0.23
	PI ₇₅	0.37	0.18
Non-Road Transport	PI ₁₀	0.29	0.19
	PI ₂₀	0.29	0.20
	PI ₇₅	0.33	0.23
Energy & Industry	PI ₁₀	0.51	0.38
	PI ₂₀	0.51	0.39
	PI ₇₅	0.49	0.36
Households	PI ₁₀	0.20	0.09
	PI ₂₀	0.20	0.09
	PI ₇₅	0.18	0.08
Others	PI ₁₀	0.04	0.03
	PI ₂₀	0.02	0.01
	PI ₇₅	0.02	0.01

Table I.5: Mean values and standard deviation of labelled contributions for NO₂, given as fraction of the base simulation [1]. All values are distinguished by station category (URBG: urban-, SUBG: suburban- and RUBG: rural background sites and station average: ALL) and time (January, February, ..., December and temporal average: Avg).

Sector	Site	Jan	Feb	Mar	Apr	May	Jun	Jul	Aug	Sep	Oct	Nov	Dec	Avg
Road	URBG	0.40±0.04	0.39±0.03	0.41±0.03	0.45±0.04	0.48±0.03	0.46±0.03	0.47±0.03	0.48±0.04	0.48±0.04	0.47±0.05	0.46±0.04	0.41±0.04	0.45±0.05
Transport	SUBG	0.41±0.04	0.39±0.03	0.43±0.03	0.46±0.04	0.50±0.04	0.48±0.04	0.50±0.03	0.50±0.04	0.50±0.04	0.48±0.05	0.48±0.04	0.41±0.04	0.46±0.05
	RUBG	0.37±0.05	0.36±0.03	0.39±0.03	0.43±0.03	0.42±0.03	0.43±0.03	0.44±0.03	0.46±0.03	0.46±0.04	0.44±0.05	0.43±0.05	0.38±0.04	0.42±0.05
	ALL	0.40±0.04	0.38±0.03	0.41±0.03	0.45±0.03	0.47±0.03	0.46±0.03	0.47±0.03	0.48±0.03	0.48±0.04	0.47±0.05	0.46±0.04	0.40±0.04	0.44±0.05
Non-Road	URBG	0.18±0.02	0.18±0.02	0.20±0.03	0.26±0.03	0.27±0.03	0.31±0.03	0.31±0.03	0.29±0.03	0.27±0.03	0.24±0.03	0.17±0.02	0.19±0.04	0.24±0.06
Transport	SUBG	0.17±0.03	0.18±0.02	0.19±0.03	0.24±0.03	0.26±0.03	0.29±0.03	0.29±0.03	0.26±0.03	0.25±0.03	0.22±0.03	0.16±0.02	0.19±0.04	0.23±0.05
	RUBG	0.19±0.03	0.20±0.03	0.21±0.04	0.27±0.05	0.31±0.04	0.32±0.04	0.34±0.04	0.29±0.03	0.26±0.04	0.23±0.03	0.18±0.02	0.20±0.04	0.25±0.07
	ALL	0.18±0.03	0.18±0.02	0.20±0.03	0.26±0.03	0.28±0.03	0.30±0.03	0.31±0.03	0.28±0.03	0.26±0.03	0.23±0.03	0.17±0.02	0.19±0.04	0.24±0.06
Energy & Industry	URBG	0.25±0.03	0.20±0.03	0.20±0.03	0.19±0.02	0.18±0.02	0.18±0.01	0.17±0.02	0.18±0.02	0.18±0.02	0.20±0.03	0.21±0.03	0.23±0.02	0.20±0.03
	SUBG	0.25±0.03	0.20±0.04	0.20±0.03	0.19±0.02	0.17±0.03	0.19±0.03	0.17±0.03	0.19±0.02	0.18±0.02	0.20±0.03	0.20±0.02	0.24±0.02	0.20±0.04
	RUBG	0.29±0.04	0.25±0.03	0.24±0.03	0.22±0.03	0.21±0.02	0.21±0.02	0.19±0.02	0.21±0.02	0.22±0.02	0.24±0.03	0.26±0.03	0.28±0.02	0.23±0.04
Households	ALL	0.26±0.03	0.21±0.03	0.21±0.03	0.19±0.02	0.18±0.02	0.19±0.02	0.18±0.02	0.19±0.02	0.19±0.02	0.21±0.03	0.22±0.02	0.25±0.02	0.21±0.03
	URBG	0.15±0.03	0.21±0.04	0.18±0.04	0.09±0.03	0.06±0.02	0.04±0.01	0.04±0.00	0.04±0.01	0.06±0.03	0.08±0.03	0.14±0.03	0.15±0.03	0.10±0.06
	SUBG	0.15±0.03	0.21±0.04	0.17±0.04	0.09±0.03	0.06±0.02	0.04±0.01	0.04±0.00	0.04±0.01	0.06±0.03	0.08±0.03	0.14±0.03	0.14±0.03	0.10±0.06
Others	RUBG	0.13±0.03	0.18±0.03	0.15±0.04	0.08±0.03	0.05±0.02	0.04±0.01	0.03±0.00	0.03±0.01	0.05±0.03	0.07±0.02	0.12±0.03	0.12±0.03	0.09±0.05
	ALL	0.14±0.03	0.20±0.04	0.17±0.04	0.09±0.03	0.06±0.02	0.04±0.01	0.04±0.00	0.04±0.01	0.06±0.03	0.08±0.03	0.13±0.03	0.14±0.03	0.10±0.06
	URBG	0.02±0.00	0.02±0.00	0.02±0.00	0.02±0.00	0.01±0.00	0.01±0.00	0.01±0.00	0.00±0.00	0.01±0.00	0.01±0.00	0.02±0.00	0.02±0.00	0.01±0.01
Others	SUBG	0.02±0.00	0.02±0.00	0.02±0.00	0.02±0.00	0.01±0.00	0.01±0.00	0.00±0.00	0.01±0.00	0.01±0.00	0.02±0.00	0.02±0.00	0.02±0.00	0.01±0.01
	RUBG	0.02±0.00	0.02±0.00	0.02±0.00	0.01±0.00	0.01±0.00	0.01±0.00	0.00±0.00	0.01±0.00	0.01±0.00	0.01±0.00	0.02±0.00	0.02±0.00	0.01±0.01
	ALL	0.02±0.00	0.02±0.00	0.02±0.00	0.02±0.00	0.01±0.00	0.01±0.00	0.01±0.00	0.00±0.00	0.01±0.00	0.01±0.00	0.02±0.00	0.02±0.00	0.01±0.01

Table I.6: Mean values and standard deviation for mass concentration levels [$\mu\text{g m}^{-3}$] of the BASE simulation, the Labelled Explained Mass (LEM) and the Single Explained Mass (SEM₂₀) are shown for NO. In addition, the ratio [1] of the LEM and SEM₂₀ with respect to the BASE simulation is provided as well as the SEM₂₀ in comparison to the LEM. All values are distinguished by station category (URBG: urban-, SUBG: suburban- and RUBG: rural background sites and station average: ALL) and time (January, February, ..., December and temporal average: Avg).

	Site	Jan	Feb	Mar	Apr	May	Jun	Jul	Aug	Sep	Oct	Nov	Dec	Avg
BASE	URBG	1.98±1.67	2.10±1.08	1.19±0.48	0.89±0.22	0.64±0.15	0.75±0.22	0.68±0.14	0.77±0.22	1.16±0.46	1.46±0.47	2.38±0.86	2.42±1.99	1.36±1.09
	SUBG	1.77±1.59	1.79±0.88	1.02±0.38	0.74±0.17	0.56±0.12	0.67±0.19	0.61±0.13	0.68±0.16	0.94±0.36	1.18±0.42	1.90±0.77	1.96±1.77	1.15±0.95
	RUBG	0.73±0.55	0.82±0.28	0.52±0.15	0.37±0.07	0.30±0.05	0.31±0.07	0.28±0.06	0.31±0.09	0.37±0.12	0.52±0.12	0.84±0.31	0.72±0.44	0.50±0.32
LEM	ALL	1.52±1.26	1.62±0.76	0.94±0.33	0.69±0.15	0.51±0.10	0.59±0.16	0.54±0.10	0.60±0.15	0.85±0.32	1.09±0.33	1.77±0.64	1.77±1.43	1.04±0.80
	URBG	1.94±1.65	2.06±1.07	1.17±0.47	0.86±0.21	0.62±0.15	0.72±0.22	0.65±0.14	0.74±0.22	1.13±0.45	1.42±0.47	2.33±0.85	2.38±1.97	1.33±1.08
	SUBG	1.72±1.56	1.76±0.87	1.00±0.37	0.72±0.17	0.54±0.12	0.64±0.18	0.58±0.13	0.65±0.15	0.91±0.36	1.14±0.41	1.85±0.76	1.92±1.75	1.12±0.93
SEM ₂₀	RUBG	0.70±0.54	0.79±0.27	0.50±0.15	0.35±0.07	0.27±0.05	0.28±0.07	0.26±0.06	0.28±0.08	0.35±0.11	0.49±0.12	0.80±0.30	0.69±0.43	0.48±0.31
	ALL	1.49±1.24	1.59±0.75	0.92±0.33	0.67±0.15	0.49±0.10	0.57±0.16	0.51±0.10	0.58±0.15	0.83±0.31	1.06±0.33	1.72±0.63	1.74±1.41	1.01±0.79
	URBG	3.32±3.03	3.72±2.09	1.91±0.86	1.27±0.41	0.80±0.27	0.96±0.39	0.83±0.22	1.10±0.41	1.80±0.83	2.37±0.92	4.13±1.67	4.38±3.76	2.21±2.09
LEM/BASE	SUBG	2.98±2.85	3.24±1.79	1.60±0.69	1.01±0.30	0.65±0.21	0.86±0.31	0.72±0.18	0.94±0.29	1.42±0.66	1.90±0.85	3.40±1.59	3.68±3.45	1.86±1.86
	RUBG	1.11±0.93	1.35±0.52	0.73±0.26	0.47±0.13	0.31±0.08	0.34±0.11	0.29±0.08	0.37±0.16	0.48±0.19	0.71±0.22	1.36±0.61	1.26±0.92	0.73±0.61
	ALL	2.53±2.28	2.86±1.48	1.46±0.60	0.95±0.27	0.61±0.18	0.75±0.27	0.63±0.15	0.83±0.29	1.29±0.58	1.73±0.66	3.07±1.27	3.23±2.79	1.65±1.55
SEM ₂₀ /BASE	URBG	0.98±0.01	0.98±0.00	0.98±0.01	0.97±0.01	0.96±0.01	0.96±0.01	0.96±0.01	0.96±0.01	0.97±0.01	0.97±0.01	0.98±0.01	0.98±0.01	0.97±0.01
	SUBG	0.97±0.01	0.98±0.00	0.98±0.01	0.96±0.01	0.95±0.01	0.96±0.01	0.95±0.01	0.96±0.01	0.96±0.01	0.97±0.01	0.97±0.01	0.97±0.01	0.97±0.01
	RUBG	0.95±0.01	0.97±0.01	0.96±0.01	0.94±0.01	0.92±0.02	0.92±0.01	0.91±0.01	0.92±0.02	0.93±0.01	0.94±0.01	0.95±0.01	0.95±0.01	0.94±0.02
SEM ₂₀ /LEM	ALL	0.97±0.01	0.98±0.00	0.97±0.01	0.96±0.01	0.95±0.01	0.95±0.01	0.95±0.01	0.95±0.01	0.96±0.01	0.97±0.01	0.97±0.01	0.97±0.01	0.96±0.01
	URBG	1.56±0.22	1.72±0.19	1.57±0.16	1.40±0.15	1.21±0.15	1.26±0.16	1.21±0.11	1.38±0.18	1.52±0.15	1.60±0.17	1.71±0.15	1.70±0.25	1.48±0.25
	SUBG	1.58±0.22	1.75±0.20	1.54±0.17	1.34±0.13	1.14±0.13	1.25±0.14	1.17±0.08	1.35±0.14	1.47±0.15	1.56±0.20	1.74±0.18	1.74±0.28	1.47±0.27
SEM ₂₀ /LEM	RUBG	1.43±0.20	1.62±0.16	1.39±0.15	1.24±0.12	1.04±0.13	1.10±0.11	1.02±0.11	1.17±0.19	1.25±0.15	1.36±0.14	1.58±0.17	1.62±0.31	1.32±0.27
	ALL	1.55±0.22	1.72±0.18	1.53±0.15	1.36±0.13	1.16±0.13	1.23±0.13	1.17±0.08	1.34±0.16	1.47±0.14	1.56±0.17	1.70±0.16	1.70±0.26	1.46±0.25
	URBG	1.60±0.22	1.75±0.19	1.60±0.16	1.45±0.14	1.26±0.14	1.30±0.16	1.26±0.11	1.43±0.18	1.57±0.14	1.64±0.16	1.75±0.15	1.73±0.25	1.53±0.24
SEM ₂₀ /LEM	SUBG	1.62±0.22	1.78±0.20	1.57±0.16	1.39±0.13	1.20±0.13	1.31±0.14	1.23±0.08	1.41±0.14	1.53±0.15	1.62±0.19	1.79±0.17	1.78±0.28	1.52±0.27
	RUBG	1.50±0.20	1.67±0.16	1.45±0.15	1.32±0.12	1.12±0.12	1.20±0.12	1.12±0.11	1.27±0.19	1.35±0.15	1.45±0.14	1.65±0.16	1.69±0.30	1.40±0.26
	ALL	1.59±0.21	1.75±0.18	1.57±0.15	1.41±0.13	1.22±0.12	1.29±0.13	1.23±0.08	1.41±0.16	1.53±0.14	1.61±0.16	1.75±0.15	1.74±0.26	1.51±0.25

Table I.7: Same as in Table I.6, but for NO₂.

	Site	Jan	Feb	Mar	Apr	May	Jun	Jul	Aug	Sep	Oct	Nov	Dec	Avg
BASE	URBG	13.27±4.78	14.53±3.93	12.43±3.13	10.44±1.75	8.07±1.46	8.14±1.56	8.04±1.48	9.38±1.25	12.61±2.48	13.58±2.98	16.10±3.42	15.06±5.55	11.78±4.14
	SUBG	12.89±4.39	13.90±3.80	11.64±2.63	9.69±1.78	7.60±1.39	7.69±1.59	7.38±1.36	8.78±1.16	11.69±2.41	12.81±2.86	15.39±3.16	14.61±5.48	11.15±4.01
	RUBG	8.73±2.67	9.11±2.18	7.36±1.59	5.56±0.84	4.53±0.54	4.21±0.67	4.11±0.65	4.96±0.65	6.37±1.01	7.78±1.19	10.26±1.80	9.67±3.13	6.87±2.68
LEM	ALL	11.75±3.98	12.67±3.32	10.65±2.49	8.73±1.47	6.85±1.13	6.81±1.28	6.63±1.16	7.85±1.01	10.44±1.98	11.58±2.33	14.10±2.81	13.30±4.80	10.09±3.62
	URBG	12.74±4.62	14.09±3.83	12.01±3.05	9.89±1.70	7.54±1.42	7.61±1.49	7.41±1.38	8.70±1.21	11.89±2.41	12.88±2.86	15.36±3.31	14.51±5.46	11.20±4.07
	SUBG	12.34±4.23	13.44±3.69	11.20±2.56	9.11±1.73	7.03±1.36	7.11±1.52	6.71±1.28	8.04±1.13	10.93±2.34	12.08±2.74	14.62±3.06	14.04±5.39	10.53±3.95
SEM ₂₀	RUBG	8.25±2.55	8.71±2.08	6.98±1.52	5.07±0.81	4.04±0.52	3.73±0.60	3.55±0.57	4.34±0.64	5.75±0.96	7.16±1.12	9.59±1.73	9.16±3.06	6.35±2.64
	ALL	11.23±3.84	12.24±3.22	10.23±2.41	8.19±1.42	6.32±1.10	6.28±1.21	6.01±1.07	7.17±0.98	9.74±1.91	10.90±2.22	13.38±2.71	12.76±4.72	9.52±3.56
	URBG	11.73±3.27	13.20±2.99	11.95±2.65	9.90±1.70	7.46±1.51	7.62±1.54	7.24±1.34	8.66±1.30	11.59±2.37	12.40±2.46	14.10±2.59	13.05±4.11	10.72±3.38
SEM ₂₀ /BASE	SUBG	11.48±3.06	12.81±3.02	11.34±2.27	9.27±1.80	7.01±1.53	7.17±1.64	6.59±1.31	8.06±1.28	10.85±2.45	11.90±2.46	13.73±2.50	12.95±4.32	10.24±3.43
	RUBG	8.56±2.47	9.26±2.25	7.57±1.57	5.36±0.99	4.07±0.72	3.87±0.73	3.47±0.60	4.54±0.92	6.06±1.26	7.59±1.27	10.04±1.70	9.57±3.26	6.65±2.82
	ALL	10.67±2.94	11.87±2.74	10.43±2.18	8.33±1.49	6.29±1.24	6.35±1.30	5.89±1.06	7.23±1.15	9.69±2.01	10.78±2.01	12.75±2.25	11.97±3.92	9.34±3.18
LEM/BASE	URBG	0.96±0.01	0.97±0.01	0.97±0.01	0.95±0.01	0.93±0.01	0.93±0.01	0.92±0.01	0.93±0.01	0.94±0.01	0.95±0.01	0.95±0.01	0.96±0.01	0.95±0.02
	SUBG	0.96±0.01	0.97±0.01	0.96±0.01	0.94±0.01	0.92±0.02	0.92±0.01	0.91±0.01	0.91±0.02	0.93±0.01	0.94±0.01	0.95±0.01	0.96±0.01	0.94±0.02
	RUBG	0.94±0.01	0.96±0.01	0.95±0.01	0.91±0.02	0.89±0.02	0.88±0.02	0.86±0.02	0.87±0.02	0.90±0.02	0.92±0.02	0.93±0.01	0.95±0.01	0.91±0.03
SEM ₂₀ /BASE	ALL	0.95±0.01	0.97±0.01	0.96±0.01	0.94±0.01	0.92±0.02	0.92±0.01	0.91±0.01	0.91±0.02	0.93±0.01	0.94±0.01	0.95±0.01	0.96±0.01	0.94±0.02
	URBG	0.91±0.07	0.92±0.06	0.97±0.05	0.95±0.04	0.92±0.04	0.93±0.03	0.90±0.03	0.92±0.04	0.92±0.03	0.92±0.03	0.88±0.04	0.88±0.06	0.92±0.05
	SUBG	0.91±0.07	0.93±0.05	0.98±0.05	0.96±0.04	0.92±0.05	0.93±0.04	0.89±0.04	0.92±0.05	0.93±0.03	0.93±0.04	0.90±0.05	0.90±0.07	0.92±0.05
SEM ₂₀ /LEM	RUBG	0.98±0.04	1.02±0.03	1.03±0.04	0.96±0.07	0.89±0.08	0.92±0.07	0.84±0.05	0.91±0.10	0.95±0.07	0.97±0.05	0.98±0.03	0.99±0.04	0.95±0.08
	ALL	0.93±0.06	0.95±0.05	0.99±0.04	0.95±0.05	0.91±0.05	0.93±0.04	0.89±0.04	0.92±0.06	0.93±0.04	0.93±0.04	0.91±0.04	0.91±0.05	0.93±0.05
	URBG	0.95±0.08	0.95±0.06	1.00±0.05	1.00±0.03	0.99±0.03	1.00±0.02	0.98±0.02	0.99±0.04	0.97±0.02	0.97±0.04	0.93±0.05	0.92±0.07	0.97±0.05
LEM	SUBG	0.95±0.07	0.96±0.05	1.02±0.04	1.02±0.04	0.99±0.03	1.00±0.04	0.98±0.03	1.00±0.05	0.99±0.03	0.99±0.04	0.95±0.05	0.94±0.08	0.98±0.05
	RUBG	1.04±0.04	1.06±0.04	1.09±0.04	1.05±0.06	1.00±0.06	1.04±0.06	0.98±0.04	1.04±0.09	1.05±0.07	1.06±0.04	1.05±0.03	1.04±0.04	1.04±0.06
	ALL	0.97±0.07	0.98±0.05	1.03±0.04	1.02±0.04	0.99±0.04	1.01±0.03	0.98±0.03	1.00±0.05	0.99±0.03	0.99±0.03	0.96±0.04	0.95±0.06	0.99±0.05

Table I.8: Same as in Table I.6, but for NO_x.

	Site	Jan	Feb	Mar	Apr	May	Jun	Jul	Aug	Sep	Oct	Nov	Dec	Avg
BASE	URBG	16.30±7.23	17.74±5.46	14.25±3.80	11.80±2.02	9.06±1.65	9.29±1.77	9.08±1.60	10.56±1.49	14.38±3.04	15.81±3.55	19.74±4.53	18.77±8.44	13.87±5.66
	SUBG	15.59±6.66	16.65±5.03	13.21±3.12	10.83±1.97	8.46±1.55	8.72±1.77	8.32±1.45	9.83±1.30	13.13±2.80	14.62±3.40	18.31±4.05	17.62±7.95	12.91±5.28
	RUBG	9.85±3.43	10.37±2.54	8.16±1.77	6.13±0.89	4.98±0.59	4.68±0.71	4.55±0.68	5.43±0.74	6.94±1.12	8.57±1.32	11.55±2.15	10.77±3.74	7.65±3.11
LEM	ALL	14.09±5.82	15.15±4.40	12.09±2.94	9.79±1.64	7.64±1.27	7.72±1.42	7.46±1.23	8.78±1.17	11.75±2.35	13.25±2.74	16.82±3.60	16.02±6.86	11.69±4.72
	URBG	15.71±7.04	17.25±5.34	13.80±3.72	11.21±1.98	8.49±1.62	8.71±1.71	8.41±1.51	9.84±1.47	13.62±2.98	15.05±3.43	18.93±4.42	18.16±8.33	13.23±5.58
	SUBG	14.98±6.47	16.14±4.90	12.74±3.04	10.21±1.92	7.86±1.52	8.10±1.69	7.60±1.37	9.04±1.28	12.32±2.73	13.83±3.28	17.46±3.95	16.99±7.83	12.24±5.20
SEM ₂₀	RUBG	9.32±3.29	9.93±2.43	7.75±1.69	5.61±0.87	4.46±0.57	4.16±0.65	3.94±0.61	4.77±0.74	6.28±1.09	7.90±1.25	10.82±2.07	10.22±3.65	7.08±3.06
	ALL	13.51±5.64	14.67±4.28	11.64±2.86	9.21±1.60	7.08±1.24	7.15±1.36	6.79±1.15	8.06±1.15	11.01±2.29	12.52±2.64	16.02±3.50	15.42±6.76	11.06±4.66
	URBG	16.72±7.57	18.83±5.94	14.85±3.85	11.83±2.22	8.66±1.89	9.08±2.00	8.48±1.58	10.31±1.84	14.32±3.45	16.00±3.67	20.34±4.71	19.61±9.38	14.05±6.21
SEM ₂₀ /BASE	SUBG	15.97±7.00	17.71±5.47	13.77±3.15	10.81±2.15	8.00±1.80	8.46±1.98	7.68±1.46	9.48±1.60	13.00±3.22	14.78±3.58	18.87±4.26	18.45±8.87	13.05±5.84
	RUBG	10.24±3.71	11.31±2.89	8.69±1.87	6.08±1.10	4.54±0.83	4.40±0.84	3.91±0.68	5.11±1.15	6.79±1.51	8.67±1.54	12.10±2.37	11.48±4.52	7.75±3.64
	ALL	14.49±6.14	16.19±4.82	12.65±3.00	9.78±1.82	7.21±1.50	7.47±1.61	6.84±1.22	8.48±1.52	11.65±2.74	13.41±2.90	17.40±3.79	16.82±7.75	11.83±5.27
LEM/BASE	URBG	0.96±0.01	0.97±0.00	0.97±0.01	0.95±0.01	0.94±0.01	0.94±0.01	0.93±0.01	0.93±0.01	0.95±0.01	0.95±0.01	0.96±0.01	0.96±0.01	0.95±0.02
	SUBG	0.96±0.01	0.97±0.01	0.96±0.01	0.94±0.01	0.93±0.02	0.93±0.01	0.91±0.01	0.92±0.01	0.94±0.01	0.94±0.01	0.95±0.01	0.96±0.01	0.94±0.02
	RUBG	0.94±0.01	0.96±0.01	0.95±0.01	0.91±0.02	0.89±0.02	0.89±0.02	0.87±0.02	0.88±0.02	0.90±0.02	0.92±0.02	0.94±0.01	0.95±0.01	0.92±0.03
SEM ₂₀ /BASE	ALL	0.96±0.01	0.97±0.01	0.96±0.01	0.94±0.01	0.92±0.02	0.93±0.01	0.91±0.01	0.92±0.02	0.94±0.01	0.94±0.01	0.95±0.01	0.96±0.01	0.94±0.02
	URBG	1.02±0.03	1.06±0.02	1.04±0.04	1.00±0.04	0.95±0.05	0.97±0.05	0.93±0.03	0.97±0.06	0.99±0.04	1.01±0.03	1.03±0.02	1.03±0.05	1.00±0.05
	SUBG	1.02±0.03	1.06±0.03	1.04±0.04	1.00±0.05	0.94±0.06	0.96±0.05	0.92±0.04	0.96±0.06	0.98±0.05	1.01±0.04	1.03±0.03	1.03±0.05	1.00±0.06
SEM ₂₀ /LEM	RUBG	1.03±0.04	1.09±0.03	1.07±0.05	0.99±0.07	0.91±0.08	0.94±0.08	0.86±0.06	0.93±0.11	0.97±0.08	1.01±0.06	1.05±0.03	1.05±0.06	0.99±0.09
	ALL	1.02±0.03	1.07±0.03	1.05±0.04	1.00±0.05	0.94±0.06	0.96±0.06	0.92±0.04	0.96±0.07	0.99±0.05	1.01±0.04	1.03±0.03	1.04±0.05	1.00±0.06
	URBG	1.06±0.02	1.09±0.02	1.08±0.03	1.05±0.04	1.01±0.04	1.04±0.04	1.01±0.03	1.04±0.05	1.05±0.04	1.06±0.03	1.08±0.02	1.07±0.04	1.05±0.04
SEM ₂₀ /LEM	SUBG	1.06±0.02	1.10±0.03	1.08±0.03	1.06±0.04	1.01±0.04	1.04±0.05	1.01±0.03	1.04±0.05	1.05±0.04	1.07±0.03	1.08±0.02	1.08±0.04	1.06±0.04
	RUBG	1.09±0.03	1.14±0.04	1.12±0.04	1.08±0.06	1.01±0.07	1.05±0.07	0.99±0.05	1.06±0.10	1.07±0.08	1.09±0.05	1.12±0.03	1.11±0.05	1.08±0.07
	ALL	1.07±0.03	1.10±0.03	1.09±0.03	1.06±0.04	1.01±0.05	1.04±0.05	1.01±0.03	1.05±0.06	1.05±0.04	1.07±0.03	1.09±0.02	1.08±0.04	1.06±0.05

Table I.9: Mean values and standard deviation of Potential Impacts (PI₂₀) for NO₂, given as fraction of the SEM₂₀ [1]. All values are distinguished by station category (URBG: urban-, SUBG: suburban- and RUBG: rural background sites and station average: ALL) and time (January, February, ..., December and temporal average: Avg).

Sector	Site	Jan	Feb	Mar	Apr	May	Jun	Jul	Aug	Sep	Oct	Nov	Dec	Avg
Road	URBG	0.41±0.05	0.39±0.03	0.41±0.04	0.45±0.04	0.47±0.03	0.44±0.04	0.46±0.03	0.46±0.03	0.48±0.04	0.47±0.06	0.47±0.05	0.42±0.04	0.44±0.05
Transport	SUBG	0.42±0.05	0.40±0.03	0.42±0.04	0.46±0.04	0.48±0.04	0.46±0.04	0.48±0.03	0.48±0.04	0.49±0.04	0.48±0.05	0.48±0.05	0.42±0.04	0.46±0.05
	RUBG	0.38±0.05	0.36±0.03	0.38±0.03	0.41±0.03	0.40±0.03	0.40±0.03	0.41±0.03	0.42±0.03	0.45±0.04	0.44±0.06	0.43±0.05	0.38±0.05	0.40±0.05
	ALL	0.40±0.05	0.39±0.03	0.41±0.03	0.44±0.04	0.46±0.03	0.44±0.03	0.45±0.03	0.46±0.03	0.48±0.04	0.47±0.05	0.47±0.05	0.41±0.04	0.44±0.05
Non-Road	URBG	0.19±0.03	0.18±0.02	0.21±0.03	0.28±0.04	0.28±0.03	0.32±0.04	0.33±0.03	0.31±0.04	0.29±0.03	0.25±0.03	0.18±0.03	0.21±0.04	0.25±0.07
Transport	SUBG	0.18±0.03	0.18±0.02	0.20±0.03	0.26±0.04	0.28±0.03	0.31±0.04	0.31±0.03	0.29±0.03	0.27±0.03	0.24±0.03	0.17±0.02	0.20±0.04	0.24±0.06
	RUBG	0.20±0.03	0.20±0.03	0.22±0.04	0.29±0.05	0.35±0.05	0.35±0.04	0.38±0.04	0.34±0.04	0.29±0.03	0.26±0.03	0.19±0.02	0.22±0.05	0.28±0.08
	ALL	0.19±0.03	0.19±0.02	0.21±0.03	0.27±0.04	0.30±0.03	0.32±0.04	0.34±0.03	0.31±0.03	0.28±0.03	0.25±0.03	0.18±0.02	0.21±0.04	0.25±0.06
Energy & Industry	URBG	0.22±0.04	0.19±0.02	0.19±0.03	0.17±0.02	0.18±0.02	0.18±0.02	0.17±0.02	0.18±0.02	0.16±0.02	0.18±0.04	0.19±0.04	0.21±0.03	0.18±0.03
	SUBG	0.22±0.04	0.19±0.03	0.19±0.03	0.17±0.03	0.16±0.03	0.18±0.03	0.17±0.03	0.18±0.03	0.17±0.02	0.18±0.04	0.18±0.03	0.21±0.03	0.18±0.03
	RUBG	0.26±0.04	0.23±0.02	0.22±0.04	0.20±0.04	0.20±0.02	0.20±0.03	0.18±0.03	0.20±0.03	0.20±0.03	0.21±0.04	0.23±0.04	0.24±0.03	0.22±0.04
Households	ALL	0.23±0.04	0.20±0.02	0.20±0.03	0.18±0.02	0.18±0.02	0.19±0.02	0.17±0.02	0.18±0.02	0.17±0.02	0.18±0.04	0.20±0.03	0.22±0.03	0.19±0.03
	URBG	0.15±0.03	0.22±0.04	0.18±0.04	0.09±0.03	0.06±0.02	0.04±0.01	0.04±0.00	0.04±0.01	0.06±0.03	0.09±0.03	0.14±0.03	0.15±0.03	0.10±0.06
	SUBG	0.15±0.03	0.22±0.04	0.18±0.04	0.09±0.03	0.06±0.02	0.04±0.01	0.04±0.00	0.04±0.01	0.06±0.03	0.09±0.03	0.14±0.03	0.15±0.03	0.10±0.06
Others	RUBG	0.14±0.03	0.19±0.03	0.16±0.04	0.08±0.03	0.05±0.02	0.04±0.01	0.03±0.00	0.03±0.01	0.05±0.03	0.08±0.02	0.13±0.03	0.13±0.03	0.09±0.06
	ALL	0.15±0.03	0.21±0.03	0.17±0.04	0.09±0.03	0.06±0.02	0.04±0.01	0.04±0.00	0.04±0.01	0.06±0.03	0.09±0.03	0.14±0.03	0.14±0.03	0.10±0.06
	URBG	0.02±0.00	0.02±0.00	0.02±0.00	0.02±0.00	0.01±0.00	0.01±0.00	0.01±0.00	0.00±0.00	0.01±0.00	0.01±0.00	0.02±0.00	0.02±0.00	0.01±0.01
Others	SUBG	0.02±0.00	0.02±0.00	0.02±0.00	0.02±0.00	0.01±0.00	0.01±0.00	0.01±0.00	0.00±0.00	0.01±0.00	0.01±0.00	0.02±0.00	0.02±0.00	0.01±0.01
	RUBG	0.02±0.00	0.02±0.00	0.02±0.00	0.01±0.00	0.01±0.00	0.01±0.00	0.00±0.00	0.01±0.00	0.01±0.00	0.02±0.00	0.02±0.00	0.02±0.00	0.01±0.01
	ALL	0.02±0.00	0.02±0.00	0.02±0.00	0.02±0.00	0.01±0.00	0.01±0.00	0.01±0.00	0.00±0.00	0.01±0.00	0.01±0.00	0.02±0.00	0.02±0.00	0.01±0.01

Paper II

Source attribution of particulate matter in Berlin

J. Pültz¹, S. Banzhaf¹, M. Thürkow¹, R. Kranenburg² and M. Schaap^{1,2}

Published in Atmospheric Environment, Volume 292, January 2023, 119416, ISSN: 1352-2310, DOI: 10.1016/j.atmosenv.2022.119416, URL: <https://www.sciencedirect.com/science/article/pii/S1352231022004812>

This article is licensed under a Creative Commons Attribution-NonCommercial-NoDerivs 4.0 International license.

Contents

II.1	Introduction	83
II.2	Methodology	85
II.3	Results	89
II.4	Discussion and conclusion	101

Highlights

- A sectoral and regional source attribution for Berlin was performed.
- The most important source sectors for PM are households and industry & energy.
- Transboundary contributions are smaller than domestic contributions.
- Missing resuspension processes may explain the underestimation of the coarse mode.

Abstract

The exposure to ambient particulate matter in metropolitan areas is a major health problem. A prerequisite for formulating effective mitigation strategies is to understand the origin of particulate matter in terms of source regions and sectors. We performed a source attribution of particulate matter (PM) for the Berlin agglomeration area covering the period from 2016 to 2018 using the LOTOS-EUROS chemistry transport model. The (3 year-) mean modelled urban background PM_{2.5} concentration ($10.4 \mu\text{g m}^{-3}$) is largely explained by households ($3.2 \mu\text{g m}^{-3}$) and industry & energy ($2.0 \mu\text{g m}^{-3}$), while the remaining source sectors contribute the other half. The modelled annual mean urban increment for PM_{2.5} is mainly attributed to households ($1.6 \mu\text{g m}^{-3}$) and traffic ($0.5 \mu\text{g m}^{-3}$). With respect to its relative shares the PM₁₀ source attribution looks similar to that of PM_{2.5} throughout the year, but with enhanced natural contributions. From a geographical perspective the main source area for the PM_{2.5} in Berlin is Germany ($5.1 \mu\text{g m}^{-3}$) itself, followed by the contributions from transboundary transport ($3.4 \mu\text{g m}^{-3}$). The German sources could be further split into Berlin ($2.6 \mu\text{g m}^{-3}$), Brandenburg ($0.7 \mu\text{g m}^{-3}$) and remaining states of Germany ($1.8 \mu\text{g m}^{-3}$). About one third of the foreign shares can be attributed to Germany's neighbouring countries Poland and Czech Republic. During episodes these contributions can significantly differ, e.g. in February 2017 the Polish contribution is about 1/3rd. The sectoral contributions agree with previous findings except that our study indicates lower contributions for traffic. The model's underestimation of total PM is largely caused by an underestimation of the coarse mode PM. Both the coarse mode urban increment as well as the regional background concentrations are underestimated by the model, especially during summer. We suggest that the enhanced coarse material (in the city) during warm seasons is predominated by (road) resuspension processes which need more of our attention to further improve our models.

Keywords: *chemistry transport model, source attribution, coarse mode, urban increment, Lenschow approach*

Author affiliation:

¹Institute of Meteorology, Freie Universität Berlin, Carl-Heinrich-Becker-Weg 6-10, 12165, Berlin, Germany

²TNO, Department Climate Air and Sustainability, Princetonlaan 6, 3584 CB, Utrecht, the Netherlands

II.1 Introduction

Air pollution remains the single largest environmental health risk in Europe according to the World Health Organization (WHO, 2015). The adverse health effects of air pollution are dominated by exposure to particulate matter (PM) (Boldo et al., 2006; Brook et al., 2010; Costa et al., 2014). Harmful effects as cardiovascular and respiratory diseases, can ultimately lead to premature death (Newby et al., 2015). In Europe, the average reduction in life expectancy due to fine particulate matter (PM_{2.5}) is estimated in the order of 8-10 months (Boldo et al., 2006; Brook et al., 2010). Although a large proportion of the European population is exposed to levels above the WHO air quality guidelines, current EU limit values for PM in Europe are exceeded to a limited extent. Exceedances of the daily limit value for PM₁₀ in Germany are measured particularly at monitoring sites close to traffic and industry in large conurbations (UBA, 2019). To protect citizens from the negative effects of air pollution and to bring PM concentration levels below the limit value, it is necessary to elaborate effective mitigation strategies. In order to develop effective mitigation strategies, it is crucial to understand which sources contribute to the particulate matter exposure (Pandolfi et al., 2020) and which mitigation options have the largest impact, especially for high concentration episodes (Belis et al., 2020). A prerequisite is that the modelling systems used for developing mitigation strategies explain the observed levels and variability in particulate matter well.

PM encompasses a wide range of particle types, regarding size (coarse:

PM₁₀ and fine: PM_{2.5}), chemical composition (e.g., mineral dust, combustion particles, sea salt, secondary inorganic aerosol, secondary organic aerosol, metals), and sources (e.g., natural, traffic, industry, domestic households, secondary processes) (Putaud et al., 2004). Its contributions depend on local sources as well as its location with respect to source regions located further away and vary strongly depending on synoptic meteorological conditions and season (Lenschow et al., 2001; Mues et al., 2012; Fuzzi et al., 2015; van Pinxteren et al., 2019). Sources of PM in urban areas are traffic, domestic heating, cooking, construction sites, industries, power generation or mineral dust (e.g., Querol et al., 2004). Long-range transport prevalent as the rural background is normally dominated by contributions from combustion processes and secondary aerosols, e.g. ammonium nitrate and sulphate (van Pinxteren et al., 2019). Whereas PM episodes may be driven by a local or regional build-up of pollution (e.g. Banzhaf et al., 2013), the urban concentration levels during episodes may also be largely controlled by long range transport to a city (Beekmann et al., 2015). Hence, many cities are unable to meet target levels for air pollutants through local action alone (van Pinxteren et al., 2019). To identify the origin and quantify both natural and anthropogenic source contributions to urban PM levels is an important task.

There are various methodologies to identify and apportion PM to different sources. Statistical data analyses of observations are often used. The Lenschow approach is a simple method, in which urban increments that correspond to the concentration difference between the urban and the regional lo-

calculations are calculated (Lenschow et al., 2001). The increment is assumed to be the impact of a city on its own air pollution. The main advantage is a simplified data treatment with low impact of mathematical artefacts (Viana et al., 2008). A weakness of the method is that the assumption of the independence of the two locations may not be fulfilled (Thunis et al., 2018). A further helpful method is to apply air trajectories to identify source regions which can be long-range or trans-boundary (e.g., Potier et al., 2019). Positive Matrix Factorization (PMF) attempt to apportion the sources based on observations (internal correlations) at the receptor site alone. A very distinct advantage is the detailed source profiles PMF provides. This method is often used for analysis because detailed prior knowledge of the sources and source profiles is not required and software to perform this type of analysis is widely available (Viana et al., 2008). Normally, receptor modelling studies can distinguish a limited number of broad source categories. An essential disadvantage is the inability to provide a source apportionment for secondary components. Furthermore, these experimental approaches do not yield information on the geographical origin. Finally, the required chemical analyses are expensive leading to many applications in campaigns and a limited availability of long time series (Hendriks et al., 2013).

Complementary to methods based on observations, deterministic Eulerian Chemistry Transport Models (CTMs) are widely used to obtain more detailed information on air pollution and its origins. By involving atmospheric process descriptions and emission inventories they provide calculations of the evolution of the air pollution situation across

a region (Baklanov et al., 2014). To gain insights in source contributions, several methodologies have been used in the past. The simplest approach is the brute force (BF) method, in which the emissions of the source sectors under investigation are reduced and compared to a base case simulation (e.g., Banzhaf et al., 2013; Belis et al., 2020). Through extrapolation of the resulting concentration changes the source sector contribution can be estimated. For inert compounds these approaches provide equivalent results (Thunis et al., 2019). It has to be highlighted that the BF method and labelling approach lead to different source attribution (SA) results due to non-linear chemical effects, such as for the formation of secondary inorganic aerosol (e.g. Thunis et al., 2020). The main advantage of the BF methodology is that it directly provides information on the effectiveness of potential measures. However, by upscaling the impacts one may over- or underestimate the baseline concentration, which becomes a larger issue in case of situation with a limiting formation process and on short time scales (Li et al., 2014; Thunis et al., 2015; Pommier et al., 2020; Thürkow et al., 2023). Moreover, in case of a limitation in the formation small sized emission sources may be given a zero or low impact and thus may be overlooked as a relevant contributor (Thunis et al., 2020; Thürkow et al., 2023). In this situation detailing a large sector as traffic further into subsectors may lead to the situation that the sum of the sub-sectors is away from the sector estimate (Clappier et al., 2017). This may be amplified in case also the spatial and temporal variability are different per subsector. Also, the resulting source apportionment is sensitive to the reduction percentage

applied (Napelenok et al., 2006). Due to the intrinsic assumption that each molecule has the same chance of reaction adopted in the labelling implementation these effects do not occur. The resulting source apportionment is additive and complete, but does not per se indicate the effectiveness. Note that above mentioned concerns disappear when the brute force apportionment is performed within its limits of applicability, i.e. for a limited range of emission reduction strengths (Clappier et al., 2017). Hence, we see a labelling based source apportionment as a valuable first step to identify and quantify the relevant sectors to be further addressed in brute force calculations to determine efficiency of potential measures. This is further supported by the fact that the labelling strategy is more computationally efficient enabling to detail a larger number of source contributions than normally feasible in brute force studies (Belis et al., 2020). Methods like Decoupled Direct Method (DDM; Dunker et al., 2002; Zhang et al., 2012) at least partly, solve this computational burden for brute force approaches. Although first operational applications are becoming available (Pommier et al., 2020), the experience using such model-based source apportionment is still relatively scarce in Europe.

In this paper, we apply the LOTOS-EUROS CTM version 2.1 to identify the most relevant sources with regards to their contributions of PM for the German capital Berlin. The model was applied to a 3-year time frame from January 2016 to December 2018 for which we quantified the urban sector contributions as well as the long-range transport contributions using a labelling approach. As CTMs do not fully explain the observed PM concentration and

variability (e.g., Belis et al., 2020), special emphasis is put on the identification of shortcomings. For comparison of modelled urban increments to observational data we adopted the Lenschow approach (Lenschow et al., 2001). Finally, we discuss our findings in comparison to earlier studies oriented at source attribution for Berlin or model-based source apportionment.

II.2 Methodology

II.2.1 Chemical transport modelling

In this paper, we apply the LOTOS-EUROS CTM version 2.1 to investigate the origin of PM in Berlin during a 3-year time frame from January 2016 to December 2018. LOTOS-EUROS is a 3D chemistry transport model (CTM) developed by the Netherlands Organization for Applied Scientific Research (TNO) and partners including the Freie Universität Berlin (FUB, Germany). The LOTOS-EUROS CTM is an Eulerian grid model, which was originally developed to simulate ozone and smog concentration levels in the lower troposphere in Europe. In the vertical a mixed-layer approach is applied (Manders et al., 2017) using 5 terrain following layers extending up to 5 km above sea level (orography). In this study we set up a European domain (D1) with a horizontal resolution of 0.5° (longitude) and 0.25° (latitude) corresponding to about $28 \times 32 \text{ km}^2$. An increased resolution is obtained for a nested domain (D2) covering Germany and Poland with 0.125° (longitude) and 0.0625° (latitude), approximately $7 \times 8 \text{ km}^2$. Poland was included in the high-resolution domain as the transboundary

II. Source attribution of particulate matter in Berlin

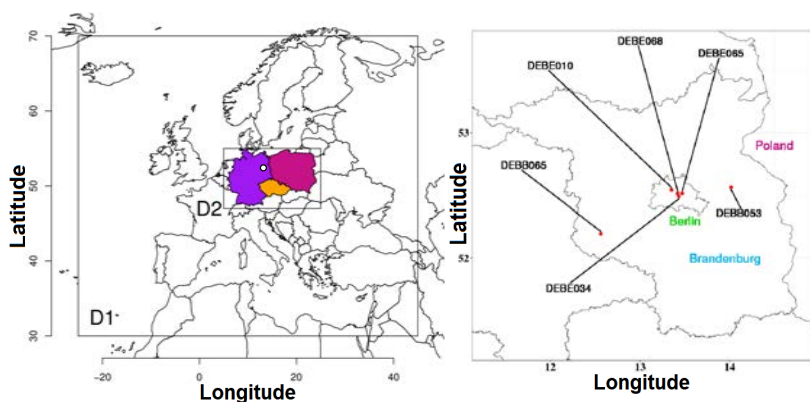


Figure II.1: The D1 domain for Europe and therein the D2 domain for Germany/ Poland/ Czech Republic, the position of Berlin is indicated with a white circle (left). Illustration of the measurement locations in Berlin and the surrounding federal state of Brandenburg (right). The colours correspond to the related labels.

component is of specific interest for the local policy (details see [Figure II.1](#)). The model describes the fate of anthropogenic primary particulate matter (ppm), including a separation of elemental carbon (EC) and organic material (POM). The formation of secondary inorganic aerosol (SO_4 , NO_3 and NH_4) from its precursor gases and the emissions of (semi-) natural emissions of sea salt and mineral dust are also described. The model follows a bulk approach for the fine (f) and coarse (c) aerosol mode (a). The total particulate matter mass is computed from the individual model compounds:

$$\begin{aligned}
 PM_{2.5} = & SO_{4_{af}} + NH_{4_{af}} + NO_{3_{af}} \\
 & + EC_f + POM_f + PPM_f + 3.26 \\
 & * Na_f + Dust_f
 \end{aligned}
 \tag{II.1}$$

$$\begin{aligned}
 PM_{10} = & PM_{2.5} + NO_{3_{ac}} + POM_c \\
 & + PPM_c + 3.26 * Na_c + Dust_c
 \end{aligned}
 \tag{II.2}$$

The LOTOS-EUROS model adopts sodium as the preserved sea salt tracer, and its concentration is multiplied by a factor 3.26 to arrive at the total sea salt contribution.

Meteorological data were taken from ECMWF (European Centre for Medium-range Weather Forecasts). The model configuration, except the domain definition, resembles the set-up used within the regional ensemble of the Copernicus Atmospheric Monitoring Service (CAMS). Within CAMS LOTOS-EUROS is applied to provide operational air quality forecasts and analyses for Europe ([Marécal et al., 2015](#)) including source apportionment information for major cities ([Pommier et al., 2020](#)). For a more detailed description of LOTOS-EUROS we refer to [Manders et al. \(2017\)](#).

The gas-phase chemistry is described by the TNO CBM-IV scheme, a modified version based on the development by [Whitten et al. \(1980\)](#). Aerosol chemistry is formulated within the thermodynamic equilibrium module

ISORROPIA2 (Fountoukis and Nenes, 2007). Coarse mode nitrate formation is modelled dynamically through a surface reaction on sea salt. Sea salt emissions are parameterized using two schemes for the fine and coarse mode (Monahan, 1986; Mårtensson et al., 2003). Resuspended mineral dust from road-traffic is parameterized using constant emission factors and depends on the traffic intensity in the respective grid cell (Schaap et al., 2009). In a similar vein, the agricultural land management emissions are parameterized using constant emission factors per activity and are allocated over the months in which the activity typically occur (Schaap et al., 2009). Both sources are switched off in case of rain. Windblown dust is parameterized by sand blasting schemes (Manders et al., 2017), but normally do not impact Berlin. Forest fire emissions were taken from the CAMS global fire assimilation system (Kaiser et al., 2012). Dry deposition fluxes for reactive gases are calculated using the resistance approach as implemented in the DEPAC (DEPosition of Acidifying Compounds) module (Kruit et al., 2012). Particle deposition follows the scheme of Zhang et al. (2001). Wet deposition is parameterized as described in Banzhaf et al. (2012). Secondary organic aerosol formation was neglected, as the VBS-module was not yet implemented in the source apportionment approach of the model.

The annual total emissions were based on the official country reporting to the UNECE and the EU for 2017. Except for Germany, emissions were gridded based on the CAMS reporting (Copernicus Atmospheric Monitoring System) database. For Germany, the gridded emissions were obtained from

the GrETa system (GRETA - Gridding Emission Tool for ArcGIS v1.1; Schneider et al. (2016)). The totals are apportioned to monthly, daily, and hourly amounts by sector-specific time factors. For CO and VOC temperature-dependent factors were used (Manders et al., 2017). The official emissions for residential wood combustion (RWC) were replaced by a scientific bottom-up inventory for Europe (van der Gon et al., 2015). This contains a consistent set of emission factors for wood combustion and includes the impact of condensable material (van der Gon et al., 2015). Overall, the RWC emissions in this study were by a factor of 2–3 higher than the officially reported. To incorporate the dependency of heating demand on temperature the temporal variability of RWC emissions was calculated using heating degree days. The heating degree demand was calculated relative to a reference temperature (18 °C). We used a fraction of 20 %, for emissions not related to heating following Mues et al. (2014).

II.2.2 Source attribution

To assess the contribution of different source sectors and regions we applied the source apportionment module implemented in the LOTOS-EUROS CTM (Hendriks et al., 2013; Kranenburg et al., 2014). Through a labelling procedure the origin of species is traced through the process descriptions for the transport and chemical reactions (Kranenburg et al., 2014). The labelling approach works for primary, inert aerosol tracers and chemically tracers in which a C, N (oxidized and reduced) or S atom is conserved. The validation of this module was done in (Kranenburg et al., 2013) in dedicated

II. Source attribution of particulate matter in Berlin

Table II.1: Labelled source regions (left) and source sectors (right).

Labelled regions	Labelled sectors
Berlin	Traffic
Brandenburg	Households
Rest of Germany	Industry & Energy
Poland	Agriculture
Czech Republic	Rest
Others	
Natural	Natural
Boundary	Boundary

experiments. The module was applied to PM (episodes) (Hendriks et al., 2013; Hendriks et al., 2015; Timmermans et al., 2017; Timmermans et al., 2020) and nitrogen oxides (Schaap et al., 2013; Curier et al., 2014). The source attribution for ammonium nitrate is calculated as a weighted mean of the source sectors contributing to the reduced and oxidized N-atom (in i.e., ammonium and nitrate) on a molar basis (Hendriks et al., 2013).

We defined 32 combinations of sectors and regions to be tracked. The 5 sectors we considered are the main source sectors for particulate matter (traffic, households, industry & energy, agriculture) and all remaining sectors combined as rest. To quantify the urban, regional, domestic, and transboundary contributions we separated 6 geographic regions: Berlin, Brandenburg, Rest of Germany, Poland, Czech Republic and all remaining countries as "other countries". In addition, the natural and boundary (incl. initial) conditions were traced (see Table II.1).

II.2.3 Monitoring data

The present work focuses on a dataset containing daily PM_{10} and $PM_{2.5}$ mass concentrations for 6 selected air quality monitoring sta-

tions of the federal states of Berlin (4) and Brandenburg (2). For comparison reasons one urban traffic station is included additionally. The data were provided by the German Federal Environmental Agency (Umweltbundesamt, UBA) and the Senat of Berlin. Classifications, geographic coordinates, component, and short names of the measurement stations are listed in Table II.2.

The observed data provides no information about the source region and/ or the source sectors. This leads to the Lenschow approach, where rural and urban stations are selected and can be investigated separately and/ or in a combined manner. As the approach can be also applied for modelled data, the modelled spatial gradient can be compared to the measured spatial gradient. Statistical indicators for the model performance were calculated in a common way (e.g., RMSE, BIAS, MEAN). For the correlation coefficient the Pearson correlation was used. When the spatial mean of a specific station type was calculated, the daily mean values were used. Suburban sites pose a challenge to the model, as the stations are located close to the city border. Grid cells which include these stations may be affected by substantial urban emissions leading to an overestimation of the rural to suburban increment. Hence, we mainly focus our analysis on the gradients between rural and urban background concentrations. The RB stations investigated are located west and east of the city, thus they show mean values for the RB, normally only upwind stations should be used. Meteorological data (such as wind and precipitation) were taken from the WMO station Berlin-Dahlem.

II.2.4 Investigation domain and periods

In this study we focus on the capital of Germany with around 4 million inhabitants. Berlin is located in the north-eastern part of Germany and surrounded by the federal state of Brandenburg. The closest neighbouring country, Poland, is about 60 km east of the city. The climate is characterized by westerlies, bringing maritime air towards Berlin while during some episodes preferably in midsummer and winter easterlies can prevail for several days up to weeks due to a continental high. For Berlin, the long-term annual precipitation amount of about 600 mm and mean temperatures of around 13 °C were observed. Prevailing wind directions are westerlies (~75 %, NW to SW) and easterlies (~25 %, NE to SE), with easterly wind directions mainly occurring during the winter season. Apart from a large power plant in the western part of the city, there is no major industry in the city or in the surrounding area.

II.3 Results

II.3.1 Observed levels for the investigation period

We provide an overview of the observed annual mean particulate matter mass concentration for 2016 to 2018 following the Lenschow's incremental approach (Figure II.2). The concentrations are classified by sub-categories of the UBA measurement network for the rural background (RB, light grey), urban background (UB, dark grey) and urban traffic (UT,

Table II.2: Measurement sites in Berlin and Brandenburg containing UBA-code, location, street, shortcut, longitude, latitude, characteristic, PM₁₀ and PM_{2.5} observed for 2018. B=Berlin, BB=Brandenburg; UT=Urban Traffic, UB=Urban Background, RB=Rural Background.

Station Code	Region & district	Address	Acronym	Geogr. latitude	Geogr. longitude	Type	PM ₁₀ [$\mu\text{g m}^{-3}$]	PM _{2.5} [$\mu\text{g m}^{-3}$]
DEBE010	B Wedding	Amrumer/ Limburger Str.	BEAMR	52.542744	13.349119	UB	21.43	15.07
DEBE034	B Neukölln	Nansenstraße 10	BENAN	52.489451	13.430844	UB	24.42	16.34
DEBE065	B Friedrichshain	Frankfurter Allee (86b)	BEFRA	52.514072	13.469931	UT	27.77	17.56
DEBE068	B Mitte	Brückenstr. 6	BEBRU	52.513606	13.418833	UB	22.74	15.44
DEBB053	BB Hasenholz	15377 Buckow	BBHAS	52.563835	14.015252	RB	19.33	14.11
DEBB065	BB Lnette (Belzig)	Die hohe Heide/Feldstr.	BBLUE	52.194225	12.561389	RB	15.03	12.01

II. Source attribution of particulate matter in Berlin

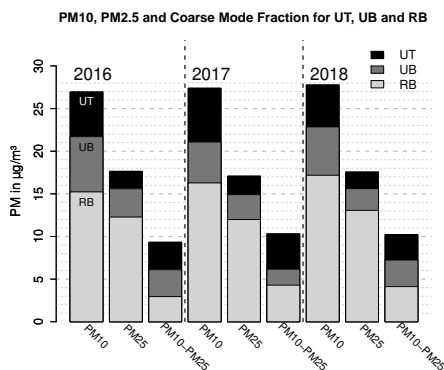


Figure II.2: Incremental Lenschow approach for observed data. For each UBA sub-category, the corresponding mean was calculated over the associated stations. Annual mean PM concentrations and increments ($\mu\text{g m}^{-3}$) between the rural background (RB, light grey), urban background (UB, dark grey) and urban traffic (UT, black) concentrations. For each year (2016, left; 2017, centre; 2018, right), a further subdivision into the three shares PM_{10} (left), $\text{PM}_{2.5}$ (centre) and the coarse mode fraction ($\text{PM}_{10}-\text{PM}_{2.5}$, right) was made.

black). We provide the overview for PM_{10} , $\text{PM}_{2.5}$ and the coarse mode fraction (PM_{CO} , difference between $\text{PM}_{10}-\text{PM}_{2.5}$) for 2016 (left), 2017 (middle) and 2018 (right), separately. The share for the urban background is the difference between the concentration in the urban background and in the rural background and is called the urban increment. The same applies to the urban traffic and is accordingly referred to as the traffic increment.

The overall annual mean PM_{10} concentration at urban traffic sites was about $27\text{--}28 \mu\text{g m}^{-3}$. The $\text{PM}_{2.5}$ level was about $17 \mu\text{g m}^{-3}$, and the coarse mode was about $10 \mu\text{g m}^{-3}$. The annual mean PM_{10} concentration in the urban background is in the range of $21\text{--}23 \mu\text{g m}^{-3}$, while that of $\text{PM}_{2.5}$ is about $15 \mu\text{g m}^{-3}$. Hence, the coarse mode contributes about $6\text{--}7 \mu\text{g m}^{-3}$.

For $\text{PM}_{2.5}$ the rural background ($12\text{--}13 \mu\text{g m}^{-3}$) is contributing about three quarters of the urban background concentrations, whereas for the coarse mode the relative contribution of the rural background is smaller, about 50% ($3\text{--}4 \mu\text{g m}^{-3}$). For PM_{10} the rural background concentration is measured to be about $15\text{--}17 \mu\text{g m}^{-3}$. For $\text{PM}_{2.5}$ the urban increment ($\sim 3 \mu\text{g m}^{-3}$) is slightly larger than the observed traffic increment ($\sim 2 \mu\text{g m}^{-3}$). A low variability from year to year can be seen for annual-averaged levels of the $\text{PM}_{2.5}$ rural background, urban increment, and traffic increment. For the coarse mode, the urban background and traffic increments are similar ($\sim 3 \mu\text{g m}^{-3}$ each).

Figure II.3 shows daily mean particulate matter mass concentrations averaged over all urban background stations from 2016 to 2018. The PM_{10} seasonal cycle reflects a pattern common to many cities in Europe. Largest PM_{10} concentrations are observed during wintertime, while smallest concentrations occur during summer. During episodes in winter, daily mean PM_{10} concentrations between 70 and $100 \mu\text{g m}^{-3}$ were observed, whereas concentrations in summer hardly exceeded $40 \mu\text{g m}^{-3}$. $\text{PM}_{2.5}$ shows a stronger seasonal cycle than PM_{10} as PM_{10} concentration episodes in winter consist mainly of fine material. The coarse mode shows the opposite seasonal cycle with maximum contributions during summer and early fall with enhanced fractions throughout the year at traffic and urban background stations.

Figure II.4 shows the observed PM_{10} daily concentrations for station DEBE034 with respect to the prevalent wind direction. During 2016 and 2017 the westerly wind directions (from NW to SW) dominate associated with low

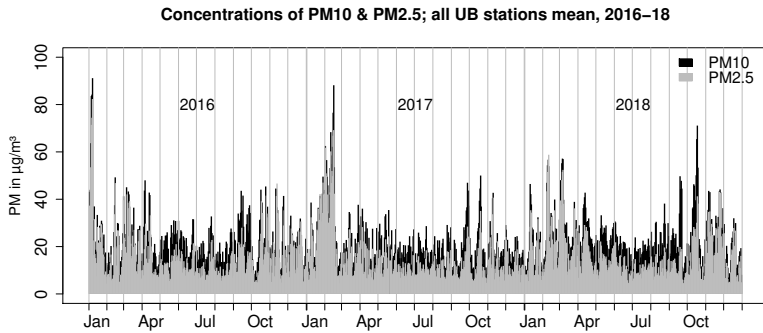


Figure II.3: PM_{10} and $\text{PM}_{2.5}$ mass concentration for the urban background (UB) stations (DEBE010, DEBE034, DEBE068) for 2016 to 2018. Observations (gravimetric) are shown as daily mean values with missing values are considered as no data available.

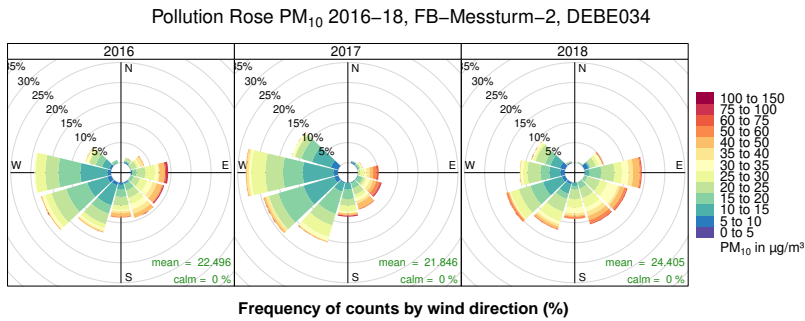


Figure II.4: Observed mass concentration for PM_{10} of the urban background (UB) station Berlin (DEBE034, Nansenstr.) for daily data (gravimetric) and wind measurement data from the wind gauge mast of the FU-Berlin for 2016 to 2018. The breaks for PM_{10} concentrations are not equally distributed, missing values are considered (this causes the sum of all contributions to be below 100 % for some cases because of the missing values).

to medium PM_{10} concentrations ($5\text{--}35 \mu\text{g m}^{-3}$). In contrast, up to 1/4 of the weather situations of the days with easterlies (from NE to SE) show concentrations above the daily limit value (up to more than $100 \mu\text{g m}^{-3}$). These situations are often associated with cold temperatures, low wind speeds and stagnation conditions with shallow boundary layers in winter or spring. 2016 and 2017 can be considered as typical for the investigation period and correspond to the common climatological conditions.

The meteorological conditions in 2018 on the other hand were atypical as easterlies were present for almost half of the year ($\sim 40\%$) and westerlies were less apparent ($\sim 45\%$). A prolonged drought characterized by low amounts of precipitation from mid-April until the end of the year occurred. Consequently, this year had the lowest annual precipitation (393 mm) on record since the beginning of measurements in Berlin/ Brandenburg in 1881, whereas the long-term mean (1961–1990) is 557

mm (DWD, 2020). During 2018 the easterly wind directions were associated with more moderate PM_{10} mass concentrations than the previous years as these easterlies occurred in the summer.

II.3.2 Model performance

To assess the robustness of the applied model to simulate PM concentrations, we compared the LOTOS-EUROS CTM results for Berlin to daily observations at UB and RB monitoring stations. Figure II.5 shows the observed and modelled $\text{PM}_{2.5}$ timeseries in the form of a bar chart and Figure II.6 shows the corresponding scatter plots. A selection of statistical measures (mean values, correlation, normalized RMSE and BIAS) for PM_{10} , $\text{PM}_{2.5}$ and PM_{CO} is presented in Table II.3. While the model can reproduce a fair part of the temporal variability of $\text{PM}_{2.5}$ concentrations throughout the year, it is not able to catch major amplitudes. The underestimation is particularly visible in summer and early autumn while wintertime peaks are better reproduced. The model performs best during spring season in capturing concentration variability and amplitude. Also, the concentration level increase starting in early autumn is well reproduced by the model. During winter, the modelled $\text{PM}_{2.5}$ concentration averaged over all UB sites captures 75 % of the observed (PM_{10} : 74 %) concentration, while during summer only 57 % (PM_{10} : 53 %) is reproduced. The annual statistics show the underestimation of the model for PM in a negative BIAS at all stations (by 13–48 % for the normalized BIAS). For all fractions - PM_{10} , $\text{PM}_{2.5}$ and PM_{CO} - the underestimation is more distinct at UB stations than at RB stations and gen-

Table II.3: Model performance statistics for all monitoring stations and the three-year period of 2016-2018. Shown are the concentrations for PM_{10} , $\text{PM}_{2.5}$ and the coarse mode fraction (PM_{CO}) for observed and modelled data: the mean values, the correlation (Pearson), the normalized RMSE (root mean squared error), the normalized BIAS (deviation of the mean). The normalization was done by dividing by the respective observational mean.

Station No.	site	Mean PM_{10}		Mean $\text{PM}_{2.5}$		Mean PM_{CO}		Correlation			Normalized RMSE			Normalized BIAS		
		OBS	SIM	OBS	SIM	OBS	SIM	PM_{10}	$\text{PM}_{2.5}$	PM_{CO}	PM_{10}	$\text{PM}_{2.5}$	PM_{CO}	PM_{10}	$\text{PM}_{2.5}$	PM_{CO}
DEBB053	RB	17.54	11.68	13.32	8.75	4.23	2.93	0.58	0.80	0.08	0.62	0.58	1.30	-0.33	-0.34	-0.31
DEBB065	RB	14.85	11.52	11.42	8.57	3.42	2.96	0.68	0.81	0.12	0.52	0.52	0.92	-0.22	-0.25	-0.13
DEBE010	UB	20.73	13.07	14.95	9.52	5.91	3.55	0.69	0.78	0.13	0.3	0.69	0.93	-0.37	-0.44	-0.40
DEBE034	UB	22.89	14.18	16.10	10.60	6.91	3.58	0.61	0.75	0.15	0.55	0.54	1.00	-0.38	-0.33	-0.48
DEBE068	UB	22.03	14.96	15.47	11.01	6.69	3.95	0.59	0.72	0.17	0.53	0.52	0.96	-0.32	-0.28	-0.41

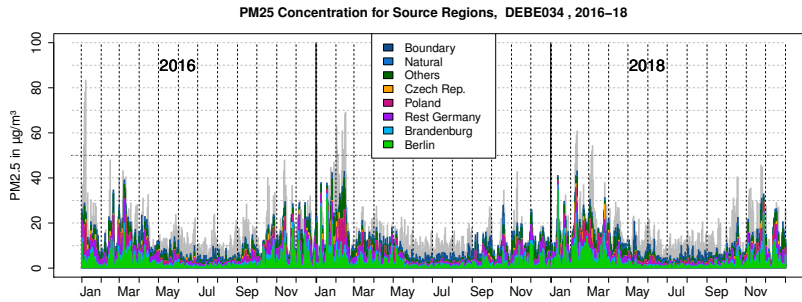


Figure II.5: Time series of the $\text{PM}_{2.5}$ mass concentration for Berlin (UB station DEBE034) for 2016 to 2018. Observations are shown in grey and modelled sector (A) and regional (B) contributions are colour coded.

erally larger during episodes. Furthermore, the correlation coefficient reveals that the model is better in capturing the variability in $\text{PM}_{2.5}$ concentrations than in those of PM_{10} . There is one RB station (DEBB065) which is slightly better simulated than all other stations, especially for $\text{PM}_{2.5}$.

When looking at the coarse mode material, modelled summertime concentration levels reflect only about fifty percent of those observed. In numbers, at RB (UB) stations the model captures 57 % (47 %) of the observed mass during summertime while during wintertime 132 % (73 %) of the observed mass at RB (UB) stations is modelled by LOTOS-EUROS. The mean observed summertime coarse mode urban increment of about $2.5 \mu\text{g m}^{-3}$ is with $0.6 \mu\text{g m}^{-3}$ considerably underestimated by the model. This is also valid for wintertime with an observed urban increment of $2.8 \mu\text{g m}^{-3}$ compared to the modelled urban increment of $0.8 \mu\text{g m}^{-3}$. The BIAS, correlation coefficients and normalized RMSE show that the coarse mode is largely underestimated, and that the temporal variability is poorly explained by the model.

The $\text{PM}_{2.5}$ and coarse mode urban increments (modelled and observed) are shown in Figure II.7. To suppress short-term fluctuations a running mean of 7 days was applied. The observed increments are shown in solid lines, while those for the simulations are dashed (colours for each year: 2016: black; 2017: red; 2018: blue). For $\text{PM}_{2.5}$ (upper panel) the observed urban increment shows a clear seasonality with increased variability from autumn to spring with values often ranging between 5 and $10 \mu\text{g m}^{-3}$. During summertime typical values are below $5 \mu\text{g m}^{-3}$ and the time series shows rather limited fluctuations. Only a few periods show a negative urban increment implying that concentrations in the rural background were higher than in the urban background. A pronounced and prolonged enhancement of the urban increment was observed from mid-January to mid-February 2017 when Berlin was hit by a PM episode during stagnant easterly flow which will be further discussed below. The modelled urban increment shows lower variability than the observed and with only few exceptions underestimates the observed

II. Source attribution of particulate matter in Berlin

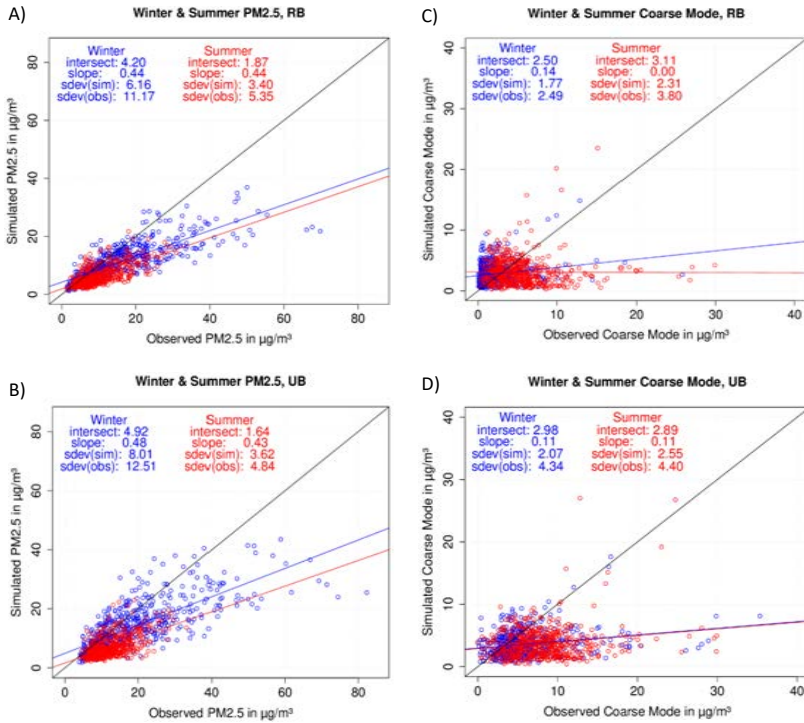


Figure II.6: Scatterplots with linear regression for 2016 to 2018 of the PM_{2.5} mass concentration at rural (A) and urban (B) sites and the coarse mode fraction at rural (C) and urban (D) sites.

increment throughout the investigation period. While the model does capture the seasonal variation with higher amplitudes from autumn to spring the model underestimation is most distinct during summertime when the modelled urban increment is almost non-existent.

For the coarse mode (Figure II.7, lower panel) the seasonal signal of the observed urban increment is less pronounced than those of PM_{2.5}. The variability between the years is large, indicating that the variability is mainly driven by synoptic meteorological variability. An increase in variability and amplitude can be found during springtime and early autumn. Furthermore, negative urban increments of the coarse

mode are more frequently observed compared to PM_{2.5}, illustrating sources of course material in the rural surrounding of Berlin. During the PM episode in early 2017 the coarse mode shows a negative urban increment. As expected from the large bias for the coarse mode, the modelled urban increment is almost non-existent throughout the seasons for all years which reveals a distinct discrepancy between modelled and observed increment. A potential reason for this underestimation is dust resuspension, which will be discussed below.

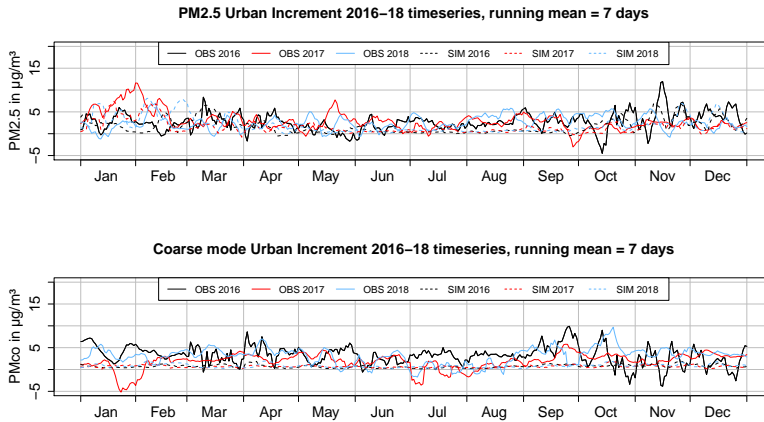


Figure II.7: Timeseries of the $\text{PM}_{2.5}$ (upper panel) and coarse mode (lower panel) urban increments for 2016–2018. The observed and modelled data were smoothed by using a 7-day running mean.

II.3.3 Source attribution for particulate matter in Berlin

Although the model systematically underestimates the observed $\text{PM}_{2.5}$ (and PM_{10}) levels, in this section we present a sectoral and regional source attribution for $\text{PM}_{2.5}$ and PM_{10} of the Berlin agglomeration area. Since the episodes with the highest particulate matter concentrations occur during the fine mode dominated cold season and the model performance is best for $\text{PM}_{2.5}$, our main focus is on the source attribution of $\text{PM}_{2.5}$. The sectoral/ regional source attribution provides insights to the most important source sectors/ regions contributing to Berlin's PM mass concentration.

An overview of the annual mean contributions of source sectors and regions for Berlin and the rural background is also presented in Table II.4. For Berlin the (3 year-) mean modelled urban background $\text{PM}_{2.5}$ concentrations for

the 2016 to 2018 ($10.4 \mu\text{g m}^{-3}$) are explained by households ($3.2 \mu\text{g m}^{-3}$), industry & energy ($2.0 \mu\text{g m}^{-3}$), boundary ($1.4 \mu\text{g m}^{-3}$), agriculture ($1.3 \mu\text{g m}^{-3}$), traffic ($1.3 \mu\text{g m}^{-3}$), rest ($0.7 \mu\text{g m}^{-3}$) and natural ($0.5 \mu\text{g m}^{-3}$). The modelled annual mean urban increment for $\text{PM}_{2.5}$ is mainly composed of households ($1.6 \mu\text{g m}^{-3}$) and traffic ($0.5 \mu\text{g m}^{-3}$). During the whole period the most important contribution to PM_{CO} comes from (semi-)natural sources, i.e., sea salt and dust. In the rural background natural sources contribute $1.6 \mu\text{g m}^{-3}$ on average to PM_{CO} . Agriculture provides a secondary contribution in the rural background, whereas in the urban background the traffic contribution ($0.8 \mu\text{g m}^{-3}$) is the second largest source sector. The modelled traffic contribution in the city is largely due to urban traffic as the modelled traffic increment is $0.55 \mu\text{g m}^{-3}$. The remaining sectors only show small modelled increments ($\pm 0.1 \mu\text{g m}^{-3}$) for PM_{CO} . As $\text{PM}_{2.5}$ is a large fraction of PM_{10} ,

II. Source attribution of particulate matter in Berlin

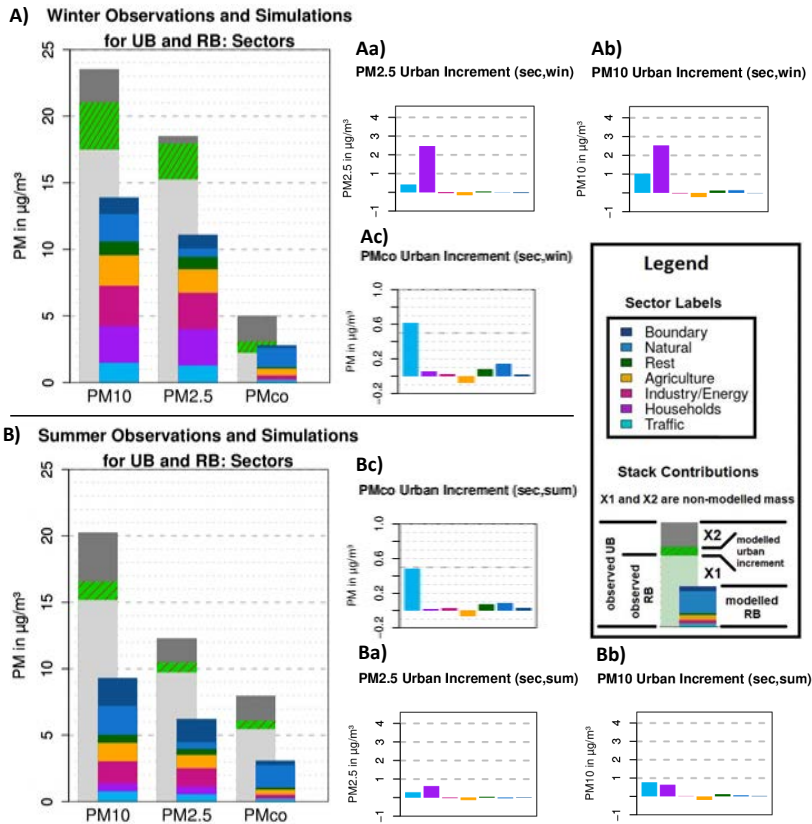


Figure II.8: Overview of observed and modelled concentrations and the increments for PM₁₀, PM_{2.5} and PM_{CO} (coarse mode fraction). The observed rural background levels provided in light grey. The urban increment is provided in dark grey. As the modelled increments underestimate the observations we provide the modelled urban increment as the green hatched in this bar. The modelled RB sectors contributions are indicated in the coloured bar. The modelled urban increment is detailed per sector in the separate graphs on the right side of the figure (Aa/ Ba for PM_{2.5}, Ab/ Bb for PM₁₀ and Ac/ Bc for the coarse mode, A for winter and B for summer).

the PM₁₀ source attribution looks similar to PM_{2.5} throughout the year with respect to the relative shares, but with enhanced natural contribution derived from the coarse mode. The sectors contributing to rural background PM₁₀ during winter show on average a fairly even distribution over the sectors industry & energy (2.9 $\mu\text{g m}^{-3}$), household (2.7 $\mu\text{g m}^{-3}$), agriculture (2.1 $\mu\text{g m}^{-3}$) and natural (2.0 $\mu\text{g m}^{-3}$) and slightly

lower contributions from traffic (1.4 $\mu\text{g m}^{-3}$). Remaining sources play a minor role. The PM₁₀ urban increment combines the PM_{2.5} and coarse mode contributions from households (winter: 2.5 $\mu\text{g m}^{-3}$) and traffic (winter: 1.0 $\mu\text{g m}^{-3}$).

From a geographical perspective the main source area for the PM_{2.5} in Berlin is Germany (5.1 $\mu\text{g m}^{-3}$) itself, followed by the contributions from

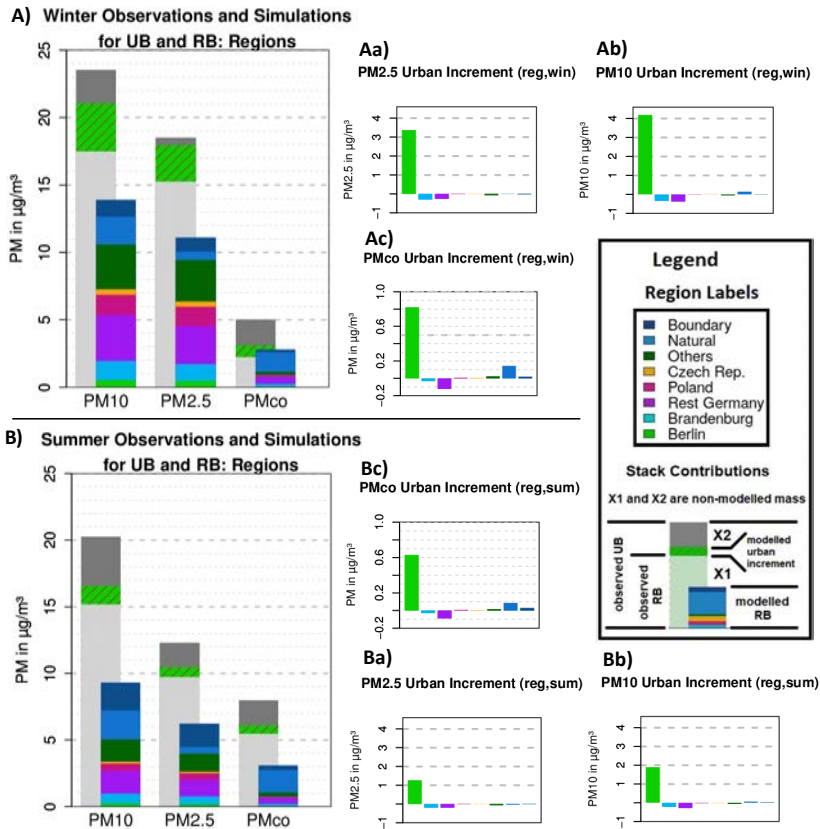


Figure II.9: Same as in Figure II.8, but for regional contributions.

transboundary transport ($3.4 \mu\text{g m}^{-3}$). The German contributions can be separated into Berlin ($2.6 \mu\text{g m}^{-3}$), Brandenburg ($0.7 \mu\text{g m}^{-3}$) and remaining states of Germany ($1.8 \mu\text{g m}^{-3}$), which reveals that on average the city contribution slightly exceeds the contribution of the remaining German sources. The modelled contribution from foreign countries to the urban background is about as large as that of Berlin and Brandenburg combined. On average, the transboundary contribution exceeds those of domestic contribution in air masses advected to Berlin. Note that Berlin also contributes to the av-

erage rural background ($\sim 0.4 \mu\text{g m}^{-3}$). About one third of foreign shares can be attributed to Germany's neighbouring countries Poland ($1 \mu\text{g m}^{-3}$) and Czech Republic ($0.3 \mu\text{g m}^{-3}$). The remaining foreign contribution ($2.2 \mu\text{g m}^{-3}$) strongly correlate to the contributions of Poland and Czech Republic, highlighting the importance of transport of PM from further (south-)east. Throughout the year the geographic origin remains similar in terms of relative contributions.

For PM_{CO} the importance of long-range transport is lower. The modelled contribution of German sources exceeds

those of the transboundary contribution, which is explained by the shorter lifetime of the coarse mode. The coarse mode fraction in the RB has largest contributions from natural ($1.6 \mu\text{g m}^{-3}$) and the rest of Germany ($0.5 \mu\text{g m}^{-3}$), while the shares of the remaining regions are forming additional $0.9 \mu\text{g m}^{-3}$. The geographic origin contributions for PM_{10} are very similar to that of $\text{PM}_{2.5}$ with the same observations regarding natural contributions as discussed above.

The urban increment ($\text{PM}_{2.5}$, annual mean: $1.7 \mu\text{g m}^{-3}$) is composed of two terms: 1) a positive increment induced by emissions in Berlin ($+2.3 \mu\text{g m}^{-3}$), and 2) a negative increment from remaining areas ($-0.6 \mu\text{g m}^{-3}$). The negative increments mean that the absolute contribution in the rural background is larger than in the city. This can be explained by a) the deposition of PM transported into the city from outside and b) the further dilution of nearby rural emissions when entering the city. Besides the positive increments explained by households and traffic emissions there is a small increment labelled natural ($\sim 0.1 \mu\text{g m}^{-3}$ annual mean), which is mainly associated with sea salt in 2016 and 2017, while in 2018 it additionally contains continental dust. This natural labelled increment results rather from the configuration of the measurement locations than from an urban source since the urban stations are slightly closer to the coast.

Figure II.8 and Figure II.9 provide a graphical overview of the source apportioned rural background concentration and urban increments. The figure is separated into two panels: the upper one highlights the winter period, the lower one the summer season. The

figure is split into several subfigures. In Figure II.8A and Figure II.8B the observational data for PM_{10} , $\text{PM}_{2.5}$ and the coarse mode is provided (grey for RB and dark grey for UB locations), while the modelled urban increment with an offset relative to the observed is shown (green, hatched). In front of the observed RB, the modelled RB (colour-shaded) is shown. Since the urban increment is the difference between the urban and rural background, subfigures Aa/ Ba ($\text{PM}_{2.5}$), Ab/ Bb (for PM_{10}) and Ac/ Bc (coarse mode) contain the increments for the absolute sector contributions. Negative contributions in the urban increment can appear (e.g., agriculture) due to larger modelled concentration outside the city than (attributed to the same sector) inside the city. The absolute contributions of the source sectors households and industry & energy show the largest variation in time. The contribution from households in the urban background dominates during the cold season (October–March) with mass concentrations of $5.2 \mu\text{g m}^{-3}$, followed by industry & energy ($2.7 \mu\text{g m}^{-3}$), traffic ($1.6 \mu\text{g m}^{-3}$) and agriculture ($1.4 \mu\text{g m}^{-3}$). During the warm season (April–September) the order of importance shifts with larger relative contributions for e.g., industry & energy ($1.5 \mu\text{g m}^{-3}$). During the warm season, the absolute contribution of the remaining source sectors is roughly halved, except for households showing a fifth of their winter contributions. Hence, in summer the largest contributions for UB $\text{PM}_{2.5}$ derive from industry & energy ($1.4 \mu\text{g m}^{-3}$), households ($1.2 \mu\text{g m}^{-3}$), agriculture ($0.9 \mu\text{g m}^{-3}$), and traffic ($0.8 \mu\text{g m}^{-3}$).

The modelled timeseries allows to address the source attribution on

a daily basis. Figure II.5 includes the contributions simulated by the LOTOS-EUROS CTM for source sectors (Figure II.5A) and source regions (Figure II.5B) at station BENAN representing the urban background of Berlin. The sectoral contributions contain traffic (light blue), households (purple), industry/ energy (dark pink), agriculture (orange), rest (green), natural (blue) and boundary (dark blue). For the regional contributions, the labels are defined as: Berlin (light green), Brandenburg (light blue), rest of Germany (purple), Poland (dark pink), Czech Republic (orange), others (green), natural (blue) and boundary (dark blue). From day-to-day and for individual periods/ episodes the (relative) source contributions and dominant sectors may differ largely from the mean. For example, during certain peaks in January 2018 the Berlin share rises up to 80 %. More frequently, Poland contributes an important fraction of total $\text{PM}_{2.5}$ mass during wintertime high-concentration episodes, with contributions up to $1/3^{\text{rd}}$ of the total modelled mass (e.g., January 2016, January/ February 2017, or March 2018). Zooming into the situation at the beginning of 2017, the variability induced by meteorological conditions is nicely illustrated. At the beginning of the episode the model estimates high Berlin contributions for $\text{PM}_{2.5}$ (with about $34 \mu\text{g m}^{-3}$) during the stagnant conditions until the weather regime changed to more diluting conditions (increased wind speeds and planetary boundary layer height). Afterwards a continental high-pressure system dominated the weather situation causing easterly flows towards Berlin. During this period the contributions from Poland, Czech Republic and remaining foreign countries (= others)

take over the dominating share with a combined contribution of $2/3^{\text{rd}}$ of the simulated mass. During this phase the energy/ industry contribution is relatively enlarged as well, although households remain the most important sector. The episode lasted until mid-February when a trough took over control of the weather causing the transport of maritime air from the north Atlantic towards Berlin. As a result, the contributions from Poland, Czech Republic and others diminished and contributions from German sources dominated the picture again.

Table II.4: Mean labelled concentrations for sectors and regions for PM_{2.5} and PM_{CO} for RB, UB and the urban increment.

Source	Label	UB ($\mu\text{g m}^{-3}$)		RB ($\mu\text{g m}^{-3}$)		Urban Increment ($\mu\text{g m}^{-3}$)		
		PM _{2.5}	PM _{CO}	PM _{2.5}	PM _{CO}	PM _{2.5}	PM _{CO}	
Sector	Traffic	1.25	0.77	0.90	0.22	0.35	0.55	
	Housholds	3.21	0.05	1.67	0.02	1.54	0.04	
	Industry & Energy	2.01	0.31	2.05	0.29	-0.03	0.02	
	Agriculture	1.25	0.38	1.38	0.45	-0.14	-0.07	
	Rest	0.74	0.20	0.70	0.12	0.04	0.08	
	Natural	0.54	1.68	0.56	1.56	-0.02	0.11	
	Boundary	1.38	0.30	1.40	0.28	-0.02	0.02	
	Sum:	10.38	3.69	8.66	2.95	1.72	0.75	
	Region	Berlin	2.62	0.78	0.31	0.06	2.31	0.72
		Brandenburg	0.68	0.13	0.92	0.16	-0.25	-0.03
		Rest Germany	1.80	0.41	2.03	0.52	-0.23	-0.11
Poland		0.95	0.08	0.96	0.07	-0.01	0.01	
Czech Republic		0.25	0.02	0.25	0.02	0.00	0.00	
Others		2.15	0.29	2.22	0.27	-0.07	0.02	
Natural		0.54	1.68	0.56	1.56	-0.02	0.11	
Boundary		1.38	0.30	1.40	0.28	-0.02	0.02	
Sum:		10.38	3.69	8.66	2.95	1.72	0.75	

II.4 Discussion and conclusion

In this paper we conducted an air pollution simulation with the LOTOS-EUROS CTM, to address the source attribution of particulate matter (PM) for the Berlin agglomeration area as a first step towards defining the relevant brute force calculations for the determination of effectivity. The modelled timeseries allows to address the source attribution on a daily basis. The (relative) source contributions and dominant source sectors vary strongly between episodes. On average, the households and industry & power contribute the largest share to the modelled PM_{2.5} levels in Berlin. Domestic contributions on average exceed those of transboundary transport, of which the city contribution slightly exceeds the contribution of the remaining German sources. During wintertime episodes the importance of source regions in Poland and further east was highlighted. The source attribution for PM₁₀ looks similar with respect to the relative shares, except that the natural contribution is enhanced compared to that in PM_{2.5}.

The evaluation of the model against UBA measurements has shown an overall underestimation for PM. Overall, the fine mode is better reproduced by the model than the coarse mode. The systematic underestimation of modelled PM is a feature that has been pointed out in earlier studies using LOTOS-EUROS (Weijers et al., 2010; Hendriks et al., 2013; Manders et al., 2017) and that is shared by many other chemistry transport models (Marécal et al., 2015; Bessagnet et al., 2016; Potier et al., 2019; Belis et al., 2020; Pommier et al., 2020). In previous studies the missing

mass modelling PM_{2.5} with LOTOS-EUROS was related to a missing share of organic carbon (OC) (Hendriks et al., 2013; Timmermans et al., 2013). This is largely solved by the inclusion of condensable material (van der Gon et al., 2015). For a general discussion on the fine mode, we refer to abovementioned publications. Below, we mainly focus on the coarse mode and the urban increment.

The modelled coarse mode urban increment is underestimated by a factor of 4. Traffic resuspension is a well-known source of coarse mode particles in the urban atmosphere (Amato et al., 2009). A study by van Pinxteren et al. (2019) found that the combined traffic exhaust and resuspension source profile contributed 17 % to urban background PM₁₀ in Berlin, whereas the contribution was around 9 % in the rural background. Applying these percentages to the observed 3-year mean concentrations of this study an indication of the typical urban increment ($2.5 \mu\text{g m}^{-3}$) for this source profile can be obtained. As the profile is dominated by crustal material and the total coarse mode increment for Berlin is about $3 \mu\text{g m}^{-3}$, the traffic crustal factor obtained by van Pinxteren et al. (2019) explains the coarse mode increment to a large part. In the receptor modelling contributions from highly correlated sources may appear in the same profile (Chan et al., 1999). Hence, other urban sources may still be included into the estimate. Nevertheless, we conclude that the modelled traffic increment ($0.8 \mu\text{g m}^{-3}$), being much lower than deduced from the observations, explains a large part of the underestimation of the coarse mode increment.

Although there is a large body of work on modelling desert dust, little

attention has been given to the modelling of crustal material from other sources in chemistry transport models. Emission inventories do not contain estimates of resuspension of e.g., traffic and land preparation, although they can be important sources (Denby et al., 2013; Thouron et al., 2018; Belis et al., 2020; Maffia et al., 2020). Most model systems do not include resuspension parameterizations for emissions from traffic and land management activities. Earlier work from Pay et al. (2011) and Schaap et al. (2009) showed that implementing a simple resuspension scheme reduced the BIAS and error in PM_{10} predictions. In our model set-up emission factors are applied to the mileage driven in each grid-cell for urban, rural and highway traffic. Implicitly, it is therefore assumed that the dust reservoir remains constant over time. Only in case of precipitation, the resuspension emission flux is set to zero. The spatial variability of the emission factors is calculated based on annual average soil water content (Schaap et al., 2009). Hence, seasonal variability as well as the impact of droughts are not included. Given the range of a factor of four in reported emission factors between regions (Gehrig et al., 2004), an impact of seasonality and especially drought periods are to be expected. In a follow-up study we plan to investigate different approaches to improve this parameterization.

Another issue that contributes to the overall underestimation of PM concentrations is the reduced capability of CTMs to model PM during stagnant weather conditions. A comparison between different CTMs showed that the models treat the vertical mixing very differently (Stern et al., 2008). A recent study connecting LOTOS-EUROS

to an ensemble of COSMO-CLM simulations with different parameterizations for boundary layer meteorology, however, did not show a systematic effect of different schemes (Thürkow et al., 2021). Currently, the LOTOS-EUROS team is assessing the possibility to move away from the mixed-boundary layer concept to a set-up with a significantly larger number of layers, which has shown to give improved temporal behavior of the major air pollutants including PM (Escudero et al., 2019; Thürkow et al., 2021).

The use of national scale emission inventories may also lead to problems due to the use of proxy data, such as population density. For instance, using population density to spatially distribute emissions neglects that urban populations are much more energy efficient than rural populations (Lobo et al., 2009; Timmermans et al., 2013). Such assumptions may lead to systematic over and underestimations of urban emissions in downscaled emission inventories, as for example shown for residential heating emissions in Paris (Timmermans et al., 2013). In this study for Berlin, we also used a national scale emission inventory, and clearly underestimate the urban increment. For NO_x Kuik et al. (2018) have shown that the emission totals of the national scale and local inventory for Berlin were only a few percent apart. In their study, Kuik et al. (2018) concluded that the large systematic BIAS between WRF-Chem modelled and observed NO_2 levels was connected to a general underestimation of NO_x emissions from traffic. Hence, primary emissions of transport need future attention. To improve the temporal and spatial variability of emissions from the residential heating sector we have applied temperature de-

pendent emissions as this leads to improved modelled pollutant concentrations (Mues et al., 2014). Similarly, dynamic approaches should also be included for other sectors like e.g., road transport, which also shows considerable variability due to ambient temperature (Matzer et al., 2017). In a follow up study, we plan to assess if these recent findings significantly affect the modelled urban increments for NO₂ and PM.

Evaluating the gradients between source regions and background levels may provide important information to get to the reason of the underestimation. We have used the traditional approach of Lenschow in this paper (Lenschow et al., 2001). Recently, using this approach to calculate the impact of a city was criticized because the rural background concentrations partly include the urban signal (Thunis et al., 2018). Hence the urban increment would underestimate the urban contribution. In our study the gradients between urban and rural sites were calculated in the same way for the modelled and observed results. The modelled urban contribution to the UB PM_{2.5} concentration is 2.62 µg m⁻³ whereas the modelled increment is 1.72 µg m⁻³. Thunis et al. (2018) used a BF approach to quantify the impact of the urban emissions on the (rural) background concentrations as function of the distance to the city for London, Paris, Berlin and Brussels using the CHIMERE model for 2010. Although the size of the urban contribution depends on the choice and configuration of the rural and urban observation sites as well as the model system used, our study confirms that the urban increment from the Lenschow approach is a lower estimate for the urban contribu-

tion in the city.

In order to reveal further shortcomings of the model system we recommend a comparison of LOTOS-EUROS results to those of receptor model results. Furthermore, a dynamic model evaluation as in Banzhaf et al. (2015) but including source attribution would help to further analyse the source attribution of the model and reveal its weaknesses. For the near future we propose the enhancement of resuspension schemes in CTMs and an improvement of the emission variability in space and time.

Code and data availability. The LOTOS-EUROS source apportionment code used in this study is property of TNO and not allowed to be shared publicly. The LOTOS-EUROS model is available as open source-version (excluding the data source attribution package) for public use via www.lotos-euros.tno.nl.

CRedit authorship contribution statement. **Joscha Pültz:** Conceptualization, Methodology, Software, Validation, Formal analysis, Investigation, Resources, Data curation, Writing – original draft, Writing – review & editing, Visualization. **Sabine Banzhaf:** Software, Writing – review & editing, Supervision. **Markus Thürkow:** Conceptualization, Methodology, Software, Resources, Writing – review & editing. **Richard Kranenburg:** Software, Resources. **Martijn Schaap:** Conceptualization, Methodology, Software, Writing – review & editing, Supervision, Project administration, Funding acquisition.

Declaration of competing interest. The authors declare that they have no known competing financial interests or

personal relationships that could have appeared to influence the work reported in this paper.

Acknowledgment. This research was funded by the Federal Ministry of Transport and Digital Infrastructure (BMVI) within the framework of the mFUND research initiative (grant no. 19F2065). It was partly supported by the Senat of Berlin and the Umweltbundesamt (UBA), which provided data. And finally, to the HPC Service of ZEDAT, Freie Universität Berlin, for computing time ([Bennett et al., 2020](#)), the [RCoreTeam \(2014\)](#) for the provision of software and Mr. Bergmann, for his support in setting up the computational environment.

Data availability. The data used in this article is partly publicly available and partly produced by own simulations. The data/ code from the simulations is partly confidential. Data will be made available on request.

A multi-meteorological comparison for episodes of PM₁₀ concentrations in the Berlin agglomeration area in Germany with the LOTOS-EUROS CTM

M. Thürkow¹, I. Kirchner¹, R. Kranenburg², R.M.A. Timmermans² and M. Schaap^{1,2}

Published in Atmospheric Environment, Volume 244, January 2021, 117946, ISSN: 1352-2310, DOI: 10.1016/j.atmosenv.2020.117946, URL: <https://www.sciencedirect.com/science/article/pii/S1352231020306804>

This article is licensed under a Creative Commons Attribution-NonCommercial-NoDerivs 4.0 International license.

Contents

III.1	Introduction	107
III.2	Methodology	108
III.3	Results	117
III.4	Discussion and conclusions	131

Highlights

- An interface of the LOTOS-EUROS CTM to the COSMO-CLM model was developed.
- PBL conditions were improved by the COSMO-CLM, but no clear bias correction is evident using different parametrizations.
- Higher resolved model simulations lead to a more realistic representation of the urban-increment.
- Impacts on PM mass concentrations of refined vertical layers are much larger compared to the meteorological input-data.
- Ammonium and Nitrate responded highly sensitive to different simulation set-ups.



Abstract

Particulate matter (PM) remains as one of the most relevant air-quality concerns in urban environments. The Berlin agglomeration area is still affected by exceedances of the daily limit value of the PM concentration, especially during wintertime PM episodes. In this study, we present test-case studies with the LOTOS-EUROS CTM to improve the representation of PM episodes in the Berlin agglomeration area. A variety of simulations were compared for two winter episodes characterized by cold stagnant conditions, using different meteorological input data (from the European Centre for Medium Weather Forecast (ECMWF) and the Consortium for Small-Scale Modelling-Climate Limited-area Modelling (COSMO-CLM)) and horizontal and vertical resolutions of the LOTOS-EUROS CTM. The LOTOS-EUROS CTM indicates too high mixing from the planetary boundary layer (PBL) to higher layers, leading to an underestimation of the PM mass concentration in the Berlin agglomeration. As major impact factor the mixing layer height (MLH) can be identified. Through applying the COSMO-CLM model the meteorological representation of the PBL and MLH can significantly be improved, whereas sensitivity studies only exhibit a small variation of the PBL meteorology and did not further improve the MLH. As the MLHs of both models are underestimated compared to observations and their derivation is questionable, we advise not to use this quantity any longer in CTMs. By contrast, applying a multi-level approach excluding the MLH, provides a considerable increase in the total PM mass concentration amount. The redistribution and increased nitrate and ammonium concentration can be mentioned as the main culprit. However, the best-fit simulations were obtained for the multi-level configuration fed by COSMO-CLM input data, additionally representing a more realistic urban increment.

Keywords: *particulate matter, LOTOS-EUROS, COSMO-CLM, planetary boundary layer, composition of PM*

Author affiliation:

¹Institute of Meteorology, Freie Universität Berlin, Carl-Heinrich-Becker-Weg 6-10, 12165, Berlin, Germany

²TNO, Department Climate Air and Sustainability, Princetonlaan 6, 3584 CB, Utrecht, the Netherlands

III.1 Introduction

Poor air quality is one of the most important environmental concerns of the 21st century (Lim et al., 2012). Exposure to particulate matter (PM) is thought to dominate the health impacts of air pollution (Boldo et al., 2006; Brook et al., 2010; Costa et al., 2014). According to the European Environment Agency each year about 62.300 premature deaths in Germany are caused by fine particulate matter (PM_{2.5}) (EEA, 2018a). Although a large part of the urban population in Germany is exposed to concentrations above the PM target value of the World Health Organization (WHO, 2005), the annual limit values for both PM_{2.5} and PM₁₀ as introduced by the European Ambient Air Quality Directive (EC, 2008) are currently not exceeded across Germany (UBA, 2019). In practice, the daily mean limit value for PM is more stringent than the annual mean limit values (Engler et al., 2012) and is still exceeded at traffic sites throughout Germany (UBA, 2019). To enable the development of cost-effective mitigation strategies to further reduce the health impacts by PM and the number of limit value exceedances it is required to understand the sources and processes leading to the enhanced concentration levels in episodes as compared to normal conditions (Belis et al., 2020).

PM concentrations are the result of processes involving direct emissions, chemical transformations, vertical mixing, long-range transport and dry and wet deposition, all depending on meteorological parameters (Zhang et al., 2015). Hence, establishing the origin of PM is complex as the contributions from local and distant, natural and anthropogenic, as well as individual

source sectors vary largely with season and synoptic situation (Tai et al., 2010; Mues et al., 2012; Zhang et al., 2015). High concentrations of PM are often associated with cold and stagnating weather conditions (Tai et al., 2010). Although the exceedances of limit values occur especially at the local urban scale (van Pinxteren et al., 2019), the regional background provides the most important mass contribution to observed PM levels in European cities (Beekmann et al., 2015; Garg and Sinha, 2017). Berlin, and East Germany in general, are affected by air masses from different European regions, i.e. western Europe through westerly air masses and central Europe through (south-) easterly air masses (Lenschow et al., 2001). In winter, the latter are associated with cold, stagnant weather conditions (Spindler et al., 2004; Brüggemann et al., 2009; Engler et al., 2012). Recent receptor modelling results showed combustion and secondary inorganic aerosols, e.g. ammonium, nitrate and sulfate, to be the main source groups during such cold spells (van Pinxteren et al., 2019). The same conditions also cause large trans-boundary contributions from Eastern European countries (van Pinxteren et al., 2019; Timmermans et al., 2020). As methodologies combining measurements and back trajectories as well as receptor models usually provide a limited number of source sectors and are less suitable to quantitatively identify the source regions (Belis et al., 2020), one cannot rely on observations alone to quantify the relevant (geographic) source contributions.

Chemistry transport models (CTMs) are deterministic and can provide quantitative source attribution estimates, which is an advantage above

III. A multi-meteorological comparison for episodes of PM₁₀ concentrations in the Berlin agglomeration area in Germany with the LOTOS-EUROS CTM

qualitative results based on empirical studies (Potier et al., 2019). Numerous model studies have been carried out to point out the sources of PM and their composition (Hendriks et al., 2013; Garg and Sinha, 2017; Thunis et al., 2018; Potier et al., 2019). However, a prerequisite for using these modelling results is that they reproduce the observed concentration levels and their variability. Previous studies have highlighted the challenges of modelling PM episodes under stable conditions. Underestimation of the observed PM concentration can be related to insufficient treatment of temporal emission variability (Mues et al., 2014) or underestimation of residential wood combustion emissions (Spindler et al., 2004; van der Gon et al., 2015). In addition, the reliability of simulations with CTMs to quantify concentrations strongly depends on the quality of the meteorological input data (Vautard et al., 2012). A multi-model comparison for an winter episode in 2003 revealed a characteristic underestimation of the PM concentrations in modern CTMs (Stern et al., 2008). Parametrizations of the mixing layer height (MLH) in meteorological models are identified as one source of the underestimation of PM under stable conditions and shallow boundary layers as shown by Seibert et al. (2000). Still, only a few studies have addressed the improvement of planetary boundary layer (PBL) variables for use in air quality model simulations (Hu et al., 2010; Buzzi et al., 2011; Banks and Baldasano, 2016).

In this study we explore if we can improve the modelling of PM episodes during winter in east-Germany by high resolution nonhydrostatic meteorological modelling (dynamical downscaling) using the COSMO-CLM model. Sensi-

tivity studies were conducted to investigate the representation of the PBL conditions. Meteorological quantities as the MLH were evaluated against radiosonde observations. The impact of different PBL parameterizations on modelled PM concentrations was analyzed. In addition, we investigated the impact of using two different vertical structures in the LOTOS-EUROS CTM. The impact of the dynamical downscaling was compared to the operational set-up of the LOTOS-EUROS CTM using the ECMWF meteorological driver.

III.2 Methodology

A dynamical downscaling approach with the COSMO-CLM model has been applied to generate high resolution meteorological input data for the LOTOS-EUROS CTM. First, we performed sensitivity studies to investigate the representation of the PBL conditions on the modelled PBL height and PM concentrations for January 2016. Accounting for the lessons learned, we applied the system to the next winter (September 2016 to March 2017) to further investigate and validate the impact of different horizontal and vertical set-ups. To assess the added value of the dynamical downscaling we used a simulation with meteorological input data of the ECMWF forecast model system (Flemming et al., 2009) as reference.

III.2.1 Study area and periods

The Berlin metropolitan area is the largest conurbation of Germany covering an area of 891 km². With more than 3.75 million inhabitants Berlin is densely populated.

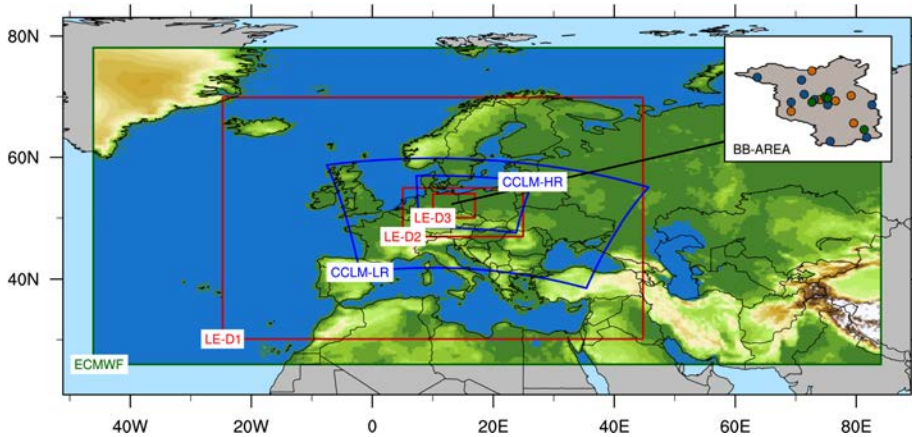


Figure III.1: Domain configuration of the model area. Three zooming domains are used for the LOTOS-EUROS CTM simulations (red). Meteorological boundary datasets are provided by the ECMWF model (green) and the COSMO-CLM (blue) model. As the COSMO-CLM model is applying a dynamical downscaling approach, two areas are needed. The investigation area of Berlin Brandenburg (BB) is attached on the right-hand side and contains the location of the rural- (orange), suburban- (blue) and urban-background observation sites.

Berlin's dynamic population increase combined with a pronounced tourist impact of about 13.50 million visitors per year is reflected in the air pollution management plan by targeting e.g. the construction (agglomeration) and traffic sectors (SenStadt, 2019). Berlin is situated in the North German Plain at $52^{\circ}30' N$ and $13^{\circ}30' E$ (Figure III.1). The neighboring republic of Poland is about 80 km from the eastern edge of the city. Berlin's conurbation is characterized by low orography features and intersected by the Spree valley. The average altitude above sea level is about 35-70 m increasing towards the border of the city. The maximum elevation is about 115 m. According to the prevailing season, Berlin is dominated by maritime climate in summer and continental climate in winter. The ambient air pollution in Berlin and its vicinity can be regarded as moderate. Annual average PM_{10} concentrations in 2016 ranged between 22.0

$\mu g m^{-3}$ and $26.8 \mu g m^{-3}$ for urban background and traffic stations, respectively (SenStadt, 2019). Levels in the surrounding rural area are typically about $17.0 \mu g m^{-3}$ and thus about $5.0 \mu g m^{-3}$ lower than recorded in the urban background (LFU, 2018). In recent years, exceedances of daily mean limit values of the PM concentration were limited and have only been recorded at traffic locations (LFU, 2018; SenStadt, 2019).

This study focuses on two periods, i.e. January 2016 and September 2016 to March 2017. These periods were selected as they contain episodes exceeding the daily PM limit value, caused by cold and stable weather conditions (Figure III.2). January 2016 was selected as this month is split into two major periods differing in their meteorological conditions. The first cold spell in the first week (2nd to 7th) was characterized by an easterly wind inflow. Temperature minima down to $-10.0^{\circ} C$ were observed at the surface.

III. A multi-meteorological comparison for episodes of PM₁₀ concentrations in the Berlin agglomeration area in Germany with the LOTOS-EUROS CTM

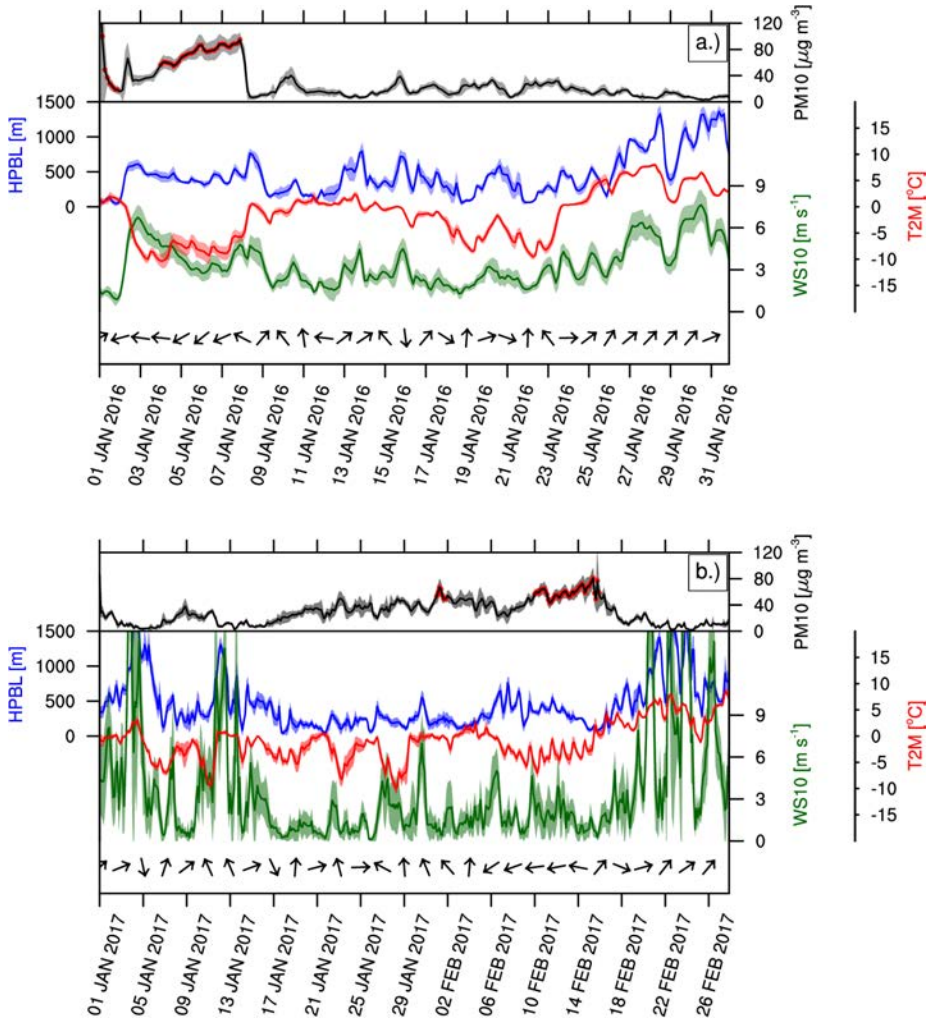


Figure III.2: Time series of investigation periods, representative for January 2016 (a) and January to February 2017 (b) for the Berlin agglomeration. PM mass concentration levels (black) are plotted on top with meteorological fields, as the mixing layer height (blue), the 2 m-temperature (red), the 10 m-wind-speed (green) and the 10 m-wind-direction above. Red dots indicate exceedances of the daily limit value. Parameters representing the spatial average of all observation sites.

A second (19th to 22nd) took place with a low pressure system crossing inducing inversion layering. Temperatures during the westerly wind period reflect the typical variation of a frontal passage and therefore vary between 0 °C and -10.5 °C. Apart from the differ-

ing wind direction the meteorological conditions during both periods were quite similar. Low wind speeds were recorded for both periods resulting in a monthly mean of about 3.4 m s⁻¹ at the surface. The MLH derived from radiosonde data was on average about

647 m and showed a large day-to-day variability. A PM episode with concentrations reaching values well above $90 \mu\text{g m}^{-3}$ was observed from the 2nd to the 7th (see Figure III.2). Despite similar meteorological conditions, during the westerly wind inflow period (19th to 22nd), no exceedances of the daily limit values were identified.

As the period of January 2016 is quite short, a second investigation period containing a winter PM episode has been examined. Therefore, the September 2016 to March 2017 was selected, with similar meteorological conditions compared to the reference period of January 2016 during wintertime of January to February 2017. The January to February 2017 was affected by low mixing and a mean mixing layer height of about 545 m. Mean temperatures were close to zero with minima of about $-10 \text{ }^\circ\text{C}$. The average wind speed below 3 m s^{-1} is quite low, whereas exceedances of the daily limit values again only occur during easterly wind periods. An advantage of investigating this winter is that we could use the data of the PM-OST campaign (van Pinxteren et al., 2019) for evaluating the modelled PM composition.

III.2.2 Nonhydrostatic meteorological modelling

A dynamical downscaling of the ERA-Interim reanalysis (Dee et al., 2011) was performed using the COSMO-CLM version 5.00 (Consortium for Small-Scale Modelling-Climate Limited-area Modelling) model (Doms et al., 2011; Doms and Baldauf, 2018) by using a double nesting approach. The first nested domain of the COSMO-

CLM model (Figure III.1) covers Europe from 4° W down to 40° E and 42° N - 59° N with a horizontal resolution of 0.0625° ($7 \times 7 \text{ km}^2$). The second nested domain covers Germany and Poland between 8° E - 25° E to 48° N - 57° N with a resolution of 0.025° ($2.8 \times 2.8 \text{ km}^2$). Independent of the spatial resolution 40 vertical levels were used, with at least 11 levels below 1 km to be able to represent the vertical behavior in the PBL. The domain configuration was chosen to resemble the DWD COSMO-DE configuration to allow for future operational use of COSMO-DE to provide air quality forecasts.

The convective scale operational numerical weather prediction model COSMO-LM, was originally developed at the German Weather Service (DWD). The aim was to be able to simulate nonhydrostatic processes which appear on the meso- β and meso- γ scale. The model focuses on deep moist convection and severe weather events. In Rockel et al. (2008) a documentation of the COSMO-CLM, the climate mode of the COSMO-LM, is given. The climate mode is designed for longer simulation periods using numerous lateral boundary conditions (e.g. sea surface temperatures, vegetation parameters). COSMO-CLM is a limited-area model defined on spherical rotated geographical coordinates, following a generalized terrain height coordinate in the vertical. A staggered Arakawa C-grid is used to represent the orthogonal discretization (Arakawa and Lamb, 1977), with a Lorenz hybrid z-layering applied in the vertical (Herzog et al., 2002a).

The representation of the PBL was investigated for January 2016 by an ensemble of turbulence parameterization schemes of the COSMO-CLM model (Table III.1). Ranging from ba-

III. A multi-meteorological comparison for episodes of PM₁₀ concentrations in the Berlin agglomeration area in Germany with the LOTOS-EUROS CTM

Table III.1: List of planetary boundary layer sensitivity parameterizations used in this work.

	PBL Parameterization		
	Turbulence Scheme	Surface Scheme	
CCLM-TC-V1-1	1-D Diagnostic Closure	Standard Bulk-Transfer Scheme	
CCLM-TC-V1-2		TKE-Based Surf. Transfer S.	
CCLM-TC-V2-1	1-D TKE-Based Diagn. Cl.	TKE-Based Surf. Transfer S.	
CCLM-TC-V2-2			
CCLM-TC-V2-3		Standard Bulk-Transfer S.	
CCLM-TC-V3-1	3-D TKE-Based Progn. Cl.	TKE-Based Surf. Transfer S.	
CCLM-TC-V3-2			
CCLM-TC-V3-3			
CCLM-TC-V3-4			
			Tuning Parameter
			lexpcor, ltmpcor, lcpfluc and ltkecon are applied
			Reduction of the turbulent length scale (50 m)
			Lowering of the diffusion coefficient of heat ($0.1 \text{ m}^2 \text{ s}^{-1}$)
			Adopting both parameters used in V3-2 and V3-3

sis meso- β flow systems to more sophisticated ones, the spectra of turbulent closure approaches is broad. Three closure approaches of the vertical diffusion and two surface flux schemes are available in the COSMO-CLM model. A detailed description of the implemented parameterizations can be found in (Doms et al., 2011). In this study a combination of all 6 parameterizations have been applied (Table III.1). The most simple closure approach as shown by Muller (1981) (1-D Diagnostic Closure) is based on the assumption of the boundary layer approximation neglecting horizontal turbulent fluxes. Mellor and Yamada (1974) developed a more extensive second-order parameterization (1-D TKE-Based Diagnostic Closure), extended by Louis (1979) with a surface flux formulation for the Prandtl-layer dependent on stability and roughness-length. The most sophisticated closure approach (3-D TKE-Based Prognostic Closure) focuses on highly resolved LES-like model simulations of subgrid-scale processes to avoid current boundary layer approximations (Herzog et al., 2002a; Herzog et al., 2002b). According to Louis (1979) analytical functions are applied to solve the transfer coefficients of roughness length and stability parameters of the surface flux formulation based on the Businger relations (Businger et al., 1971) (Standard Bulk-Transfer Scheme). Based on the coefficients of the Mellor-Yamada closure, the second surface flux scheme applies two layers by using a transport resistance of the laminar turbulent roughness layer and a constant Prandtl-layer. As described in Doms et al. (2011) an advanced surface layer scheme (TKE-Based Surface Transfer Scheme) is implemented into COSMO-CLM relating to the Mellor-Yamada

closure approach (Mellor and Yamada, 1974). The surface layer is sub-divided into roughness layer and Prandtl-layer. Additional control parameters like as the turbulent length and the diffusion coefficients of heat enlarge the range of possible configuration options. Different setups such as the impact of the turbulent heat and moisture fluxes and their reliance to condensation processes (lexpcor), the computation of thermal sources (ltmpcor) as well as the consideration of the convective buoyancy (ltkecon) for the TKE equation and variations in the heat capacity of air (lcpfluc) have been used as further test properties (Table III.1). A more detailed description of the applied control parameters are available in the COSMO-CLM users guide (Schättler et al., 2019). For the winter of 2016-2017 we performed a single dynamical downscaling using the advised setup using the "1-D TKE-Based Diagnostic Closure" and the "TKE-Based Surface Transfer Scheme".

III.2.3 Chemical transport modelling

Air quality simulations were performed using the chemistry transport model (CTM) LOTOS-EUROS version 2.1 (Manders et al., 2017). LOTOS-EUROS is an open-source 3D CTM, developed at TNO (Netherlands Organization for Applied Scientific Research) in cooperation with partners such as the FUB (Freie Universität Berlin). The aim of the model is to analyze and forecast air pollution concentrations in the lower troposphere. The model is part of the European regional ensemble of the Copernicus Atmospheric Monitoring Service (CAMS) (Marécal et al.,

2015), providing operational forecasts and analyses for Europe. An important application of the model is for source apportionment in different regions worldwide, e.g. Netherlands, China, and Germany (Kranenburg et al., 2013; Timmermans et al., 2017; Timmermans et al., 2020).

LOTOS-EUROS is based on a regular Eulerian grid with variable horizontal resolution over Europe (Manders et al., 2017) and terrain following vertical coordinates. The gas-phase chemistry is solved with the TNO CBM-IV scheme, a simplified version of the original scheme by Whitten et al. (1980). The hydrolysis of N_2O_5 (Schaap et al., 2004) and the cloud chemistry sulfate formation (Banzhaf et al., 2012) are explicitly treated. Computations for aerosol chemistry are performed with the ISORROPIA-II module (Fountoukis and Nenes, 2007). Dry deposition processes for the gas-phase are derived based on the DEPAC (DEPosition of Acidifying Compounds) module (Van Zanten et al., 2010; Kruit et al., 2012). Dry deposition of particles is implemented using the scheme of Zhang et al. (2001). Wet deposition processes are solved as described by Banzhaf et al. (2012). The horizontal advection of pollutants is calculated applying a monotonic advection scheme as shown by Walcek (2000). For a more detailed description of the LOTOS-EUROS model we refer to Manders et al. (2017) and references therein.

Table III.2: Model runs and settings performed for the LOTOS-EUROS model.

		COSMO-CLM		ECMWF IFS 12 h forecasts
Meteorological Input Data	Spatial Resolution	0.0625°x0.0625° @ 7x7 km ² (LR)	0.025°x0.025° @ 2.8x2.8 km ² (HR)	0.14°x0.14° @ 15x15 km ²
	Vertical Resolution	Lorenz hybrid z-level (40 layers)		3-layer-interval-averaged product of the ECMWF-L91 hybrid-sigma pressure levels (20 layers)
	Domain	4° W - 40° E to 42° N - 59° N	8° E - 25° E to 48° N - 57° N	46° W - 84° E to 26° N - 78° N
	PBL Sensitivity	see Table III.1		/
Chemical Transport Model Set-Up	Spatial Resolution	0.125°x0.0625° @ 7x8 km ² (D2)		0.0625°x0.03125° @ 4x4 km ² (D3)
	Vertical Structure	Multi layering approach @ 15 layers up to 2 km	Mixed layer approach @ 5 layers up to 5 km	Multi layering approach @ 15 layers up to 12 km
	Domain	5° E - 25° E to 47° N - 55° N		10° E - 12° E to 50° N - 54° N
	Period	January 2016		September 2016 - March 2017
	Boundary Conditions	LOTOS-EUROS climatological simulation with ECMWF IFS 12 h forecast conditions (0.5°x0.25° @ 28x32 km ²)		
Anthrop. Emissions	CAMS-RWC-AP 2015 (v1.1) and CAMS-2015-RWC-update-GrETa-gridding (v1.1) (van der Gon et al., 2015)			

For Europe, a regional inventory of the CAMS emissions developed by the TNO for 2015 was applied. The GRETA (Gridding Emission Tool for ArcGIS, Schneider et al. (2016)) inventory is used for the German anthropogenic emission distribution (Table III.2). A separate annual time profile for each source category represents the temporal variation that breaks down the annual emission totals. The CAMS fire product (Kaiser et al., 2012) provides information on wildfire emission sources. Chemical boundary conditions were taken from the Integrated Forecasting System provided by ECMWF (European Centre for Medium-Range Weather Forecasts) (C-IFS, Marécal et al. (2015)).

The standard meteorological input data of the LOTOS-EUROS CTM is derived from the operational meteorological dataset of the IFS (Integrated Forecasting System) provided by the ECMWF (Flemming et al., 2009). The meteorological forecasts offer a spatial resolution of about 0.14° , with hybrid-sigma pressure layers define the vertical coordinate system (Eckermann, 2009). The vertical resolution of the input data corresponds to a selection of 20 layers by vertical interval averaging of 3 layers derived from the ECMWF-L91 product, with the lowest level matching the initial layer of the ECMWF meteorology. The meteorological forecast is stored to enable re-analyses of past periods. The ECMWF data cover Europe from 46° W down to 84° E and 26° N - 78° N (Figure III.1).

The standard approach for increasing resolution by nesting the LOTOS-EUROS air pollution modelling is performed by a statistical downscaling of the ECMWF meteorological input data. In this study an interface

between COSMO-CLM and LOTOS-EUROS was developed to make further use of the dynamically downscaled COSMO-CLM meteorology. To implement the meteorological input data of the COSMO-CLM model, the spherical rotated horizontal and the hybrid z-layering vertical grid information's has been described within the LOTOS-EUROS CTM. A corresponding specification of the transformation of the available COSMO-CLM variables into the required fields within the LOTOS-EUROS CTM was performed like it was already implemented for the ECMWF model (Manders et al., 2017) and for the WRF model (Escudero et al., 2019). Both the horizontal and vertical grid configuration correspond to the model specification as provided by the DWD model family, avoiding interpolation of the data. The LOTOS-EUROS simulations were performed for three different regions and spatial resolutions using a one-way nesting approach (Figure III.1). The large scale European simulation ($28 \times 32 \text{ km}^2$) was performed with ECMWF meteorology, the higher resolution nests over Germany-Poland ($7 \times 8 \text{ km}^2$) and East-Germany ($4 \times 4 \text{ km}^2$) were performed by both meteorological drivers (Figure III.1).

Two concepts of the vertical structure were tested in the LOTOS-EUROS CTM. The current operational LOTOS-EUROS model set-up uses a dynamic mixed layer approach (MIX) consisting of 5 layers extending up to 5 km above sea level to determine the vertical (Manders et al., 2017). The vertical is structured by using a static surface layer of 25 m followed by a dynamic layer. The height of the dynamic layer equals the MLH, derived by the meteorological input data. Up to 3.5 km two equally thick dynamic reservoir layers

III. A multi-meteorological comparison for episodes of PM₁₀ concentrations in the Berlin agglomeration area in Germany with the LOTOS-EUROS CTM

are implemented. Hence, the depth of the vertical layers varies in time and space. To resolve free tropospheric transport processes like mineral dust transport, a fifth layer exceeding the 3.5 km altitude is used. As prerequisite for applying the dynamic mixed layer approach a homogenous pollutant distribution is presumed within the PBL. However, assuming a well-mixed PBL can lead to a wrong representation of the vertical mixing in the model system. Due to deep reservoir layers over-estimated mixing, particular during stable weather conditions with low MLHs, occurs. Therefore, recent model developments apply a much larger number of vertical layers in the LOTOS-EUROS CTM to reproduce the vertical structure of the planetary boundary layer (Escudero et al., 2019) and to provide a better understanding of the vertical distribution of pollutants, the multi-level version (MUL) negates the assumption of a well-mixed PBL and better accounts for the residual layer dynamics. The multi-level model version uses the vertical level information as provided by the meteorological input data. Here, the multi-level approach of LOTOS-EUROS was applied using the lowest 15 hybrid z-level of COSMO-CLM and hybrid-sigma pressure layers of the ECMWF as input data.

III.2.4 Observational data and metrics

The meteorological simulations were evaluated compared to radiosonde observation from Lindenberg, Schleswig, Greifswald in Germany and Leba, Legionowa and Wroclaw in Poland. To compare to both meteorological model systems, the radiosonde observations were vertically interpo-

lated to the corresponding model layering. To derive the MLH for both, observations and model results, the bulk Richardson method was used (Seibert et al., 2000). Defined as a dimensionless quantity and used in the turbulent kinetic energy (TKE) equation, the bulk Richardson number describes the bulk-ratio of the buoyant consumption term and the mechanical production term (Stull, 1988). The MLH refers to the altitude at which the bulk Richardson number is reaching a pre-set threshold, known as the critical Richardson number. Critical values of 0.2–1.0 are indicated in literature. Here we used the COSMO-CLM thresholds of 0.33 at stable conditions (Wetzel, 1982) and 0.22 during convection (Vogelezang and Holtslag, 1996) to determine the MLH based on the thermo-dynamical parameters and moisture variables.

To evaluate the modelled PM mass concentrations, observation data were collected from the ground-based monitoring networks in Germany collected by the German Environment agency UBA (www.uba.de). As we evaluated relatively short time periods, we chose to ensure full data coverage by using monitoring sites with 99 % data availability. Traffic sites were neglected as these are not representative for the model resolution. The monitoring sites were clustered into rural-background (6), suburban-background (10) and urban-background (4). To determine the contribution of individual components to the total PM concentration, data from the PM-OST monitoring campaign were used (van Pinxteren et al., 2019). The spatial-temporal mass concentration characteristics were illustrated by box plots. Mean diurnal and weekly cycles were calculated for all sites clustered by station type to ex-

amine the temporal variability of modelled and measured mass concentration. When analyzing the mass concentration per station type the data for all stations within a type were averaged in advance. To quantify the impact of meteorological conditions on the PM mass concentration level, a classification was carried out. The classification is based on three meteorological quantities. 2m-temperature ($T_C \leq 273.15$ K and $T_W > 273.15$ K), 10m-wind speed ($WS10_L \leq 3.3$ m s⁻¹ and $WS10_H > 3.3$ m s⁻¹ and 10m-wind direction ($WD10 [0^\circ \dots 360^\circ, 90^\circ]$). Equally sized clusters were defined by using a bootstrapping algorithm. To include vertical mixing, the classified PM concentration data were plotted against the MLHs of both meteorological input data sets. To assess the different model configurations used in this study, model statistics based on Chang and Hanna (2004) were used.

III.3 Results

III.3.1 January 2016

A comparison of both meteorological data from COSMO-CLM and ECMWF against radiosonde data was carried out for January 2016 before investigating the impact on the chemical transport modelling. Here we focus on thermodynamic parameters such as the MLH, temperature and wind speed. To evaluate the COSMO-CLM model, an ensemble of the PBL parameterization simulations is used.

Observed temperature profiles of the lower PBL are rather well captured by both meteorological input datasets (Figure III.3, left). The ensemble of the COSMO-CLM model predicts systematically lower temperatures in the model domain compared to

the ECMWF model, with an underestimation of observed values increasing towards the surface. The ECMWF model overestimates the temperatures compared to observations, most pronounced above the 700 m altitude. The structure of the vertical profile in the observations is considerably better reflected by the COSMO-CLM ensemble than the ECMWF model. Both models do not represent the cold easterly wind inflow period as well as the westerly wind inflow period.

For wind speed both meteorological datasets show a striking underestimation (of up to a factor of three) of the measured values (Figure III.3, right). The underestimations are visible over the entire vertical of the PBL and are most pronounced at about the 700 m altitude. The ensemble of the COSMO-CLM model provides higher wind speeds and a closer resemblance of the observed profile than the ECMWF model.

In general, the MLHs (Figure III.4) derived from both model simulations are lower compared to those derived from radiosonde measurements. The monthly mean bias of the ECMWF model is about -226 m and about -123 m for the COSMO-CLM ensemble mean. This could be attributed to an insufficient representation of the sensible and latent heat flux of the used model systems in the target area, which leads to lower near surface temperature estimates compared to the observations and the subsequent formation of inversion layers. Further research studies are required to investigate this issue. Deviations from the mean provide information of the variability and the temporal evolution. With this respect a large spatial variability between observation sites can be recognized, with

III. A multi-meteorological comparison for episodes of PM₁₀ concentrations in the Berlin agglomeration area in Germany with the LOTOS-EUROS CTM

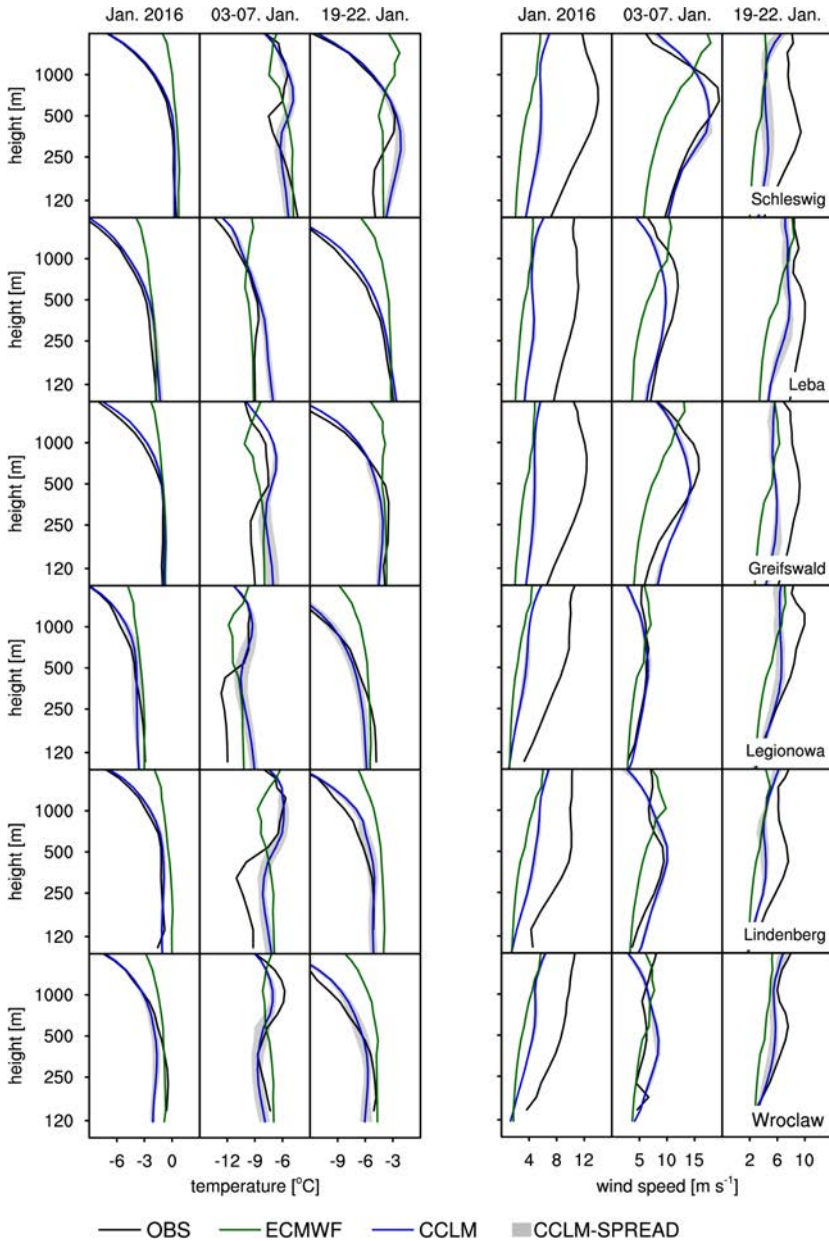


Figure III.3: Profiles of the temperature (left hand side) and the wind-speed (right hand side) for January 2016, split into sub-periods of 01.-31., 03.-07. and 19.-22.01.2016. Observation data are selected out of radiosonde measurements at Schleswig, Leba, Greifswald, Legionowa, Lindenberg and Wroclaw and color-coded in black. Model simulations are color-coded in green (ECMWF) and blue (COSMO-CLM). The COSMO-CLM model data is plotted as ensemble mean of the boundary layer parameterizations with their related spread marked as grey area.

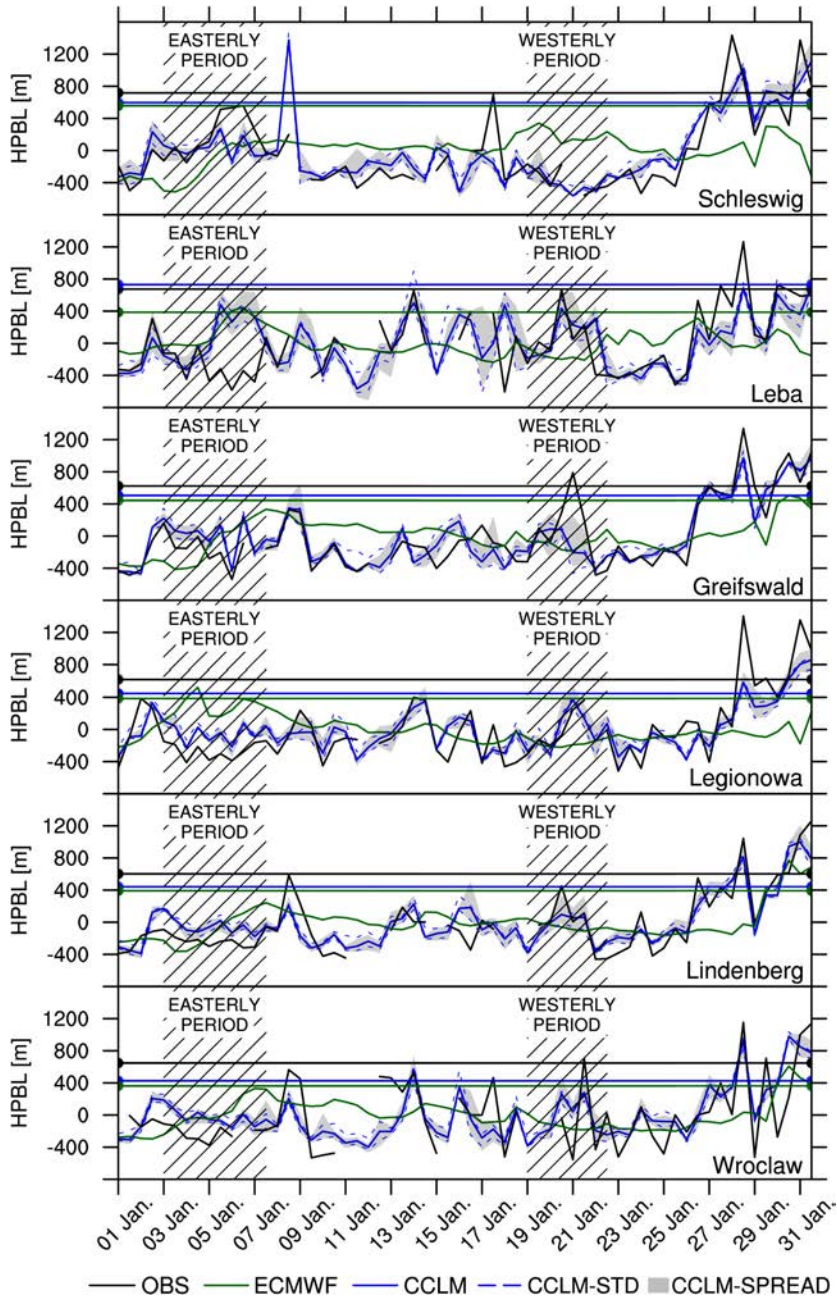


Figure III.4: Time series of the mixing layer height and deviation from mean, for January 2016. Observations are derived from radiosonde data in Schleswig, Leba, Greifswald, Legionowa, Lindenberg and Wroclaw and is color-coded in black. Meteorological boundary data is color-coded in green (ECMWF) and blue (COSMO-CLM). The COSMO-CLM data is plotted as ensemble mean of the boundary layer parameterizations, the related spread marked as grey area and with the standard deviation coded as dashed line.

III. A multi-meteorological comparison for episodes of PM₁₀ concentrations in the Berlin agglomeration area in Germany with the LOTOS-EUROS CTM

the largest variation appearing in Leba. A rather good representation of the temporal evolution, with a correlation coefficient of 0.76, can be achieved using the COSMO-CLM ensemble. The ECMWF model, on the other hand, has weaknesses representing the temporal evolution (correlation coefficient 0.13) of the MLH. The main weakness of both models is indicated by the standard deviation of the MLH. Even though the standard deviation of the COSMO-CLM ensemble MLH is closer to the observation, modelled values (about 340 m) are lower than observed (424 m). A noticeable lower standard deviation around the mean MLH is computed for the ECMWF model (189 m). Hence, the dynamical downscaling using COSMO-CLM provides improved meteorological information compared to the standard dataset from ECMWF.

The impact of different PBL parameterizations of the COSMO-CLM model can be regarded as small (grey area in Figure III.3). Main impact can be noted in the lower atmosphere, with largest differences near the surface compared to the ensemble mean, which can be explained by a lower vertical layer thickness near the surface. Lowering the diffusion coefficient of heat leads to cooler conditions with increased wind speeds, whereas e.g. the 3-D TKE-based prognostic closure approach leads to a warming in the PBL. Largest differences with a temperature variance of about 1 K can be observed especially during cooling events. Changes in wind speed are about 1 ms⁻¹ during the PM episode and about 0.5 ms⁻¹ for the entire month. The MLH and the corresponding temporal evolution are not significantly affected (see grey area in Figure III.4). Although the spread between members is up to 200 m and

thus comparatively large, no single ensemble member provides a consistent indication of a better performance in representing the PBL meteorology.

Below, the COSMO-CLM ensemble and the reference ECMWF data are used to drive the LOTOS-EUROS CTM.

Monthly mean PM mass concentration levels in the rural background during January 2016 were about 24 µg m⁻³ (see Figure III.5 and Table III.3). The LOTOS-EUROS CTM simulations fed with the COSMO-CLM ensemble underestimate the observed concentrations by 8.1 µg m⁻³ on average. The modelled variability is much lower than observed in reality. This can be explained by an overestimation during the westerly wind period of about 0.5 µg m⁻³, and a relatively large underestimation during the easterly wind regime (up to -43.6 µg m⁻³). Despite of a similar meteorological situation with a stagnant weather condition, this discrepancy can be explained by a high transboundary PM contribution. The simulations with the COSMO-CLM ensemble of PBL parameterizations do not provide large differences in the modelled PM mass concentration (Table III.3). On average, PM levels modelled by individual members are deviating less than 0.4 µg m⁻³ from the ensemble mean (Figure III.5). The model performance statistics for the ensemble mean of all LOTOS-EUROS simulations show small positive impacts on the temporal correlation and the normalized mean squared error compared to the individual simulation members (Table III.3). In Table III.3 we also compare the validation statistics of simulations using ECMWF and different model resolutions. Using ECMWF meteorological data instead

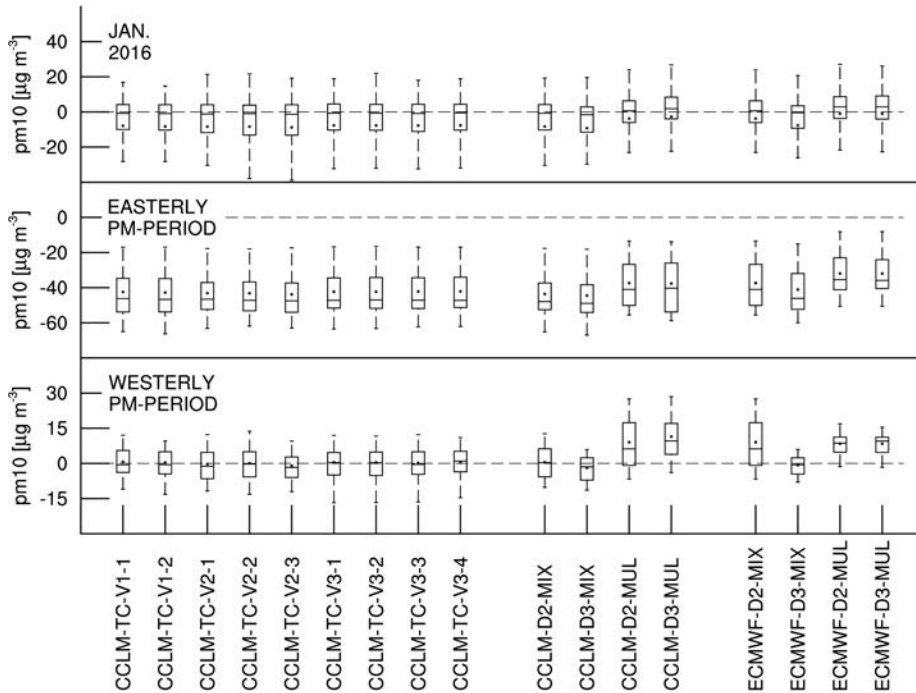


Figure III.5: PM mass concentration of the LOTOS-EUROS CTM dependent on the meteorological boundary conditions, the boundary layer parameterization, the horizontal resolution, and the vertical grid structure for the Berlin agglomeration. Three sub-periods have been investigated and are presented from top to bottom (01.-31., 03.-07. and 19.-22.01.2016).

of COSMO-CLM provides larger correlation coefficients and lower error statistics. Independent on meteorological driver the vertical structure leads to a substantial increase in levels and modelled variation. The increase in horizontal resolution (D3 vs D2) leads to a slightly larger increment between rural and urban sites.

In short, the impacts of the COSMO-CLM ensemble (members) is small compared to the use of different meteorological input data (COSMO-CLM vs ECMWF) and using different vertical model resolutions. The latter are discussed in more detail below for the winter 2016-2017, for which we did not pursue to perform the full ensemble calculations.

Table III.3: Statistics on modelled and observed means (μ), standard deviation (σ), temporal correlation coefficient (R_T), spatial correlation coefficient (R_S), geometric mean bias (MG), normalized mean square error (NMSE), geometric variance (VG), fractional bias (FB) and number of sites (NoS) for January 2016.

COSMO-CLM	MIX	D2	15.70 ± 06.43	23.99 ± 21.76	0.53	0.52	1.68	1.25	1.16	0.42	6 RUBG	
		_____	15.23 ± 06.20	27.26 ± 25.61	0.50	0.53	1.74	1.46	1.64	0.57	10 SUBG	
		_____	20.08 ± 09.47	31.88 ± 35.17	0.24	0.88	1.80	1.36	2.03	0.45	4 URBG	
	D3	_____	14.77 ± 06.19	23.99 ± 21.76	0.55	0.59	1.72	1.34	1.27	0.48	6 RUBG	
		_____	14.16 ± 05.50	27.26 ± 25.61	0.51	0.58	1.82	1.57	1.82	0.64	10 SUBG	
		_____	21.31 ± 10.74	31.88 ± 35.17	0.17	0.94	1.82	1.28	1.96	0.40	4 URBG	
	ENS	_____	15.93 ± 06.63	23.99 ± 21.76	0.58	0.53	1.62	1.24	1.09	0.40	6 RUBG	
		_____	15.55 ± 06.36	27.26 ± 25.61	0.51	0.57	1.69	1.44	1.57	0.55	10 SUBG	
		_____	20.18 ± 09.49	31.88 ± 35.17	0.26	0.89	1.76	1.35	2.00	0.45	4 URBG	
	MUL	D2	_____	20.20 ± 11.41	23.99 ± 21.76	0.56	0.65	1.42	1.06	0.70	0.17	6 RUBG
			_____	19.75 ± 11.29	27.26 ± 25.61	0.50	0.64	1.42	1.24	1.02	0.32	10 SUBG
		D3	_____	23.32 ± 13.14	31.88 ± 35.17	0.36	0.90	1.42	1.24	1.55	0.31	4 URBG
_____			21.33 ± 11.31	23.99 ± 21.76	0.51	0.71	1.43	0.98	0.70	0.12	6 RUBG	
D3		_____	20.92 ± 10.99	27.26 ± 25.61	0.47	0.74	1.38	1.15	0.95	0.27	10 SUBG	
		_____	26.09 ± 14.07	31.88 ± 35.17	0.28	0.94	1.48	1.08	1.43	0.20	4 URBG	
ECMWF IFS	MIX	D2	20.15 ± 06.69	23.99 ± 21.76	0.62	0.64	1.42	1.17	1.00	0.37	6 RUBG	
		_____	16.72 ± 06.66	27.26 ± 25.61	0.57	0.62	1.46	1.31	1.35	0.48	10 SUBG	
		_____	19.39 ± 08.51	31.88 ± 35.17	0.36	0.88	1.56	1.35	2.01	0.49	4 URBG	
	D3	_____	16.35 ± 06.76	23.99 ± 21.76	0.64	0.72	1.41	1.17	0.99	0.38	6 RUBG	
		_____	16.77 ± 06.67	27.26 ± 25.61	0.60	0.58	1.45	1.31	1.30	0.48	10 SUBG	
		_____	20.12 ± 08.98	31.88 ± 35.17	0.36	0.95	1.54	1.31	1.91	0.45	4 URBG	
	D2	_____	23.02 ± 11.00	23.99 ± 21.76	0.67	0.86	1.35	0.87	0.50	0.04	6 RUBG	
		_____	22.91 ± 11.05	27.26 ± 25.61	0.60	0.69	1.30	1.00	0.73	0.17	10 SUBG	
		_____	24.61 ± 12.00	31.88 ± 35.17	0.46	0.95	1.33	1.10	1.32	0.26	4 URBG	
	MUL	_____	22.95 ± 11.00	23.99 ± 21.76	0.67	0.93	1.35	0.87	0.50	0.05	6 RUBG	
		_____	23.00 ± 11.08	27.26 ± 25.61	0.61	0.61	1.29	1.00	0.70	0.18	10 SUBG	
		_____	24.98 ± 12.14	31.88 ± 35.17	0.46	0.95	1.33	1.08	1.30	0.24	4 URBG	

III.3.2 September 2016 to March 2017

III.3.2.1 Meteorological input data

Classifying the PM concentration by meteorological conditions for September 2016 to March 2017, more detailed information can be obtained on their relationship to thermodynamical quantities. [Figure III.6](#) illustrates the well-known feature of high PM concentration levels predominant during cold periods when a shallow mixing layer is observed. By contrast, a low mass concentration is evident during relative mild winter periods. Periods with weak wind speeds are linked to local impacts like urban emissions, high wind speeds are associated to long-range transport. Concentration levels are higher at south-east wind directions than at north-west ones in the investigation area of Berlin. Summarizing, high concentration levels in Berlin can be linked to long-range transport of air masses from East-European countries, during cold stagnant conditions. PM concentrations during westerly wind periods are well represented while an underestimation of PM concentrations is present for all mixed-layer model versions during easterly wind periods with respect to the UBA measurements. Warm periods are better reproduced than colder episodes. Largest PM underestimations for September 2016 to March 2017 are obvious for conditions with cold south-easterly high wind periods by up to $15.0 \mu\text{g m}^{-3}$ compared to the observation. LOTOS-EUROS CTM simulations driven by the COSMO-CLM model and ECMWF input data differ, depending on the meteorological condition, in their mean MLH by about 75 m with the ECMWF

model providing lower values for most of the time. Related PM mass concentration levels vary within $5.0 \mu\text{g m}^{-3}$, with largest deviations during cold periods. Simulation results of the LOTOS-EUROS CTM using input data of the COSMO-CLM model are on average about $-1.4 \mu\text{g m}^{-3}$ lower in rural areas than ones computed by using the ECMWF model, with the more striking difference of about $-7.4 \mu\text{g m}^{-3}$ evident during cold stagnant PM episodes, which could be related to higher wind speeds of the COSMO-CLM model.

For winter December 2016 to February 2017, the monthly mean rural background concentration was $21.7 \mu\text{g m}^{-3}$, with the major impact attributed to urban agglomerations of about $27.4 \mu\text{g m}^{-3}$ ([Figure III.7](#) and [Table III.4](#)). This corresponds to an urban increment of about $5.7 \mu\text{g m}^{-3}$. The rural background concentration levels for the mixed-layer model versions are underestimated by about $-2.7 \mu\text{g m}^{-3}$ on average with respect to the UBA measurements. Especially urban background ($-5.2 \mu\text{g m}^{-3}$) influenced areas cannot be captured by the LOTOS-EUROS CTM. Therefore, the modelled urban increment is underestimated by about $3.2 \mu\text{g m}^{-3}$ on average. The average urban increment of the COSMO-CLM model system, applying the dynamical downscaling approach, lowers the underestimation of the increment of modelled PM mass concentration levels in the LOTOS-EUROS CTM seen in UBA measurements ([Figure III.7](#)).

This particularly affects the enhanced PM mass concentration levels of urban agglomerations. More gradients are visible in the PM distribution across highly polluted areas such as Berlin. Whereas the rural background concentration estimates for win-

III. A multi-meteorological comparison for episodes of PM₁₀ concentrations in the Berlin agglomeration area in Germany with the LOTOS-EUROS CTM

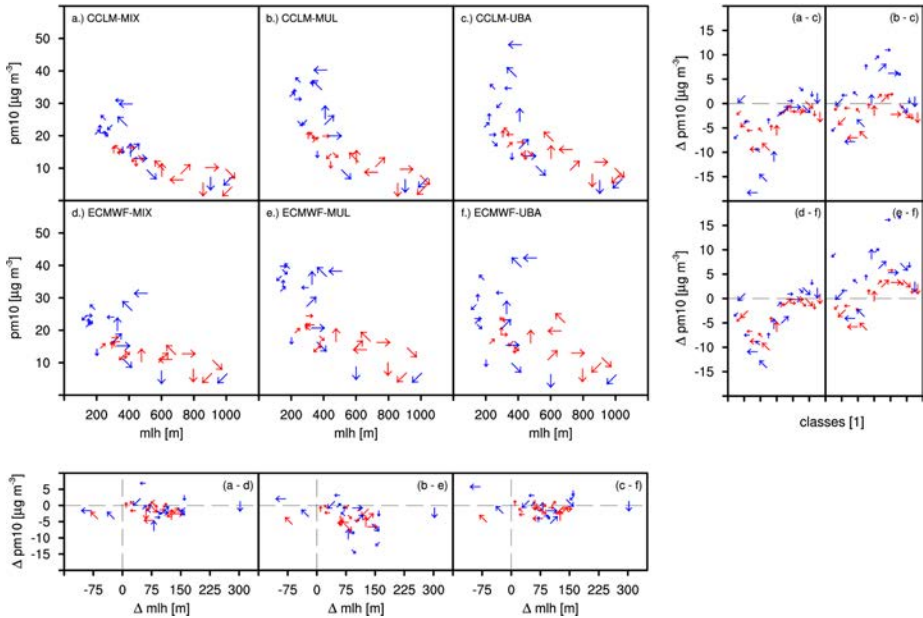


Figure III.6: Modelled (left: mixed layer approach [MIX], middle: multi-layering concept [MUL]) and observed (right) PM mass concentration levels are plotted over the MLH (a–f) for September 2016 to March 2017. Rural-background sites are used as evaluation sites, with the COSMO-CLM model (top) and ECMWF model (bottom) representing the meteorological boundary data. The PM mass concentration levels are divided into different classes depending on the meteorological condition. Anomalies of the different configurations are plotted on each side. The temperature impact is color-coded: $T_C \leq 273.15$ K as blue and $T_W > 273.15$ K as red. Wind speed is marked by the arrow length: $WS_{10L} \leq 3.3$ m s^{-1} and $WS_{10H} > 3.3$ m s^{-1} . The wind direction is associated to the arrow direction: $WD_{10} [0^\circ \dots 360^\circ, 90^\circ]$

ter December 2016 to February 2017 are slightly higher by using the COSMO-CLM model compared to the observations (bias of $-3.1 \mu\text{g m}^{-3}$) than those of the ECMWF model system. In the urban background area, an underestimation of $-4.4 \mu\text{g m}^{-3}$ is obvious with respect to the observations. This results in an urban increment of $4.4 \mu\text{g m}^{-3}$.

Figure III.8 provides observed and modelled diurnal and weekly cycles of surface PM concentration levels for winter December 2016 to February 2017. The observed diurnal cycle is characterized by a minimum during lunchtime and a maximum at night, caused by the natural development of the MLH.

Whereas, in the urban area two peak values are observed during daytime, between 8-11 GMT and 19-22 GMT, mainly attributed to the impact of traffic rush hours and heating in conurbation areas. Diurnal cycles are too pronounced in the LOTOS-EUROS CTM simulations. Lower concentration levels are predominant in the early morning hours from midnight to 6:00 GMT, with about $-5.5 \mu\text{g m}^{-3}$ in rural areas and about $-6.8 \mu\text{g m}^{-3}$ in the urban background compared to the observation. Towards the evening the bias is reduced to about $-3.5 \mu\text{g m}^{-3}$ in rural areas and about $-2 \mu\text{g m}^{-3}$ in the urban background with respect to the UBA

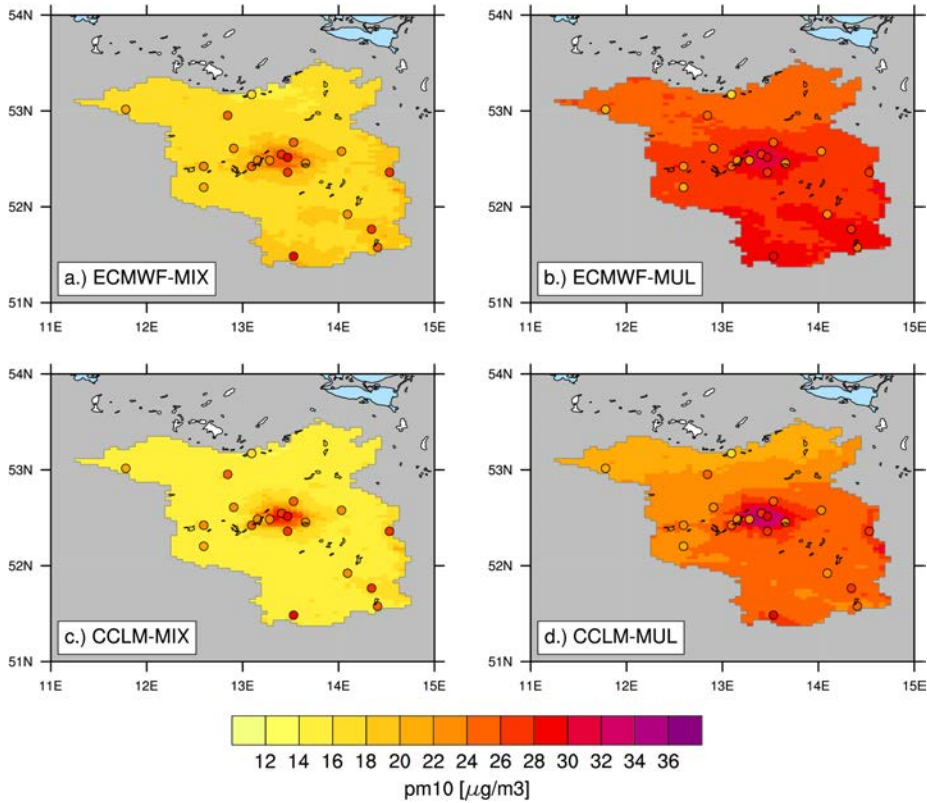


Figure III.7: Map of the observed (dots) and the modelled (ECMWF-MIX: a, ECMWF-MUL: b, COSMO-CLM-MIX: c and COSMO-CLM-MUL: d) PM mass concentration level for December 2016 to February 2017.

measurements. The mean correlation of the diurnal cycle for urban sites is 0.81, with simulations driven by COSMO-CLM input data showing smaller correlation coefficients by about 0.07. The more pronounced overshooting of peak concentration levels in urban areas by using the COSMO-CLM model reduces the temporal correlation to 0.57. Overall higher correlations can be provided using the ECMWF input data in the rural and sub-urban background area by about 0.05.

As the impact for different horizontal (D2 vs. D3) and vertical resolutions (MIX vs. MUL) of the LOTOS-EUROS

CTM simulations is similar for varying meteorological input-data, we will focus on the COSMO-CLM model system.

III.3.2.2 Model resolution

Differences by increasing the horizontal resolution are particularly evident when applying the dynamical downscaling approach of the COSMO-CLM model, with the major benefit of the higher resolution recognized in a more detailed representation of the spatial concentration distribution. For instance, increasing the horizontal resolution applying the zooming

III. A multi-meteorological comparison for episodes of PM₁₀ concentrations in the Berlin agglomeration area in Germany with the LOTOS-EUROS CTM

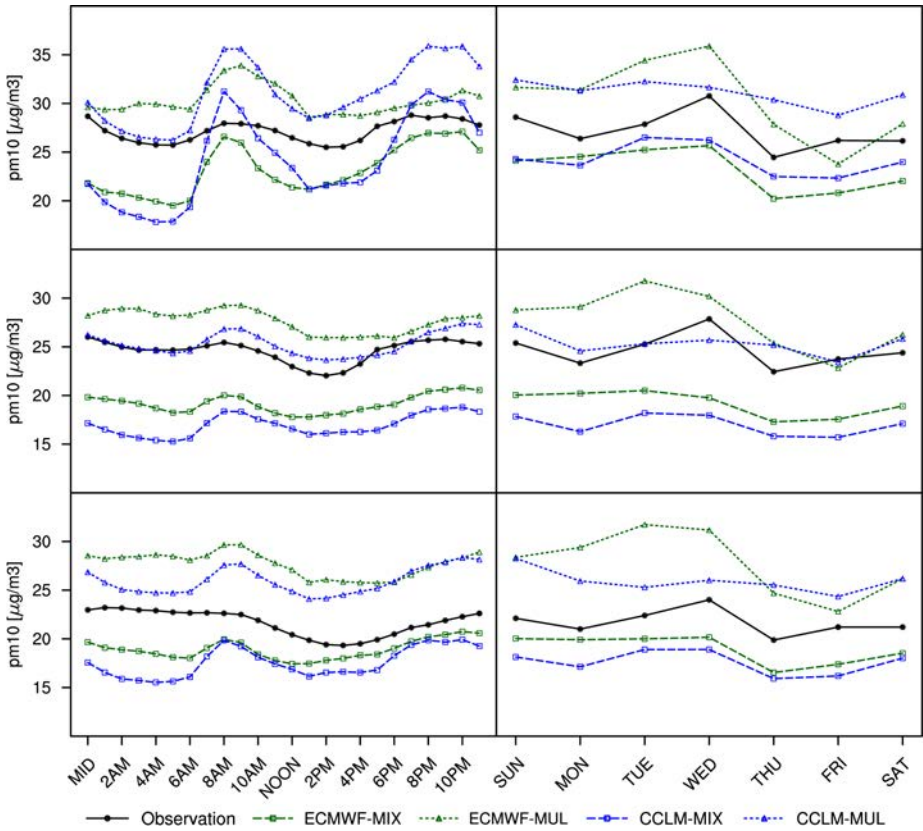


Figure III.8: Diurnal (left) and weekly (right) cycle of the observed (black solid line) and the modelled (green: dashed line - ECMWF-MIX, dotted line - ECMWF-MUL; blue: dashed line - COSMO-CLM-MIX, dotted line - COSMO-CLM-MUL) PM mass concentration levels for December 2016 to February 2017, split into urban- (top), suburban- (mid) and rural-background (bottom) areas.

approach of the LOTOS-EUROS CTM (D2 to D3) is slightly affecting the PM mass concentration and reduces the rural background levels of the LOTOS-EUROS CTM model (Table III.4 and Figure III.7). On average lower values of $-1.1 \mu\text{g m}^{-3}$ were computed compared to the coarser resolution for winter December 2016 to February 2017. In contrary, the concentration amount in the urban background of the LOTOS-EUROS CTM is increased by about $0.9 \mu\text{g m}^{-3}$ when increasing the resolution from 7 km to 2 km. This increases the

urban increment to about $6.4 \mu\text{g m}^{-3}$. Simulation results show that different horizontal resolutions applying different vertical structures delivered similar results, thus for the remainder discussions we will stick with the higher resolved model version.

Changing the vertical structure (MIX vs. MUL) of the LOTOS-EUROS CTM exhibits a larger impact than increasing the horizontal resolution. By applying the multi-level approach, higher levels of the PM mass concentration are obvious in almost all me-

teorological conditions with respect to the mixed layer approach (Figure III.6). The multi-level version leads to a considerably reduction of the underestimation during cold south-easterly high wind periods from $-14 \mu\text{g m}^{-3}$ to about $-4.0 \mu\text{g m}^{-3}$ compared to the observations. At the same time, an overestimation during cold westerly wind conditions is apparent by now of up to $10.0 \mu\text{g m}^{-3}$ with respect to the observations. Regarding warm westerly conditions a mean overestimation of about $4.0 \mu\text{g m}^{-3}$ system can be recognized applying the multi-layering concept compared to the UBA measurements. Increased PM mass concentration levels are predominant in the whole model domain when using the multi-level model version (Table III.4 and Figure III.7). In particular, the rural background concentration levels are increased by up to $8.4 \mu\text{g m}^{-3}$ on average compared to the mixed layer approach. This leads to an average overestimation of rural background concentrations of up to $4.3 \mu\text{g m}^{-3}$. The urban concentration levels are overestimated by up to $3.5 \mu\text{g m}^{-3}$. The urban increment is about $4.9 \mu\text{g m}^{-3}$ but is only slightly underestimated compared to the UBA measurements.

III.3.2.3 Model performance

Model statistics show high agreement of the model simulations compared with observations (Table III.4). An overall good representation of the observations can be achieved, with highest model performance evident for the multi-level version of the LOTOS-EUROS CTM. On average, high-resolution model simulations of the LOTOS-EUROS CTM show the best spatial performance with spatial

and temporal correlation increasing with higher vertical model resolution. Best agreements can be observed for the dynamical downscaling approach of the COSMO-CLM input data combined with increased vertical resolution of the LOTOS-EUROS CTM, with spatial averaged model statistics of about 0.74 for the temporal correlation, 0.70 for the spatial correlation, -0.11 for the fractional bias, 0.23 for the normalized mean square error, 1.29 for the geometric variance and 0.91 for the geometric mean bias.

III.3.2.4 Composition of PM

In the following section, the comparison of the observed and modelled PM concentration is extended by chemical compounds (Figure III.9 and Figure III.10). This provides more information on the mechanisms causing to different results in the applied model configurations. The modelled and observed data were spatially averaged over the entire investigation area.

The observed PM composition shows high levels of nitrate (18 %), ammonium (10 %) and sulfate (13 %) as well as organic matter (23 %) for January to February 2017. Lower contributions can be attributed to sodium (1 %) and elemental carbon (3 %). The predominant compound is classified as undefined (34 %) which includes mineral dust, oxides, and other trace materials.

Table III.4: Statistics on modelled and observed means (μ), standard deviation (σ), temporal correlation coefficient (R_T), spatial correlation coefficient (R_S), geometric mean bias (MG), normalized mean square error (NMSE), geometric variance (VG), fractional bias (FB) and number of sites (NoS) for December 2016 to February 2017.

COSMO-CLM	MIX	D2	18.55 ± 09.75	21.67 ± 14.89	0.72	0.54	1.37	1.09	0.29	0.16	6 RUBG
		D2	18.39 ± 09.52	24.71 ± 16.27	0.76	0.29	1.36	1.25	0.35	0.29	10 SUBG
		D2	23.01 ± 12.62	27.36 ± 18.69	0.65	0.76	1.36	1.15	0.35	0.17	4 URBG
		D2	17.50 ± 08.84	21.67 ± 14.89	0.71	0.59	1.38	1.13	0.35	0.21	6 RUBG
		D3	17.24 ± 08.41	24.71 ± 16.27	0.75	0.24	1.39	1.30	0.45	0.36	10 SUBG
	MUL	D2	23.86 ± 12.74	27.36 ± 18.69	0.57	0.78	1.38	1.08	0.39	0.14	4 URBG
		D2	24.45 ± 15.64	21.67 ± 14.89	0.77	0.74	1.36	0.93	0.22	-0.12	6 RUBG
		D2	24.38 ± 15.54	24.71 ± 16.27	0.80	0.43	1.28	1.06	0.17	0.01	10 SUBG
		D2	28.32 ± 18.42	27.36 ± 18.69	0.71	0.78	1.32	1.03	0.26	-0.03	4 URBG
		D3	25.92 ± 15.43	21.67 ± 14.89	0.76	0.80	1.34	0.85	0.23	-0.18	6 RUBG
ECMWF IFS	MIX	D3	25.68 ± 15.04	24.71 ± 16.27	0.79	0.50	1.24	0.97	0.17	-0.03	10 SUBG
		D3	30.88 ± 18.32	27.36 ± 18.69	0.67	0.79	1.29	0.90	0.28	-0.12	4 URBG
		D2	18.93 ± 09.49	21.67 ± 14.89	0.76	0.63	1.25	1.06	0.25	0.14	6 RUBG
		D2	19.55 ± 09.68	24.71 ± 16.27	0.80	0.41	1.23	1.16	0.28	0.23	10 SUBG
		D2	22.20 ± 11.68	27.36 ± 18.69	0.69	0.66	1.26	1.17	0.34	0.21	4 URBG
	MUL	D2	18.86 ± 09.45	21.67 ± 14.89	0.76	0.68	1.25	1.06	0.26	0.14	6 RUBG
		D3	19.41 ± 09.52	24.71 ± 16.27	0.80	0.41	1.22	1.16	0.29	0.25	10 SUBG
		D2	23.02 ± 12.33	27.36 ± 18.69	0.67	0.78	1.26	1.13	0.34	0.17	4 URBG
		D2	28.04 ± 16.54	21.67 ± 14.89	0.76	0.84	1.30	0.74	0.27	-0.26	6 RUBG
		D2	28.28 ± 15.86	24.71 ± 16.27	0.81	0.59	1.20	0.82	0.16	-0.13	10 SUBG
MUL	D2	30.06 ± 18.45	27.36 ± 18.69	0.67	0.79	1.20	0.88	0.29	-0.09	4 URBG	
	D2	27.70 ± 16.18	21.67 ± 14.89	0.76	0.87	1.30	0.74	0.26	-0.24	6 RUBG	
	D3	27.98 ± 15.69	24.71 ± 16.27	0.81	0.61	1.19	0.83	0.16	-0.12	10 SUBG	
			30.44 ± 19.02	27.36 ± 18.69	0.64	0.85	1.21	0.87	0.32	-0.11	4 URBG

As mentioned in the previous section model simulations of the mixed-layer version indicate an overall underestimation of the total PM mass concentration especially during PM episodes in comparison to the observations. The largest part of the model bias can be attributed to an underestimation of sulfate, primary organic matter (POM), and the undefined fraction with estimated average underestimations ranging between $-1.2 \mu\text{g m}^{-3}$ for Sulfate and POM and of $-8.0 \mu\text{g m}^{-3}$ for the undefined fraction, respectively. By contrast, the components sodium, and elemental carbon show positive biases up to $1.4 \mu\text{g m}^{-3}$ compared to the observations. Ammonium is slightly underestimated, whereas nitrate shows a small overestimation (both about $\pm 0.2 \mu\text{g m}^{-3}$).

Simulations by using different model resolutions in the horizontal or the vertical grid structure and different meteorological input data, especially affects individual chemical components as e.g. nitrate, and sulfate, which are highly sensitive compounds in the used model systems (Figure III.10). These observed sensitivities and their related overestimation of PM concentration levels compared to observations are primarily induced by the multi-level version of the LOTOS-EUROS CTM. The largest gain in mass concentration in the order of about $4.5 \mu\text{g m}^{-3}$ is evident for nitrate, leading to an averaged overestimation of the same order of magnitude compared to the observations. Similar results are obvious for ammonium, which results in an overestimation of the averaged fraction of about $1.3 \mu\text{g m}^{-3}$ compared to the measurements. Ammonium nitrate is a semi-volatile component and its formation depends a combination of

factors including temperature, relative humidity, stability, and the precursor concentrations. In this case, the absence of the meteorological impact on ammonia emissions may increase the effects as the rise of ammonium nitrate occurs at (colder) moments when ammonia emissions are below average. The mass concentration of POM is increasing with higher vertical layering also by about $0.6 \mu\text{g m}^{-3}$. By contrast, the sodium mass concentration was reduced and leads to a reduction of the model bias ($0.2 \mu\text{g m}^{-3}$). In all simulations a below average performance is found for the formation of sulfate. Compared to the observations, the model bias ($-0.4 \mu\text{g m}^{-3}$) for sulfate is considerably reduced on average, but still the temporal trend is difficult to capture.

Using different meteorological input data is not as large reflected in the distribution of the chemical compounds. The results differ in the concentration mass corresponding to the conclusions mentioned above with small changes in the model bias of nitrate and POM ranging within $0.5 \mu\text{g m}^{-3}$ when using the COSMO-CLM model. By contrast, the fraction of sulfate is changed for January to February 2017 and counteracts the model bias. In comparison to the ECMWF driven model system, a negative difference prior to and a positive one during the PM episode appears.

The smallest variations in the component distribution can be observed by increasing the model resolution using the zooming approach in the LOTOS-EUROS CTM, with higher POM concentration and lower nitrate levels modelled for the observation sites for January to February 2017. Averaged differences of up to $0.3 \mu\text{g m}^{-3}$

III. A multi-meteorological comparison for episodes of PM₁₀ concentrations in the Berlin agglomeration area in Germany with the LOTOS-EUROS CTM

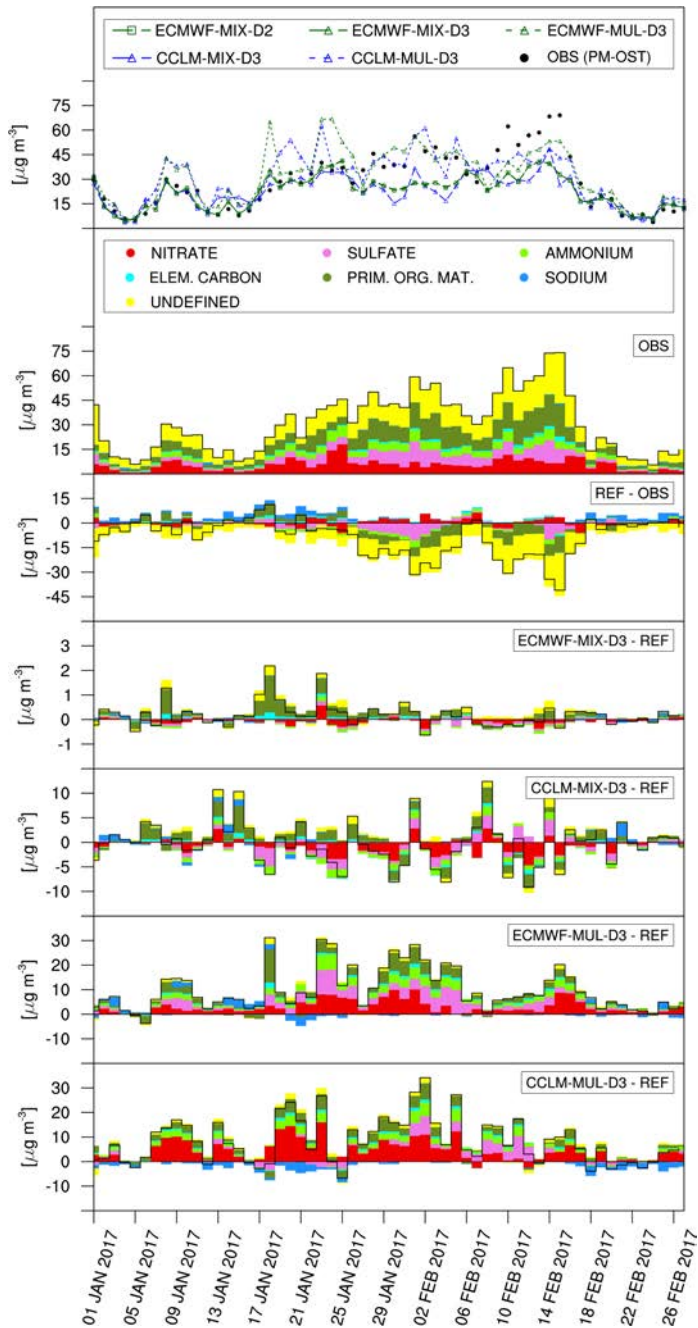


Figure III.9: Time series of observed (PM-OST) and modelled PM mass concentration levels (on top) for January to February 2017. Difference (black line) to the Observation (PM-OST) and the reference model (ECMWF-MIX-D2) are listed below and separated into their chemical composition (bar charts).

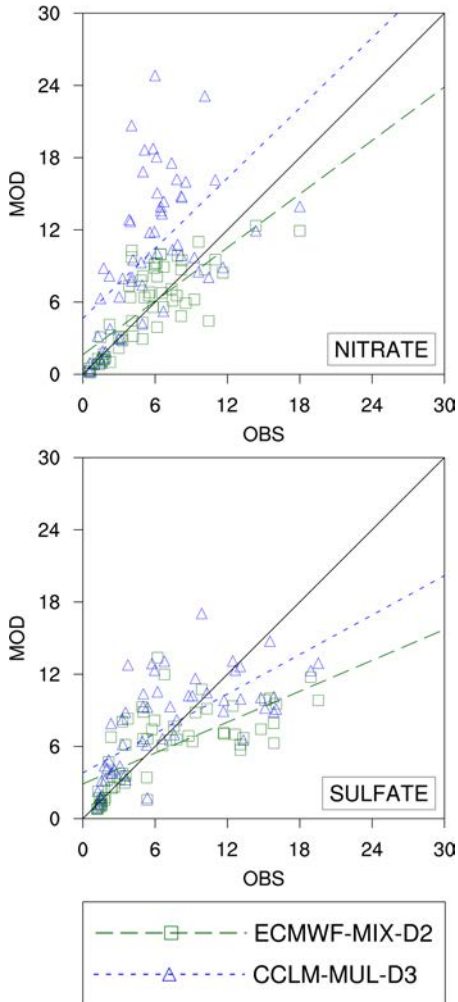


Figure III.10: Scatter plot of modelled (MOD) compared to of observed (OBS: PM-OST) mass concentration levels of nitrate (on top) and sulfate (bottom) for January to February 2017.

with respect to the lower resolution can be recognized. The impact of elemental carbon becomes more relevant with higher resolution increasing the mass concentration in the order of $0.1 \mu\text{g m}^{-3}$, which results in a larger overestimation of about $0.4 \mu\text{g m}^{-3}$ compared to the observation.

III.4 Discussion and conclusions

We successfully developed an interface to the COSMO-CLM model and explored the impact of different meteorological input data and horizontal and vertical resolutions for the LOTOS-EUROS CTM. The quality of the meteorological input data are a major impact factor on chemical transport modelling and can thus be one reason for excessive mixing (Vautard et al., 2012). Our study shows that meteorological conditions can significantly be improved by applying the dynamical downscaling approach of the COSMO-CLM model compared to the ECMWF reference data. Especially the comparison to observed MLHs, derived from radiosonde data using the bulk Richardson method (Seibert et al., 2000), exhibits a good agreement. Weaknesses are apparent representing the MLH top with a low bias, while the temporal evolution and the variability are well reflected. Previous studies also mentioned a systematic underestimation of the PBL height of the COSMO model during convective situations or frontal crossings, comparable to the prevailing conditions during the selected investigation period (Fay and Neunhuserer, 2005). Baars et al. (2008) also published model simulation results of the COSMO model

III. A multi-meteorological comparison for episodes of PM_{10} concentrations in the Berlin agglomeration area in Germany with the LOTOS-EUROS CTM

indicating a too low MLH of about 20 %. In the study of Baars et al. (2008) the dependency to cloud cover was emphasized with highest underestimation appearing when clouds are predicted by the model but are not existent at all. By contrast, the study by Coen et al. (2014) indicates a general overestimation of the COSMO model caused by a too rapid increase in the early morning hours, with larger differences during cloudy conditions as well. As reason of these positive and negative model bias compared to the observations, differences in the stratification of atmospheric parameters can be regarded as the main impact factor, caused in particular by the orographic situation in the studies mentioned above.

To provide reliable meteorological conditions of the PBL for the investigation area of Berlin, we attempted to improve the variability of the MLH by using different PBL parameterizations of the COSMO-CLM model. Neither the simulation of the mean nor the representation of the variability can be improved much by the sensitivity simulations of the COSMO-CLM model. The overall total variation caused by the parameterizations is small and no clear bias correction can be achieved. Previous studies already mentioned similar difficulties adopting parametrizations. Buzzi et al. (2011) for instance indicates a loss of information of the near-surface temperature inversion when too low diffusion coefficients are applied, with high values are required to avoid low mixing. A further study by Meissner et al. (2009) indicates minor impact of varying physical model parameters compared to changing meteorological driving data of the COSMO-CLM model. This may indicate that the downscaling domain

of COSMO should be increased substantially in the future to widen the ensemble spread.

In fact, the MLH is not a physical parameter, it is simply a diagnostic quantity and cannot be directly measured with the determination associated with certain limitations (Schäfer et al., 2006). However, studies on the comparability of MLH retrievals deliver significant differences especially depending on the meteorological conditions. Based on the algorithm used to derive the MLH, such as temperature profiles, sodar results and lidar, various solutions can be obtained (Coulter, 1979; Seidel et al., 2010; Beyrich and Leps, 2012; Haeffelin et al., 2012). The differences even increase when complex methods are used to distinguish between several PBL types (Coen et al., 2014). This leads to a validation and implementation problem in CTMs. To avoid the issue of the derivation problem, we advise not to use the MLH as input or validation data for CTMs in contrast to previous recommendations by studies like as Geiß et al. (2017). In accordance with the suggestion of Hanna and Yang (2001) we therefore increased the vertical grid resolution of the model to better reflect shallow inversion conditions by applying the recent multi-layering version of the LOTOS-EUROS CTM.

The impact on the PM mass concentration of the vertical layering in the LOTOS-EUROS CTM is much larger than the planetary boundary layer meteorology, with the multi-level approach of the LOTOS-EUROS CTM significantly increasing the concentration mass in the investigation area of Berlin. Major impact can be associated to cold stagnant weather conditions, especially easterly wind periods and

a better representation of high trans-boundary PM contributions. By contrast, warm periods are not as large modified by using the high vertical grid structure. This can be attributed to a modified distribution of the chemical compounds, especially nitrate, and ammonium, which responded highly sensitive within the used model set-ups. Compared to the mixed-layer version the nitrate and ammonium concentration levels are increased and lead to an increased total PM mass concentration when applying the higher resolved vertical layering structure.

This study and recent assessment for NO₂ and ozone show that the multi-level approach of the LOTOS-EUROS CTM keeps the pollutants closer to the surface than the mixed layer approach (Escudero et al., 2019; Fallah et al., 2020). Fallah et al. (2020) further reveals a seasonal relationship of the nitrogen oxide mass concentration levels dependent on the applied vertical set-up, with an overestimated mixing in the mixed-layer version of the LOTOS-EUROS CTM. The similarity of the results for summer was large, where a better performance for the multi-level model version was found for the winter season compared to the mixed-layer approach. However, the refined vertical layering still results in too high PM concentration levels in urban areas and non-polluted periods, thus further investigations of the model set-up must be carried out.

Higher resolved model simulations and the use of the COSMO-CLM model as meteorological input data, leads to a more realistic representation of the urban-increment compared to coarser model simulations driven by the ECMWF model. Especially the spatial distribution of the PM background

concentration is considerably improved. The higher horizontal resolution of the LOTOS-EUROS CTM in combination with high resolution meteorological input data hence leads to less artificial dilution in urban areas.

Individual chemical compounds should be examined and considered separately by applying a labelling approach. Underestimated processes like as resuspension due to traffic, construction or agriculture could then easily be identified to improve the emission inventory for the Berlin agglomeration. Further investigations based on source apportionment and receptor studies and their comparison to PMF observations should be carried out to further enhance the insight of long-range and local contributions in the investigation area of Berlin.

CRedit authorship contribution statement. **M. Thürkow:** Conceptualization, Writing-review & editing, Formal analysis, Data curation, conceived the study, analyzed the data and produced the figures. **M. Schaap:** Conceptualization, Writing-review & editing, conceived the study. **I. Kirchner:** Formal analysis, Data curation, Writing-review & editing. **R. Kranenburg** and **R.M.A. Timmermans:** Writing-review & editing.

Declaration of competing interest. The authors declare that they have no known competing financial interests or personal relationships that could have appeared to influence the work reported in this paper.

Acknowledgment. The work presented here was funded through the German Environment Agency (UBA), Dessau-Roßlau, Project number: FKZ 3716 51 203 0. The authors gratefully

III. A multi-meteorological comparison for episodes of PM_{10} concentrations in the Berlin agglomeration area in Germany with the LOTOS-EUROS CTM

acknowledge the provision of data in the project "PM-Ost" from the Berlin Senate Department for the Environment, Transport and Climate Protection, Berlin, the Saxon State Office for Environment, Agriculture and Geology (LfULG), Dresden-Pillnitz, the State Office for Environment (LfU) of the Federal State of Brandenburg, Potsdam, and the State Office for Environment, Nature and Geology (LUNG) of the Federal State of Mecklenburg-Western Pomerania, Güstrow.

Paper IV

Dynamic evaluation of modeled ozone concentrations in Germany with four regional chemistry transport models

M. Thürkow¹, M. Schaap^{1,2}, R. Kranenburg², F. Pfäfflin³, L. Neunhäuserer³, R. Wolke⁴, B. Heinold⁴, J. Stoll⁴, A. Lupăscu^{5,*}, S. Nordmann⁶, A. Minkos⁶ and T. Butler^{1,5}

Published in Science of The Total Environment, Volume 906, January 2024, 167665, ISSN: 0048-9697, DOI: 10.1016/j.scitotenv.2023.167665, URL: <https://www.sciencedirect.com/science/article/pii/S0048969723062927>

This publication is licensed under a <https://creativecommons.org/licenses/by/4.0/>.

Contents

IV.1	Introduction	137
IV.2	Description of models and experimental design	139
IV.3	Results and discussions	146
IV.4	Summary and conclusion	162
IV.5	Appendix - figures	165
IV.6	Appendix - statistical indicators	166

Highlights

- A high resolution (national scale) multi-model intercomparison study was applied.
- The models show room for improvement predicting O₃ at night and MDA8 O₃ > 120 µg m⁻³.
- To evaluate the ozone sensitivity to temperature a new metric was developed.
- A large spread was found between the CTMs for the ozone sensitivity to temperature.

Abstract

Simulating the ozone variability at regional scales using chemistry transport models (CTMs) remains a challenge. We designed a multi-model intercomparison to evaluate, for the first time, four regional CTMs on a national scale for Germany. Simulations were conducted with LOTOS-EUROS, REM-CALGRID, COSMO-MUSCAT and WRF-Chem for January 1st to December 31st, 2019, using prescribed emission information. In general, all models show good performance in the operational evaluation with average temporal correlations of MDA8 O₃ in the range of 0.77-0.87 and RMSE values between 16.3 $\mu\text{g m}^{-3}$ and 20.6 $\mu\text{g m}^{-3}$. On average, better model skill has been observed for rural background stations than for the urban background stations as well as for springtime compared to summertime. Our study confirms that the ensemble mean provides a better model-measurement agreement than individual models. All models capture the larger local photochemical production in summer compared to springtime and observed differences between the urban and the rural background. We introduce a new indicator to evaluate the dynamic response of ozone to temperature. During summertime a large ensemble spread in the ozone sensitivities to temperature is found with (on average) an underestimation of the ozone sensitivity to temperature, which can be linked to a systematic underestimation of mid-level ozone concentrations. During springtime we observed an ozone episode that is not covered by the models which is likely due to deficiencies in the representation of background ozone in the models. We recommend to focus on a diagnostic evaluation aimed at the model descriptions for biogenic emissions and dry deposition as a follow up and to repeat the operational and dynamic analysis for longer timeframes.

Keywords: *air quality, model evaluation, inter-comparison, ozone, nitrogen oxides*

Author affiliation:

¹FUB, Institute of Meteorology, Freie Universität Berlin, Carl-Heinrich-Becker-Weg 6-10, 12165 Berlin, Germany

²TNO, Department Climate, Air and Sustainability, Princetonlaan 6, 3584 CB Utrecht, the Netherlands

³IVU Umwelt GmbH, Emmy-Noether-Straße 2, 79110 Freiburg, Germany

⁴TROPOS, Leibniz Institute for Tropospheric Research, Permoserstraße 15, 04318 Leipzig, Germany

⁵RIFS Potsdam, Research Institute for Sustainability, Helmholtz Zentrum Potsdam, Berlinerstraße 130, 14467 Potsdam, Germany

⁶UBA, Umweltbundesamt, Wörlitzer Platz 1, 06844 Dessau-Roßlau, Germany

*Now at ECMWF, Bonn, Germany

IV.1 Introduction

Ozone (O_3) remains one of the most toxic and ecologically detrimental air pollutants in Europe. Alongside particulate matter and nitrogen oxides, exposure to ozone causes a substantial burden of diseases in Germany (e.g., Krug et al., 2019; Krug et al., 2020). Millions of people are exposed to ozone levels above the WHO guideline values (EEA, 2018a). Ozone is not emitted but rather formed through complex chemical reactions in the atmosphere. Processes influencing ozone in the troposphere act over a range of spatial scales, from the global scale (Crutzen, 1973), through the regional scale (Schnell et al., 2015), down to the urban scale (Churkina et al., 2017). Ozone at a given location consists of the transported baseline concentration and the local production (Parrish et al., 2017; Derwent et al., 2018). The oxidation of methane in the remote troposphere and the subsequent long-range transport of remotely produced ozone into Europe contributes to about one third of the annual average baseline ozone concentration over Europe (Butler et al., 2020). The long-range contribution to the background is strongest in spring, while the local production is strongest in summer (HTAP, 2010). High local ozone concentrations associated with ozone threshold exceedance episodes are primarily attributable to regionally emitted ozone precursors (e.g., Reidmiller et al., 2009; Huang et al., 2017; Jonson et al., 2018; Lupaşcu and Butler, 2019; Lupaşcu et al., 2022).

The regional buildup of ozone is highly sensitive to several meteorological parameters such as temperature, moisture, and solar radiation and has

been documented in numerous scientific studies based on both measurements and modeling (e.g., Seo et al., 2014; Coates et al., 2016; Otero et al., 2016; Kavassalis and Murphy, 2017; Otero et al., 2018; Luo et al., 2020). The synoptic state, such as high-pressure systems and/or blocking conditions, can boost the formation of ozone over a period of several days (Black et al., 2004). Biogenic volatile organic compound (BVOC) emissions are highly temperature dependent (Jacob and Winner, 2009; Monks et al., 2015) and correlate to clear sky conditions (Guenther et al., 2006; Guenther et al., 2012). Their largest impact on ozone formation can be observed on warm and cloud-free days (Tawfik and Steiner, 2013) as photolysis is another crucial factor. Under high nitrogen oxide (NO_x) conditions the photochemical formation of ozone is enhanced with strong solar radiation (Kleinman, 1994), especially during summer when the solar insolation is at its largest (Schaap et al., 2015; Bessagnet et al., 2016). The photolysis of ozone can also act as a sink for ozone, for example in the remote marine boundary layer where NO_x concentrations are low (Oltmans and Levy, 1994). In high NO_x and low NMVOC (non-methane volatile organic compounds) conditions, the same occurs through the production of OH and subsequent reaction with nitrogen dioxide (NO_2). Vegetation is also an important sink of ozone through dry deposition. High temperatures along with low humidity cause plants to close their stomata to conserve water. This reduces the ozone removal (Fowler et al., 2009; Kavassalis and Murphy, 2017). A similar correlation was mentioned by Lin et al. (2020) for low soil moisture content when plants

IV. Dynamic evaluation of modeled ozone concentrations in Germany with four regional chemistry transport models

will tend to conserve water. Such a reduction in ozone dry deposition due to vegetative water stress can often be observed during extended episodes of high ozone levels related to heatwaves and droughts (Lin et al., 2020). Churkina et al. (2017) emphasized the role of enhanced precursor emissions such as VOCs and the removal effect of vegetation during heatwaves. Many of the chemical reactions involved in the production of ozone are also faster at higher temperatures (e.g., Sillman, 1995; Atkinson, 2007; Fischer et al., 2014; Coates et al., 2016).

Extensive modeling efforts are required to encompass ozone formation and removal processes with a sufficient high quality representation notably observed for intense episodes. To hindcast- and forecast the ambient air pollution of ozone at all scales, a hierarchy of numerical models is commonly used, consisting of global models (e.g., Young et al., 2018), regional models (e.g., Colette et al., 2017), and depending on the application, urban models (e.g., Maronga et al., 2019). Nowadays, it is common practice to conduct modeling frameworks using a multi-model (ensemble) approach with unified input data (emissions and/ or meteorology) as done for example in the Copernicus Atmosphere Monitoring Service (CAMS). Results of an ensemble are often more robust compared to a single simulation and can increase the validity of the model results (Colette et al., 2017; Chen et al., 2019). Numerous model intercomparison studies for ozone have been performed on both global and regional scales (e.g., Rao et al., 2011; Foley et al., 2015a; Foley et al., 2015b; Bessagnet et al., 2016; Colette et al., 2017; Galmarini et al., 2017; Otero et al., 2018; Chen et al., 2019).

The response of ozone to a uniform changing emission dataset has been studied in the HTAP framework (e.g., Galmarini et al., 2017; Jonson et al., 2018). Model performance assessments and the evaluation of model processes have been performed within the inter-comparison studies of ACCMIP (e.g., Lamarque et al., 2013; Stevenson et al., 2013) and CCMi (e.g., Morgenstern et al., 2017; Dhomse et al., 2018) for the global scale. The AQMEII (e.g., Rao et al., 2011; Solazzo and Galmarini, 2016; Galmarini et al., 2017), CAMS (e.g., Flemming et al., 2017; Inness et al., 2019) and EURODELTA (e.g., Colette et al., 2017) frameworks can be mentioned as examples for regional model evaluations. Within CAMS the needs for the development of regional air quality modeling aspects have been developed and described in detail. The CAMS_g1 service provides information on how to handle daily forecasts- and hindcasts using multi-model (ensemble) simulations. Only a few studies for air quality benchmarking on a national level have been reported so far.

The quality of model (ensemble) simulations in the past has predominantly been assessed by determining the model errors with respect to in-situ measurements using the operational evaluation. This can be done using different model quality indicators, such as those provided by the FAIRMODE initiative (Forum for AIR quality MODELing in Europe, <https://fairmode.jrc.ec.europa.eu/>). To assess the model errors in more detail, the dynamic (model) evaluation can be used (e.g., Dennis et al., 2010; Lecœur and Seigneur, 2013; Hennehan et al., 2017). The dynamic evaluation allows a quality assessment of model simulations, based on the

analysis of the relationship between air pollutants and different input drivers, such as emissions and/ or meteorology. While the operational model evaluation compares the absolute modeled concentration to measurements, the dynamic evaluation is based on the comparison of changes in modeled and observed concentration levels (Dennis et al., 2010; Lecœur and Seigneur, 2013). This assesses whether the models can capture changes in concentrations related to different meteorological conditions or emission changes (Dennis et al., 2010). Modeled and observed sensitivities to different processes can further be diagnosed (Dennis et al., 2010; Hennehan et al., 2017). Ozone metrics can be correlated with meteorological parameters as shown in previous studies (e.g., Lecœur and Seigneur, 2013; Otero et al., 2016; Otero et al., 2018). In Lecœur and Seigneur (2013), correlations were estimated for chemistry transport model simulations of particulate matter related to temperature, precipitation, and wind speed and their 0 to 10 subsequent days. In Otero et al. (2016) and Otero et al. (2018), a multiple linear regression analysis for different meteorological conditions was applied to estimate their relevance for ozone. Otero et al. (2016) also indicate the correlation of probabilistic threshold exceedances and estimates the meteorological impact to ozone extreme values.

In this study we (1) perform a model inter-comparison study with uniform input data (notably emissions and meteorology) to (2) assess the model quality on the regional (national) scale for Germany in 2019, by (3) a combined approach of the operational and the dynamic evaluation, aiming (4) to examine model specific behavior

as a function of meteorology. In Section IV.2, we describe the experimental design of the model inter-comparison study, give information on all four models applied and the framework used for the operational and the dynamic evaluation. In Section IV.3 the results are provided, discussed and put in a broader perspective. In Section IV.4 the conclusion is presented.

IV.2 Description of models and experimental design

IV.2.1 Participating Models

In the context of this study four Eulerian chemistry transport models have been evaluated and compared: LOTOS-EUROS, REM-CALGRID, COSMO-MUSCAT and WRF-Chem (Table IV.1 & Table IV.2). All models are designed as regional-scale, limited-area models to perform air quality assessments on short- and long time scales in the lower troposphere and can be used for process studies in scientific research activities as well as for regulatory efforts and policy advice. All models applied have previously participated in several model inter-comparison studies, such as EURODELTA (Colette et al., 2017) and/or AQMEII (Solazzo et al., 2012; Im et al., 2015a; Im et al., 2015b), in which the performance of the models have been assessed to its peers. The models are also widely used for ozone applications (e.g., Flemming and Stern, 2007; Mar et al., 2016; Escudero et al., 2019). The models differ in their complexity with respect to chemical formation processes, vertical layering and especially in their meteorological driving. We

IV. Dynamic evaluation of modeled ozone concentrations in Germany with four regional chemistry transport models

employed two offline (LOTOS-EUROS & REM-CALGRID) and two online models (COSMO-MUSCAT & WRF-Chem). Characteristics relevant for the model's ozone prediction are summarized in Table IV.1 & Table IV.2. For a complete description with application examples of the models we refer to the key references given in the tables.

IV.2.2 Experimental Design

To guarantee the comparability of the results as much as possible, an intercomparison protocol was developed to harmonize anthropogenic emissions, meteorological input data, boundary conditions, model domains and resolutions as far as possible.

The simulations were conducted for the year 2019 over a domain encompassing Germany (Figure IV.1, upper panel). Each model simulation has been performed in a nested approach with the outer domain covering Europe. The outer model domain has been employed to encompass the impacts of long-range transport on air quality in Germany. The target domain over Germany is defined by a regular longitude-latitude grid with a spatial resolution of approximately $2 \times 2 \text{ km}^2$ and also covers parts of the neighboring countries, e.g. the Netherlands, Belgium, Luxembourg, and Poland. We allow all models to freely select the number of required intermediate nested grids. By doing so, the expert knowledge for each model system could be used to represent the air quality in the most accurate manner. Note that, the model simulations for the inner nest are performed either with a grid definition matching or with a native grid definition close to the target grid, with all modeled concentrations

harmonized to the target $2 \times 2 \text{ km}^2$ grid for the purposes of intercomparison.

The model simulations were driven by meteorological input data provided by the German Weather Service (Deutscher Wetterdienst, DWD, e.g. Reinert et al. (2016b)). For the large-scale European simulation, the ICON-EU meteorology with a horizontal resolution of about $7 \times 7 \text{ km}^2$ was selected. Over Germany, the higher-resolved COSMO-D2 model ($\sim 2.2 \text{ km}^2$) has been applied. With the operational setup, the DWD provides 60 vertical layers for ICON-EU and 65 for COSMO-D2. The offline models (LOTOS-EUROS & REM-CALGRID) directly make use of these meteorological datasets as 1-hourly input for their chemical transport modeling. WRF-Chem and COSMO-MUSCAT (both online models) use their own methods for further processing the meteorological information according to the needs of their model specifics. For WRF-Chem and COSMO-MUSCAT, the meteorology is simulated as a hindcast itself, driven by initial and boundary conditions of the DWD models. To stay close to the DWD product, the model simulations are re-/ initialized every 24-72 hours. Aside from the reinitialization of meteorological input fields, WRF-Chem and COSMO-MUSCAT also nudge the 3-D meteorological fields of winds, potential temperature, water vapor mixing ratio, and geopotential every hour to ensure that the fields are not largely diverging from the DWD models.

For Germany, the officially reported anthropogenic emissions were provided by the German Environment Agency (Umweltbundesamt, UBA, www.uba.de) for all participating models individually, gridded using

the GRETA system (Gridding Emission Tool for ArcGIS, [Schneider et al. \(2016\)](#)). For the rest of Europe, the regional inventory of CAMS for 2018 (CAMS-REG, [Kuenen et al. \(2022\)](#)) was used. The sector classification for both emission inventories follows the Gridded Nomenclature for Reporting (GNFR). The breakdown of the GNFR sector F (road transport) in GRETA towards the sub-categories F1-F4 is based on a factor split derived from CAMS-REG ([Table IV.3](#)). Area sources from GRETA's GNFR sectors A, B, D, J, and H have been vertically distributed by using the height profile presented in [Table IV.4](#). All remaining area sources were to be emitted into the lowest model layers. Point sources from GRETA were vertically distributed using the height information that comes with the product. Profiles for the CAMS-recommended height distribution for point and area sources were adjusted by each model group individually on the corresponding grids of the outer nests. For all sectors, the emission time profiles were set to the CAMS temporal profiles to account for the hourly evolution from their emitting activity sectors. For road transport (GNFR sector F) the direct NO₂ emission percentage was set to 20 %. All other NO_x emission sources are distributed with a 97 % to 3 % (NO to NO₂) ratio. The composition of PM and NMVOCs corresponds to CAMS-REG and has been adjusted to the chemical mechanism of the respective models.

The land use classification is based on the EU-wide Corine Land Cover (CLC) dataset for 2018 ([EEA, 2021](#)). Over Germany, the dataset of the Federal Agency for Cartography and Geodesy (BKG,

<https://mis.bkg.bund.de>) with a finer resolution of 5 ha was used. Global reanalysis data (ECMWF Atmospheric Composition Reanalysis 4: EAC4) of CAMS were used as boundary conditions around the outer European domain including the model top ([Inness et al., 2019](#)). The EAC4 data are based on global chemistry transport calculations in a horizontal resolution of 0.75° and are available in time steps of 3 hours.

Table IV.1: Description of basic structures, schemes and relevant parameters of the four participating models (part 1).

	LOTOS-EUROS	REM-CALGRID	COSMO-MUSCAT	WRF-Chem
MODEL OVERVIEW				
Key references	Manders et al. (2017)	Stern (2003)	Wolke et al. (2012)	Grell et al. (2005) and Fast et al. (2006)
Version	2.2.002	4.0	5.05-02	3.9.1
Research group	TNO	IVU Umwelt	TROPOS	RIFS
Two-way feedback	offline	offline	online	online
INTERNAL MODEL GRID STRUCTURE				
Nesting & horizontal resolution	3 domains (28x32 km ² ; 7x8 km ² ; 2x2 km ²)	3 domains (28x32 km ² ; 7x8 km ² ; 2x2 km ²)	2 domains (14x14 km ² ; 2x2 km ²)	3 domains (30x30 km ² ; 10x10 km ² ; 2x2 km ²)
Vertical layers	13	10/8	40/65	38
Vertical extent	8000/4000 m (7/10 layers below 1500 m)	3000 m (8 layers below 1300 m)	8000 m (MUSCAT: 11/20 layers below 1000 m)	20000 m (11 layers below 3000 m)
Depth of first layer	20 m	20 m	20 m	25 m
INPUT DATA (HARMONIZED)				
Meteorology	ICON-EU & COSMO-D2 (both DWD)			
Emissions	German Environment Agency (UBA) for Germany & CAMS-REG (Kuenen et al., 2022) for Europe			
Boundary conditions	CAMS-EAC4 (Inness et al., 2019)			
Land use	Corine Land Cover 2018 (EEA, 2021) & the 5 ha dataset of the Federal Agency for Cartography and Geodesy (BKG)			
MODEL PROCESSES				
Advection	based on Walcek (2000)	based on Walcek (2000) , modified by Yamartino (2003)	based on Hundsdoerfer et al. (1995) , Wolke and Knoth (2000) , and Schlegel et al. (2012)	third-order Runge–Kutta time-integration (Skamarock et al., 2008)
Vertical diffusion	K _z -theory, with K _z values calculated in the stability parametrization	based on K-theory	provided online by COSMO	vertical turbulent mixing calculated online
Dry deposition	DEPAC (Van Zanten et al., 2010)	DEPAC (Van Zanten et al., 2010)	based on Seinfeld and Pandis (2006) and Schlunzen et al. (2012)	based on Wesely (1989)

Table IV.2: Description of basic structures, schemes and relevant parameters of the four participating models (part 2).

	LOTOS-EUROS	REM-CALGRID	COSMO-MUSCAT	WRF-Chem
MODEL PROCESSES				
Wet deposition	Banzhaf et al. (2012)	simple wash-out approach, scavenging rates are calculated from temperature- and species-dependent Henry's Law solubility and rainfall rate	based on Simpson et al. (2012)	based on Neu and Prather (2012)
Gas phase chemistry	CBM-IV (Gery et al., 1989) with 38 species and 96 reactions	CBM-IV (Gery et al., 1989) with 36 species and 93 reactions	RACM-MIM2-ext (Stockwell et al., 1997; Karl et al., 2006; Luttkus et al., 2022) with 140 species and 335 reactions	MOZART4 (Emmons et al., 2010) with 140 species and 335 reactions
Cloud chemistry	ph dependent oxidation scheme	no explicit cloud chemistry, simple parameterization of sulfate oxidation in clouds	based on Schaap et al. (2004)	double microphysics scheme (Morrison and Gettelman, 2008)
Photolysis	computed offline with the solar-zenith angle and adjusted online by clouds	offline computed clear sky rates based on the TUV radiative transfer model, online modified by cloud cover from the meteorological driver	computed offline with the solar-zenith angle and adjusted online by clouds	provided online based on clear-sky rates as function of solar-zenith angle and cloud shading factors
Biogenic emissions	similar to Steinbrecher et al. (2009)	based on Simpson et al. (1995a), Simpson et al. (1995b), and Simpson et al. (1999)	based on Steinbrecher et al. (2009)	based on Guenther et al. (2006)
SOA formation	not included here	SORGAM (Schell et al., 2001)	based on Schrödner et al. (2014) and Luttkus et al. (2022)	based on Knote et al. (2014)
Sea salt emissions	based on Monahan (1986) and Mårtensson et al. (2003)	based on Monahan (1986), Gong et al. (1997a), and Gong et al. (1997b)	based on Long et al. (2011) and Sofiev et al. (2011)	based on Monahan (1986), Gong et al. (1997a), Gong et al. (1997b), and O'Dowd et al. (1997)

IV. Dynamic evaluation of modeled ozone concentrations in Germany with four regional chemistry transport models

Table IV.3: Breakdown of the GNFR sector F (GRETA) into the transport sub-categories F1 (exhaust-gasoline), F2 (exhaust-diesel), F3 (exhaust-LPG) to F4 (non-exhaust) from CAMS-REG [fraction of the total].

	F1	F2	F3	F4
CO	0.75	0.24	0.01	0.00
CO ₂	0.33	0.66	0.01	0.00
NH ₃	0.74	0.20	0.05	0.00
NMVOOC	0.58	0.16	0.03	0.23
NO _x	0.03	0.97	0.00	0.00
PM ₁₀	0.05	0.20	0.00	0.75
PM ₂₅	0.07	0.31	0.00	0.62
SO ₂	0.30	0.70	0.00	0.00

IV.2.3 Evaluation metrics and measurement data

The modeling results were sampled for locations of the monitoring network from the German Environment Agency and the German federal states, as available in the central database at UBA. Based on the 2x2 km² mesh size of the target grid resolution, we only incorporated background sites (urban, suburban, and rural) into the model performance evaluation. Sites located above 900 m were excluded from the analysis. In total, 238/ 247 (O₃/ NO₂) measurement sites were included (Figure IV.1). The classification into urban (93/ 108), suburban (72/ 71), and rural (73/ 68) background sites was used to discriminate between more and less polluted areas in Germany. The distinction between rural and urban sites is used to consider any (potential) titration effects and provides information on the modeled ozone production efficiency, which may vary considerably with the location and timing of NO_x emissions.

Annual mean concentration maps were created to illustrate differences in the spatial distribution between all models. A regression analysis was per-

Table IV.4: Height distribution of area sources for GRETA (A: Public power; B: Industry; D: Fugitive; H: Aviation; J: Waste).

sector	0-20 m	20-92 m	92-184 m	184-324 m	324-522 m	522-781 m	781-1106 m
H	0.25	0.25	0.1	0.1	0.1	0.1	0.1
A, B, D, J	0.1	0.8	0.1	0	0	0	0

formed to quantify the spatial correlation with measurements. Besides the evaluation of the spatial distribution, we generated time series for all stations from which we show selected sites in rural (Westerland: DEUB001), suburban (Augsburg: DEBY099) and urban (Berlin: DEBE034) locations as well as for all monitoring sites averaged. Time series of the daily mean and the mean values of the daily maximum 8-hour average (MDA8) for ozone provide more insight into the synoptic variability. Difference plots address the specific dissimilarities between the individual model simulations. By analyzing average weekly and daily variations, the meteorological impact can be largely removed, and the effect of anthropogenic emissions is emphasized. We therefore calculated average diurnal cycles for all days of the week. For ozone we distinguished between the growing season (April-September) and the winter period (January-March & October-December). We further subdivided the growing season into April-June and July-September, as it was anticipated that during the April-June period ozone concentrations are predominantly affected by long-range transport, while from July to September the local photochemical production plays a more important role (Otero et al., 2018; Butler et al., 2020).

We calculated an ensemble mean from the four models to verify possible benefits when using a simple poor man's ensemble approach. The performance between the individual model members can thus be compared against each other and to this ensemble mean. To evaluate the capability of the ensemble mean to represent different concentration regimes for ozone, we grouped the MDA8 O₃ into discrete bins based

on concentration.

A wide range of statistical indicators were computed to benchmark the model performance. We used mean bias (MB), root mean squared error (RMSE), index of agreement (IOA) and correlation coefficient (R) (see appendix). Due to the large number of stations we calculated average statistics over all sites. Exceedances of the calculated values of the 120 µg m⁻³ EU long-term target value for MDA8 O₃ have been investigated as well. All four models were evaluated on their ability to capture the observed threshold exceedances using time series and statistics. We scored the models on their rate of false alarms (FA), missed alarms (MA), good values below (GA⁻), and good values above (GA⁺) the threshold for MDA8 O₃ of 120 µg m⁻³. In an ideal case, the number of false and missed alarms is small compared to the number of good values below and above the threshold. We provide the probability of detection (POD) and the success ratio (SR), that is "comparing the (correct) modeled alerts with the (observed) alerts and the (correct) modeled alerts with (all) alerts issued by the model", respectively (Janssen and Thunis, 2022).

We made use of the air quality modeling benchmarking indicators provided by the FAIRMODE initiative (Janssen and Thunis, 2022). In FAIRMODE, scientific model assessment methods are combined and harmonized using modeling quality indicators (MQIs) and modeling performance indicators (MPIs). All indicators are based on the uncertainty of measurements for each pollutant (RMS_U). Note, that the calculation of the RMS_U differs for time series and annual averaged values. The MQIs are calculated using the ratio between

IV. Dynamic evaluation of modeled ozone concentrations in Germany with four regional chemistry transport models

the model error and the RMS_U , scaled by a factor $\beta=2$, so that the differences between modeled results and observations are allowed to be twice as large as the RMS_U . To emphasize further needs for model improvements we make use of the MPIs that are related to the temporal variation in terms of correlation (MPI_R), bias (MPI_{Bias}), standard deviation (MPI_σ) and high percentile values (MPI_{Perc}). In FAIRMODE the 92.9th percentile of the MDA8 O_3 is used to calculate the MPI_{Perc} . Similar to ozone, the MPI_{Perc} is assessed for nitrogen dioxide that equals the 19th occurrence in 8760 hours (99.8th percentile). In FAIRMODE, defined modeling quality objectives (MQO) and modeling performance criteria (MPC) are being used to indicate the limits of applicability of a modeling approach. The MQO and the MQC are fulfilled when the 90th percentile value of corresponding MQI and MPI values are ≤ 1 . For a more detailed description of all indicators, the objective and criteria we refer to [Janssen and Thunis \(2022\)](#). The calculation of all indicators applied in this study is given in the appendix.

We further assessed the quality of all four models and the ensemble using a dynamic (model) evaluation. The MDA8 for ozone has been used for this evaluation. We classified the prevailing weather conditions by categorizing the meteorological parameters into discrete bins. Similar straightforward methods of clustering meteorological conditions to determine the accumulation of air pollutants have also been applied in previous research activities (e.g., [van Pinxteren et al., 2019](#); [Thürkow et al., 2021](#)). The MDA8 for ozone was assigned to each of these discrete classes. As a measure for the meteorological conditions, we selected the daytime maximum tem-

perature (T_{max}) and the corresponding humidity at 2 m altitude ($\text{RH}@T_{\text{max}}$). We used the DWD COSMO-D2 forecasts as a proxy for observations, as they were applied as input dataset to all four individual models. For statistical robustness we require for each bin that the number count of the observations is larger than the number of stations being used. We further tried to quantify the relationship between temperature and MDA8 O_3 by a very basic calculation. For this, the average mean MDA8 O_3 values of the binned temperature clusters for ($T_{\text{max}} = 30$ to 32 °C) and ($T_{\text{max}} = 20$ to 22 °C) were subtracted from each other and divided by the 10 °C temperature difference between these bins. We performed the dynamic evaluation for urban and rural sites as well as for different periods of the year separately as described above.

IV.3 Results and discussions

IV.3.1 Spatial distribution

Figure IV.1 shows maps of the annual averaged MDA8 O_3 over Germany, for all models and the measured background concentration. A regression analysis compares the modeled and the measured concentrations and is shown below the maps for each model. The ensemble mean is presented aside. In [Figure IV.2](#) the same information as in [Figure IV.1](#) is given for the nitrogen dioxide concentration.

The spatial ozone distribution calculated by all models shows a very similar pattern ([Figure IV.1](#)). Largest concentrations in Germany are found in the rural background, including a clear signal of the orography. Here, we found

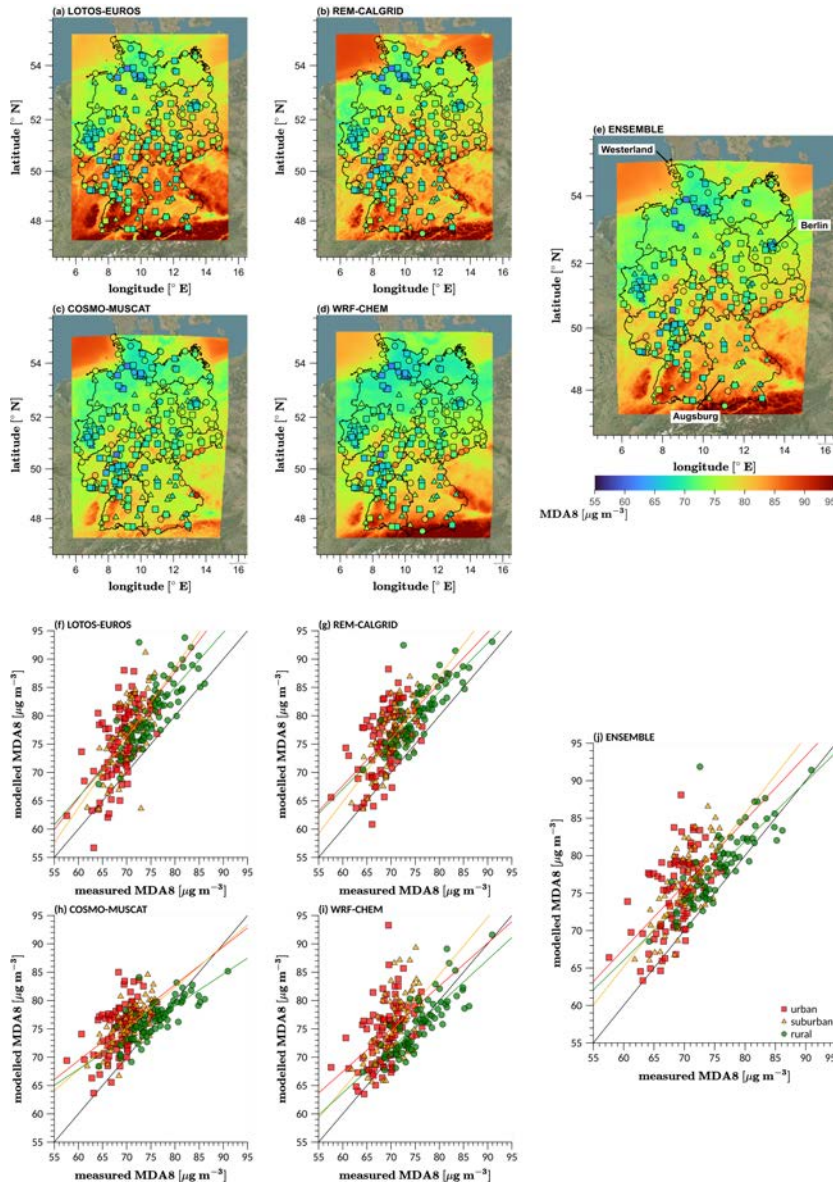


Figure IV.1: Annual averaged MDA8 O₃ over Germany for LOTOS-EUROS (a), REM-CALGRID (b), COSMO-MUSCAT (c) and WRF-Chem (d). Measured concentrations of the urban (square), suburban (triangle) and rural (circle) background are shown on top. A regression analysis compares the modeled and the measured concentrations and is shown below the maps for each model (f-i). The ensemble mean of all models is shown in subplots (e) and (j).

IV. Dynamic evaluation of modeled ozone concentrations in Germany with four regional chemistry transport models

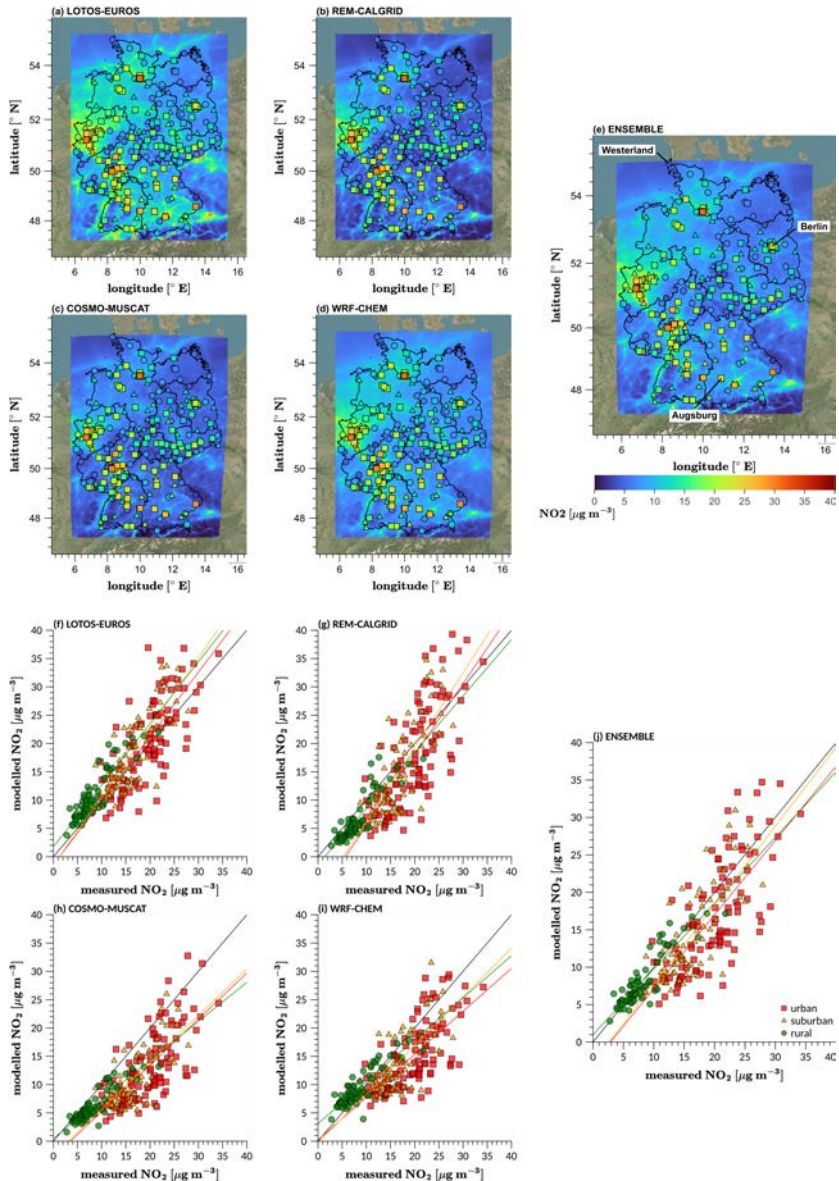


Figure IV.2: Same as in Figure IV.1 with information given for the nitrogen dioxide concentration.

for all four models the well-known elevated ozone concentration pattern in the Alps. The lowest values are found in and near NO_x source regions, like the Main-Rhein area, the Ruhr area as well as the larger cities like Berlin, Hamburg, Bremen, and Munich. These minima are due to the well known titration of ozone by nitrogen monoxide. All models show increased ozone levels above the sea, consistent with a smaller dry deposition sink in comparison to land areas.

The regression analysis for ozone summarizes the average model-measurement comparison indicating different fit slopes for the participating models (Figure IV.1). All models overestimate the measured MDA8 O_3 levels on annual average in the German background for rural, suburban and urban areas. Systematic differences among the model participants become obvious in the rural background, over the large cities, the sea, and the Alps. The model members differ mainly in terms of the differentiation between urban and rural regions, with the largest absolute mean bias seen for urban areas. This corresponds with larger fraction errors in the urban background than in the rural background. Rural regions show an overall larger model-measurement agreement. In addition, the spatial pattern varies between the models, e.g., over the sea, at higher elevations, and with respect to the gradient between northern and southern Germany.

Modeled distributions for nitrogen dioxide clearly show the same pattern as the input emissions due to its short lifetime in the atmosphere (Figure IV.2). All major cities and highways can be seen in the annual distribution. Most models show an average negative bias for the nitrogen

dioxide background concentration. In the urban background larger variations can be recognized for all model participants compared to the rural area.

IV.3.2 Temporal analysis

Figure IV.3 shows daily time series of the MDA8 O_3 , for the models and measured ozone as average at all background monitoring sites in Germany. The difference for each model against the measured concentration is presented in the lower panel. In Figure IV.4 we classified the MDA8 for ozone for observed discrete bins of $20 \mu\text{g m}^{-3}$ to investigate how well the models can reproduce different ozone concentration regimes. Daily mean time series for three example sites (Westerland, Augsburg and Berlin-Neukölln) are presented in Figure IV.5.

The time series (Figure IV.3 & Figure IV.5) show that the highest ozone levels in 2019 were measured for a few single days in June and two episodes in the second half of July and at the end of August. The dynamic range across the year of the simulated ozone concentration differs between the models, as the ordering of the model systems changes from season to season (Figure IV.3 & Figure IV.4). Figure IV.4 shows that the MDA8 O_3 of about $80\text{--}120 \mu\text{g m}^{-3}$ in summer and about $40\text{--}80 \mu\text{g m}^{-3}$ in winter are captured well by the models. Observed concentration bins of the MDA8 for ozone are overestimated by the models below $80 \mu\text{g m}^{-3}$ in summer. For winter, the models are biased high for concentration bins of the MDA8 O_3 below $40 \mu\text{g m}^{-3}$ and biased low for MDA8 O_3 above $80 \mu\text{g m}^{-3}$.

We also found that the models capture MDA8 O_3 values above $120 \mu\text{g m}^{-3}$ during summer and fall to a

IV. Dynamic evaluation of modeled ozone concentrations in Germany with four regional chemistry transport models

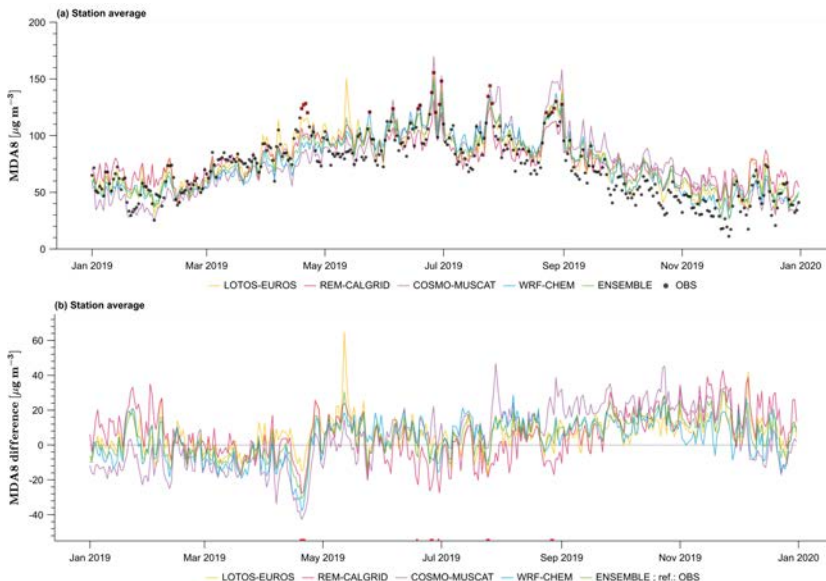


Figure IV.3: Time series (a) of the MDA8 O₃ for LOTOS-EUROS (yellow), REM-CALGRID (magenta), COSMO-MUSCAT (purple), WRF-Chem (blue) and the ensemble mean (green). Plotted values reflect the average background concentration of all available monitoring sites in Germany. Measured concentrations are indicated with black circles. The difference for each model and the ensemble mean to the measured concentration is shown in subplot (b). Exceedances above the MDA8 O₃ target value of 120 $\mu\text{g m}^{-3}$ are indicated with red dots.

fairly large extent (Figure IV.3 & Figure IV.4). However, on average, the model ensemble underestimates the MDA8 for ozone above the 120 $\mu\text{g m}^{-3}$ air quality target threshold. Especially, the observed high ozone levels during the end of April are not captured by any of the model participants (Figure IV.3). Inspection of the individual example sites further reveals model specific features (Figure IV.5). We found that all four models can represent the conditions present in coastal areas for example in the German location of Westerland. Ozone background concentrations for large agglomerations like in Berlin and for suburban areas in middle-sized cities represented by the station Augsburg can be captured as well.

As the MDA8 O₃ is thought to be

rather insensitive to titration regimes the analysis of the diurnal behavior provides additional information on the ozone concentration itself. In Figure IV.6 the day of the week cycles for modeled ozone and the measured levels are shown for rural and urban background sites and in Figure IV.7 the same information is presented for nitrogen dioxide.

All models reproduce the early morning ozone minimum at the same time and the increase of ozone levels at a similar rate afterwards (Figure IV.6). We also found that the models capture the morning and the evening daytime maxima for nitrogen dioxide concentrations (Figure IV.7). However, the timing of the daytime ozone maximum between the models can be slightly shifted.

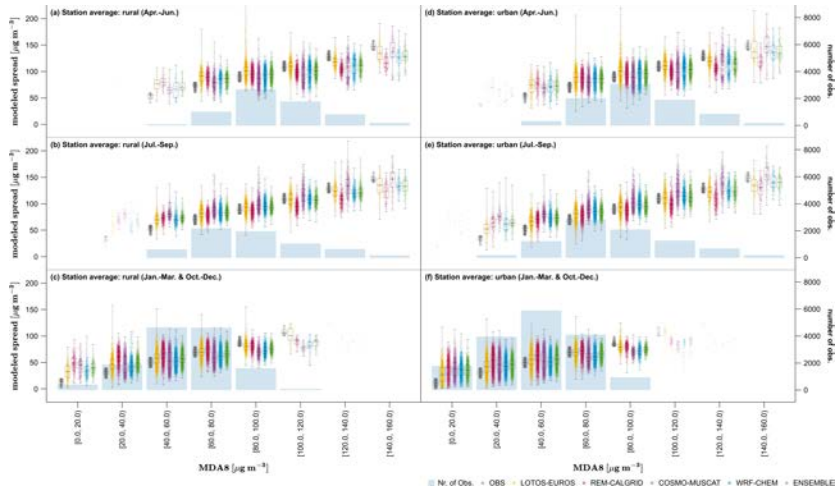


Figure IV.4: Modeled ozone concentration (MDA8 O_3) in relation to the measured ozone levels for LOTOS-EUROS (yellow), REM-CALGRID (magenta), COSMO-MUSCAT (purple), WRF-Chem (blue) and the ensemble (green). Observations are shown in grey. Plotted values are binned by the measured background concentration levels of all available monitoring sites in Germany. Each single dot represents one observation (one day of the MDA8 O_3 in the corresponding bin from one station). The box plot shows the mean, median, 25th and 75th percentile as well as the min and max values. Different station classes are separated out for rural (a-c) and urban (d-f) areas. The periods of April-June and July-September are shown in the subplots (a,d) and (b,e) as well as the winter months January-March and October-December in subplots (c,f).

We also found that the modeled absolute concentrations largely differ between the model groups. All models hardly capture the low ozone levels at night in summer and winter. Especially in the urban background, the models do not decrease as far and overestimate the ozone levels up to $20 \mu\text{g m}^{-3}$ during the night. LOTOS-EUROS shows the deepest nighttime dips, which could be related to larger NO_2 concentrations at night.

We also found on average better model-measurement agreement during the growing season than in winter. Especially in July-September the results largely vary between the ensemble members, with the models sometimes showing better agreement and sometimes not. During the middle of the day, the

nitrogen dioxide levels are often underestimated by all models. The models slightly tend to overestimate the afternoon maxima of NO_2 in rural areas and in the urban background at weekends. LOTOS-EUROS shows too pronounced morning daytime maxima for NO_2 . In winter the treatment of stability and the titration of NO play a key role and still remain difficult. REM-CALGRID converts NO_2 cycles rather well except for rural background areas during the winter season, where the model substantially differs from the model ensemble.

Simulated ground-level ozone has already been shown to be sensitive to the model representation of the local production which can be influenced e.g. by vertical mixing processes in the free troposphere and the planetary bound-

IV. Dynamic evaluation of modeled ozone concentrations in Germany with four regional chemistry transport models

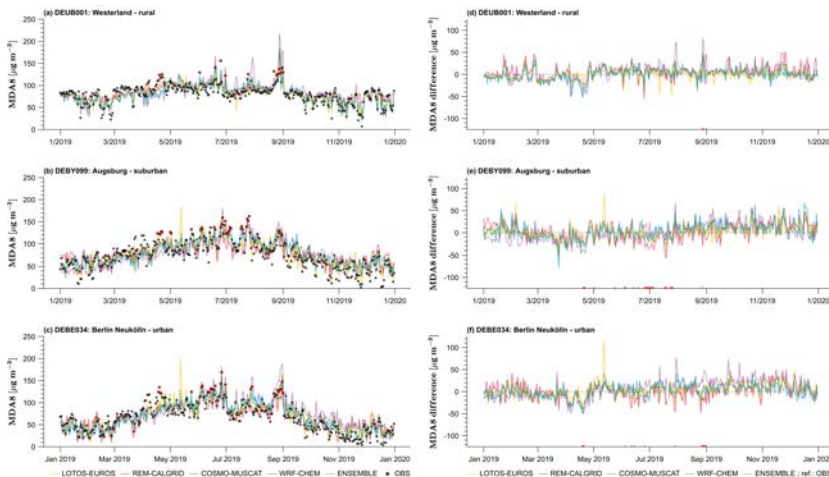


Figure IV.5: Same as in Figure IV.3 with the information of Westerland (a,d), Augsburg (b,e) and Berlin Neukölln (c,f) instead of the station average over Germany. Time series of the MDA8 O_3 are presented in subplot (a-c). The differences for modeled and measured levels are subdivided in (d-f).

ary layer (Jang et al., 1995; Hogrefe et al., 2018). In addition, the ozone simulated by regional models can be affected by long-range transport and thus can be highly sensitive to the choice of chemical boundary conditions. The concentrations predicted for the outer domain act as boundary conditions and also impact the inflow of ozone through the edges of the inner model domain(s) (Colette et al., 2017; Im et al., 2018). The information on causes for (high) ozone episodes can be obtained from simulations that account for the attribution of different source sectors and source regions (e.g., Lupaşcu and Butler, 2019; Pay et al., 2019; Butler et al., 2020; Lupaşcu et al., 2022; Schaap et al., 2023) and could give further indication on the reasons why the model results largely vary for threshold exceedances of $MDA8 O_3 > 120 \mu g m^{-3}$ in April compared to the observations.

Ozone exceedance events in the summertime are mainly affected by re-

gional photochemistry (Schaap et al., 2023). Figure IV.7 shows (on average) lower nitrogen dioxide concentrations in the observed afternoon rush-hour peak (caused by lower emissions in urban areas) on weekends than during the week. This leads to a lowered titration on weekends. Accordingly, lower ozone concentrations can be expected during the rest of the week than on weekends (Koo et al., 2012) in many urban areas. In NO_x limited regions, such as in rural areas or some urban locations, the ozone level can also be lowered with decreased NO_x levels at daytime. This uncertainty to changes in NO_x emissions with respect to O_3 and their response to local photochemistry can be in principle captured by the models. However, addressing the weekend effect requires to analyse several years of data meaning that our single year simulation is not sufficiently long to quantify the effect. In addition, the emission information needs to

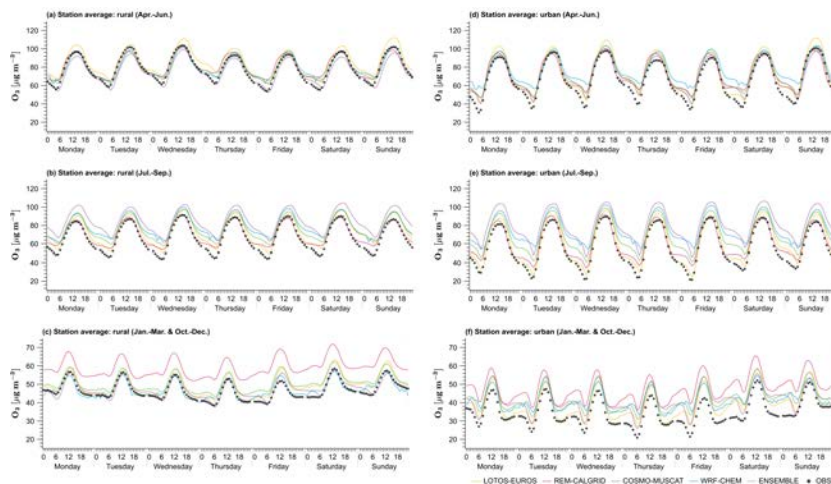


Figure IV.6: Day of the week ozone concentration for LOTOS-EUROS (yellow), REM-CALGRID (magenta), COSMO-MUSCAT (purple), WRF-Chem (blue) and the ensemble mean (green). Plotted values reflect the average background concentration of all available monitoring sites in Germany. Measured concentrations are indicated with black circles. Different station classes are separated out for rural (a-c) and urban (d-f) areas. The periods of April-June and July-September are shown in the subplots (a,d) and (b,e) as well as the winter months January-March and October-December in subplots (c,f).

be refined for this purpose as generic (monthly, weekly and daily) temporal profiles per sector have been used.

IV.3.3 Model performance evaluation by comparison with measurements

In Figure IV.8 the mean bias (MB), root mean squared error (RMSE), index of agreement (IOA) and temporal correlation (R) averaged over all German background sites are presented. The statistics for ozone and nitrogen dioxide concentrations were calculated for hourly and daily time series. For ozone, we also provide statistics of the MDA8 and the daytime maximum. Each indicator's value (lowest to largest skill) has been color coded (from dark to light red) to improve the readability and comparability.

The information presented in Figure IV.8 illustrates the common behavior that chemistry transport models perform (slightly) better for daily than for hourly time series. Hourly ozone correlation coefficients for all models are between 0.68 and 0.80. Corresponding values of the daily mean time series are between 0.67 and 0.85. Higher correlation coefficients can be observed for the daytime maximum for ozone and the MDA8 O₃ ranging between 0.78-0.86 and 0.77-0.87, respectively. For the hourly time series, the models show a larger root mean squared error (20.4-25.4 µg m⁻³) than calculated for the daily time series (14.4-21.3 µg m⁻³) as expected. The root mean squared errors for the daytime maxima and the MDA8 O₃ are comparable to numbers we calculate for the daily time series (both about 16.3-20.6 µg m⁻³). Modeled mean biases for the daily and

IV. Dynamic evaluation of modeled ozone concentrations in Germany with four regional chemistry transport models

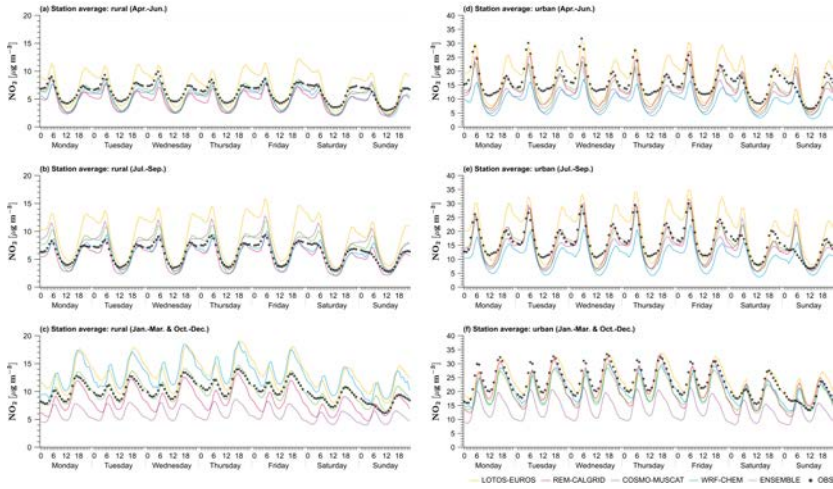


Figure IV.7: Same as in Figure IV.6 with information given for the nitrogen dioxide concentration.

hourly time series are comparable to each other ($5.3\text{--}8.8\ \mu\text{g m}^{-3}$). The mean bias of the daytime maximum and the MDA8 for ozone ($2.9\text{--}6.9\ \mu\text{g m}^{-3}$) are lower compared to the daily and hourly time series. For the index of agreement we also calculate for hourly and daily time series quite similar numbers (0.78–0.89, each). The index of agreement for the daytime maximum and the MDA8 for ozone is about 0.83–0.91. The overall lowest model skills were calculated for MDA8 O_3 values above the target value of $120\ \mu\text{g m}^{-3}$. This can be shown for example for the correlation coefficients (0.53–0.61) and the index of agreement (0.56–0.72). We also found the largest spread between the models in terms of the mean error (-14.1 to $8.2\ \mu\text{g m}^{-3}$) and root mean squared error ($12.6\text{--}19.6\ \mu\text{g m}^{-3}$) for MDA8 O_3 values above $120\ \mu\text{g m}^{-3}$. As shown in the previous section, the models tend to overestimate the observed ozone mass concentration at night. This reduces the model-measurement agreement of the ozone depletion at night and its

production afterwards. The challenging representation of the nighttime titration can explain the lower model performance for the hourly ozone assessment compared to daily time series and the daytime maximum or MDA8 for ozone. The low skill of the models to represent MDA8 O_3 values above $120\ \mu\text{g m}^{-3}$ illustrates the challenging nature of chemistry transport models to capture peak ozone concentrations or in fact episodes.

For the nitrogen dioxide concentration the models show consistent results in the ranking of the model skills. For daily time series we calculate a mean absolute bias of 1.8 to $5.0\ \mu\text{g m}^{-3}$, a root mean squared error between 7.1 and $9.0\ \mu\text{g m}^{-3}$, an index of agreement of about 0.57–0.78 and 0.43–0.71 for the correlation coefficient. As expected, the performances for the hourly time series are lower compared to the daily time series (Figure IV.8). LOTOS-EUROS is overestimating the measured NO_2 levels on average, whereas the other model members simulate lower nitrogen

(a) O ₃					(b) NO ₂					
		MB	RMSE	IOA	R		MB	RMSE	IOA	R
Hourly	LOTOS-EUROS	5.37	20.43	0.88	0.80	LOTOS-EUROS	1.79	10.82	0.74	0.61
	REM-CALGRID	8.83	22.90	0.81	0.74	REM-CALGRID	-1.84	10.94	0.70	0.59
	COSMO-MUSCAT	8.40	25.36	0.80	0.68	COSMO-MUSCAT	-4.94	11.54	0.60	0.44
	WRF-CHEM	8.54	23.39	0.82	0.73	WRF-CHEM	-2.45	10.37	0.73	0.60
	ENSEMBLE	7.80	19.49	0.87	0.82	ENSEMBLE	-1.86	9.29	0.75	0.66
Daily	LOTOS-EUROS	5.26	14.41	0.89	0.85	LOTOS-EUROS	1.78	7.10	0.78	0.71
	REM-CALGRID	8.77	17.93	0.79	0.76	REM-CALGRID	-1.86	7.71	0.72	0.69
	COSMO-MUSCAT	8.34	21.31	0.78	0.67	COSMO-MUSCAT	-4.96	8.97	0.57	0.43
	WRF-CHEM	8.53	17.91	0.83	0.78	WRF-CHEM	-2.45	7.39	0.77	0.71
	ENSEMBLE	7.72	15.35	0.86	0.83	ENSEMBLE	-1.87	6.61	0.77	0.74
DailyMax	LOTOS-EUROS	6.85	17.74	0.90	0.85					
	REM-CALGRID	5.91	19.57	0.83	0.81					
	COSMO-MUSCAT	3.86	20.56	0.87	0.78					
	WRF-CHEM	2.86	16.42	0.91	0.86					
	ENSEMBLE	4.87	15.53	0.92	0.88					
MDA8	LOTOS-EUROS	6.05	16.30	0.91	0.87					
	REM-CALGRID	5.94	18.73	0.84	0.82					
	COSMO-MUSCAT	4.31	20.64	0.87	0.77					
	WRF-CHEM	3.50	16.44	0.91	0.85					
	ENSEMBLE	4.95	15.13	0.92	0.88					
MDA8>120	LOTOS-EUROS	-2.15	13.16	0.72	0.61					
	REM-CALGRID	-14.14	19.58	0.56	0.53					
	COSMO-MUSCAT	8.18	17.19	0.67	0.58					
	WRF-CHEM	-3.84	12.64	0.71	0.60					
	ENSEMBLE	0.21	11.33	0.74	0.61					

Figure IV.8: Statistics for ozone (a) and nitrogen dioxide (b). The calculated values of the mean bias (MB), root mean squared error (RMSE), index of agreement (IOA) and correlation coefficient (R) reflect the average over all available background sites. All statistics were calculated for hourly and daily input data. For ozone the MDA8 O₃, MDA8 O₃>120 µg m⁻³ and daytime maximum is shown. The model skill has been color coded (from dark to light red: lowest to highest skill) to improve the readability and comparability of each statistical index.

dioxide concentrations than observed.

The mean model-measurement agreement and skill for the calculated statistics is often highest for the model ensemble, calculated as a simple four model mean, for ozone as well as for nitrogen dioxide. Figure IV.8 shows that the ensemble mean almost always ranks highest for correlation and index of agreement. Error statistics for mean bias and root mean squared error are also low and often outperform most of the individual ensemble members. Even the performance for MDA8 O₃ values above 120 µg m⁻³ is higher than for the single models.

IV.3.4 Air quality model benchmarking following FAIRMODE

Figure IV.9 summarizes the air quality model benchmarking following guidelines within FAIRMODE for ozone and nitrogen dioxide. We found that for ozone all four models fulfill the modeling quality objectives (MQOs) for annually averaged values and for time series of the MDA8, at all German background locations as well as in each subclass (MQI ≤ 1 for 90 % of analyzed stations; indicated with green boxes). Note that the MQIs in rural areas are substantially lower (yearly: 0.24-0.45; MDA8 O₃: 0.42-0.58) than

IV. Dynamic evaluation of modeled ozone concentrations in Germany with four regional chemistry transport models

(a) O ₃							(b) NO ₂							
	MQI (Yearly)	MQI (MDA8)	MPI (Bias)	MPI (R)	MPI (Sigma)	MPI (Perc)		MQI (Yearly)	MQI (Hourly)	MPI (Bias)	MPI (R)	MPI (Sigma)	MPI (Perc)	
All	LOTOS-EUROS	0.60	0.51	0.32	0.16	0.11	0.23	LOTOS-EUROS	0.84	0.68	0.35	0.35	0.17	0.56
	REM-CALGRID	0.56	0.57	0.30	0.17	0.34	0.42	REM-CALGRID	0.95	0.73	0.39	0.36	0.24	0.82
	COSMO-MUSCAT	0.48	0.61	0.26	0.32	0.11	0.30	COSMO-MUSCAT	1.12	0.72	0.47	0.32	0.29	1.04
	WRF-CHEM	0.51	0.52	0.27	0.20	0.13	0.25	WRF-CHEM	0.91	0.65	0.38	0.31	0.23	0.76
	ENSEMBLE	0.52	0.48	0.28	0.14	0.20	0.25	ENSEMBLE	0.81	0.61	0.34	0.25	0.24	0.88
Urban	LOTOS-EUROS	0.64	0.52	0.34	0.16	0.11	0.24	LOTOS-EUROS	0.91	0.71	0.38	0.37	0.14	0.59
	REM-CALGRID	0.66	0.58	0.35	0.18	0.32	0.38	REM-CALGRID	1.07	0.74	0.44	0.38	0.24	0.82
	COSMO-MUSCAT	0.58	0.62	0.31	0.31	0.10	0.35	COSMO-MUSCAT	1.26	0.76	0.53	0.35	0.31	1.06
	WRF-CHEM	0.58	0.55	0.31	0.21	0.12	0.24	WRF-CHEM	1.07	0.69	0.44	0.32	0.24	0.83
	ENSEMBLE	0.59	0.50	0.31	0.14	0.19	0.22	ENSEMBLE	0.96	0.65	0.40	0.27	0.26	0.96
SubUrban	LOTOS-EUROS	0.61	0.53	0.32	0.18	0.12	0.23	LOTOS-EUROS	0.88	0.68	0.36	0.37	0.17	0.51
	REM-CALGRID	0.52	0.58	0.28	0.18	0.35	0.40	REM-CALGRID	0.94	0.75	0.39	0.43	0.26	0.76
	COSMO-MUSCAT	0.40	0.61	0.22	0.33	0.11	0.28	COSMO-MUSCAT	1.07	0.68	0.43	0.36	0.31	1.03
	WRF-CHEM	0.49	0.53	0.26	0.21	0.15	0.20	WRF-CHEM	0.80	0.65	0.34	0.36	0.23	0.73
	ENSEMBLE	0.48	0.50	0.26	0.14	0.23	0.22	ENSEMBLE	0.77	0.63	0.32	0.27	0.25	0.88
Rural	LOTOS-EUROS	0.45	0.45	0.24	0.16	0.09	0.20	LOTOS-EUROS	0.60	0.53	0.24	0.19	0.20	0.58
	REM-CALGRID	0.40	0.52	0.21	0.15	0.34	0.47	REM-CALGRID	0.47	0.49	0.19	0.19	0.17	0.84
	COSMO-MUSCAT	0.26	0.58	0.14	0.32	0.11	0.26	COSMO-MUSCAT	0.42	0.50	0.18	0.19	0.21	0.91
	WRF-CHEM	0.24	0.42	0.12	0.16	0.11	0.27	WRF-CHEM	0.37	0.47	0.16	0.19	0.12	0.45
	ENSEMBLE	0.28	0.41	0.14	0.13	0.19	0.29	ENSEMBLE	0.37	0.41	0.16	0.13	0.13	0.68

Figure IV.9: Summary of indicators for air quality model benchmarking following the Air Quality Directive 2008/50/EC (AQD) from FAIRMODE. The modeling quality indicator (MQI) and the modeling performance indicators (MPIs) were calculated for ozone (a) and nitrogen dioxide (b). Statistics for the MQI were calculated separately, for yearly averaged model results (Yearly) as well as for hourly (Hourly, nitrogen dioxide) and the MDA8 O₃ (MDA8, ozone) input data. The MPIs are calculated in relation to the temporal variability and show modeled discrepancies for the bias (Bias), correlation (R), standard deviation (σ) and high percentile values (Perc). All indicators are calculated for all available background sites in Germany (All) or their selection of site classes (Urban, SubUrban, Rural). The model skill has been color coded (from light to dark green: lowest to highest skill) to improve the readability and comparability of each statistical index. Red color-coded boxes are used to indicate that the modeling quality objective (MQO) or modeling performance criteria (MPC) are not fulfilled.

in the urban background (yearly: 0.58-0.66; MDA8 O₃: 0.52-0.62). We found that the MQIs for the annual assessment are often larger than MQI values for time series of the MDA8 in urban areas. This can be simply explained as the measurement uncertainty for the annual assessment is smaller as opposed to time series of the MDA8. In contrast, for rural and suburban areas the MQIs for annual averaged values are lower for most of the model results.

Modeling performance indicators (MPIs) for ozone with respect to bias, correlation, standard deviation and high percentile values were also calculated. MPI values with respect to bias (MPI_{Bias}) for all German background sites are similar between all model sys-

tems (0.26-0.32). Values found in the urban background are larger (0.31-0.35) than shown for the rural area (0.12-0.24). Largest differences for MPIs of the ozone assessment between the models were calculated for the correlation, the standard deviation and the representation of high percentile values. We found that the models largely vary in terms of correlation for high ozone concentrations, illustrated by MPI_R values between 0.17-0.32. We also identified differences between the models for MPI _{σ} values of about 0.11-0.34, that reflects the lower season-to-season variation for the models applied.

Table IV.5: Threshold exceedance events of MDA8 O₃>120 μg m⁻³ as total of all background stations used, per model and station type (good values below threshold: GA⁻; good values above threshold: GA⁺; missed alarms: MA; false alarms: FA; probability of detection: POD; success ratio: SR).

period	site class	GA ⁻	GA ⁺	MA	FA	POD	SR
LOTOS-EUROS	all	77992	3438	2266	2608	0.60	0.57
	rural	23927	1135	798	710	0.59	0.62
	suburban	23550	1074	669	785	0.62	0.58
	urban	30515	1229	799	1113	0.61	0.52
REM-CALGRID	all	80352	1431	4273	248	0.25	0.85
	rural	24580	396	1537	57	0.20	0.87
	suburban	24284	445	1298	51	0.26	0.90
	urban	31488	590	1438	140	0.29	0.81
COSMO-MUSCAT	all	77412	3776	1928	3188	0.66	0.54
	rural	23856	1201	732	781	0.62	0.61
	suburban	23354	1156	587	981	0.66	0.54
	urban	30202	1419	609	1426	0.70	0.50
WRF-Chem	all	78862	3237	2467	1738	0.57	0.65
	rural	24314	962	971	323	0.50	0.75
	suburban	23773	1050	693	562	0.60	0.65
	urban	30775	1225	803	853	0.60	0.59
ENSEMBLE	all	79551	2906	2798	1049	0.51	0.73
	rural	24427	873	1060	210	0.45	0.81
	suburban	24033	901	842	302	0.52	0.75
	urban	31091	1132	896	537	0.56	0.68

IV. Dynamic evaluation of modeled ozone concentrations in Germany with four regional chemistry transport models

Similar to ozone, we found for NO_2 that the annual averaged values of the MQI are larger in the urban background than in rural areas compared to input data for time series (for NO_2 , hourly values). All four models as well fulfill the MQI for nitrogen dioxide of the hourly assessment for all German background locations and their split into sub-categories for urban to rural sites. Except for LOTOS-EUROS, the MQI for annual averaged values of nitrogen dioxide is not fulfilled by the models in the urban background (MQI > 1; indicated with red boxes). However, the parameters for the calculation of the MQI on annual basis are still under discussion in FAIRMODE. Nevertheless, the MPIs for nitrogen dioxide can all be fulfilled for most of the applied models. COSMO-MUSCAT in addition misses the criteria for high percentile values for all background stations and for the urban and suburban regions.

In agreement to the performance evaluation presented in the previous section, the result of the ensemble mean is often more reliable than the single ensemble members and ranks lowest in terms of numbers for the MQIs and the MPIs for ozone as well as for nitrogen dioxide. All MQI and MPI values as calculated and presented for the ensemble mean are fulfilling the MQO and MPC, respectively.

Table IV.5 provides statistical information on exceedances for MDA8 O_3 above $120 \mu\text{g m}^{-3}$ using false alarms (FA), missed alarms (MA), good values above (GA^+) and below (GA^-) the threshold as well as the probability of detection (POD) and the success ratio (SR) for German background sites differentiated per station type and model. We found that on average all models lack performance capturing

exceedances of MDA8 O_3 above $120 \mu\text{g m}^{-3}$. The number of false (248-3188) and missed alarms (1928-4273) largely varies between the models and are large compared to the number of good values above the threshold (1431-3776) for all German background sites. The averaged model's performance is expressed by both, the probability of detection (POD) and the success ratio (SR). For all German sites, we calculate numbers of the probability of detection ranging between 25 and 66 % and a success ratio of about 54 to 85 %. REM-CALGRID shows by far the largest SR (85 %), but also the lowest POD (25 %). The other three ensemble members show a very consistent picture in the ranking of the SR (54-65 %) and the POD (57-66 %). Statistics calculated for the ensemble mean are biased to the lowest model performance and thus show high values for the success ratio (73 %) but a low probability of detection (51 %) for all German background sites. We also noticed that the values of the POD are larger in the urban background than in rural areas. Vice versa, the SR is larger in the rural background.

In FAIRMODE it has already been stated that large inconsistencies may occur for different indicators depending on whether time series (daily/ hourly) or annual averaged values are included in the analysis (Monteiro et al., 2018). Following Monteiro et al. (2018), the MQO for hourly or daily time series is often attained, whereas it is not the case for annual values. We could show that all models fulfill the quality standards set by the FAIRMODE guideline values for annual averages as well as for time series in the background locations, whereas for specific regions (e.g. rural vs. urban areas) the model performance can differ. The ca-

pability to reproduce extreme events in model intercomparison and evaluation studies is often ignored as many times only averaged values were obtained or only high percentile values were investigated (Monteiro et al., 2018). We therefore also focused on threshold exceedances as recommended by FAIRMODE and which are typically highly coherent in time and space over scales of hundreds of kilometers (Schnell et al., 2015; Carro-Calvo et al., 2017). Regional models are most suited to simulate human exposure to ozone events when the grid resolution is considering the spatial extent of the urban background in the region of interest (Kuik et al., 2016), while for simulation of large-scale ozone exceedance events in the rural background in Europe, grid resolutions between 10-20 km have been shown to be optimal (Schaap et al., 2015). However, in our study we could show that the representation of ozone threshold exceedance events in urban areas for MDA8 $O_3 > 120 \mu\text{g m}^{-3}$ is limited even on a $2 \times 2 \text{ km}^2$ scale.

IV.3.5 Dynamic (ozone) model evaluation

As introduced, ozone is highly correlated to temperature which is an important driver especially during ozone episodes. In Figure IV.10 we show the common relation that higher ozone concentrations occur more often during warmer weather conditions, while at colder temperatures the ozone concentrations more likely remain low. Due to the physical relation between the daytime maxima of temperature and their corresponding humidity, lower levels of the relative humidity are more often connected to higher ozone concentrations and vice versa.

Figure IV.10 shows that the ensemble mean reports a good agreement of the measured concentration in relation to temperature for April-June. Largest differences to the observed ozone-temperature dependence were found for July-September. In July-September, the measured ozone levels for temperatures lower than $\sim 18^\circ\text{C}$ are biased high for the ensemble mean and for all models. In winter, all models and the ensemble mean are biased high for temperatures higher than $\sim 14^\circ\text{C}$. Differences between urban and rural sites are on average smaller compared to seasonal deviations (see appendix Figure IV.12).

However, we also observed a large spread for all models in their ozone sensitivity to different temperature regimes. The ozone-temperature dependence for temperatures higher than $\sim 26^\circ\text{C}$ in April-September has been well captured by WRF-Chem and LOTOS-EUROS. For COSMO-MUSCAT and WRF-Chem we observed good agreement capturing the ozone sensitivity to temperature for temperatures lower than $\sim 18^\circ\text{C}$ in April-June. In winter, COSMO-MUSCAT is in good agreement with observed concentrations for temperatures lower than $\sim 14^\circ\text{C}$. On the other hand, COSMO-MUSCAT shows on average larger ozone sensitivity to temperature for warmer conditions in spring- and summertime. Vice versa, the lowest sensitivity of ozone to temperature was found for REM-CALGRID. This too high and too low sensitivity to temperature observed for COSMO-MUSCAT and REM-CALGRID causes an overestimation (COSMO-MUSCAT) and underestimation (REM-CALGRID) of the ozone levels for temperatures higher than $\sim 26^\circ\text{C}$ in spring- and summer-

IV. Dynamic evaluation of modeled ozone concentrations in Germany with four regional chemistry transport models

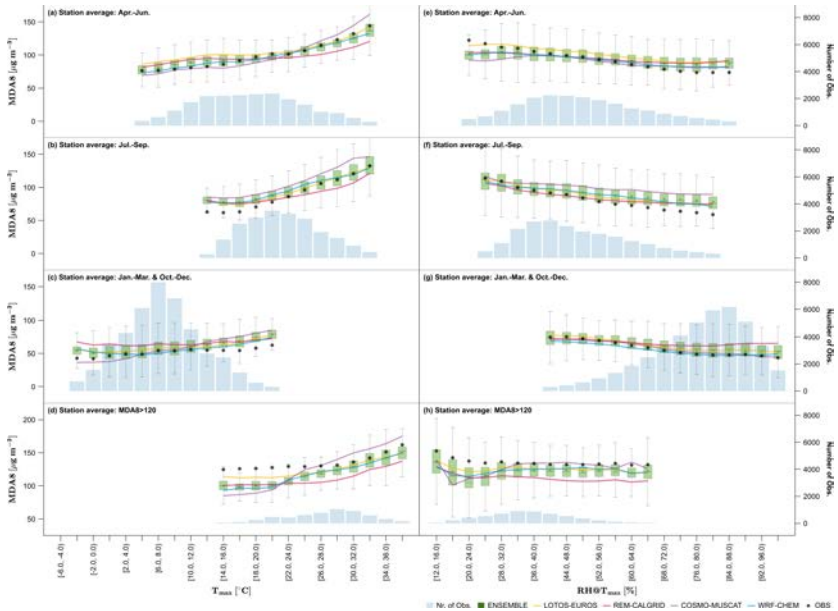


Figure IV.10: Ozone concentration (MDA8 O_3) in relation to temperature (a-d) and humidity (e-h) for LOTOS-EUROS (yellow), REM-CALGRID (magenta), COSMO-MUSCAT (purple), WRF-Chem (blue) and the ensemble (boxplots). Plotted values reflect the average background concentration of all available monitoring sites in Germany. Measured concentrations are indicated with black circles. Box plots of the ensemble show the mean, median, 25th and 75th percentile as well as the two times standard deviation as min and max. Mean values are used for the ensemble members and the measurements. The periods of April-June and July-September are shown in the subplots (a,e) and (b,f) as well as the wintermonth January-March & October-December in subplots (c,g). The relation to temperature and humidity for exceedances above the MDA8 O_3 target value of $120 \mu\text{g m}^{-3}$ are shown in subplots (d) and (h).

time. For temperatures lower than ~ 14 and ~ 18 °C in April-June, we observed slightly biased high ozone levels for REM-CALGRID and for LOTOS-EUROS. For colder conditions in winter, we also observed high biased ozone concentrations for LOTOS-EUROS, WRF-Chem and REM-CALGRID.

The observed timeseries show values of MDA8 O_3 just over $120 \mu\text{g m}^{-3}$ already in the temperature range from ~ 15 to ~ 24 °C which are systematically underestimated by all models (Figure IV.10). LOTOS-EUROS comes closest to covering MDA8 $O_3 > 120 \mu\text{g m}^{-3}$ for temperatures lower than

~ 24 °C. REM-CALGRID captures the ozone-temperature dependence for MDA8 $O_3 > 120 \mu\text{g m}^{-3}$ to a fairly large extent but is on average biased low as well. The models show a similar ozone temperature-dependence for temperatures higher than ~ 28 °C. However, temperatures at which the MDA8 O_3 typically starts to rise largely differ between the models (~ 22 - 26 °C) and the observations (~ 30 °C). COSMO-MUSCAT shows the most pronounced ozone-temperature sensitivity and therefore the largest underestimation for temperatures lower than ~ 24 °C and high biased MDA8 $O_3 > 120 \mu\text{g m}^{-3}$

for temperatures larger than ~ 30 °C.

In Table IV.6 we present the temperature increase per Celsius between ~ 21 °C and ~ 31 °C. The ensemble mean and nearly all models underestimate the observed ozone dependence to temperature in April-June and July-September for all locations. Nevertheless, the higher temperature sensitivity in July-September (OBS: $4.3 \mu\text{g m}^{-3} \text{ }^\circ\text{C}^{-1}$; ENS_{ALL}: $3.5 \mu\text{g m}^{-3} \text{ }^\circ\text{C}^{-1}$) compared with April to June (OBS: $3.1 \mu\text{g m}^{-3} \text{ }^\circ\text{C}^{-1}$; ENS_{ALL}: $2.9 \mu\text{g m}^{-3} \text{ }^\circ\text{C}^{-1}$) is captured by most of the models. All models also capture the observed lower ozone sensitivity to temperature for urban areas compared to rural stations in April-June and vice versa in July-September (see Table IV.6). For MDA8 $\text{O}_3 > 120 \mu\text{g m}^{-3}$, all models show a too large ozone dependence on temperature (OBS_{ALL}: $0.8 \mu\text{g m}^{-3} \text{ }^\circ\text{C}^{-1}$; ENS_{ALL}: $2.8 \mu\text{g m}^{-3} \text{ }^\circ\text{C}^{-1}$), where REM-CALGRID comes closest covering the temperature increase per 10 °C for MDA8 $\text{O}_3 > 120 \mu\text{g m}^{-3}$.

In Figure IV.10 we show the sensitivity to the relative humidity and observed consistent results with an overall good model-measurement agreement for all models. The models slightly overestimate the ozone concentrations for humid conditions equal to relative humidities larger than ~ 68 % in April-June and larger than ~ 64 % in July-September. Largest high biased concentrations for humid conditions have been found for COSMO-MUSCAT in July-September and for REM-CALGRID in winter. Except for LOTOS-EUROS, in April-June the models are also biased low for relative humidities lower than ~ 28 %. MDA8 O_3 values above $120 \mu\text{g m}^{-3}$ are biased low as well for relative humidities lower than ~ 28 %

Table IV.6: Dependence of ozone concentration on temperature, for ~ 21 °C to ~ 31 °C [$\mu\text{g m}^{-3} \text{ }^\circ\text{C}^{-1}$].

	site class	obs.	LOTOS-EUROS		REM-CALGRID		COSMO-MUSCAT		WRF-Chem		ENSEMBLE	
			EUROS	CALGRID	REM-CALGRID	MUSCAT	WRF-Chem	ENSEMBLE				
April-June	all	3.06	2.71	1.65	1.65	5.10	2.72	2.86				
	rural	3.60	3.08	1.82	1.43	5.14	2.80	3.06				
	urban	2.88	2.47	1.43	2.56	5.05	2.62	2.68				
July-September	all	4.29	3.77	2.56	2.44	4.98	3.06	3.45				
	rural	4.13	3.38	2.44	2.66	4.78	2.80	3.17				
	urban	4.47	4.06	2.66	1.30	5.22	3.34	3.68				
MDA8 $\text{O}_3 > 120 \mu\text{g m}^{-3}$	all	0.82	1.87	1.30	1.32	5.57	2.97	2.82				
	rural	1.08	1.97	1.32	1.25	4.77	2.61	2.66				
	urban	0.69	1.77	1.25	1.25	6.03	3.23	2.90				

for all models. For REM-CALGRID a good agreement to the ozone-humidity dependence is observed. However, similar to results shown before for the ozone sensitivity to temperature, a too low modeled concentration for MDA8 $O_3 > 120 \mu\text{g m}^{-3}$ is observed.

In Otero et al. (2018) the influence of meteorology on ozone has been calculated for a model ensemble and the observations using a multiple linear regression analysis on a multi-decadal time scale. The study showed that the models can reproduce the temperature (T_{max}) response to a fairly large extent. We precise this finding and argue that the observed ozone-temperature dependence shows highest agreement for warmer conditions, but the models can also largely vary in the modeled ozone sensitivity to temperature. In contrast to our results, Otero et al. (2018) identified a better model-measurement agreement for summer compared to spring. We found large season-to-season differences and high biased ozone levels for July-September that seem to be connected with moderate temperatures and thus higher relative humidities during the summertime, especially at night. Following Otero et al. (2018) the relation between humidity and ozone is more difficult to capture. We found an overall good agreement of the modeled ozone-humidity dependence. However, the models largely underestimate high ozone concentrations ($\text{MDA8 } O_3 > 120 \mu\text{g m}^{-3}$) for dry conditions during springtime. We speculate that this could be connected with an insufficient representation of modeled deposition velocities covering vegetative water stress and low sensitivity of NO_x and BVOC emissions (e.g., Churkina et al., 2017; Lin et al., 2020).

IV.4 Summary and conclusion

We have successfully compared and evaluated the performance of four regional chemistry transport models and their ensemble. Our work shares similar features with previous multi-model intercomparison studies for ozone but focuses on a higher grid resolution and performs a national scale quality assessment, which might be more relevant with a future revision of the European air quality directive.

The results demonstrate that all models satisfy the modeling quality objectives and criteria (MQO/ MQC) set by the FAIRMODE initiative for every modeling quality and performance indicator (MQI/ MPI) for annual averaged ozone concentrations as well as for time series of the MDA8 O_3 . All models showed good performance of the operational evaluation using standard statistical indicators such as bias, correlation or for high percentile values. The analysis of the model skills demonstrate better performance in rural areas than in the urban background and for springtime compared to summertime. We also showed an improved performance for the ensemble over the individual model participants. Despite the high model-measurement agreement, the individual models and their ensemble show room for improvement at simulating threshold exceedances for MDA8 O_3 above $120 \mu\text{g m}^{-3}$. Here, we compute high values for missed alarms and false alarms. We also found rather low model-measurement agreement for observed lower ozone concentrations at night, which is likely related to difficulties in simulating the stable nocturnal boundary layer.

A novel feature of this study is the dynamic evaluation of modeled ozone with respect to temperature. In general, the models correctly reproduced the observed higher sensitivity of ozone with respect to temperature in summer than in springtime, which is linked to overall higher local photochemical production of ozone in summer. The models also correctly captured the differences in the temperature sensitivity of ozone between rural and urban areas in both spring and summer seasons, with a lower temperature sensitivity in urban areas in springtime and a higher sensitivity in summertime, showing that the $2 \times 2 \text{ km}^2$ model resolution used in this study is adequate for simulating the dynamic response of ozone to temperature in urban background areas. Despite capturing the observed spring to summer and urban to rural differences in the temperature sensitivity of ozone, there was still a large spread in the modeled temperature sensitivities. The sensitivity of ozone to temperature also depends on the ratio of NO_x and BVOC. For example, in NO_x rich urbanized regions the temperature-sensitivity to ozone is higher than in NO_x limited regions [Otero et al., 2021](#). Future work should focus on the representation of temperature sensitive processes in models, such as BVOC and nitrogen oxide emissions.

In general, the models underestimated the observed temperature sensitivity of ozone in summer, despite showing high bias in simulated ozone concentrations compared with the measurements. Both, the high bias and the underestimated temperature sensitivity can be linked to a systematic overestimation of ozone concentrations in the $60\text{--}80 \text{ }\mu\text{g m}^{-3}$ range, which make up most of the observed ozone concentra-

tions in summer and tend to occur at moderate temperatures. The models also show a high bias with respect to observations in the same concentration range in spring. However, this is not reflected in the overall springtime model bias due to a systematic underestimation of higher values (over $100 \text{ }\mu\text{g m}^{-3}$) in spring, which tend to occur at relatively low temperatures (below $25 \text{ }^\circ\text{C}$) compared with similar exceedance events in summer. The missed springtime exceedance events and the general overestimation of concentrations in the $60\text{--}80 \text{ }\mu\text{g m}^{-3}$ range could be linked to deficiencies in the representation of background ozone, including long-range transport, which can be further addressed with source apportionment techniques and validation at the European scale. An important caveat in this context is that these results are based only on observations and model simulations for the year of 2019. Future work should focus on longer periods to determine whether these results can be generalized to longer timeframes.

In this study we focused on an operational and dynamic evaluation of four chemistry transport models for ozone in Germany. The dynamic evaluation would benefit from an extension to a decadal time scale as shown e.g. by [Colette et al. \(2017\)](#) and [Banzhaf et al. \(2015\)](#). We used a poor man's ensemble to assess the added value of the combined information in the ensemble. The evaluation of larger ensembles of chemistry transport models is currently taking place within the Copernicus Atmosphere Monitoring Service, enabling it to address additional ensemble properties which are not covered here. An important next step for the work pre-

sented here is to diagnose the reasons for the mismatches with observations and differences between the models. Such diagnostic evaluation requires investigating the process descriptions in more detail. As the uncertainties related to the biogenic emissions and the dry deposition parametrizations are large (e.g., Im et al., 2015a), we recommend to focus on the representation of these process descriptions by evaluation of dedicated simulations for research campaigns providing the relevant process information.

CRedit authorship contribution

statement. **M. Thürkow:** Conceptualization, Methodology, Software, Validation, Formal analysis, Investigation, Data curation, Writing – original draft, Visualization. **T. Butler:** Conceptualization, Methodology, Writing – original draft, Supervision, Project administration, Funding acquisition. **M. Schaap:** Conceptualization, Methodology, Writing – original draft, Supervision. **All authors:** Resources, Writing – review & editing. All authors have read and agreed to the published version of the manuscript.

Declaration of competing interest.

The authors declare that they have no known competing financial interests or personal relationships that could have appeared to influence the work reported in this paper. Thanks to Hanna Thürkow for proofreading and the final assistance when submitting the article.

Acknowledgment. This research was funded by the German Environment Agency (Umweltbundesamt - UBA), Dessau-Roßlau within the framework of the "OzonEval" research initiative (project number: FKZ 3720 51 201 0).

IV.5 Appendix - figures

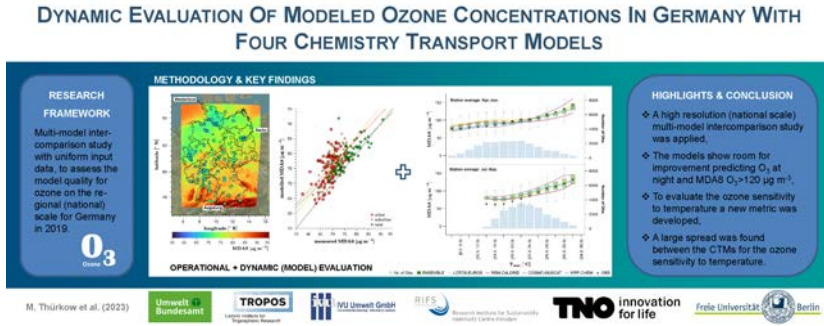


Figure IV.11: Graphical abstract

IV.6 Appendix - statistical indicators

IV.6.1 operational evaluation

mean bias:

$$MB = \frac{1}{N} \sum_{i=1}^n (M_i - O_i) \quad (\text{IV.1})$$

root mean squared error:

$$RMSE = \sqrt{\frac{1}{N} \sum_{i=1}^n (M_i - O_i)^2} \quad (\text{IV.2})$$

index of agreement:

$$IOA = 1 - \frac{\sum_{i=1}^n (M_i - O_i)^2}{\sum_{i=1}^n (|M_i - \bar{O}| + |O_i - \bar{O}|)^2} \quad (\text{IV.3})$$

correlation coefficient:

$$R = \frac{\sum_{i=1}^n (M_i - \bar{M})(O_i - \bar{O})}{\sqrt{\sum_{i=1}^n (M_i - \bar{M})^2} \sqrt{\sum_{i=1}^n (O_i - \bar{O})^2}} \quad (\text{IV.4})$$

IV.6.2 threshold exceedances indicators

probability of detection:

$$POD = \frac{GA^+}{MA + GA^+} \quad (\text{IV.5})$$

success ratio:

$$SR = \frac{GA^+}{FA + GA^+} \quad (\text{IV.6})$$

IV.6.3 reporting model performance - FAIRMODE (Janssen and Thunis, 2022)

measured uncertainty:

- for time series

$$RMS_U = U_r(RV) \sqrt{(1 - \alpha^2)(\bar{O}^2 + \sigma_O^2) + \alpha^2 RV^2} \quad (\text{IV.7})$$

- for annual averaged values

$$RMS_U \approx U_r(RV) \sqrt{\frac{(1 - \alpha^2)}{N_p} \bar{O}^2 + \frac{\alpha^2 RV^2}{N_{np}}} \quad (\text{IV.8})$$

- with parameters for O₃

$$U_r(RV) = 0.18 ; RV = 120.0 \mu g m^{-3} ; \alpha = 0.79 ; N_p = 11.0 ; N_{np} = 3.0 \text{ (IV.9)}$$

- and parameters for NO₂

$$U_r(RV) = 0.24 ; RV = 200.0 \mu g m^{-3} ; \alpha = 0.20 ; N_p = 5.2 ; N_{np} = 5.5 \text{ (IV.10)}$$

modeling quality indicator:

$$MQI = \frac{RMSE}{\beta RMS_U} \text{ (IV.11)}$$

- with $\beta = 2$

modeling performance indicators:

$$MPI_R = \frac{1 - R}{0.5\beta^2 \frac{RMS_U^2}{\sigma_O \sigma_M}} \text{ (IV.12)}$$

$$MPI_{Bias} = \frac{|Bias|}{\beta RMS_U} \text{ (IV.13)}$$

$$MPI_\sigma = \frac{|\sigma_M - \sigma_O|}{\beta RMS_U} \text{ (IV.14)}$$

$$MPI_{Perc} = \frac{RMSE_{Perc}}{\beta RMS_{U_{Perc}}} \text{ (IV.15)}$$

- with $\beta = 2$

IV. Dynamic evaluation of modeled ozone concentrations in Germany with four regional chemistry transport models

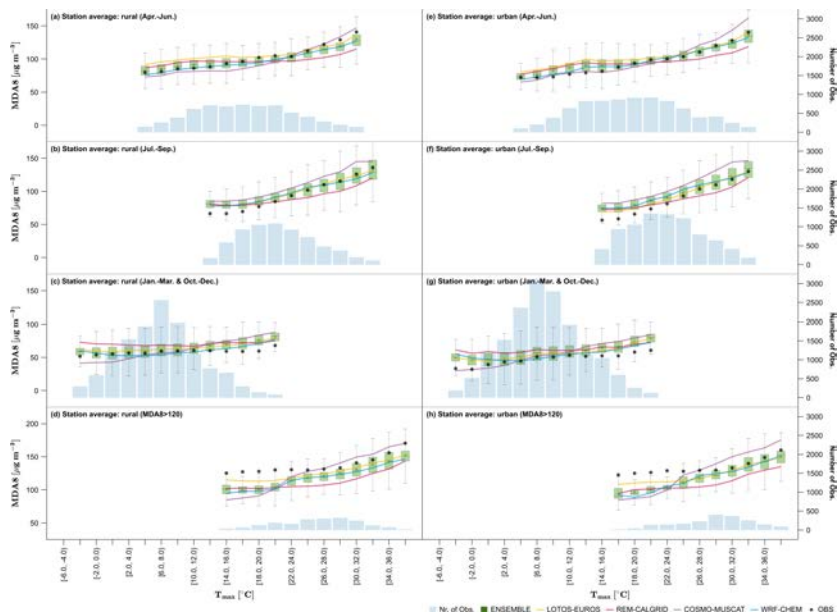


Figure IV.12: Ozone concentration (MDA8 O₃) in relation to temperature for LOTOS-EUROS (yellow), REM-CALGRID (magenta), COSMO-MUSCAT (purple), WRF-CHEM (blue) and the ensemble (boxplots). Plotted values reflect the average for rural (left) and urban (right) background concentrations of all available monitoring sites in Germany. Measured concentrations are indicated with black circles. Box plots of the ensemble show the mean, median, 25th and 75th percentile as well as the two times standard deviation as min and max. Mean values are used for the ensemble members and the measurements. The periods of April-June and July-September are shown in the subplots (a,e) and (b,f) as well as the wintermonth January-March & October-December in subplots (c,g). The relation to temperature for exceedances above the MDA8 O₃ target value of 120 µg m⁻³ are shown in subplots (d) and (h).

References

References

- Amann, M., Bertok, I., Borken-Kleefeld, J., Cofala, J., Heyes, C., Höglund-Isaksson, L., Klimont, Z., Nguyen, B., Posch, M., Rafaj, P., Sandler, R., Schöpp, W., Wagner, F., and Winiwarter, W. (Dec. 2011). “Cost-effective control of air quality and greenhouse gases in Europe: Modeling and policy applications”. In: *Environmental Modelling & Software* vol. 26 (12), pp. 1489–1501. ISSN: 13648152. DOI: [10.1016/j.envsoft.2011.07.012](https://doi.org/10.1016/j.envsoft.2011.07.012). URL: <https://linkinghub.elsevier.com/retrieve/pii/S1364815211001733>.
- Amato, F., Zandveld, P., Keuken, M., Jonkers, S., Querol, X., Reche, C., Gon, H. A. C. D. van der, and Schaap, M. (2016). “Improving the modeling of road dust levels for Barcelona at urban scale and street level”. In: *Atmospheric Environment* vol. 125. Cited By :5

Export Date: 17 January 2020, pp. 231–242. DOI: [10.1016/j.atmosenv.2015.10.078](https://doi.org/10.1016/j.atmosenv.2015.10.078). URL: <https://www.scopus.com/inward/record.uri?eid=2-s2.0-84947790561&doi=10.1016%2Fj.atmosenv.2015.10.078&partnerID=40&md5=3df0a241155ba52d7c53a13af785997d>.
- Amato, F., Pandolfi, M., Escrig, A., Querol, X., Alastuey, A., Pey, J., Perez, N., and Hopke, P. (2009). “Quantifying road dust resuspension in urban environment by Multilinear Engine: A comparison with PMF2”. In: *Atmospheric Environment* vol. 43, no. 17, pp. 2770–2780. ISSN: 1352-2310. DOI: <https://doi.org/10.1016/j.atmosenv.2009.02.039>. URL: <https://www.sciencedirect.com/science/article/pii/S135223100900171X>.
- Amato, F., Pandolfi, M., Moreno, T., Furger, M., Pey, J., Alastuey, A., Bukowiecki, N., Prevot, A., Baltensperger, U., and Querol, X. (2011). “Sources and variability of inhalable road dust particles in three European cities”. In: *Atmospheric Environment* vol. 45, no. 37, pp. 6777–6787. ISSN: 1352-2310. DOI: <https://doi.org/10.1016/j.atmosenv.2011.06.003>. URL: <https://www.sciencedirect.com/science/article/pii/S1352231011005942>.
- Amato, F., Schaap, M., Denier van der Gon, H. A., Pandolfi, M., Alastuey, A., Keuken, M., and Querol, X. (2012). “Effect of rain events on the mobility of road dust load in two Dutch and Spanish roads”. In: *Atmospheric Environment* vol. 62, pp. 352–358. ISSN: 1352-2310. DOI: <https://doi.org/10.1016/j.atmosenv.2012.08.042>. URL: <https://www.sciencedirect.com/science/article/pii/S135223101200814X>.
- Anderson, J. O., Thundiyil, J. G., and Stolbach, A. (June 2012). “Clearing the Air: A Review of the Effects of Particulate Matter Air Pollution on Human Health”. In: *Journal of Medical Toxicology* vol. 8 (2), pp. 166–175. ISSN: 1556-9039. DOI: [10.1007/s13181-011-0203-1](https://doi.org/10.1007/s13181-011-0203-1).
- Annesi-Maesano, I. (Dec. 2017). “The air of Europe: where are we going?” In: *European Respiratory Review* vol. 26 (146), p. 170024. ISSN: 0905-9180. DOI: [10.1183/16000617.0024-2017](https://doi.org/10.1183/16000617.0024-2017).
- Arakawa, A. and Lamb, V. R. (1977). *Computational Design of the Basic Dynamical Processes of the UCLA General Circulation Model*. Ed. by CHANG, J. DOI: <https://doi.org/10.1016/B978-0-12-460817-7.50009-4>. URL: <http://www.sciencedirect.com/science/article/pii/B9780124608177500094>.
- Arias-Pérez, R. D., Taborda, N. A., Gómez, D. M., Narvaez, J. F., Porras, J., and Hernandez, J. C. (Dec. 2020). “Inflammatory effects of particulate matter air

-
- pollution”. In: *Environmental Science and Pollution Research* vol. 27 (34), pp. 42390–42404. ISSN: 0944-1344. DOI: [10.1007/s11356-020-10574-w](https://doi.org/10.1007/s11356-020-10574-w).
- Atkinson, R. (2007). “Rate constants for the atmospheric reactions of alkoxy radicals: An updated estimation method”. In: *Atmospheric Environment* vol. 41, no. 38, pp. 8468–8485. ISSN: 1352-2310. DOI: <https://doi.org/10.1016/j.atmosenv.2007.07.002>. URL: <https://www.sciencedirect.com/science/article/pii/S1352231007006152>.
- Baars, H., Ansmann, A., Engelmann, R., and Althausen, D. (2008). “Continuous monitoring of the boundary-layer top with lidar”. In: *Atmospheric Chemistry and Physics* vol. 8 (23), pp. 7281–7296. DOI: [10.5194/acp-8-7281-2008](https://doi.org/10.5194/acp-8-7281-2008). URL: <https://www.atmos-chem-phys.net/8/7281/2008/>.
- Baklanov, A. et al. (2014). “Online coupled regional meteorology chemistry models in Europe: current status and prospects”. In: *Atmospheric Chemistry and Physics* vol. 14, no. 1, pp. 317–398. DOI: [10.5194/acp-14-317-2014](https://doi.org/10.5194/acp-14-317-2014). URL: <https://acp.copernicus.org/articles/14/317/2014/>.
- Baklanov, A. and Zhang, Y. (2020). “Advances in air quality modeling and forecasting”. In: *Global Transitions* vol. 2, pp. 261–270. ISSN: 25897918. DOI: [10.1016/j.glt.2020.11.001](https://doi.org/10.1016/j.glt.2020.11.001).
- Banks, R. F. and Baldasano, J. M. (Dec. 2016). “Impact of WRF model PBL schemes on air quality simulations over Catalonia, Spain”. In: *Science of the Total Environment* vol. 572, pp. 98–113. ISSN: 18791026. DOI: [10.1016/j.scitotenv.2016.07.167](https://doi.org/10.1016/j.scitotenv.2016.07.167).
- Banzhaf, S., Schaap, M., Kerschbaumer, A., Reimer, E., Stern, R., Swaluw, E. V. D., and Bultjes, P. (2012). “Implementation and evaluation of pH-dependent cloud chemistry and wetdeposition in the chemical transport model REM-Calgrid”. In: *Atmospheric Environment*. ISSN: 13522310. DOI: [10.1016/j.atmosenv.2011.10.069](https://doi.org/10.1016/j.atmosenv.2011.10.069).
- Banzhaf, S., Schaap, M., Kranenburg, R., Manders, A. M. M., Segers, A. J., Visschedijk, A. J. H., Gon, H. A. C. D. van der, Kuenen, J. J. P., Meijgaard, E. van, Ulft, L. H. van, Cofala, J., and Bultjes, P. J. H. (Apr. 2015). “Dynamic model evaluation for secondary inorganic aerosol and its precursors over Europe between 1990 and 2009”. In: *Geoscientific Model Development* vol. 8 (4), pp. 1047–1070. ISSN: 1991-9603. DOI: [10.5194/gmd-8-1047-2015](https://doi.org/10.5194/gmd-8-1047-2015). URL: <https://gmd.copernicus.org/articles/8/1047/2015/>.
- Banzhaf, S., Schaap, M., Wichink Kruit, R. J., Denier van der Gon, H. A. C., Stern, R., and Bultjes, P. J. H. (2013). “Impact of emission changes on secondary inorganic aerosol episodes across Germany”. In: *Atmospheric Chemistry and Physics* vol. 13, no. 23, pp. 11675–11693. DOI: [10.5194/acp-13-11675-2013](https://doi.org/10.5194/acp-13-11675-2013). URL: <https://acp.copernicus.org/articles/13/11675/2013/>.
- Beekmann, M. et al. (2015). “In situ, satellite measurement and model evidence on the dominant regional contribution to fine particulate matter levels in the Paris megacity”. In: *Atmospheric Chemistry and Physics* vol. 15 (16), pp. 9577–9591. ISSN: 16807324. DOI: [10.5194/acp-15-9577-2015](https://doi.org/10.5194/acp-15-9577-2015).
- Beelen, R. et al. (Mar. 2014). “Effects of long-term exposure to air pollution on natural-cause mortality: an analysis of 22 European cohorts within the multicentre ESCAPE project”. In: *The Lancet* vol. 383 (9919), pp. 785–

References

795. ISSN: 01406736. DOI: 10.1016/S0140-6736(13)62158-3. URL: <https://linkinghub.elsevier.com/retrieve/pii/S0140673613621583>.
- Beirle, S., Borger, C., Dörner, S., Li, A., Hu, Z., Liu, F., Wang, Y., and Wagner, T. (Nov. 2019). "Pinpointing nitrogen oxide emissions from space". In: *Science Advances* vol. 5 (11). ISSN: 2375-2548. DOI: 10.1126/sciadv.aax9800.
- Belis, C. et al. (Jan. 2020). "Evaluation of receptor and chemical transport models for PM10 source apportionment". In: *Atmospheric Environment: X* vol. 5, p. 100053. ISSN: 2590-1621. DOI: 10.1016/J.AEAOA.2019.100053. URL: <https://www.sciencedirect.com/science/article/pii/S2590162119300565?pes=vor>.
- Bell, M. L. and Davis, D. L. (June 2001). "Reassessment of the lethal London fog of 1952: novel indicators of acute and chronic consequences of acute exposure to air pollution." In: *Environmental Health Perspectives* vol. 109 (suppl 3), pp. 389–394. ISSN: 0091-6765. DOI: 10.1289/ehp.01109s3389.
- Bennett, L., Melchers, B., and Proppe, B. (2020). *Curta: A General-purpose High-Performance Computer at ZEDAT, Freie Universität Berlin*.
- Berg, W. (2003). "Legislation for the Reduction of Exhaust Gas Emissions". In: pp. 175–253. DOI: 10.1007/b10463.
- Bergqvist, R., Turesson, M., and Weddmark, A. (June 2015). "Sulphur emission control areas and transport strategies -the case of Sweden and the forest industry". In: *European Transport Research Review* vol. 7 (2), p. 10. ISSN: 1867-0717. DOI: 10.1007/s12544-015-0161-9.
- Bessagnet, B. et al. (2016). "Presentation of the EURODELTA III intercomparison exercise – evaluation of the chemistry transport models' performance on criteria pollutants and joint analysis with meteorology". In: *Atmospheric Chemistry and Physics* vol. 16, no. 19, pp. 12667–12701. DOI: 10.5194/acp-16-12667-2016. URL: <https://acp.copernicus.org/articles/16/12667/2016/>.
- Beyrich, F. and Leps, J. P. (Aug. 2012). "An operational mixing height data set from routine radiosoundings at Lindenberg: Methodology". In: *Meteorologische Zeitschrift* vol. 21 (4), pp. 337–348. ISSN: 09412948. DOI: 10.1127/0941-2948/2012/0333.
- Black, E., Blackburn, M., Harrison, G., Hoskins, B., and Methven, J. (2004). "Factors contributing to the summer 2003 European heatwave". In: *Weather* vol. 59, no. 8, pp. 217–223. DOI: <https://doi.org/10.1256/wea.74.04>. eprint: <https://rmets.onlinelibrary.wiley.com/doi/pdf/10.1256/wea.74.04>. URL: <https://rmets.onlinelibrary.wiley.com/doi/abs/10.1256/wea.74.04>.
- Boldo, E., Medina, S., LeTertre, A., Hurley, F., Mücke, H. G., Ballester, F., Aguilera, I., and Eilstein, D. (2006). "Aphis: Health impact assessment of long-term exposure to PM2.5 in 23 European cities". In: *European Journal of Epidemiology* vol. 21 (6), pp. 449–458. ISSN: 03932990. DOI: 10.1007/s10654-006-9014-0. URL: <https://doi.org/10.1007/s10654-006-9014-0>.
- Borrego, C., Costa, A., Ginja, J., Amorim, M., Coutinho, M., Karatzas, K., Sioumis, T., Katsifarakis, N., Konstantinidis, K., Vito, S. D., Esposito, E., Smith, P., André, N., Gérard, P., Francis, L., Castell, N., Schneider, P., Viana, M., Minguillón, M., Reimringer, W., Otjes, R., Sicard, O. von, Pohle, R., Elen, B., Suriano, D., Pfister, V., Prato, M., Dipinto, S., and Penza, M. (Dec.

-
- 2016). “Assessment of air quality microsensors versus reference methods: The EuNetAir joint exercise”. In: *Atmospheric Environment* vol. 147, pp. 246–263. ISSN: 13522310. DOI: 10.1016/j.atmosenv.2016.09.050.
- Brook, R. D., Rajagopalan, S., Pope, C. A., Brook, J. R., Bhatnagar, A., Diez-Roux, A. V., Holguin, F., Hong, Y., Luepker, R. V., Mittleman, M. A., Peters, A., Siscovick, D., Smith, S. C., Whitsel, L., and Kaufman, J. D. (June 2010). *Particulate matter air pollution and cardiovascular disease: An update to the scientific statement from the american heart association*. DOI: 10.1161/CIR.0b013e3181dbee1.
- Brüggemann, E., Gerwig, H., Gnauk, T., Müller, K., and Herrmann, H. (May 2009). “Influence of seasons, air mass origin and day of the week on size-segregated chemical composition of aerosol particles at a kerbside”. In: *Atmospheric Environment* vol. 43 (15), pp. 2456–2463. ISSN: 1352-2310. DOI: 10.1016/J.ATMOSENV.2009.01.054. URL: <https://www.sciencedirect.com/science/article/pii/S1352231009000958#fig1>.
- Burnett, R. et al. (Sept. 2018). “Global estimates of mortality associated with long-term exposure to outdoor fine particulate matter”. In: *Proceedings of the National Academy of Sciences* vol. 115 (38), pp. 9592–9597. ISSN: 0027-8424. DOI: 10.1073/pnas.1803222115.
- Businger, J. A., Wyngaard, J. C., Izumi, Y., and Bradley, E. F. (Mar. 1971). “Flux-Profile Relationships in the Atmospheric Surface Layer”. In: *Journal of the Atmospheric Sciences* vol. 28 (2), pp. 181–189. ISSN: 0022-4928. DOI: 10.1175/1520-0469(1971)028<0181:fpri>2.0.co;2.
- Butler, T., Lupascu, A., Coates, J., and Zhu, S. (July 2018). “TOAST 1.0: Tropospheric Ozone Attribution of Sources with Tagging for CESM 1.2.2”. In: *Geoscientific Model Development* vol. 11 (7). ISSN: 1991-9603. DOI: 10.5194/gmd-11-2825-2018.
- Butler, T., Lupascu, A., and Nalam, A. (Sept. 2020). “Attribution of ground-level ozone to anthropogenic and natural sources of nitrogen oxides and reactive carbon in a global chemical transport model”. In: *Atmospheric Chemistry and Physics* vol. 20 (17). ISSN: 1680-7324. DOI: 10.5194/acp-20-10707-2020.
- Buzzi, M., Rotach, M. W., Holtslag, M., and Holtslag, A. A. (June 2011). “Evaluation of the COSMO-SC turbulence scheme in a shear-driven stable boundary layer”. In: *Meteorologische Zeitschrift* vol. 20 (3), pp. 335–350. ISSN: 0941-2948. DOI: 10.1127/0941-2948/2011/0050. URL: http://www.schweizerbart.de/papers/metz/detail/20/76134/Evaluation_of_the_COSMO_SC_turbulence_scheme_in_a_af=crossref.
- Calderón-Garcidueñas, L., Franco-Lira, M., Torres-Jardón, R., Henriquez-Roldán, C., Barragán-Mejía, G., Valencia-Salazar, G., González-Maciél, A., Reynoso-Robles, R., Villarreal-Calderón, R., and Reed, W. (Jan. 2007). “Pediatric Respiratory and Systemic Effects of Chronic Air Pollution Exposure: Nose, Lung, Heart, and Brain Pathology”. In: *Toxicologic Pathology* vol. 35 (1), pp. 154–162. ISSN: 0192-6233. DOI: 10.1080/01926230601059985.
- Carnevale, C., Angelis, E. D., Finzi, G., Pederzoli, A., Turrini, E., and Volta, M. (2018). “A non linear model approach to define priority for air quality control”. In: *IFAC-PapersOnLine* vol. 51 (13), pp. 210–215. ISSN: 24058963.

References

- DOI: 10.1016/j.ifacol.2018.07.280. URL: <https://linkinghub.elsevier.com/retrieve/pii/S2405896318310334>.
- Carro-Calvo, L., Ordóñez, C., García-Herrera, R., and Schnell, J. L. (2017). "Spatial clustering and meteorological drivers of summer ozone in Europe". In: *Atmospheric Environment* vol. 167, pp. 496–510. ISSN: 1352-2310. DOI: <https://doi.org/10.1016/j.atmosenv.2017.08.050>. URL: <https://www.sciencedirect.com/science/article/pii/S1352231017305630>.
- Castro, M. and Pires, J. C. (May 2019). "Decision support tool to improve the spatial distribution of air quality monitoring sites". In: *Atmospheric Pollution Research* vol. 10 (3), pp. 827–834. ISSN: 13091042. DOI: 10.1016/j.apr.2018.12.011.
- Chan, Y., Simpson, R., Mctainsh, G., Vowles, P., Cohen, D., and Bailey, G. (1999). "Source apportionment of PM_{2.5} and PM₁₀ aerosols in Brisbane (Australia) by receptor modelling". In: *Atmospheric Environment* vol. 33, no. 19, pp. 3251–3268. ISSN: 1352-2310. DOI: [https://doi.org/10.1016/S1352-2310\(99\)00090-4](https://doi.org/10.1016/S1352-2310(99)00090-4). URL: <https://www.sciencedirect.com/science/article/pii/S1352231099000904>.
- Chang, J. C. and Hanna, S. R. (Oct. 2004). "Air quality model performance evaluation". In: *Meteorology and Atmospheric Physics* vol. 87 (1-3), pp. 167–196. ISSN: 01777971. DOI: 10.1007/s00703-003-0070-7.
- Chen, L., Gao, Y., Zhang, M., Fu, J. S., Zhu, J., Liao, H., Li, J., Huang, K., Ge, B., Wang, X., Lam, Y. F., Lin, C.-Y., Itahashi, S., Nagashima, T., Kajino, M., Yamaji, K., Wang, Z., and Kurokawa, J. (2019). "MICS-Asia III: multi-model comparison and evaluation of aerosol over East Asia". In: *Atmospheric Chemistry and Physics* vol. 19, no. 18, pp. 11911–11937. DOI: 10.5194/acp-19-11911-2019. URL: <https://acp.copernicus.org/articles/19/11911/2019/>.
- Chen, T.-M., Kuschner, W. G., Gokhale, J., and Shofer, S. (Apr. 2007). "Outdoor Air Pollution: Nitrogen Dioxide, Sulfur Dioxide, and Carbon Monoxide Health Effects". In: *The American Journal of the Medical Sciences* vol. 333 (4), pp. 249–256. ISSN: 00029629. DOI: 10.1097/MAJ.0b013e31803b900f.
- China, S. and James, D. E. (Dec. 2012). "Influence of pavement macrotexture on PM₁₀ emissions from paved roads: A controlled study". In: *Atmospheric Environment* vol. 63, pp. 313–326. ISSN: 1352-2310. DOI: 10.1016/J.ATMOENV.2012.09.018. URL: <https://www.sciencedirect.com/science/article/abs/pii/S1352231012008771?via%3Dihub>.
- Churkina, G., Kuik, F., Bonn, B., Lauer, A., Grote, R., Tomiak, K., and Butler, T. M. (June 2017). "Effect of VOC Emissions from Vegetation on Air Quality in Berlin during a Heatwave". In: *Environmental Science & Technology* vol. 51 (11). ISSN: 0013-936X. DOI: 10.1021/acs.est.6b06514.
- Clappier, A., Thunis, P., Pirovano, G., Riffault, V., Gilardoni, S., Pisoni, E., Guerreiro, C., Monteiro, A., Dupont, H., Wærsted, E., Hellebust, S., Stocker, J., Eriksson, A., Angyal, A., Bonafe, G., Montanari, F., Matejovica, J., Bartzis, J., and Gianelle, V. (2022). "Source apportionment to support air quality management practices". In: no. KJ-NA-31-222-EN-N (online). ISSN: 1831-9424 (online). DOI: 10.2760/781626 (online).

-
- Clappier, A., Belis, C. A., Pernigotti, D., and Thunis, P. (Nov. 2017). *Source apportionment and sensitivity analysis: Two methodologies with two different purposes*. DOI: 10.5194/gmd-10-4245-2017.
- Coates, J., Mar, K. A., Ojha, N., and Butler, T. M. (2016). “The influence of temperature on ozone production under varying NO_x conditions – a modelling study”. In: *Atmospheric Chemistry and Physics* vol. 16, no. 18, pp. 11601–11615. DOI: 10.5194/acp-16-11601-2016. URL: <https://acp.copernicus.org/articles/16/11601/2016/>.
- Coen, M. C., Praz, C., Haefele, A., Ruffieux, D., Kaufmann, P., and Calpini, B. (2014). “Determination and climatology of the planetary boundary layer height above the Swiss plateau by in situ and remote sensing measurements as well as by the COSMO-2 model”. In: *Atmospheric Chemistry and Physics* vol. 14 (23), pp. 13205–13221. DOI: 10.5194/acp-14-13205-2014. URL: <https://www.atmos-chem-phys.net/14/13205/2014/>.
- Colette, A. et al. (2017). “EURODELTA-Trends, a multi-model experiment of air quality hindcast in Europe over 1990–2010”. In: *Geoscientific Model Development* vol. 10, no. 9, pp. 3255–3276. DOI: 10.5194/gmd-10-3255-2017. URL: <https://gmd.copernicus.org/articles/10/3255/2017/>.
- Collett, R. S. and Oduyemi, K. (Sept. 1997). “Air quality modelling: a technical review of mathematical approaches”. In: *Meteorological Applications* vol. 4 (3), S1350482797000455. ISSN: 13504827. DOI: 10.1017/S1350482797000455.
- Conti, G. O., Heibati, B., Kloog, I., Fiore, M., and Ferrante, M. (Mar. 2017). “A review of AirQ Models and their applications for forecasting the air pollution health outcomes”. In: *Environmental Science and Pollution Research* vol. 24 (7), pp. 6426–6445. ISSN: 0944-1344. DOI: 10.1007/s11356-016-8180-1.
- Cooter, E. J., Bash, J. O., Benson, V., and Ran, L. (Oct. 2012). “Linking agricultural crop management and air quality models for regional to national-scale nitrogen assessments”. In: *Biogeosciences* vol. 9 (10), pp. 4023–4035. ISSN: 1726-4189. DOI: 10.5194/bg-9-4023-2012.
- Costa, S., Ferreira, J., Silveira, C., Costa, C., Lopes, D., Relvas, H., Borrego, C., Roebeling, P., Miranda, A. I., and Teixeira, J. P. (Aug. 2014). *Integrating health on air quality assessment - Review report on health risks of two major european outdoor air pollutants: PM and NO₂*. doi: 10.1080/10937404.2014.946164. DOI: 10.1080/10937404.2014.946164. URL: <https://doi.org/10.1080/10937404.2014.946164>.
- Coulter, R. L. (Nov. 1979). “A Comparison of Three Methods for Measuring Mixing-Layer Height”. In: *Journal of Applied Meteorology* vol. 18 (11). doi: 10.1175/1520-0450(1979)0182.0.CO;2, pp. 1495–1499. ISSN: 0021-8952. DOI: 10.1175/1520-0450(1979)018<1495:ACOTMF>2.0.CO;2. URL: [https://doi.org/10.1175/1520-0450\(1979\)018%3C1495:ACOTMF%3E2.0.CO%20http://0.0.0.2](https://doi.org/10.1175/1520-0450(1979)018%3C1495:ACOTMF%3E2.0.CO%20http://0.0.0.2).
- Crippa, M., Guizzardi, D., Muntean, M., Schaaf, E., Dentener, F., Van Aardenne, J. A., Monni, S., Doering, U., Olivier, J. G., Pagliari, V., et al. (2018). “Gridded emissions of air pollutants for the period 1970–2012 within EDGAR v4.3.2”. In: *Earth Syst. Sci. Data* vol. 10, no. 4, pp. 1987–2013.

References

- Crippa, M., Janssens-Maenhout, G., Dentener, F., Guizzardi, D., Sindelarova, K., Muntean, M., Dingenen, R. V., and Granier, C. (Mar. 2016). “Forty years of improvements in European air quality: regional policy-industry interactions with global impacts”. In: *Atmospheric Chemistry and Physics* vol. 16 (6), pp. 3825–3841. ISSN: 1680-7324. DOI: [10.5194/acp-16-3825-2016](https://doi.org/10.5194/acp-16-3825-2016).
- Cromar, K. R., Duncan, B. N., Bartonova, A., Benedict, K., Brauer, M., Habre, R., Hagler, G. S. W., Haynes, J. A., Khan, S., Kilaru, V., Liu, Y., Pawson, S., Peden, D. B., Quint, J. K., Rice, M. B., Sasser, E. N., Seto, E., Stone, S. L., Thurston, G. D., and Volckens, J. (2019). “Air Pollution Monitoring for Health Research and Patient Care. An Official American Thoracic Society Workshop Report”. In: *Annals of the American Thoracic Society* vol. 16, no. 10. PMID: 31573344, pp. 1207–1214. DOI: [10.1513/AnnalsATS.201906-477ST](https://doi.org/10.1513/AnnalsATS.201906-477ST). eprint: <https://doi.org/10.1513/AnnalsATS.201906-477ST>. URL: <https://doi.org/10.1513/AnnalsATS.201906-477ST>.
- Crutzen, P. (Dec. 1973). “A discussion of the chemistry of some minor constituents in the stratosphere and troposphere”. In: *Pure and Applied Geophysics* vol. 106-108 (1), pp. 1385–1399. ISSN: 0033-4553. DOI: [10.1007/BF00881092](https://doi.org/10.1007/BF00881092).
- Curier, R. L., Kranenburg, R., Segers, A. J., Timmermans, R. M., and Schaap, M. (2014). “Synergistic use of OMI NO₂ tropospheric columns and LOTOS-EUROS to evaluate the NO_x emission trends across Europe”. In: *Remote Sensing of Environment* vol. 149, pp. 58–69. ISSN: 00344257. DOI: [10.1016/j.rse.2014.03.032](https://doi.org/10.1016/j.rse.2014.03.032).
- D’Amato, G., Liccardi, G., D’Amato, M., and Cazzola, M. (Sept. 2002). “Outdoor air pollution, climatic changes and allergic bronchial asthma”. In: *European Respiratory Journal* vol. 20 (3), pp. 763–776. ISSN: 0903-1936. DOI: [10.1183/09031936.02.00401402](https://doi.org/10.1183/09031936.02.00401402).
- Dabass, A., Talbott, E., Brink, L., Rager, J., and Holguin, F. (Oct. 2014). “Long Term Chronic Exposure to Ozone Air Pollution and Biomarkers of Cardiovascular Diseases in Adult National Health and Nutrition Examination Survey Participants”. In: *ISEE Conference Abstracts* vol. 2014 (1). ISSN: 1078-0475. DOI: [10.1289/isee.2014.O-034](https://doi.org/10.1289/isee.2014.O-034).
- Dahl, A., Gharibi, A., Swietlicki, E., Gudmundsson, A., Bohgard, M., Ljungman, A., Blomqvist, G., and Gustafsson, M. (Mar. 2006). “Traffic-generated emissions of ultrafine particles from pavement-tire interface”. In: *Atmospheric Environment* vol. 40 (7), pp. 1314–1323. ISSN: 13522310. DOI: [10.1016/j.atmosenv.2005.10.029](https://doi.org/10.1016/j.atmosenv.2005.10.029).
- Daiber, A., Kuntic, M., Hahad, O., Delogu, L. G., Rohrbach, S., Lisa, F. D., Schulz, R., and Münzel, T. (Dec. 2020). “Effects of air pollution particles (ultrafine and fine particulate matter) on mitochondrial function and oxidative stress – Implications for cardiovascular and neurodegenerative diseases”. In: *Archives of Biochemistry and Biophysics* vol. 696, p. 108662. ISSN: 00039861. DOI: [10.1016/j.abb.2020.108662](https://doi.org/10.1016/j.abb.2020.108662).
- Dee, D. P. et al. (2011). “The ERA-Interim reanalysis: configuration and performance of the data assimilation system”. In: *Quarterly Journal of the Royal Meteorological Society* vol. 137 (656), pp. 553–597. DOI: [10.1002/qj.828](https://doi.org/10.1002/qj.828). URL: <https://rmets.onlinelibrary.wiley.com/doi/abs/10.1002/qj.828>.

-
- Denby, B., Sundvor, I., Johansson, C., Pirjola, L., Ketzel, M., Norman, M., Kupiainen, K., Gustafsson, M., Blomqvist, G., and Omstedt, G. (2013). “A coupled road dust and surface moisture model to predict non-exhaust road traffic induced particle emissions (NORTRIP). Part 1: Road dust loading and suspension modelling”. In: *Atmospheric Environment* vol. 77, pp. 283–300. ISSN: 1352-2310. DOI: <https://doi.org/10.1016/j.atmosenv.2013.04.069>. URL: <https://www.sciencedirect.com/science/article/pii/S1352231013003336>.
- Denby, B. R., Kupiainen, K. J., and Gustafsson, M. (2018). “Chapter 9 - Review of Road Dust Emissions”. In: *Non-Exhaust Emissions*. Ed. by Amato, F. Academic Press, pp. 183–203. ISBN: 978-0-12-811770-5. DOI: <https://doi.org/10.1016/B978-0-12-811770-5.00009-1>. URL: <https://www.sciencedirect.com/science/article/pii/B9780128117705000091>.
- Dennis, R., Fox, T., Fuentes, M., Gilliland, A., Hanna, S., Hogrefe, C., Irwin, J., Rao, S. T., Scheffe, R., Schere, K., Steyn, D., and Venkatram, A. (Aug. 2010). “A framework for evaluating regional-scale numerical photochemical modeling systems”. In: *Environmental Fluid Mechanics* vol. 10 (4). ISSN: 1567-7419. DOI: [10.1007/s10652-009-9163-2](https://doi.org/10.1007/s10652-009-9163-2).
- Derwent, R. G., Manning, A. J., Simmonds, P. G., Spain, T. G., and O’Doherty, S. (2018). “Long-term trends in ozone in baseline and European regionally-polluted air at Mace Head, Ireland over a 30-year period”. In: *Atmospheric Environment* vol. 179, pp. 279–287. ISSN: 1352-2310. DOI: <https://doi.org/10.1016/j.atmosenv.2018.02.024>. URL: <https://www.sciencedirect.com/science/article/pii/S135223101830102X>.
- Dhomse, S. S. et al. (2018). “Estimates of ozone return dates from Chemistry-Climate Model Initiative simulations”. In: *Atmospheric Chemistry and Physics* vol. 18, no. 11, pp. 8409–8438. DOI: [10.5194/acp-18-8409-2018](https://doi.org/10.5194/acp-18-8409-2018). URL: <https://acp.copernicus.org/articles/18/8409/2018/>.
- Dingenen, R. V., Dentener, F., Crippa, M., Leitao, J., Marmer, E., Rao, S., Solazzo, E., and Valentini, L. (Nov. 2018). “TM5-FASST: a global atmospheric source–receptor model for rapid impact analysis of emission changes on air quality and short-lived climate pollutants”. In: *Atmospheric Chemistry and Physics* vol. 18 (21), pp. 16173–16211. ISSN: 1680-7324. DOI: [10.5194/acp-18-16173-2018](https://doi.org/10.5194/acp-18-16173-2018). URL: <https://acp.copernicus.org/articles/18/16173/2018/>.
- Dinoi, A., Donato, A., Belosi, F., Conte, M., and Contini, D. (Aug. 2017). “Comparison of atmospheric particle concentration measurements using different optical detectors: Potentiality and limits for air quality applications”. In: *Measurement* vol. 106, pp. 274–282. ISSN: 02632241. DOI: [10.1016/j.measurement.2016.02.019](https://doi.org/10.1016/j.measurement.2016.02.019).
- Doms, G. and Baldauf, M. (2018). *A Description of the Nonhydrostatic Regional COSMO-Model Part I: Dynamics and Numerics - COSMO-Model 5.5*. Deutscher Wetterdienst.
- Doms, G., Förstner, J., Heise, E., Herzog, H.-J., Mironov, D., Raschendorfer, M., Reinhardt, T., Ritter, B., Schrodin, R., Schulz, J.-P., and Vogel, G. (Sept. 2011). *A Description of the Nonhydrostatic Regional COSMO-Model Part II: Physical Parameterization - LM_F90 4.20*. Deutscher Wetterdienst.

- Dunker, A. M., Yarwood, G., Ortmann, J. P., and Wilson, G. M. (July 2002). “The Decoupled Direct Method for Sensitivity Analysis in a Three-Dimensional Air Quality Model Implementation, Accuracy, and Efficiency”. In: *Environmental Science & Technology* vol. 36 (13), pp. 2965–2976. ISSN: 0013-936X. DOI: 10.1021/es0112691.
- DWD (2020). *Klimastatusbericht Deutschland, Jahr 2018. Deutscher Wetterdienst (DWD) - Wetter und Klima aus einer Hand*. URL: https://www.dwd.de/DE/leistungen/klimastatusbericht/publikationen/ksb_2018.pdf?__blob=publicationFile&v=5.
- EC (2008). “Directive 2008/50/EC on ambient air quality and cleaner air for Europe”. In: *Official Journal of the European Communities* vol. 51, pp. 1–43. DOI: <http://eur-lex.europa.eu/LexUriServ/LexUriServ.do?uri=OJ:L:2008:152:0001:0044:EN:PDF>.
- Eckermann, S. (2009). “Hybrid σ -p coordinate choices for a global model”. In: *Monthly Weather Review* vol. 137 (1), pp. 224–245. ISSN: 00270644. DOI: 10.1175/2008MWR2537.1.
- EEA (2018a). “Air quality in Europe - 2018 report”. In: *European Environment Agency (EEA) Report No 12/2018*. Created 09 Jul 2018. ISSN: 978-92-9213-990-2. URL: <https://www.eea.europa.eu/publications/air-quality-in-europe-2018>.
- (2018b). “Unequal exposure and unequal impacts: social vulnerability to air pollution, noise and extreme temperatures in Europe”. In: *European Environment Agency (EEA) Report No 22/2018*. Created 11 Jan 2019. ISSN: 978-92-9480-047-3. URL: <https://www.eea.europa.eu/publications/unequal-exposure-and-unequal-impacts#additional-files>.
- (2021). “CORINE Land Cover - User Manual”. In: *Copernicus Land Monitoring Service* vol. 1.0 (European Environment Agency, European Topic Centre Urban Land and Soil).
- Emmons, L. K., Walters, S., Hess, P. G., Lamarque, J.-F., Pfister, G. G., Fillmore, D., Granier, C., Guenther, A., Kinnison, D., Laepple, T., Orlando, J., Tie, X., Tyndall, G., Wiedinmyer, C., Baughcum, S. L., and Kloster, S. (2010). “Description and evaluation of the Model for Ozone and Related chemical Tracers, version 4 (MOZART-4)”. In: *Geoscientific Model Development* vol. 3, no. 1, pp. 43–67. DOI: 10.5194/gmd-3-43-2010. URL: <https://gmd.copernicus.org/articles/3/43/2010/>.
- Engler, C., Birmili, W., Spindler, G., and Wiedensohler, A. (2012). “Analysis of exceedances in the daily PM 10 mass concentration ($50 \mu\text{g m}^{-3}$) at a roadside station in Leipzig, Germany”. In: *Atmospheric Chemistry and Physics* vol. 12 (21), pp. 10107–10123. ISSN: 16807316. DOI: 10.5194/acp-12-10107-2012. URL: <https://www.atmos-chem-phys.net/12/10107/2012/>.
- EPA, U. (Jan. 2008). *Latest Findings on National Air Quality - Status and Trends Through 2006, Contract No. EP-D-05-004 Work Assignment No. 3-4, U.S. Environmental Protection Agency, Office of Air Quality Planning and Standards, Air Quality Assessment Division, Research Triangle Park, North Carolina*.

-
- Escudero, M., Segers, A., Kranenburg, R., Querol, X., Alastuey, A., Borge, R., Paz, D. de la, Gangoiti, G., and Schaap, M. (Apr. 2019). "Analysis of summer O₃ in the Madrid air basin with the LOTOS-EUROS chemical transport model". In: *Atmospheric Chemistry and Physics Discussions*, pp. 1–40. ISSN: 1680-7375. DOI: [10.5194/acp-2019-334](https://doi.org/10.5194/acp-2019-334).
- Fallah, B., Thürkow, M., Jäkel, I., Segers, A., Kranenburg, R., and Schaap, M. (2020). "Tropospheric NO₂ column over Germany: A comparison between LOTUS-EUROS model and Copernicus sentinel-5 precursor satellite." In: *submitted to Atmospheric Environment*.
- Fang, Y., Naik, V., Horowitz, L. W., and Mauzerall, D. L. (2013). "Air pollution and associated human mortality: the role of air pollutant emissions, climate change and methane concentration increases from the preindustrial period to present". In: *Atmospheric Chemistry and Physics* vol. 13, no. 3, pp. 1377–1394. DOI: [10.5194/acp-13-1377-2013](https://doi.org/10.5194/acp-13-1377-2013). URL: <https://acp.copernicus.org/articles/13/1377/2013/>.
- Fast, J. D., Gustafson Jr., W. I., Easter, R. C., Zaveri, R. A., Barnard, J. C., Chapman, E. G., Grell, G. A., and Peckham, S. E. (2006). "Evolution of ozone, particulates, and aerosol direct radiative forcing in the vicinity of Houston using a fully coupled meteorology-chemistry-aerosol model". In: *Journal of Geophysical Research: Atmospheres* vol. 111, no. D21. DOI: <https://doi.org/10.1029/2005JD006721>. eprint: <https://agupubs.onlinelibrary.wiley.com/doi/pdf/10.1029/2005JD006721>. URL: <https://agupubs.onlinelibrary.wiley.com/doi/abs/10.1029/2005JD006721>.
- Favre, C., May, J., and Bosteels, D. (2016). "Emissions control technologies to meet current and future European vehicle emissions legislation". In: URL: www.aecc.eu.
- Fay, B. and Neunhäuserer, L. (Nov. 2005). "Evaluation of very high-resolution simulations with the non-hydrostatic numerical weather prediction model Lokalmodell for urban air pollution episodes in Helsinki, Oslo and Valencia". In: *Atmospheric Chemistry and Physics Discussions* vol. 5. DOI: [10.5194/acpd-5-8233-2005](https://doi.org/10.5194/acpd-5-8233-2005).
- Finlayson-Pitts, B. J. and Pitts, J. N. (2000). *Global Tropospheric Chemistry and Climate Change*. DOI: [10.1016/B978-012257060-5/50016-2](https://doi.org/10.1016/B978-012257060-5/50016-2). URL: <https://linkinghub.elsevier.com/retrieve/pii/B9780122570605500162>.
- Fischer, E. V., Jacob, D. J., Yantosca, R. M., Sulprizio, M. P., Millet, D. B., Mao, J., Paulot, F., Singh, H. B., Roiger, A., Ries, L., Talbot, R. W., Dzepina, K., and Pandey Deolal, S. (2014). "Atmospheric peroxyacetyl nitrate (PAN): a global budget and source attribution". In: *Atmospheric Chemistry and Physics* vol. 14, no. 5, pp. 2679–2698. DOI: [10.5194/acp-14-2679-2014](https://doi.org/10.5194/acp-14-2679-2014). URL: <https://acp.copernicus.org/articles/14/2679/2014/>.
- Fischer, P. H., Marra, M., Ameling, C. B., Hoek, G., Beelen, R., Hoogh, K. de, Breugelmans, O., Kruize, H., Janssen, N. A., and Houthuijs, D. (July 2015). "Air Pollution and Mortality in Seven Million Adults: The Dutch Environmental Longitudinal Study (DUELS)". In: *Environmental Health Perspectives* vol. 123 (7), pp. 697–704. ISSN: 0091-6765. DOI: [10.1289/ehp.1408254](https://doi.org/10.1289/ehp.1408254). URL: <https://ehp.niehs.nih.gov/doi/10.1289/ehp.1408254>.

References

- Flemming, J., Benedetti, A., Inness, A., Engelen, R. J., Jones, L., Huijnen, V., Remy, S., Parrington, M., Suttie, M., Bozzo, A., Peuch, V.-H., Akritidis, D., and Katragkou, E. (2017). “The CAMS interim Reanalysis of Carbon Monoxide, Ozone and Aerosol for 2003–2015”. In: *Atmospheric Chemistry and Physics* vol. 17, no. 3, pp. 1945–1983. DOI: [10.5194/acp-17-1945-2017](https://doi.org/10.5194/acp-17-1945-2017). URL: <https://acp.copernicus.org/articles/17/1945/2017/>.
- Flemming, J., Inness, A., Flentje, H., Huijnen, V., Moinat, P., Schultz, M. G., and Stein, O. (Dec. 2009). “Coupling global chemistry transport models to ECMWF’s integrated forecast system”. In: *Geoscientific Model Development* vol. 2 (2), pp. 253–265. ISSN: 19919603. DOI: [10.5194/gmd-2-253-2009](https://doi.org/10.5194/gmd-2-253-2009).
- Flemming, J. and Stern, R. (2007). “Testing model accuracy measures according to the EU directives—examples using the chemical transport model REM-CALGRID”. In: *Atmospheric Environment* vol. 41, no. 39, pp. 9206–9216. ISSN: 1352-2310. DOI: <https://doi.org/10.1016/j.atmosenv.2007.07.050>. URL: <https://www.sciencedirect.com/science/article/pii/S1352231007006838>.
- Foley, K. M., Dolwick, P., Hogrefe, C., Simon, H., Timin, B., and Possiel, N. (2015a). “Dynamic evaluation of CMAQ part II: Evaluation of relative response factor metrics for ozone attainment demonstrations”. In: *Atmospheric Environment* vol. 103, pp. 188–195. ISSN: 1352-2310. DOI: <https://doi.org/10.1016/j.atmosenv.2014.12.039>. URL: <https://www.sciencedirect.com/science/article/pii/S135223101400987X>.
- Foley, K. M., Hogrefe, C., Pouliot, G., Possiel, N., Roselle, S. J., Simon, H., and Timin, B. (2015b). “Dynamic evaluation of CMAQ part I: Separating the effects of changing emissions and changing meteorology on ozone levels between 2002 and 2005 in the eastern US”. In: *Atmospheric Environment* vol. 103, pp. 247–255. ISSN: 1352-2310. DOI: <https://doi.org/10.1016/j.atmosenv.2014.12.038>. URL: <https://www.sciencedirect.com/science/article/pii/S1352231014009868>.
- Fountoukis, C. and Nenes, A. (2007). “ISORROPIA II: a computationally efficient thermodynamic equilibrium model for K^+ - Ca^{2+} - Mg^{2+} - NH_4^+ - Na^+ - SO_4^{2-} - NO_3^- - Cl^- - H_2O aerosols”. In: *Atmospheric Chemistry and Physics* vol. 7, no. 17, pp. 4639–4659. DOI: [10.5194/acp-7-4639-2007](https://doi.org/10.5194/acp-7-4639-2007). URL: <https://acp.copernicus.org/articles/7/4639/2007/>.
- Fowler, D. et al. (2009). “Atmospheric composition change: Ecosystems–Atmosphere interactions”. In: *Atmospheric Environment* vol. 43, no. 33. ACCENT Synthesis, pp. 5193–5267. ISSN: 1352-2310. DOI: <https://doi.org/10.1016/j.atmosenv.2009.07.068>. URL: <https://www.sciencedirect.com/science/article/pii/S1352231009006633>.
- Fowler, D., Coyle, M., Skiba, U., Sutton, M. A., Cape, J. N., Reis, S., Sheppard, L. J., Jenkins, A., Grizzetti, B., Galloway, J. N., Vitousek, P., Leach, A., Bouwman, A. F., Butterbach-Bahl, K., Dentener, F., Stevenson, D., Amann, M., and Voss, M. (July 2013). “The global nitrogen cycle in the twenty-first century”. In: *Philosophical Transactions of the Royal Society B: Biological Sciences* vol. 368 (1621). ISSN: 0962-8436. DOI: [10.1098/rstb.2013.0164](https://doi.org/10.1098/rstb.2013.0164).
- Fuzzi, S., Baltensperger, U., Carslaw, K., Decesari, S., Denier van der Gon, H., Facchini, M. C., Fowler, D., Koren, I., Langford, B., Lohmann, U., Nemitz, E.,

-
- Pandis, S., Riipinen, I., Rudich, Y., Schaap, M., Slowik, J., Spracklen, D. V., Vignati, E., Wild, M., Williams, M., and Gilardoni, S. (2015). "Particulate matter, air quality and climate: lessons learned and future needs". en. In: *Atmospheric Chemistry and Physics* vol. 15, no. 14, pp. 8217–8299. ISSN: 1680-7375. DOI: [10.3929/ethz-b-000103253](https://doi.org/10.3929/ethz-b-000103253).
- Galmarini, S., Koffi, B., Solazzo, E., Keating, T., Hogrefe, C., Schulz, M., Benedictow, A., Griesfeller, J. J., Janssens-Maenhout, G., Carmichael, G., Fu, J., and Dentener, F. (2017). "Technical note: Coordination and harmonization of the multi-scale, multi-model activities HTAP2, AQMEII3, and MICS-Asia3: simulations, emission inventories, boundary conditions, and model output formats". In: *Atmospheric Chemistry and Physics* vol. 17, no. 2, pp. 1543–1555. DOI: [10.5194/acp-17-1543-2017](https://doi.org/10.5194/acp-17-1543-2017). URL: <https://acp.copernicus.org/articles/17/1543/2017/>.
- Garg, B. D., Cadle, S. H., Mulawa, P. A., Groblicki, P. J., Laroo, C., and Parr, G. A. (Nov. 2000). "Brake wear particulate matter emissions". In: *Environmental Science and Technology* vol. 34 (21), pp. 4463–4469. ISSN: 0013936X. DOI: [10.1021/es001108h](https://doi.org/10.1021/es001108h).
- Garg, S. and Sinha, B. (Oct. 2017). "Determining the contribution of long-range transport, regional and local source areas, to PM10 mass loading in Hessen, Germany using a novel multi-receptor based statistical approach". In: *Atmospheric Environment* vol. 167, pp. 566–575. ISSN: 18732844. DOI: [10.1016/j.atmosenv.2017.08.029](https://doi.org/10.1016/j.atmosenv.2017.08.029). URL: <https://www.sciencedirect.com/science/article/abs/pii/S1352231017305344>.
- Gauderman, W. J., Avol, E., Gilliland, F., Vora, H., Thomas, D., Berhane, K., McConnell, R., Kuenzli, N., Lurmann, F., Rappaport, E., Margolis, H., Bates, D., and Peters, J. (Sept. 2004). "The Effect of Air Pollution on Lung Development from 10 to 18 Years of Age". In: *New England Journal of Medicine* vol. 351 (11), pp. 1057–1067. ISSN: 0028-4793. DOI: [10.1056/NEJMoa040610](https://doi.org/10.1056/NEJMoa040610).
- Ge, X., Schaap, M., Kranenburg, R., Segers, A., Reinds, G. J., Kros, H., and Vries, W. de (2020). "Modeling atmospheric ammonia using agricultural emissions with improved spatial variability and temporal dynamics". In: *Atmospheric Chemistry and Physics* vol. 20, no. 24, pp. 16055–16087. DOI: [10.5194/acp-20-16055-2020](https://doi.org/10.5194/acp-20-16055-2020). URL: <https://acp.copernicus.org/articles/20/16055/2020/>.
- Gehrig, R., Hill, M., Buchmann, B., Imhof, D., Weingartner, E., and Baltensperger, U. (2004). "Separate determination of PM10 emission factors of road traffic for tailpipe emissions and emissions from abrasion and resuspension processes". In: *International Journal of Environment and Pollution* vol. 22, no. 3, pp. 312–325. DOI: [10.1504/IJEP.2004.005549](https://doi.org/10.1504/IJEP.2004.005549). eprint: <https://www.inderscienceonline.com/doi/pdf/10.1504/IJEP.2004.005549>. URL: <https://www.inderscienceonline.com/doi/abs/10.1504/IJEP.2004.005549>.
- Geiß, A., Wiegner, M., Bonn, B., Schäfer, K., Forkel, R., Schneidmesser, E. V., Münkler, C., Chan, K. L., and Nothard, R. (Aug. 2017). "Mixing layer height as an indicator for urban air quality?" In: *Atmospheric Measurement Techniques* vol. 10 (8), pp. 2969–2988. ISSN: 18678548. DOI: [10.5194/amt-10-2969-2017](https://doi.org/10.5194/amt-10-2969-2017).

References

- Gerard, D. and Lave, L. B. (Sept. 2005). "Implementing technology-forcing policies: The 1970 Clean Air Act Amendments and the introduction of advanced automotive emissions controls in the United States". In: *Technological Forecasting and Social Change* vol. 72 (7), pp. 761–778. ISSN: 00401625. DOI: [10.1016/j.techfore.2004.08.003](https://doi.org/10.1016/j.techfore.2004.08.003).
- Gery, M. W., Whitten, G. Z., Killus, J. P., and Dodge, M. C. (1989). "A photochemical kinetics mechanism for urban and regional scale computer modeling". In: *Journal of Geophysical Research: Atmospheres* vol. 94, no. D10, pp. 12925–12956. DOI: <https://doi.org/10.1029/JD094iD10p12925>. eprint: <https://agupubs.onlinelibrary.wiley.com/doi/pdf/10.1029/JD094iD10p12925>. URL: <https://agupubs.onlinelibrary.wiley.com/doi/abs/10.1029/JD094iD10p12925>.
- Giannakis, E., Kushta, J., Bruggeman, A., and Lelieveld, J. (Dec. 2019). "Costs and benefits of agricultural ammonia emission abatement options for compliance with European air quality regulations". In: *Environmental Sciences Europe* vol. 31 (1), p. 93. ISSN: 2190-4707. DOI: [10.1186/s12302-019-0275-0](https://doi.org/10.1186/s12302-019-0275-0).
- Gon, H. D. van der, Jozwicka, M., Hendriks, E., Gondwe, M., and Schaap, M. (2010). "Mineral Dust as a component of particulate matter". In: *PBL Netherlands Environmental Assessment Agency* vol. 160. URL: <https://www.pbl.nl/en/publications/Mineral-Dust-component-particulate-matter>.
- Gong, S. L., Barrie, L. A., and Blanchet, J.-P. (1997a). "Modeling sea-salt aerosols in the atmosphere: 1. Model development". In: *Journal of Geophysical Research: Atmospheres* vol. 102, no. D3, pp. 3805–3818. DOI: <https://doi.org/10.1029/96JD02953>. eprint: <https://agupubs.onlinelibrary.wiley.com/doi/pdf/10.1029/96JD02953>. URL: <https://agupubs.onlinelibrary.wiley.com/doi/abs/10.1029/96JD02953>.
- Gong, S. L., Barrie, L. A., Prospero, J. M., Savoie, D. L., Ayers, G. P., Blanchet, J.-P., and Spacek, L. (1997b). "Modeling sea-salt aerosols in the atmosphere: 2. Atmospheric concentrations and fluxes". In: *Journal of Geophysical Research: Atmospheres* vol. 102, no. D3, pp. 3819–3830. DOI: <https://doi.org/10.1029/96JD03401>. eprint: <https://agupubs.onlinelibrary.wiley.com/doi/pdf/10.1029/96JD03401>. URL: <https://agupubs.onlinelibrary.wiley.com/doi/abs/10.1029/96JD03401>.
- Gozzi, F., Marcelli, A., and Lucci, F. (Sept. 2017). "Current status of particulate matter pollution in Europe and future perspectives: A review". In: vol. 8, pp. 1901–1909.
- Granier, C., Bessagnet, B., Bond, T., D'Angiola, A., Gon, H. D. van der, Frost, G. J., Heil, A., Kaiser, J. W., Kinne, S., Klimont, Z., Kloster, S., Lamarque, J.-F., Liousse, C., Masui, T., Meleux, F., Mieville, A., Ohara, T., Raut, J.-C., Riahi, K., Schultz, M. G., Smith, S. J., Thompson, A., Aardenne, J. van, Werf, G. R. van der, and Vuuren, D. P. van (Nov. 2011). "Evolution of anthropogenic and biomass burning emissions of air pollutants at global and regional scales during the 1980–2010 period". In: *Climatic Change* vol. 109 (1-2), pp. 163–190. ISSN: 0165-0009. DOI: [10.1007/s10584-011-0154-1](https://doi.org/10.1007/s10584-011-0154-1). URL: <http://link.springer.com/10.1007/s10584-011-0154-1>.

-
- Granier, C., Darras, S., Der Gon, H. D. van, Jana, D., Elguindi, N., Bo, G., Michael, G., Marc, G., Jalkanen, J.-P., Kuenen, J., et al. (2019). “The Copernicus atmosphere monitoring service global and regional emissions (April 2019 version)”. PhD thesis. Copernicus Atmosphere Monitoring Service.
- Grell, G. and Baklanov, A. (Dec. 2011). “Integrated modeling for forecasting weather and air quality: A call for fully coupled approaches”. In: *Atmospheric Environment* vol. 45 (38), pp. 6845–6851. ISSN: 13522310. DOI: [10.1016/j.atmosenv.2011.01.017](https://doi.org/10.1016/j.atmosenv.2011.01.017).
- Grell, G. A. (2004). “Online versus offline air quality modeling on cloud-resolving scales”. In: *Geophysical Research Letters* vol. 31 (16), p. L16117. ISSN: 0094-8276. DOI: [10.1029/2004GL020175](https://doi.org/10.1029/2004GL020175).
- Grell, G. A., Peckham, S. E., Schmitz, R., McKeen, S. A., Frost, G., Skamarock, W. C., and Eder, B. (2005). “Fully coupled “online” chemistry within the WRF model”. In: *Atmospheric Environment* vol. 39, no. 37, pp. 6957–6975. ISSN: 1352-2310. DOI: <https://doi.org/10.1016/j.atmosenv.2005.04.027>. URL: <https://www.sciencedirect.com/science/article/pii/S1352231005003560>.
- Grigoratos, T. and Martini, G. (2015). “Brake wear particle emissions: a review”. In: *Environmental Science and Pollution Research* vol. 22 (4). Cited By :188
Export Date: 17 January 2020, pp. 2491–2504. DOI: [10.1007/s11356-014-3696-8](https://doi.org/10.1007/s11356-014-3696-8). URL: <https://www.scopus.com/inward/record.uri?eid=2-s2.0-84925483947&doi=10.1007%2Fs11356-014-3696-8&partnerID=40&md5=e5892d1456036abd41c9bafb1ad0997e>.
- Guenther, A., Jiang, X., Heald, C. L., Sakulyanontvittaya, T., Duhl, T., Emmons, L. K., and Wang, X. (2012). “The Model of Emissions of Gases and Aerosols from Nature version 2.1 (MEGAN2.1): an extended and updated framework for modeling biogenic emissions”. In: *Geoscientific Model Development* vol. 5, no. 6, pp. 1471–1492. DOI: [10.5194/gmd-5-1471-2012](https://doi.org/10.5194/gmd-5-1471-2012). URL: <https://gmd.copernicus.org/articles/5/1471/2012/>.
- Guenther, A., Karl, T., Harley, P., Wiedinmyer, C., Palmer, P. I., and Geron, C. (2006). “Estimates of global terrestrial isoprene emissions using MEGAN (Model of Emissions of Gases and Aerosols from Nature)”. In: *Atmospheric Chemistry and Physics* vol. 6, no. 11, pp. 3181–3210. DOI: [10.5194/acp-6-3181-2006](https://doi.org/10.5194/acp-6-3181-2006). URL: <https://acp.copernicus.org/articles/6/3181/2006/>.
- Guerreiro, C. B., Foltescu, V., and Leeuw, F. de (Dec. 2014). “Air quality status and trends in Europe”. In: *Atmospheric Environment* vol. 98, pp. 376–384. ISSN: 13522310. DOI: [10.1016/j.atmosenv.2014.09.017](https://doi.org/10.1016/j.atmosenv.2014.09.017).
- Guevara, M., Jorba, O., Tena, C., Gon, H. van der, Kuenen, J., Elguindi, N., Darras, S., Granier, C., and Garc{1}a-Pando, C. P. (2021). “Copernicus Atmosphere Monitoring Service TEMPORal profiles (CAMs-TEMPO): global and European emission temporal profile maps for atmospheric chemistry modelling”. In: *Earth System Science Data* vol. 13 (2), pp. 367–404. DOI: [10.5194/essd-13-367-2021](https://doi.org/10.5194/essd-13-367-2021). URL: <https://essd.copernicus.org/articles/13/367/2021/>.

References

- Gulia, S., Goyal, P., Goyal, S. K., and Kumar, R. (Mar. 2019). *Re-suspension of road dust: contribution, assessment and control through dust suppressants—a review*. DOI: 10.1007/s13762-018-2001-7.
- Gurjar, B., Jain, A., Sharma, A., Agarwal, A., Gupta, P., Nagpure, A., and Lelieveld, J. (Nov. 2010). “Human health risks in megacities due to air pollution”. In: *Atmospheric Environment* vol. 44 (36), pp. 4606–4613. ISSN: 13522310. DOI: 10.1016/j.atmosenv.2010.08.011.
- Gustafsson, M., Blomqvist, G., Gudmundsson, A., Dahl, A., Jonsson, P., and Swietlicki, E. (Oct. 2009). “Factors influencing PM10 emissions from road pavement wear”. In: *Atmospheric Environment* vol. 43 (31), pp. 4699–4702. ISSN: 1352-2310. DOI: 10.1016/J.ATMOSENV.2008.04.028. URL: <https://www.sciencedirect.com/science/article/abs/pii/S1352231008004731?via%3Dihub>.
- Haefelin, M., Angelini, F., Morille, Y., Martucci, G., Frey, S., Gobbi, G. P., Lolli, S., O’Dowd, C. D., Sauvage, L., Xueref-Rémy, I., Wastine, B., and Feist, D. G. (Apr. 2012). “Evaluation of Mixing-Height Retrievals from Automatic Profiling Lidars and Ceilometers in View of Future Integrated Networks in Europe”. In: *Boundary-Layer Meteorology* vol. 143 (1), pp. 49–75. ISSN: 00068314. DOI: 10.1007/s10546-011-9643-z.
- Hagino, H., Oyama, M., and Sasaki, S. (Apr. 2016). “Laboratory testing of airborne brake wear particle emissions using a dynamometer system under urban city driving cycles”. In: *Atmospheric Environment* vol. 131, pp. 269–278. ISSN: 1352-2310. DOI: 10.1016/J.ATMOSENV.2016.02.014. URL: <https://www.sciencedirect.com/science/article/pii/S135223101630125X?via%3Dihub>.
- Hanna, S. R. and Yang, R. (2001). “Evaluations of mesoscale models’ simulations of near-surface winds, temperature gradients, and mixing depths”. In: *Journal of Applied Meteorology* vol. 40 (6), pp. 1095–1104. ISSN: 08948763. DOI: 10.1175/1520-0450(2001)040<1095:EOMMSO>2.0.CO;2.
- Harrison, R. M., Jones, A. M., Gietl, J., Yin, J., and Green, D. C. (June 2012). “Estimation of the Contributions of Brake Dust, Tire Wear, and Resuspension to Nonexhaust Traffic Particles Derived from Atmospheric Measurements”. In: *Environmental Science & Technology* vol. 46 (12). ISSN: 0013-936X. DOI: 10.1021/es300894r.
- Heinold, B., Tegen, I., Schepanski, K., Tesche, M., Esselborn, M., Freudenthaler, V., Gross, S., Kandler, K., Knippertz, P., Müller, D., Schladitz, A., Toledano, C., Weinzierl, B., Ansmann, A., Althausen, D., Müller, T., Petzold, A., and Wiedensohler, A. (Jan. 2011). “Regional modelling of Saharan dust and biomass-burning smoke: Part 1: Model description and evaluation”. In: *Tellus B: Chemical and Physical Meteorology* vol. 63 (4), p. 781. ISSN: 1600-0889. DOI: 10.1111/j.1600-0889.2011.00570.x.
- Hendriks, C., Kranenburg, R., Kuenen, J., Bril, B. V. den, Verguts, V., and Schaap, M. (Apr. 2016). “Ammonia emission time profiles based on manure transport data improve ammonia modelling across north western Europe”. In: *Atmospheric Environment* vol. 131, pp. 83–96. ISSN: 1352-2310. DOI: 10.1016/J.ATMOSENV.2016.01.043. URL: <https://www.sciencedirect.com/science/article/abs/pii/S1352231016300668?via%3Dihub>.

-
- Hendriks, C., Kranenburg, R., Kuenen, J., Gijlswijk, R. van, Kruit, R. W., Segers, A., Gon, H. D. van der, and Schaap, M. (2013). “The origin of ambient particulate matter concentrations in the Netherlands”. In: *Atmospheric Environment*. ISSN: 13522310. DOI: [10.1016/j.atmosenv.2012.12.017](https://doi.org/10.1016/j.atmosenv.2012.12.017).
- Hendriks, C., Kuenen, J., Kranenburg, R., Scholz, Y., and Schaap, M. (2015). “A shift in emission time profiles of fossil fuel combustion due to energy transitions impacts source receptor matrices for air quality”. In: *Environ. Sci.: Processes Impacts* vol. 17 (3), pp. 510–524. DOI: [10.1039/C4EM00444B](https://doi.org/10.1039/C4EM00444B). URL: <http://dx.doi.org/10.1039/C4EM00444B>.
- Henneman, L. R., Liu, C., Hu, Y., Mulholland, J. A., and Russell, A. G. (2017). “Air quality modeling for accountability research: Operational, dynamic, and diagnostic evaluation”. In: *Atmospheric Environment* vol. 166, pp. 551–565. ISSN: 1352-2310. DOI: <https://doi.org/10.1016/j.atmosenv.2017.07.049>. URL: <https://www.sciencedirect.com/science/article/pii/S1352231017304983>.
- Herzog, H.-J., Schubert, U., Vogel, G., Fiedler, A., and . Kirchner, R. (2002a). “LLM- the high-resolving nonhydrostatic simulation model in the DWD-project LITFASS.Part I: Modelling technique and simulation method.” In: *Technical Report No. 4*. URL: https://www.dwd.de/SharedDocs/downloads/DE/modelldokumentationen/nwv/veroeffentlichungen/Cosmo_tech_rep/costr4.pdf?__blob=publicationFile&v=2.
- Herzog, H.-J., Vogel, G., and Schubert, U. (2002b). “LLM - a nonhydrostatic model applied to high-resolving simulations of turbulent fluxes over heterogeneous terrain”. In: *Theoretical and Applied Climatology* vol. 73 (1-2), pp. 67–86. DOI: [10.1007/s00704-002-0694-4](https://doi.org/10.1007/s00704-002-0694-4).
- Hogrefe, C., Liu, P., Pouliot, G., Mathur, R., Roselle, S., Flemming, J., Lin, M., and Park, R. J. (2018). “Impacts of different characterizations of large-scale background on simulated regional-scale ozone over the continental United States”. In: *Atmospheric Chemistry and Physics* vol. 18, no. 5, pp. 3839–3864. DOI: [10.5194/acp-18-3839-2018](https://doi.org/10.5194/acp-18-3839-2018). URL: <https://acp.copernicus.org/articles/18/3839/2018/>.
- Hossain, A. and Davies, P. (May 2013). “Pyrolysis liquids and gases as alternative fuels in internal combustion engines – A review”. In: *Renewable and Sustainable Energy Reviews* vol. 21, pp. 165–189. ISSN: 13640321. DOI: [10.1016/j.rser.2012.12.031](https://doi.org/10.1016/j.rser.2012.12.031).
- HTAP (2010). *Hemispheric Transport of Air Pollution 2010*. United Nations. URL: <https://www.un-ilibrary.org/content/books/9789210541091>.
- Hu, X. M., Nielsen-Gammon, J. W., and Zhang, F. (Sept. 2010). “Evaluation of three planetary boundary layer schemes in the WRF model”. In: *Journal of Applied Meteorology and Climatology* vol. 49 (9), pp. 1831–1844. ISSN: 15588424. DOI: [10.1175/2010JAMC2432.1](https://doi.org/10.1175/2010JAMC2432.1).
- Huang, M., Carmichael, G. R., Pierce, R. B., Jo, D. S., Park, R. J., Flemming, J., Emmons, L. K., Bowman, K. W., Henze, D. K., Davila, Y., Sudo, K., Jonson, J. E., Tronstad Lund, M., Janssens-Maenhout, G., Dentener, F. J., Keating, T. J., Oetjen, H., and Payne, V. H. (2017). “Impact of intercontinental pollution transport on North American ozone air pollution: an HTAP phase 2 multi-model study”. In: *Atmospheric Chemistry and Physics* vol. 17, no. 9,

- pp. 5721–5750. DOI: 10.5194/acp-17-5721-2017. URL: <https://acp.copernicus.org/articles/17/5721/2017/>.
- Huang, Y., Deng, T., Li, Z., Wang, N., Yin, C., Wang, S., and Fan, S. (Sept. 2018). “Numerical simulations for the sources apportionment and control strategies of PM_{2.5} over Pearl River Delta, China, part I: Inventory and PM_{2.5} sources apportionment”. In: *Science of The Total Environment* vol. 634, pp. 1631–1644. ISSN: 00489697. DOI: 10.1016/j.scitotenv.2018.04.208. URL: <https://linkinghub.elsevier.com/retrieve/pii/S0048969718313858>.
- Hundsdoerfer, W., Koren, B., vanLoon, M., and Verwer, J. (1995). “A Positive Finite-Difference Advection Scheme”. In: *Journal of Computational Physics* vol. 117, no. 1, pp. 35–46. ISSN: 0021-9991. DOI: <https://doi.org/10.1006/jcph.1995.1042>. URL: <https://www.sciencedirect.com/science/article/pii/S002199918571042X>.
- Hůnová, I., Novák, M., Kurfürst, P., Škáchová, H., Štěpánová, M., Přečková, E., Komárek, A., Čuřík, J., Veselovský, F., and Bohdálková, L. (Feb. 2022). “Contribution of rime to atmospheric sulphur deposition in Central Europe: A combined empirical and modelling approach”. In: *Atmospheric Environment* vol. 270, p. 118877. ISSN: 13522310. DOI: 10.1016/j.atmosenv.2021.118877.
- Im, U. et al. (2018). “Influence of anthropogenic emissions and boundary conditions on multi-model simulations of major air pollutants over Europe and North America in the framework of AQMEII3”. In: *Atmospheric Chemistry and Physics* vol. 18, no. 12, pp. 8929–8952. DOI: 10.5194/acp-18-8929-2018. URL: <https://acp.copernicus.org/articles/18/8929/2018/>.
- Im, U. et al. (2015a). “Evaluation of operational on-line-coupled regional air quality models over Europe and North America in the context of AQMEII phase 2. Part I: Ozone”. In: *Atmospheric Environment* vol. 115, pp. 404–420. ISSN: 1352-2310. DOI: <https://doi.org/10.1016/j.atmosenv.2014.09.042>. URL: <https://www.sciencedirect.com/science/article/pii/S1352231014007353>.
- Im, U. et al. (2015b). “Evaluation of operational online-coupled regional air quality models over Europe and North America in the context of AQMEII phase 2. Part II: Particulate matter”. In: *Atmospheric Environment* vol. 115, pp. 421–441. ISSN: 1352-2310. DOI: <https://doi.org/10.1016/j.atmosenv.2014.08.072>. URL: <https://www.sciencedirect.com/science/article/pii/S1352231014006839>.
- Inness, A., Ades, M., Agustí-Panareda, A., Barré, J., Benedictow, A., Blechschmidt, A.-M., Dominguez, J. J., Engelen, R., Eskes, H., Flemming, J., Huijnen, V., Jones, L., Kipling, Z., Massart, S., Parrington, M., Peuch, V.-H., Razinger, M., Remy, S., Schulz, M., and Suttie, M. (2019). “The CAMS reanalysis of atmospheric composition”. In: *Atmospheric Chemistry and Physics* vol. 19, no. 6, pp. 3515–3556. DOI: 10.5194/acp-19-3515-2019. URL: <https://acp.copernicus.org/articles/19/3515/2019/>.
- Jacob, D. J. and Winner, D. A. (2009). “Effect of climate change on air quality”. In: *Atmospheric Environment* vol. 43, no. 1. Atmospheric Environment - Fifty Years of Endeavour, pp. 51–63. ISSN: 1352-2310. DOI: <https://doi.org/10.1016/j.atmosenv.2008.09.051>. URL: <https://www.sciencedirect.com/science/article/pii/S1352231008008571>.

-
- Jafari, A. J., Charkhloo, E., and Pasalari, H. (Dec. 2021). “Urban air pollution control policies and strategies: a systematic review”. In: *Journal of Environmental Health Science and Engineering* vol. 19 (2), pp. 1911–1940. ISSN: 2052-336X. DOI: [10.1007/s40201-021-00744-4](https://doi.org/10.1007/s40201-021-00744-4).
- Jang, J.-C. C., Jeffries, H. E., and Tonnesen, S. (1995). “Sensitivity of ozone to model grid resolution — II. Detailed process analysis for ozone chemistry”. In: *Atmospheric Environment* vol. 29, no. 21. A and WMA International Specialty Conference on Regional Photochemical Measurements and Modeling, pp. 3101–3114. ISSN: 1352-2310. DOI: [https://doi.org/10.1016/1352-2310\(95\)00119-J](https://doi.org/10.1016/1352-2310(95)00119-J). URL: <https://www.sciencedirect.com/science/article/pii/S135223109500119J>.
- Janssen, S. and Thunis, P. (2022). *FAIRMODE guidance document on modelling quality objectives and benchmarking : version 3.3*. Publications Office of the European Union. DOI: [doi/10.2760/41988](https://doi.org/10.2760/41988).
- Jonson, J. E., Schulz, M., Emmons, L., Flemming, J., Henze, D., Sudo, K., Tronstad Lund, M., Lin, M., Benedictow, A., Koffi, B., Dentener, F., Keating, T., Kivi, R., and Davila, Y. (2018). “The effects of intercontinental emission sources on European air pollution levels”. In: *Atmospheric Chemistry and Physics* vol. 18, no. 18, pp. 13655–13672. DOI: [10.5194/acp-18-13655-2018](https://doi.org/10.5194/acp-18-13655-2018). URL: <https://acp.copernicus.org/articles/18/13655/2018/>.
- Kaiser, J. W., Heil, A., Andreae, M. O., Benedetti, A., Chubarova, N., Jones, L., Morcrette, J.-J., Razinger, M., Schultz, M. G., Suttie, M., and Werf, G. R. van der (2012). “Biomass burning emissions estimated with a global fire assimilation system based on observed fire radiative power”. In: *Biogeosciences* vol. 9 (1), pp. 527–554. DOI: [10.5194/bg-9-527-2012](https://doi.org/10.5194/bg-9-527-2012). URL: <https://www.biogeosciences.net/9/527/2012/>.
- Kalina, M. F., Stopper, S., Zambo, E., and Puxbaum, H. (Mar. 2002). “Altitude-dependent wet, dry and occult nitrogen deposition in an Alpine Region”. In: *Environmental Science and Pollution Research* vol. 9 (S2), pp. 16–22. ISSN: 0944-1344. DOI: [10.1007/BF02987473](https://doi.org/10.1007/BF02987473).
- Kampa, M. and Castanas, E. (Jan. 2008). “Human health effects of air pollution”. In: *Environmental Pollution* vol. 151 (2), pp. 362–367. ISSN: 02697491. DOI: [10.1016/j.envpol.2007.06.012](https://doi.org/10.1016/j.envpol.2007.06.012). URL: <https://linkinghub.elsevier.com/retrieve/pii/S0269749107002849>.
- Karl, M., Dorn, H.-P., Holland, F., Koppmann, R., Poppe, D., Rupp, L., Schaub, A., and Wahner, A. (Sept. 2006). “Product study of the reaction of OH radicals with isoprene in the atmosphere simulation chamber SAPHIR”. In: *Journal of Atmospheric Chemistry* vol. 55 (2), pp. 167–187. ISSN: 0167-7764. DOI: [10.1007/s10874-006-9034-x](https://doi.org/10.1007/s10874-006-9034-x).
- Kasstele, J. van de and Velders, G. J. (May 2006). “Uncertainty assessment of local NO₂ concentrations derived from error-in-variable external drift kriging and its relationship to the 2010 air quality standard”. In: *Atmospheric Environment* vol. 40 (14). ISSN: 13522310. DOI: [10.1016/j.atmosenv.2005.12.023](https://doi.org/10.1016/j.atmosenv.2005.12.023).
- Kavassalis, S. C. and Murphy, J. G. (2017). “Understanding ozone-meteorology correlations: A role for dry deposition”. In: *Geophysical Research Letters*

- vol. 44, no. 6, pp. 2922–2931. DOI: <https://doi.org/10.1002/2016GL071791>. eprint: <https://agupubs.onlinelibrary.wiley.com/doi/pdf/10.1002/2016GL071791>. URL: <https://agupubs.onlinelibrary.wiley.com/doi/abs/10.1002/2016GL071791>.
- Kimbrough, S., Owen, R. C., Snyder, M., and Richmond-Bryant, J. (2017). “NO to NO₂ conversion rate analysis and implications for dispersion model chemistry methods using Las Vegas, Nevada near-road field measurements”. In: *Atmospheric Environment* vol. 165, pp. 23–34. ISSN: 18732844. DOI: [10.1016/j.atmosenv.2017.06.027](https://doi.org/10.1016/j.atmosenv.2017.06.027).
- Kleinman, L. I. (1994). “Low and high NO_x tropospheric photochemistry”. In: *Journal of Geophysical Research: Atmospheres* vol. 99, no. D8, pp. 16831–16838. DOI: <https://doi.org/10.1029/94JD01028>. eprint: <https://agupubs.onlinelibrary.wiley.com/doi/pdf/10.1029/94JD01028>. URL: <https://agupubs.onlinelibrary.wiley.com/doi/abs/10.1029/94JD01028>.
- Knote, C., Hodzic, A., Jimenez, J. L., Volkamer, R., Orlando, J. J., Baidar, S., Brioude, J., Fast, J., Gentner, D. R., Goldstein, A. H., Hayes, P. L., Knighton, W. B., Oetjen, H., Setyan, A., Stark, H., Thalman, R., Tyndall, G., Washenfelder, R., Waxman, E., and Zhang, Q. (2014). “Simulation of semi-explicit mechanisms of SOA formation from glyoxal in aerosol in a 3-D model”. In: *Atmospheric Chemistry and Physics* vol. 14, no. 12, pp. 6213–6239. DOI: [10.5194/acp-14-6213-2014](https://doi.org/10.5194/acp-14-6213-2014). URL: <https://acp.copernicus.org/articles/14/6213/2014/>.
- Köble, R. and Seufert, G. (2001). “Novel Maps for Forest Tree Species in Europe”. In: *Proceedings of the 8th European Symposium on the Physico-Chemical Behaviour of Air Pollutants: "A changing Atmosphere!"*, pp. 1–6.
- Koo, B., Jung, J., Pollack, A. K., Lindhjem, C., Jimenez, M., and Yarwood, G. (2012). “Impact of meteorology and anthropogenic emissions on the local and regional ozone weekend effect in Midwestern US”. In: *Atmospheric Environment* vol. 57, pp. 13–21. ISSN: 1352-2310. DOI: <https://doi.org/10.1016/j.atmosenv.2012.04.043>. URL: <https://www.sciencedirect.com/science/article/pii/S1352231012003731>.
- Koo, B., Wilson, G. M., Morris, R. E., Dunker, A. M., and Yarwood, G. (Sept. 2009). “Comparison of Source Apportionment and Sensitivity Analysis in a Particulate Matter Air Quality Model”. In: *Environmental Science & Technology* vol. 43 (17), pp. 6669–6675. ISSN: 0013-936X. DOI: [10.1021/es9008129](https://doi.org/10.1021/es9008129). URL: <https://pubs.acs.org/doi/10.1021/es9008129>.
- Kranenburg, R., Segers, A. J., Hendriks, C., and Schaap, M. (June 2013). “Source apportionment using LOTOS-EUROS: module description and evaluation”. In: *Geoscientific Model Development* vol. 6 (3), pp. 721–733. ISSN: 1991-9603. DOI: [10.5194/gmd-6-721-2013](https://doi.org/10.5194/gmd-6-721-2013).
- Kranenburg, R., Schaap, M., Huibregtse, E., Hendriks, C., and Segers, A. (2014). “Source Apportionment in the LOTOS-EUROS Air Quality Model”. In: *Air Pollution Modeling and its Application XXII*. Ed. by Steyn, D. G., Builtjes, P. J., and Timmermans, R. M. Dordrecht: Springer Netherlands, pp. 387–390. ISBN: 978-94-007-5577-2.

-
- Krotkov, N. A., McLinden, C. A., Li, C., Lamsal, L. N., Celarier, E. A., Marchenko, S. V., Swartz, W. H., Bucsela, E. J., Joiner, J., Duncan, B. N., Boersma, K. F., Veefkind, J. P., Levelt, P. F., Fioletov, V. E., Dickerson, R. R., He, H., Lu, Z., and Streets, D. G. (2016). “Aura OMI observations of regional SO₂ and NO₂ pollution changes from 2005 to 2015”. In: *Atmospheric Chemistry and Physics* vol. 16, no. 7, pp. 4605–4629. DOI: 10.5194/acp-16-4605-2016. URL: <https://acp.copernicus.org/articles/16/4605/2016/>.
- Krug, A., Fenner, D., Mücke, H.-G., and Scherer, D. (2020). “The contribution of air temperature and ozone to mortality rates during hot weather episodes in eight German cities during the years 2000 and 2017”. In: *Natural Hazards and Earth System Sciences* vol. 20, no. 11, pp. 3083–3097. DOI: 10.5194/nhess-20-3083-2020. URL: <https://nhess.copernicus.org/articles/20/3083/2020/>.
- Krug, A., Fenner, D., Holtmann, A., and Scherer, D. (2019). “Occurrence and Coupling of Heat and Ozone Events and Their Relation to Mortality Rates in Berlin, Germany, between 2000 and 2014”. In: *Atmosphere* vol. 10, no. 6. ISSN: 2073-4433. DOI: 10.3390/atmos10060348. URL: <https://www.mdpi.com/2073-4433/10/6/348>.
- Kruit, R. J. W., Schaap, M., Sauter, F. J., Zanten, M. C. van, and Pul, W. A. J. van (2012). “Modeling the distribution of ammonia across Europe including bi-directional surface–atmosphere exchange”. In: *Biogeosciences* vol. 9 (12), pp. 5261–5277. DOI: 10.5194/bg-9-5261-2012. URL: <https://www.biogeosciences.net/9/5261/2012/>.
- Kuenen, J., Dellaert, S., Visschedijk, A., Jalkanen, J.-P., Super, I., and Denier van der Gon, H. (2022). “CAMS-REG-v4: a state-of-the-art high-resolution European emission inventory for air quality modelling”. In: *Earth System Science Data* vol. 14, no. 2, pp. 491–515. DOI: 10.5194/essd-14-491-2022. URL: <https://essd.copernicus.org/articles/14/491/2022/>.
- Kuenen, J., Visschedijk, A., Jozwicka, M., and Denier van der Gon, H. (2014). “TNO-MACC_II emission inventory; a multi-year (2003–2009) consistent high-resolution European emission inventory for air quality modelling”. In: *Atmospheric Chemistry and Physics* vol. 14, no. 20, pp. 10963–10976. DOI: 10.5194/acp-14-10963-2014. URL: <https://acp.copernicus.org/articles/14/10963/2014/>.
- Kuik, F., Lauer, A., Churkina, G., Denier van der Gon, H. A. C., Fenner, D., Mar, K. A., and Butler, T. M. (2016). “Air quality modelling in the Berlin–Brandenburg region using WRF-Chem v3.7.1: sensitivity to resolution of model grid and input data”. In: *Geoscientific Model Development* vol. 9, no. 12, pp. 4339–4363. DOI: 10.5194/gmd-9-4339-2016. URL: <https://gmd.copernicus.org/articles/9/4339/2016/>.
- Kuik, F., Kerschbaumer, A., Lauer, A., Lupascu, A., Schneidemesser, E. V., and Butler, T. M. (2018). “Top-down quantification of NO_x emissions from traffic in an urban area using a high-resolution regional atmospheric chemistry model”. In: *Atmospheric Chemistry and Physics* vol. 18 (11). ISSN: 16807324. DOI: 10.5194/acp-18-8203-2018.
- Kukkonen, J., Olsson, T., Schultz, D. M., Baklanov, A., Klein, T., Miranda, A. I., Monteiro, A., Hirtl, M., Tarvainen, V., Boy, M., Peuch, V.-H., Poupkou, A.,

- Kioutsioukis, I., Finardi, S., Sofiev, M., Sokhi, R., Lehtinen, K. E. J., Karatzas, K., José, R. S., Astitha, M., Kallos, G., Schaap, M., Reimer, E., Jakobs, H., and Eben, K. (Jan. 2012). “A review of operational, regional-scale, chemical weather forecasting models in Europe”. In: *Atmospheric Chemistry and Physics* vol. 12 (1), pp. 1–87. ISSN: 1680-7324. DOI: [10.5194/acp-12-1-2012](https://doi.org/10.5194/acp-12-1-2012).
- Kupiainen, K., Stojiljkovic, A., Paunu, V.-V., Karvosenoja, N., Karppinen, A., Kukkonen, J., Kangas, L., Kauhaniemi, M., Denby, B., and Hänninen, O. (2020). “Characteristics and Mitigation of Vehicular Non-exhaust Particle Emissions in Nordic Conditions”. In: *Air Pollution Modeling and its Application XXVI*. Ed. by Mensink, C., Gong, W., and Hakami, A. Cham: Springer International Publishing, pp. 211–216. ISBN: 978-3-030-22055-6.
- Kwok, R. H. F., Baker, K. R., Napelenok, S. L., and Tonnesen, G. S. (Jan. 2015). “Photochemical grid model implementation and application of VOC, NO_x, and O₃ source apportionment”. In: *Geoscientific Model Development* vol. 8 (1), pp. 99–114. ISSN: 1991-9603. DOI: [10.5194/gmd-8-99-2015](https://doi.org/10.5194/gmd-8-99-2015). URL: <https://gmd.copernicus.org/articles/8/99/2015/>.
- Lamarque, J.-F., Shindell, D. T., Josse, B., Young, P. J., Cionni, I., Eyring, V., Bergmann, D., Cameron-Smith, P., Collins, W. J., Doherty, R., Dalsoren, S., Faluvegi, G., Folberth, G., Ghan, S. J., Horowitz, L. W., Lee, Y. H., MacKenzie, I. A., Nagashima, T., Naik, V., Plummer, D., Righi, M., Rumbold, S. T., Schulz, M., Skeie, R. B., Stevenson, D. S., Strode, S., Sudo, K., Szopa, S., Voulgarakis, A., and Zeng, G. (2013). “The Atmospheric Chemistry and Climate Model Intercomparison Project (ACCMIP): overview and description of models, simulations and climate diagnostics”. In: *Geoscientific Model Development* vol. 6, no. 1, pp. 179–206. DOI: [10.5194/gmd-6-179-2013](https://doi.org/10.5194/gmd-6-179-2013). URL: <https://gmd.copernicus.org/articles/6/179/2013/>.
- Lecœur, È. and Seigneur, C. (2013). “Dynamic evaluation of a multi-year model simulation of particulate matter concentrations over Europe”. In: *Atmospheric Chemistry and Physics* vol. 13, no. 8, pp. 4319–4337. DOI: [10.5194/acp-13-4319-2013](https://doi.org/10.5194/acp-13-4319-2013). URL: <https://acp.copernicus.org/articles/13/4319/2013/>.
- Leighton, P. (1961). *Photochemistry of air pollution*. 1st Edition. Academic Press, p. 312. ISBN: 9780323156455. URL: <https://www.elsevier.com/books/photochemistry-of-air-pollution/leighton/978-0-12-442250-6>.
- Lenschow, P., Abraham, H. J., Kutzner, K., Lutz, M., Preuß, J. D., and Reichenbacher, W. (2001). “Some ideas about the sources of PM₁₀”. In: *Atmospheric Environment* vol. 35 (SUPPL. 1). ISSN: 13522310. DOI: [10.1016/S1352-2310\(01\)00122-4](https://doi.org/10.1016/S1352-2310(01)00122-4).
- Lepeule, J., Litonjua, A. A., Coull, B., Koutrakis, P., Sparrow, D., Vokonas, P. S., and Schwartz, J. (Sept. 2014). “Long-Term Effects of Traffic Particles on Lung Function Decline in the Elderly”. In: *American Journal of Respiratory and Critical Care Medicine* vol. 190 (5), pp. 542–548. ISSN: 1073-449X. DOI: [10.1164/rccm.201402-0350OC](https://doi.org/10.1164/rccm.201402-0350OC).
- LFU (2018). *Luftqualität in Brandenburg Jahresbericht 2018*. Landesamt für Umwelt (LfU), p. 52. URL: https://lfu.brandenburg.de/cms/media.php/lbm1.a.3310.de/Luftqualitaet_BB_2018.pdf.

-
- Li, G., Bei, N., Zavala, M., and Molina, L. T. (2014). “Ozone formation along the California–Mexican border region during Cal–Mex 2010 field campaign”. In: *Atmospheric Environment* vol. 88, pp. 370–389. ISSN: 1352-2310. DOI: <https://doi.org/10.1016/j.atmosenv.2013.11.067>. URL: <https://www.sciencedirect.com/science/article/pii/S1352231013009175>.
- Lim, S. S. et al. (2012). “A comparative risk assessment of burden of disease and injury attributable to 67 risk factors and risk factor clusters in 21 regions, 1990-2010: A systematic analysis for the Global Burden of Disease Study 2010”. In: *The Lancet* vol. 380 (9859), pp. 2224–2260. ISSN: 1474547X. DOI: [10.1016/S0140-6736\(12\)61766-8](https://doi.org/10.1016/S0140-6736(12)61766-8).
- Lin, M., Horowitz, L. W., Xie, Y., Paulot, F., Malyshev, S., Shevliakova, E., Finco, A., Gerosa, G., Kubistin, D., and Pilegaard, K. (May 2020). “Vegetation feedbacks during drought exacerbate ozone air pollution extremes in Europe”. In: *Nature Climate Change* vol. 10 (5). ISSN: 1758-678X. DOI: [10.1038/s41558-020-0743-y](https://doi.org/10.1038/s41558-020-0743-y).
- Linquist, B. A., Adviento-Borbe, M. A., Pittelkow, C. M., Kessel, C. van, and Groenigen, K. J. van (Aug. 2012). “Fertilizer management practices and greenhouse gas emissions from rice systems: A quantitative review and analysis”. In: *Field Crops Research* vol. 135, pp. 10–21. ISSN: 03784290. DOI: [10.1016/j.fcr.2012.06.007](https://doi.org/10.1016/j.fcr.2012.06.007).
- Lobo, J., Strumsky, D., and Bettencourt, L. (2009). “Metropolitan areas and CO₂ emissions: large is beautiful”. In: *Martin Prosperity Institute, University of Toronto*.
- Long, M. S., Keene, W. C., Kieber, D. J., Erickson, D. J., and Maring, H. (2011). “A sea-state based source function for size- and composition-resolved marine aerosol production”. In: *Atmospheric Chemistry and Physics* vol. 11, no. 3, pp. 1203–1216. DOI: [10.5194/acp-11-1203-2011](https://doi.org/10.5194/acp-11-1203-2011). URL: <https://acp.copernicus.org/articles/11/1203/2011/>.
- López-Aizpún, M., Horrocks, C. A., Charteris, A. F., Marsden, K. A., Ciganda, V. S., Evans, J. R., Chadwick, D. R., and Cárdenas, L. M. (Apr. 2020). “Meta-analysis of global livestock urine-derived nitrous oxide emissions from agricultural soils”. In: *Global Change Biology* vol. 26 (4), pp. 2002–2013. ISSN: 1354-1013. DOI: [10.1111/gcb.15012](https://doi.org/10.1111/gcb.15012).
- Louis, J.-F. (Sept. 1979). “A parametric model of vertical eddy fluxes in the atmosphere”. In: *Boundary-Layer Meteorology* vol. 17 (2), pp. 187–202. ISSN: 1573-1472. DOI: [10.1007/BF00117978](https://doi.org/10.1007/BF00117978). URL: <https://doi.org/10.1007/BF00117978>.
- Luo, H., Yang, L., Yuan, Z., Zhao, K., Zhang, S., Duan, Y., Huang, R., and Fu, Q. (2020). “Synoptic condition-driven summertime ozone formation regime in Shanghai and the implication for dynamic ozone control strategies”. In: *Science of The Total Environment* vol. 745, p. 141130. ISSN: 0048-9697. DOI: <https://doi.org/10.1016/j.scitotenv.2020.141130>. URL: <https://www.sciencedirect.com/science/article/pii/S0048969720346593>.
- Lupaşcu, A., Otero, N., Minkos, A., and Butler, T. (2022). “Attribution of surface ozone to NO_x and volatile organic compound sources during two different high ozone events”. In: *Atmospheric Chemistry and Physics* vol. 22,

- no. 17, pp. 11675–11699. DOI: [10.5194/acp-22-11675-2022](https://doi.org/10.5194/acp-22-11675-2022). URL: <https://acp.copernicus.org/articles/22/11675/2022/>.
- Lupaşcu, A. and Butler, T. (Dec. 2019). “Source attribution of European surface O₃ using a tagged O₃ mechanism”. In: *Atmospheric Chemistry and Physics* vol. 19 (23), pp. 14535–14558. ISSN: 16807324. DOI: [10.5194/acp-19-14535-2019](https://doi.org/10.5194/acp-19-14535-2019).
- Luttkus, M. L., Hoffmann, E. H., Poulain, L., Tilgner, A., and Wolke, R. (2022). “The Effect of Land Use Classification on the Gas-Phase and Particle Composition of the Troposphere: Tree Species Versus Forest Type Information”. In: *Journal of Geophysical Research: Atmospheres* vol. 127, no. 7. e2021JD035305 2021JD035305, e2021JD035305. DOI: <https://doi.org/10.1029/2021JD035305>. eprint: <https://agupubs.onlinelibrary.wiley.com/doi/pdf/10.1029/2021JD035305>. URL: <https://agupubs.onlinelibrary.wiley.com/doi/abs/10.1029/2021JD035305>.
- Maffia, J., Dinuccio, E., Amon, B., and Balsari, P. (2020). “PM emissions from open field crop management: Emission factors, assessment methods and mitigation measures – A review”. In: *Atmospheric Environment* vol. 226, p. 117381. ISSN: 1352-2310. DOI: <https://doi.org/10.1016/j.atmosenv.2020.117381>. URL: <https://www.sciencedirect.com/science/article/pii/S1352231020301205>.
- Mailler, S., Menut, L., Khvorostyanov, D., Valari, M., Couvidat, F., Siour, G., Turquety, S., Briant, R., Tuccella, P., Bessagnet, B., Colette, A., Létinois, L., Markakis, K., and Meleux, F. (June 2017). “CHIMERE-2017: from urban to hemispheric chemistry-transport modeling”. In: *Geoscientific Model Development* vol. 10 (6), pp. 2397–2423. ISSN: 1991-9603. DOI: [10.5194/gmd-10-2397-2017](https://doi.org/10.5194/gmd-10-2397-2017).
- Manders, A. M. M., Builtjes, P. J. H., Curier, L., Gon, H. A. C. van der, Hendriks, C., Jonkers, S., Kranenburg, R., Kuenen, J. J. P., Segers, A. J., Timmermans, R. M. A., Visschedijk, A. J. H., Kruit, R. J. W., Pul, W. A. J. van, Sauter, F. J., Swaluw, E. van der, Swart, D. P. J., Douros, J., Eskes, H., Meijgaard, E. van, Ulft, B. van, Velthoven, P. van, Banzhaf, S., Mues, A. C., Stern, R., Fu, G., Lu, S., Heemink, A., Velzen, N. van, and Schaap, M. (2017). “Curriculum vitae of the LOTOS–EUROS (v2.0) chemistry transport model”. In: *Geoscientific Model Development* vol. 10 (11), pp. 4145–4173. DOI: [10.5194/gmd-10-4145-2017](https://doi.org/10.5194/gmd-10-4145-2017). URL: <https://www.geosci-model-dev.net/10/4145/2017/>.
- Mar, K., Ojha, N., Pozzer, A., and Butler, T. (Oct. 2016). “Ozone air quality simulations with WRF-Chem (v3.5.1) over Europe: Model evaluation and chemical mechanism comparison”. In: *Geoscientific Model Development* vol. 9, pp. 3699–. DOI: [10.5194/gmd-9-3699-2016](https://doi.org/10.5194/gmd-9-3699-2016).
- Marécal, V. et al. (2015). “A regional air quality forecasting system over Europe: the MACC-II daily ensemble production”. In: *Geoscientific Model Development* vol. 8 (9), pp. 2777–2813. DOI: [10.5194/gmd-8-2777-2015](https://doi.org/10.5194/gmd-8-2777-2015). URL: <https://www.geosci-model-dev.net/8/2777/2015/>.
- Maronga, B., Gross, G., Raasch, S., Banzhaf, S., Forkel, R., Heldens, W., Kanani-Sühring, F., Matzarakis, A., Mauder, M., Pavlik, D., Pfafferott,

-
- J., Schubert, S., Seckmeyer, G., Sieker, H., and Winderlich, K. (June 2019). “Development of a new urban climate model based on the model PALM - Project overview, planned work, and first achievements”. In: *Meteorologische Zeitschrift* vol. 28, no. 2, pp. 105–119. DOI: [10.1127/metz/2019/0909](https://doi.org/10.1127/metz/2019/0909). URL: <http://dx.doi.org/10.1127/metz/2019/0909>.
- Mårtensson, E. M., Nilsson, E. D., Leeuw, G. de, Cohen, L. H., and Hansson, H.-C. (2003). “Laboratory simulations and parameterization of the primary marine aerosol production”. In: *Journal of Geophysical Research: Atmospheres* vol. 108, no. D9. DOI: <https://doi.org/10.1029/2002JD002263>. eprint: <https://agupubs.onlinelibrary.wiley.com/doi/pdf/10.1029/2002JD002263>. URL: <https://agupubs.onlinelibrary.wiley.com/doi/abs/10.1029/2002JD002263>.
- Masiol, M. and Harrison, R. M. (Oct. 2014). “Aircraft engine exhaust emissions and other airport-related contributions to ambient air pollution: A review”. In: *Atmospheric Environment* vol. 95, pp. 409–455. ISSN: 13522310. DOI: [10.1016/j.atmosenv.2014.05.070](https://doi.org/10.1016/j.atmosenv.2014.05.070).
- Matzer, C., Hausberger, S., Lipp, S., and Rexeis, M. (2017). “A new approach for systematic use of PEMS data in emission simulation”. In: *Journal of Earth Sciences and Geotechnical Engineering* vol. 7, no. 1, pp. 33–50.
- Mayer, H., Holst, J., Schindler, D., and Ahrens, D. (June 2008). “Evolution of the air pollution in SW Germany evaluated by the long-term air quality index LAQx”. In: *Atmospheric Environment* vol. 42 (20), pp. 5071–5078. ISSN: 13522310. DOI: [10.1016/j.atmosenv.2008.02.020](https://doi.org/10.1016/j.atmosenv.2008.02.020).
- Meissner, C. S., Panitz, H.-J. F., and Kottmeier, C. (Mar. 2009). “High-resolution sensitivity studies with the regional climate model COSMO-CLM”. In: *Meteorologische Zeitschrift* vol. 18 (5), pp. 543–557. DOI: [10.1127/0941-2948/2009/0400](https://doi.org/10.1127/0941-2948/2009/0400). URL: <http://dx.doi.org/10.1127/0941-2948/2009/0400>.
- Mellor, G. L. and Yamada, T. (1974). “A Hierarchy of Turbulence Closure Models for Planetary Boundary Layers”. In: *Journal of the Atmospheric Sciences* vol. 31 (7), pp. 1791–1806. DOI: [10.1175/1520-0469\(1974\)031<1791:AHOTCM>2.0.CO;2](https://doi.org/10.1175/1520-0469(1974)031<1791:AHOTCM>2.0.CO;2). URL: [https://doi.org/10.1175/1520-0469\(1974\)031%3C1791:AHOTCM%3E2.0.CO;2](https://doi.org/10.1175/1520-0469(1974)031%3C1791:AHOTCM%3E2.0.CO;2).
- Mertens, M., Grewe, V., Rieger, V. S., and Jöckel, P. (Apr. 2018). “Revisiting the contribution of land transport and shipping emissions to tropospheric ozone”. In: *Atmospheric Chemistry and Physics* vol. 18 (8), pp. 5567–5588. ISSN: 16807324. DOI: [10.5194/acp-18-5567-2018](https://doi.org/10.5194/acp-18-5567-2018).
- Monahan, E. C. (1986). “The Ocean as a Source for Atmospheric Particles”. In: *The Role of Air-Sea Exchange in Geochemical Cycling*. Ed. by Buat-Ménard, P. Dordrecht: Springer Netherlands, pp. 129–163. ISBN: 978-94-009-4738-2. DOI: [10.1007/978-94-009-4738-2_6](https://doi.org/10.1007/978-94-009-4738-2_6). URL: https://doi.org/10.1007/978-94-009-4738-2_6.
- Monks, P. S., Archibald, A. T., Colette, A., Cooper, O., Coyle, M., Derwent, R., Fowler, D., Granier, C., Law, K. S., Mills, G. E., Stevenson, D. S., Tarasova, O., Thouret, V., Schneidemesser, E. von, Sommariva, R., Wild, O., and Williams, M. L. (2015). “Tropospheric ozone and its precursors from the urban to the global scale from air quality to short-lived climate forcer”. In: *Atmospheric*

- Chemistry and Physics* vol. 15, no. 15, pp. 8889–8973. DOI: 10.5194/acp-15-8889-2015. URL: <https://acp.copernicus.org/articles/15/8889/2015/>.
- Monteiro, A., Durka, P., Flandorfer, C., Georgieva, E., Guerreiro, C., Kushta, J., Malherbe, L., Maiheu, B., Miranda, A. I., Santos, G., Stocker, J., Trimpeneers, E., Tognet, F., Stortini, M., Wesseling, J., Janssen, S., and Thunis, P. (May 2018). “Strengths and weaknesses of the FAIRMODE benchmarking methodology for the evaluation of air quality models”. In: *Air Quality, Atmosphere & Health* vol. 11 (4), pp. 373–383. ISSN: 1873-9318. DOI: 10.1007/s11869-018-0554-8.
- Morgenstern, O. et al. (2017). “Review of the global models used within phase 1 of the Chemistry–Climate Model Initiative (CCMI)”. In: *Geoscientific Model Development* vol. 10, no. 2, pp. 639–671. DOI: 10.5194/gmd-10-639-2017. URL: <https://gmd.copernicus.org/articles/10/639/2017/>.
- Morrison, H. and Gettelman, A. (2008). “A New Two-Moment Bulk Stratiform Cloud Microphysics Scheme in the Community Atmosphere Model, Version 3 (CAM3). Part I: Description and Numerical Tests”. In: *Journal of Climate* vol. 21, no. 15, pp. 3642–3659. DOI: <https://doi.org/10.1175/2008JCLI2105.1>. URL: <https://journals.ametsoc.org/view/journals/clim/21/15/2008jcli2105.1.xml>.
- Mues, A., Manders, A., Schaap, M., Kerschbaumer, A., Stern, R., and Builtjes, P. (2012). “Impact of the extreme meteorological conditions during the summer 2003 in Europe on particulate matter concentrations”. In: *Atmospheric Environment* vol. 55, pp. 377–391. ISSN: 13522310. DOI: 10.1016/j.atmosenv.2012.03.002. URL: <http://www.sciencedirect.com/science/article/pii/S1352231012002348>.
- Mues, A., Kuenen, J., Hendriks, C., Manders, A., Segers, A., Scholz, Y., Hueglin, C., Builtjes, P., and Schaap, M. (Jan. 2014). “Sensitivity of air pollution simulations with LOTOS-EUROS to the temporal distribution of anthropogenic emissions”. In: *Atmospheric Chemistry and Physics* vol. 14 (2), pp. 939–955. ISSN: 16807316. DOI: 10.5194/acp-14-939-2014.
- Muller, E. (1981). “Turbulent flux parameterization in a regional-scale model”. In: ECMWF, pp. 193–220. URL: <https://www.ecmwf.int/node/11313>.
- Munir, S. (Jan. 2016). “Modelling the non-linear association of particulate matter (PM10) with meteorological parameters and other air pollutants—a case study in Makkah”. In: *Arabian Journal of Geosciences* vol. 9 (1), p. 64. ISSN: 1866-7511. DOI: 10.1007/s12517-015-2207-7. URL: <http://link.springer.com/10.1007/s12517-015-2207-7>.
- Napelenok, S. L., Cohan, D. S., Hu, Y., and Russell, A. G. (2006). “Decoupled direct 3D sensitivity analysis for particulate matter (DDM-3D/PM)”. In: *Atmospheric Environment* vol. 40, no. 32, pp. 6112–6121. ISSN: 1352-2310. DOI: <https://doi.org/10.1016/j.atmosenv.2006.05.039>. URL: <https://www.sciencedirect.com/science/article/pii/S1352231006005012>.
- Neu, J. L. and Prather, M. J. (2012). “Toward a more physical representation of precipitation scavenging in global chemistry models: cloud overlap and ice physics and their impact on tropospheric ozone”. In: *Atmospheric Chemistry and Physics* vol. 12, no. 7, pp. 3289–3310. ISSN: 1680-7316. DOI: doi:10.5194/

-
- acp-12-3289-2012. URL: <https://www.ingentaconnect.com/content/doi/16807316/2012/00000012/00000007/art00013>.
- Newby, D. E., Mannucci, P. M., Tell, G. S., Baccarelli, A. A., Brook, R. D., Donaldson, K., Forastiere, F., Franchini, M., Franco, O. H., Graham, I., Hoek, G., Hoffmann, B., Hoylaerts, M. F., Künzli, N., Mills, N., Pekkanen, J., Peters, A., Piepoli, M. F., Rajagopalan, S., and Storey, R. F. (Jan. 2015). “Expert position paper on air pollution and cardiovascular disease”. In: *European Heart Journal* vol. 36 (2), pp. 83–93. ISSN: 1522-9645. DOI: 10.1093/eurheartj/ehu458.
- Novak, J. H. and Pierce, T. E. (1993). “Natural emissions of oxidant precursors”. In: *Water, Air, & Soil Pollution* vol. 67 (1-2), pp. 57–77. ISSN: 0049-6979. DOI: 10.1007/BF00480814.
- O’Dowd, C. D., Smith, M. H., Consterdine, I. E., and Lowe, J. A. (1997). “Marine aerosol, sea-salt, and the marine sulphur cycle: a short review”. In: *Atmospheric Environment* vol. 31, no. 1, pp. 73–80. ISSN: 1352-2310. DOI: [https://doi.org/10.1016/S1352-2310\(96\)00106-9](https://doi.org/10.1016/S1352-2310(96)00106-9). URL: <https://www.sciencedirect.com/science/article/pii/S1352231096001069>.
- Oltmans, S. J. and Levy, H. (1994). “Surface ozone measurements from a global network”. In: *Atmospheric Environment* vol. 28, no. 1, pp. 9–24. ISSN: 1352-2310. DOI: [https://doi.org/10.1016/1352-2310\(94\)90019-1](https://doi.org/10.1016/1352-2310(94)90019-1). URL: <https://www.sciencedirect.com/science/article/pii/S1352231094900191>.
- Omstedt, G., Bringfelt, B., and Johansson, C. (2005). “A model for vehicle-induced non-tailpipe emissions of particles along Swedish roads”. In: *Atmospheric Environment* vol. 39, no. 33, pp. 6088–6097. ISSN: 1352-2310. DOI: <https://doi.org/10.1016/j.atmosenv.2005.06.037>. URL: <https://www.sciencedirect.com/science/article/pii/S1352231005005558>.
- Otero, N., Sillmann, J., Schnell, J. L., Rust, H. W., and Butler, T. (Feb. 2016). “Synoptic and meteorological drivers of extreme ozone concentrations over Europe”. In: *Environmental Research Letters* vol. 11, no. 2, p. 024005. DOI: 10.1088/1748-9326/11/2/024005. URL: <https://dx.doi.org/10.1088/1748-9326/11/2/024005>.
- Otero, N., Sillmann, J., Mar, K. A., Rust, H. W., Solberg, S., Andersson, C., Engardt, M., Bergström, R., Bessagnet, B., Colette, A., Couvidat, F., Cuvelier, C., Tsyro, S., Fagerli, H., Schaap, M., Manders, A., Mircea, M., Briganti, G., Cappelletti, A., Adani, M., D’Isidoro, M., Pay, M.-T., Theobald, M., Vivanco, M. G., Wind, P., Ojha, N., Raffort, V., and Butler, T. (2018). “A multi-model comparison of meteorological drivers of surface ozone over Europe”. In: *Atmospheric Chemistry and Physics* vol. 18, no. 16, pp. 12269–12288. DOI: 10.5194/acp-18-12269-2018. URL: <https://acp.copernicus.org/articles/18/12269/2018/>.
- Otero, N., Rust, H. W., and Butler, T. (2021). “Temperature dependence of tropospheric ozone under NO_x reductions over Germany”. In: *Atmospheric Environment* vol. 253, p. 118334. ISSN: 1352-2310. DOI: <https://doi.org/10.1016/j.atmosenv.2021.118334>. URL: <https://www.sciencedirect.com/science/article/pii/S1352231021001527>.

References

- Padoan, E. and Amato, F. (2018). “Chapter 2 - Vehicle Non-Exhaust Emissions: Impact on Air Quality”. In: *Non-Exhaust Emissions*. Ed. by Amato, F. Academic Press, pp. 21–65. ISBN: 978-0-12-811770-5. DOI: <https://doi.org/10.1016/B978-0-12-811770-5.00002-9>. URL: <https://www.sciencedirect.com/science/article/pii/B9780128117705000029>.
- Pandolfi, M., Mooibroek, D., Hopke, P., Pinxteren, D. van, Querol, X., Herrmann, H., Alastuey, A., Favez, O., Hüglin, C., Perdrix, E., Riffault, V., Sauvage, S., Swaluw, E. van der, Tarasova, O., and Colette, A. (2020). “Long-range and local air pollution: what can we learn from chemical speciation of particulate matter at paired sites?” In: *Atmospheric Chemistry and Physics* vol. 20, no. 1, pp. 409–429. DOI: [10.5194/acp-20-409-2020](https://doi.org/10.5194/acp-20-409-2020). URL: <https://acp.copernicus.org/articles/20/409/2020/>.
- Panteliadis, P., Strak, M., Hoek, G., Weijers, E., Zee, S. van der, and Dijkema, M. (Apr. 2014). “Implementation of a low emission zone and evaluation of effects on air quality by long-term monitoring”. In: *Atmospheric Environment* vol. 86, pp. 113–119. ISSN: 13522310. DOI: [10.1016/j.atmosenv.2013.12.035](https://doi.org/10.1016/j.atmosenv.2013.12.035).
- Parrish, D. D., Petropavlovskikh, I., and Oltmans, S. J. (2017). “Reversal of Long-Term Trend in Baseline Ozone Concentrations at the North American West Coast”. In: *Geophysical Research Letters* vol. 44, no. 20, pp. 10, 675–10, 681. DOI: <https://doi.org/10.1002/2017GL074960>. eprint: <https://agupubs.onlinelibrary.wiley.com/doi/pdf/10.1002/2017GL074960>. URL: <https://agupubs.onlinelibrary.wiley.com/doi/abs/10.1002/2017GL074960>.
- Pay, M. T., Gangoiti, G., Guevara, M., Napelenok, S., Querol, X., Jorba, O., and Pérez García-Pando, C. (2019). “Ozone source apportionment during peak summer events over southwestern Europe”. In: *Atmospheric Chemistry and Physics* vol. 19, no. 8, pp. 5467–5494. DOI: [10.5194/acp-19-5467-2019](https://doi.org/10.5194/acp-19-5467-2019). URL: <https://acp.copernicus.org/articles/19/5467/2019/>.
- Pay, M. T., Jiménez-Guerrero, P., and Baldasano, J. M. (2011). “Implementation of resuspension from paved roads for the improvement of CALIOPE air quality system in Spain”. In: *Atmospheric Environment* vol. 45, no. 3, pp. 802–807. ISSN: 1352-2310. DOI: <https://doi.org/10.1016/j.atmosenv.2010.10.032>. URL: <https://www.sciencedirect.com/science/article/pii/S1352231010009076>.
- Per, N., Lund, H. L., Torbjørn, W., Frederick, G., Bente, O., Ingar, H., Ingvar, H., and Paul, L. (Apr. 2004). “Urban air pollution and mortality in a cohort of Norwegian men.” In: *Environmental Health Perspectives* vol. 112 (5). doi: [10.1289/ehp.6684](https://doi.org/10.1289/ehp.6684), pp. 610–615. DOI: [10.1289/ehp.6684](https://doi.org/10.1289/ehp.6684). URL: <https://doi.org/10.1289/ehp.6684>.
- Philip, S., Martin, R. V., Donkelaar, A. van, Lo, J. W.-H., Wang, Y., Chen, D., Zhang, L., Kasibhatla, P. S., Wang, S., Zhang, Q., Lu, Z., Streets, D. G., Bittman, S., and Macdonald, D. J. (2014). “Global Chemical Composition of Ambient Fine Particulate Matter for Exposure Assessment”. In: *Environmental Science & Technology* vol. 48, no. 22. PMID: 25343705, pp. 13060–13068. DOI: [10.1021/es502965b](https://doi.org/10.1021/es502965b). eprint: <https://doi.org/10.1021/es502965b>. URL: <https://doi.org/10.1021/es502965b>.
- Pierce, T., Hogrefe, C., Rao, S. T., Porter, P. S., and Ku, J. Y. (Sept. 2010). “Dynamic evaluation of a regional air quality model: Assessing the emissions-

-
- induced weekly ozone cycle”. In: *Atmospheric Environment* vol. 44 (29), pp. 3583–3596. ISSN: 13522310. DOI: [10.1016/j.atmosenv.2010.05.046](https://doi.org/10.1016/j.atmosenv.2010.05.046).
- Pommier, M., Fagerli, H., Schulz, M., Valdebenito, A., Kranenburg, R., and Schaap, M. (2020). “Prediction of source contributions to urban background PM10 concentrations in European cities: A case study for an episode in December 2016 using EMEP/MSC-W rv4.15 and LOTOS-EUROS v2.0 - Part 1: The country contributions”. In: *Geoscientific Model Development* vol. 13 (4). ISSN: 19919603. DOI: [10.5194/gmd-13-1787-2020](https://doi.org/10.5194/gmd-13-1787-2020).
- Pope, C. A. (Aug. 2000). “Epidemiology of fine particulate air pollution and human health: biologic mechanisms and who’s at risk?” In: *Environmental Health Perspectives* vol. 108 (suppl 4), pp. 713–723. ISSN: 0091-6765. DOI: [10.1289/ehp.108-1637679](https://doi.org/10.1289/ehp.108-1637679).
- Potier, E., Waked, A., Bourin, A., Minvielle, F., Péré, J. C., Perdrix, E., Michoud, V., Riffault, V., Alleman, L. Y., and Sauvage, S. (2019). “Characterizing the regional contribution to PM10 pollution over northern France using two complementary approaches: Chemistry transport and trajectory-based receptor models”. In: *Atmospheric Research* vol. 223, pp. 1–14. ISSN: 0169-8095. DOI: <https://doi.org/10.1016/j.atmosres.2019.03.002>. URL: <http://www.sciencedirect.com/science/article/pii/S0169809518312687>.
- Pujol, J., Martínez-Vilavella, G., Macià, D., Fenoll, R., Alvarez-Pedrerol, M., Rivas, I., Forns, J., Blanco-Hinojo, L., Capellades, J., Querol, X., Deus, J., and Sunyer, J. (Apr. 2016). “Traffic pollution exposure is associated with altered brain connectivity in school children”. In: *NeuroImage* vol. 129, pp. 175–184. ISSN: 10538119. DOI: [10.1016/j.neuroimage.2016.01.036](https://doi.org/10.1016/j.neuroimage.2016.01.036).
- Pulles, T. and Heslinga, D. (Sept. 2007). *The Art of Emission Inventorying*. ISBN: 9789059863415. DOI: [10.13140/RG.2.1.2082.8007](https://doi.org/10.13140/RG.2.1.2082.8007).
- Putaud, J.-P., Raes, F., Van Dingenen, R., Brüggemann, E., Facchini, M.-C., Decesari, S., Fuzzi, S., Gehrig, R., Hüglin, C., Laj, P., Lorbeer, G., Maenhaut, W., Mihalopoulos, N., Müller, K., Querol, X., Rodriguez, S., Schneider, J., Spindler, G., Brink, H. ten, Tørseth, K., and Wiedensohler, A. (2004). “A European aerosol phenomenology—2: chemical characteristics of particulate matter at kerbside, urban, rural and background sites in Europe”. In: *Atmospheric Environment* vol. 38, no. 16, pp. 2579–2595. ISSN: 1352-2310. DOI: <https://doi.org/10.1016/j.atmosenv.2004.01.041>. URL: <https://www.sciencedirect.com/science/article/pii/S1352231004000949>.
- Querol, X., Alastuey, A., Ruiz, C., Artiñano, B., Hansson, H., Harrison, R., Buringh, E., ten Brink, H., Lutz, M., Bruckmann, P., Straehl, P., and Schneider, J. (2004). “Speciation and origin of PM10 and PM2.5 in selected European cities”. In: *Atmospheric Environment* vol. 38, no. 38. Contains Special Issue section on Measuring the composition of Particulate Matter in the EU, pp. 6547–6555. ISSN: 1352-2310. DOI: <https://doi.org/10.1016/j.atmosenv.2004.08.037>. URL: <https://www.sciencedirect.com/science/article/pii/S1352231004008143>.
- Raaschou-Nielsen, O., Andersen, Z. J., Jensen, S. S., Ketzel, M., Sørensen, M., Hansen, J., Loft, S., Tjønneland, A., and Overvad, K. (2012). “Traffic air pollution and mortality from cardiovascular disease and all causes: A Danish

- cohort study”. In: *Environmental Health: A Global Access Science Source*. ISSN: 1476069X. DOI: 10.1186/1476-069X-11-60.
- Rafaj, P., Amann, M., Siri, J., and Wuester, H. (2015). “Changes in European greenhouse gas and air pollutant emissions 1960–2010: decomposition of determining factors”. In: Springer International Publishing, pp. 27–54. DOI: 10.1007/978-3-319-15901-0_3.
- Räisänen, M., Kupiainen, K., and Tervahattu, H. (2005). “The effect of mineralogy, texture and mechanical properties of anti-skid and asphalt aggregates on urban dust, stages II and III”. In: *Bulletin of Engineering Geology and the Environment* vol. 64 (3), pp. 247–256. ISSN: 1435-9537. DOI: 10.1007/s10064-004-0267-0. URL: <https://doi.org/10.1007/s10064-004-0267-0>.
- Rao, S. T., Galmarini, S., and Puckett, K. (2011). “Air Quality Model Evaluation International Initiative (AQMEII): Advancing the State of the Science in Regional Photochemical Modeling and Its Applications”. In: *Bulletin of the American Meteorological Society* vol. 92, no. 1, pp. 23–30. DOI: <https://doi.org/10.1175/2010BAMS3069.1>. URL: https://journals.ametsoc.org/view/journals/bams/92/1/2010bams3069_1.xml.
- RCoreTeam (2014). “R: A Language and Environment for Statistical Computing.” In: *R Foundation for Statistical Computing, Vienna, Austria (2014)*. URL: <http://www.r-project.org/>.
- Reidmiller, D. R., Fiore, A. M., Jaffe, D. A., Bergmann, D., Cuvelier, C., Dentener, F. J., Duncan, B. N., Folberth, G., Gauss, M., Gong, S., Hess, P., Jonson, J. E., Keating, T., Lupu, A., Marmer, E., Park, R., Schultz, M. G., Shindell, D. T., Szopa, S., Vivanco, M. G., Wild, O., and Zuber, A. (2009). “The influence of foreign vs. North American emissions on surface ozone in the US”. In: *Atmospheric Chemistry and Physics* vol. 9, no. 14, pp. 5027–5042. DOI: 10.5194/acp-9-5027-2009. URL: <https://acp.copernicus.org/articles/9/5027/2009/>.
- Reinert, D., Prill, F., Frank, H., Denhard, M., Baldauf, M., Schraff, C., Gebhardt, C., Marsigli, C., and Zängl, G. (2016a). “DWD Database Reference for the Global and Regional ICON and ICON-EPS Forecasting System - Version 2.2.2”. In: *Deutscher Wetterdienst (DWD), Research and Development*.
- (2016b). “DWD Database Reference for the Global and Regional ICON and ICON-EPS Forecasting System - Version 2.2.2”. In: *Deutscher Wetterdienst (DWD), Research and Development*.
- Rexeis, M. and Hausberger, S. (Oct. 2009). “Trend of vehicle emission levels until 2020 - Prognosis based on current vehicle measurements and future emission legislation”. In: *Atmospheric Environment* vol. 43 (31), pp. 4689–4698. ISSN: 13522310. DOI: 10.1016/j.atmosenv.2008.09.034.
- Richmond-Bryant, J., Owen, R. C., Graham, S., Snyder, M., McDow, S., Oakes, M., and Kimbrough, S. (June 2017). “Estimation of on-road NO₂ concentrations, NO₂/NO_x ratios, and related roadway gradients from near-road monitoring data”. In: *Air Quality, Atmosphere and Health* vol. 10 (5), pp. 611–625. ISSN: 18739326. DOI: 10.1007/s11869-016-0455-7.

-
- Rockel, B., Will, A., and Hense, A. (2008). “The Regional Climate Model COSMO-CLM (CCLM)”. In: *Meteorologische Zeitschrift* vol. 17 (4), pp. 347–348. DOI: [10.1127/0941-2948/2008/0309](https://doi.org/10.1127/0941-2948/2008/0309). URL: <http://dx.doi.org/10.1127/0941-2948/2008/0309>.
- S-VELD (Apr. 2022). *Schlussbericht zur Forschungsinitiative S-VELD: Verbundprojekt im Rahmen des datenbasierten FuE-Förderprogramms „Modernitätsfonds“ (mFUND, Förderlinie 2) des BMDV*.
- Sangeeta, Moka, S., Pande, M., Rani, M., Gakhar, R., Sharma, M., Rani, J., and Bhaskarwar, A. N. (Apr. 2014). “Alternative fuels: An overview of current trends and scope for future”. In: *Renewable and Sustainable Energy Reviews* vol. 32, pp. 697–712. ISSN: 13640321. DOI: [10.1016/j.rser.2014.01.023](https://doi.org/10.1016/j.rser.2014.01.023).
- Sardar, P. R. A. (2015). “SO₂ Emission Control and Finding a Way Out to Produce Sulphuric Acid from Industrial SO₂ Emission”. In: *Journal of Chemical Engineering & Process Technology* vol. 06 (02). ISSN: 21577048. DOI: [10.4172/2157-7048.1000230](https://doi.org/10.4172/2157-7048.1000230).
- Schaap, M., Loon, M. van, Brink, H. M. ten, Dentener, F. J., and Builtjes, P. J. H. (2004). “Secondary inorganic aerosol simulations for Europe with special attention to nitrate”. In: *Atmospheric Chemistry and Physics* vol. 4 (3), pp. 857–874. DOI: [10.5194/acp-4-857-2004](https://doi.org/10.5194/acp-4-857-2004). URL: <https://www.atmoschem-phys.net/4/857/2004/>.
- Schaap, M., Cuvelier, C., Hendriks, C., Bessagnet, B., Baldasano, J., Colette, A., Thunis, P., Karam, D., Fagerli, H., Graff, A., Kranenburg, R., Nyiri, A., Pay, M., Rouil, L., Schulz, M., Simpson, D., Stern, R., Terrenoire, E., and Wind, P. (July 2015). “Performance of European chemistry transport models as function of horizontal resolution”. In: *Atmospheric Environment* vol. 112, pp. 90–105. ISSN: 1352-2310. DOI: [10.1016/J.ATMOENV.2015.04.003](https://doi.org/10.1016/J.ATMOENV.2015.04.003). URL: <https://www.sciencedirect.com/science/article/abs/pii/S1352231015300066?via%3Dihub>.
- Schaap, M., Kranenburg, R., Thürkow, M., Lupaşcu, A., and Butler, T. (2023). “Ozone source apportionment with a tagging approach in the LOTOS-EUROS model”. In: *EGU General Assembly 2023, Vienna, Austria, 24–28 Apr 2023, EGU23-12861*. DOI: <https://doi.org/10.5194/egusphere-egu23-12861>.
- Schaap, M., Manders, A., Hendriks, E., Cnossen, J., Segers, A., Gon, H. D. van der, Jozwicka, M., Sauter, F., Velders, G., Matthijssen, J., and Builtjes, P. (2009). “Regional Modelling of Particulate Matter for the Netherlands”. In: *PBL Netherlands Environmental Assessment Agency*.
- Schaap, M., Kranenburg, R., Curier, L., Jozwicka, M., Dammers, E., and Timmermans, R. (2013). “Assessing the sensitivity of the OMI-NO₂ product to emission changes across europe”. In: *Remote Sensing* vol. 5 (9), pp. 4187–4208. ISSN: 20724292. DOI: [10.3390/rs5094187](https://doi.org/10.3390/rs5094187).
- Schaap, M., Weijers, E., Mooibroek, D., Nguyen, L., and Hoogerbrugge, R. (Dec. 2010). “Composition and origin of Particulate Matter in the Netherlands”. In: .
- Schäfer, K., Emeis, S., Hoffmann, H., and Jahn, C. (2006). “Influence of mixing layer height upon air pollution in urban and sub-urban areas”. In: .

References

- Meteorologische Zeitschrift* vol. 15 (6), pp. 647–658. ISSN: 09412948. DOI: 10.1127/0941-2948/2006/0164.
- Schättler, U., Doms, G., and Schraff, C. (2019). *A Description of the Nonhydrostatic Regional COSMO-Model Part VII: User's Guide*. Deutscher Wetterdienst.
- Schell, B., Ackermann, I. J., Hass, H., Binkowski, F. S., and Ebel, A. (2001). “Modeling the formation of secondary organic aerosol within a comprehensive air quality model system”. In: *Journal of Geophysical Research: Atmospheres* vol. 106, no. D22, pp. 28275–28293. DOI: <https://doi.org/10.1029/2001JD000384>. eprint: <https://agupubs.onlinelibrary.wiley.com/doi/pdf/10.1029/2001JD000384>. URL: <https://agupubs.onlinelibrary.wiley.com/doi/abs/10.1029/2001JD000384>.
- Schlegel, M., Knoth, O., Arnold, M., and Wolke, R. (2012). “Implementation of multirate time integration methods for air pollution modelling”. In: *Geoscientific Model Development* vol. 5, no. 6, pp. 1395–1405. DOI: 10.5194/gmd-5-1395-2012. URL: <https://gmd.copernicus.org/articles/5/1395/2012/>.
- Schlünzen, K. H., Bungert, U., Flagg, D. D., Fock, B. H., and Gierisch, A. (2012). “Technical Documentation of the Multiscale Model System M-SYS (METRAS, MITRAS, MECTM, MICTM, MESIM). MEMI Technical Report 3”. In: *Meteorologisches Institut, KlimaCampus, Universität Hamburg*.
- Schneider, C., Pelzer, M., Toenges-Schuller, N., Nacken, M., and Niederau, A. (2016). “ArcGIS basierte Lösung zur detaillierten, deutschlandweiten Verteilung (Gridding) nationaler Emissionsjahreswerte auf Basis des Inventars zur Emissionsberichterstattung - Kurzfassung ; UBA TEXTE 71/2016”. In: *Für Mensch & Umwelt*. Ed. by Reaktorsicherheit des Bundesministeriums für Umwelt Naturschutz, B. und. ISSN: 1862-4804. URL: <http://www.umweltbundesamt.de/publikationen>.
- Schnell, J. L., Prather, M. J., Josse, B., Naik, V., Horowitz, L. W., Cameron-Smith, P., Bergmann, D., Zeng, G., Plummer, D. A., Sudo, K., Nagashima, T., Shindell, D. T., Faluvegi, G., and Strode, S. A. (2015). “Use of North American and European air quality networks to evaluate global chemistry–climate modeling of surface ozone”. In: *Atmospheric Chemistry and Physics* vol. 15, no. 18, pp. 10581–10596. DOI: 10.5194/acp-15-10581-2015. URL: <https://acp.copernicus.org/articles/15/10581/2015/>.
- Schöpp, W., Posch, M., Mylona, S., and Johansson, M. (Aug. 2003). “Long-term development of acid deposition (1880–2030) in sensitive freshwater regions in Europe”. In: *Hydrology and Earth System Sciences* vol. 7 (4), pp. 436–446. ISSN: 1607-7938. DOI: 10.5194/hess-7-436-2003.
- Schrödner, R., Tilgner, A., Wolke, R., and Herrmann, H. (2014). “Modeling the multiphase processing of an urban and a rural air mass with COSMO–MUSCAT”. In: *Urban Climate* vol. 10. Source apportionment and modelling of urban air pollution, pp. 720–731. ISSN: 2212-0955. DOI: <https://doi.org/10.1016/j.uclim.2014.02.001>. URL: <https://www.sciencedirect.com/science/article/pii/S221209551400011X>.

-
- Seibert, P., Beyrich, F., Gryning, S. E., Joffre, S., Rasmussen, A., and Tercier, P. (2000). *Review and intercomparison of operational methods for the determination of the mixing height*. DOI: 10.1016/S1352-2310(99)00349-0.
- Seidel, D. J., Ao, C. O., and Li, K. (Aug. 2010). “Estimating climatological planetary boundary layer heights from radiosonde observations: Comparison of methods and uncertainty analysis”. In: *Journal of Geophysical Research: Atmospheres* vol. 115 (D16). doi: 10.1029/2009JD013680. ISSN: 0148-0227. DOI: 10.1029/2009JD013680. URL: <https://doi.org/10.1029/2009JD013680>.
- Seinfeld, J. H. and Pandis, S. N. (2006). “Atmospheric Chemistry and Physics; From Air Pollution to Climate Change (second edition).” In: *John Wiley and Sons, United States of America*.
- SenStadt (2019). *Luftreinhalteplan für Berlin 2. Fortschreibung (Air pollution management plan Berlin 2. Update)*. Senate Department for the Environment, Transport and Climate Protection. URL: https://www.berlin.de/senuvk/umwelt/luft/luftreinhaltung/luftreinhalteplan_2025/download/Luftreinhalteplan.pdf.
- Seo, J., Youn, D., Kim, J. Y., and Lee, H. (2014). “Extensive spatiotemporal analyses of surface ozone and related meteorological variables in South Korea for the period 1999–2010”. In: *Atmospheric Chemistry and Physics* vol. 14, no. 12, pp. 6395–6415. DOI: 10.5194/acp-14-6395-2014. URL: <https://acp.copernicus.org/articles/14/6395/2014/>.
- Shaddick, G. and Zidek, J. V. (Aug. 2014). “A case study in preferential sampling: Long term monitoring of air pollution in the UK”. In: *Spatial Statistics* vol. 9, pp. 51–65. ISSN: 22116753. DOI: 10.1016/j.spasta.2014.03.008.
- Sharma, S., Sharma, P., and Khare, M. (June 2017). “Photo-chemical transport modelling of tropospheric ozone: A review”. In: *Atmospheric Environment* vol. 159, pp. 34–54. ISSN: 13522310. DOI: 10.1016/j.atmosenv.2017.03.047.
- Sillman, S. (1995). “The use of NO_y, H₂O₂, and HNO₃ as indicators for ozone-NO_x-hydrocarbon sensitivity in urban locations”. In: *Journal of Geophysical Research* vol. 100 (D7). ISSN: 01480227. DOI: 10.1029/94jd02953.
- Silveira, F. da, Machado, F. M., Farias, M. S. de, and Schlosser, J. F. (2023). “Fuel consumption by agricultural machinery: a review of pollutant emission control technologies”. In: *Ciência Rural* vol. 53 (5). ISSN: 1678-4596. DOI: 10.1590/0103-8478cr20220029.
- Simpson, D., Benedictow, A., Berge, H., Bergström, R., Emberson, L. D., Fagerli, H., Flechard, C. R., Hayman, G. D., Gauss, M., Jonson, J. E., Jenkin, M. E., Nyíri, A., Richter, C., Semeena, V. S., Tsyro, S., Tuovinen, J.-P., Valdebenito, Á., and Wind, P. (2012). “The EMEP MSC-W chemical transport model - technical description”. In: *Atmospheric Chemistry and Physics* vol. 12, no. 16, pp. 7825–7865. DOI: 10.5194/acp-12-7825-2012. URL: <https://acp.copernicus.org/articles/12/7825/2012/>.
- Simpson, D., Guenther, A., Hewitt, C. N., and Steinbrecher, R. (1995a). “Biogenic emissions in Europe: 1. Estimates and uncertainties”. In: *Journal of Geophysical Research: Atmospheres* vol. 100, no. D11, pp. 22875–22890. DOI: <https://doi.org/10.1029/95JD02368>. eprint: <https://agupubs.onlinelibrary>.

- wiley.com/doi/pdf/10.1029/95JD02368. URL: <https://agupubs.onlinelibrary.wiley.com/doi/abs/10.1029/95JD02368>.
- Simpson, D., Guenther, A., Hewitt, C. N., and Steinbrecher, R. (1995b). “Biogenic emissions in Europe: 1. Estimates and uncertainties”. In: *Journal of Geophysical Research: Atmospheres* vol. 100, no. D11, pp. 22875–22890. DOI: <https://doi.org/10.1029/95JD02368>. eprint: <https://agupubs.onlinelibrary.wiley.com/doi/pdf/10.1029/95JD02368>. URL: <https://agupubs.onlinelibrary.wiley.com/doi/abs/10.1029/95JD02368>.
- Simpson, D., Winiwarter, W., Börjesson, G., Cinderby, S., Ferreiro, A., Guenther, A., Hewitt, C. N., Janson, R., Khalil, M. A. K., Owen, S., Pierce, T. E., Puxbaum, H., Shearer, M., Skiba, U., Steinbrecher, R., Tarrasón, L., and Öquist, M. G. (1999). “Inventorying emissions from nature in Europe”. In: *Journal of Geophysical Research: Atmospheres* vol. 104, no. D7, pp. 8113–8152. DOI: <https://doi.org/10.1029/98JD02747>. eprint: <https://agupubs.onlinelibrary.wiley.com/doi/pdf/10.1029/98JD02747>. URL: <https://agupubs.onlinelibrary.wiley.com/doi/abs/10.1029/98JD02747>.
- Skamarock, W., Klemp, J., Dudhia, J., Gill, D., Barker, D., Wang, W., and Powers, J. (Jan. 2008). “A Description of the Advanced Research WRF Version 3”. In: vol. 27, pp. 3–27.
- Sofiev, M., Soares, J., Prank, M., Leeuw, G. de, and Kukkonen, J. (2011). “A regional-to-global model of emission and transport of sea salt particles in the atmosphere”. In: *Journal of Geophysical Research: Atmospheres* vol. 116, no. D21. DOI: <https://doi.org/10.1029/2010JD014713>. eprint: <https://agupubs.onlinelibrary.wiley.com/doi/pdf/10.1029/2010JD014713>. URL: <https://agupubs.onlinelibrary.wiley.com/doi/abs/10.1029/2010JD014713>.
- Solazzo, E. and Galmarini, S. (2016). “Error apportionment for atmospheric chemistry-transport models – a new approach to model evaluation”. In: *Atmospheric Chemistry and Physics* vol. 16, no. 10, pp. 6263–6283. DOI: [10.5194/acp-16-6263-2016](https://doi.org/10.5194/acp-16-6263-2016). URL: <https://acp.copernicus.org/articles/16/6263/2016/>.
- Solazzo, E., Bianconi, R., Vautard, R., Appel, W., Moran, M., Hogrefe, C., Bessagnet, B., Brandt, J., Christensen, J., Chemel, C., Coll, I., Denier van der Gon, H., Ferreira, J., Forkel, R., Francis, X., Grell, G., Grossi, P., Hansen, A., Jeričević, A., and Galmarini, S. (June 2012). “Model evaluation and ensemble modelling of surface-level ozone in Europe and North America in the context of AQMEII”. In: *Atmospheric Environment* vol. 53, pp. 60–74. DOI: [10.1016/j.atmosenv.2012.01.003](https://doi.org/10.1016/j.atmosenv.2012.01.003).
- Spindler, G., Müller, K., Brüggemann, E., Gnauk, T., and Herrmann, H. (Oct. 2004). “Long-term size-segregated characterization of PM₁₀, PM_{2.5}, and PM₁ at the IfT research station Melpitz downwind of Leipzig (Germany) using high and low-volume filter samplers”. In: vol. 38, pp. 5333–5347. DOI: [10.1016/j.atmosenv.2003.12.047](https://doi.org/10.1016/j.atmosenv.2003.12.047).
- Steinbrecher, R., Smiatek, G., Köble, R., Seufert, G., Theloke, J., Hauff, K., Ciccioli, P., Vautard, R., and Curci, G. (2009). “Intra- and inter-annual variability of VOC emissions from natural and semi-natural vegetation in Europe and neighbouring countries”. In: *Atmospheric Environment*

-
- vol. 43, no. 7. Natural and Biogenic Emissions of Environmentally Relevant Atmospheric Trace Constituents in Europe, pp. 1380–1391. ISSN: 1352-2310. DOI: <https://doi.org/10.1016/j.atmosenv.2008.09.072>. URL: <https://www.sciencedirect.com/science/article/pii/S1352231008008868>.
- Stern, R., Builtjes, P., Schaap, M., Timmermans, R., Vautard, R., Hodzic, A., Memmesheimer, M., Feldmann, H., Renner, E., Wolke, R., and Kerschbaumer, A. (2008). “A model inter-comparison study focussing on episodes with elevated PM10 concentrations”. In: *Atmospheric Environment* vol. 42 (19), pp. 4567–4588. ISSN: 1352-2310. DOI: <https://doi.org/10.1016/j.atmosenv.2008.01.068>. URL: <http://www.sciencedirect.com/science/article/pii/S1352231008001179>.
- Stern, R. (2003). “Development and application of the chemical transport model REM/CALGRID - UFOPLAN-Ref. No. 298 41 252”. In: *Umweltbundesamt*. URL: <http://www.umweltbundesamt.de/publikationen>.
- Stevenson, D. S. et al. (2013). “Tropospheric ozone changes, radiative forcing and attribution to emissions in the Atmospheric Chemistry and Climate Model Intercomparison Project (ACCMIP)”. In: *Atmospheric Chemistry and Physics* vol. 13, no. 6, pp. 3063–3085. DOI: [10.5194/acp-13-3063-2013](https://doi.org/10.5194/acp-13-3063-2013). URL: <https://acp.copernicus.org/articles/13/3063/2013/>.
- Stockwell, W. R., Kirchner, F., Kuhn, M., and Seefeld, S. (1997). “A new mechanism for regional atmospheric chemistry modeling”. In: *Journal of Geophysical Research: Atmospheres* vol. 102, no. D22, pp. 25847–25879. DOI: <https://doi.org/10.1029/97JD00849>. eprint: <https://agupubs.onlinelibrary.wiley.com/doi/pdf/10.1029/97JD00849>. URL: <https://agupubs.onlinelibrary.wiley.com/doi/abs/10.1029/97JD00849>.
- Stull, R. B. (1988). *An Introduction to Boundary Layer Meteorology*. Kluwer Academic Publishers. DOI: <http://dx.doi.org/10.1007/978-94-009-3027-8>.
- Sullivan, T. J., Driscoll, C. T., Beier, C. M., Burtraw, D., Fernandez, I. J., Galloway, J. N., Gay, D. A., Goodale, C. L., Likens, G. E., Lovett, G. M., and Watmough, S. A. (June 2018). “Air pollution success stories in the United States: The value of long-term observations”. In: *Environmental Science & Policy* vol. 84, pp. 69–73. ISSN: 14629011. DOI: [10.1016/j.envsci.2018.02.016](https://doi.org/10.1016/j.envsci.2018.02.016).
- Tai, A. P., Mickley, L. J., and Jacob, D. J. (2010). “Correlations between fine particulate matter (PM2.5) and meteorological variables in the United States: Implications for the sensitivity of PM2.5 to climate change”. In: *Atmospheric Environment*. ISSN: 13522310. DOI: [10.1016/j.atmosenv.2010.06.060](https://doi.org/10.1016/j.atmosenv.2010.06.060).
- Tawfik, A. B. and Steiner, A. L. (2013). “A proposed physical mechanism for ozone-meteorology correlations using land-atmosphere coupling regimes”. In: *Atmospheric Environment* vol. 72, pp. 50–59. ISSN: 1352-2310. DOI: <https://doi.org/10.1016/j.atmosenv.2013.03.002>. URL: <https://www.sciencedirect.com/science/article/pii/S1352231013001672>.
- Theobald, M. R., Vivanco, M. G., Aas, W., Andersson, C., Ciarelli, G., Couvidat, F., Cuvelier, K., Manders, A., Mircea, M., Pay, M.-T., Tsyro, S., Adani, M., Bergström, R., Bessagnet, B., Briganti, G., Cappelletti, A., D’Isidoro, M., Fagerli, H., Mar, K., Otero, N., Raffort, V., Roustan, Y., Schaap, M., Wind, P., and Colette, A. (Jan. 2019). “An evaluation of European nitrogen and

- sulfur wet deposition and their trends estimated by six chemistry transport models for the period 1990–2010”. In: *Atmospheric Chemistry and Physics* vol. 19 (1), pp. 379–405. ISSN: 1680-7324. DOI: [10.5194/acp-19-379-2019](https://doi.org/10.5194/acp-19-379-2019).
- Thouaron, L., Seigneur, C., Kim, Y., Mahé, F., André, M., Lejri, D., Villegas, D., Bruge, B., Chanut, H., and Pellan, Y. (2018). “Intercomparison of three modeling approaches for traffic-related road dust resuspension using two experimental data sets”. In: *Transportation Research Part D: Transport and Environment* vol. 58, pp. 108–121. ISSN: 1361-9209. DOI: <https://doi.org/10.1016/j.trd.2017.11.003>. URL: <https://www.sciencedirect.com/science/article/pii/S136192091730202X>.
- Thunis, P., Clappier, A., and Pirovano, G. (2020). *Source apportionment to support air quality management practices, A fitness-for-purpose guide (V 3.1)*, EUR30263. Publications Office of the European Union. DOI: [10.2760/47145](https://doi.org/10.2760/47145).
- Thunis, P., Clappier, A., Pisoni, E., and Degraeuwe, B. (2015). “Quantification of non-linearities as a function of time averaging in regional air quality modeling applications”. In: *Atmospheric Environment* vol. 103, pp. 263–275. ISSN: 1352-2310. DOI: <https://doi.org/10.1016/j.atmosenv.2014.12.057>. URL: <https://www.sciencedirect.com/science/article/pii/S135223101401005X>.
- Thunis, P., Clappier, A., Tarrason, L., Cuvelier, C., Monteiro, A., Pisoni, E., Wesseling, J., Belis, C. A., Pirovano, G., Janssen, S., Guerreiro, C., and Peduzzi, E. (2019). “Source apportionment to support air quality planning: Strengths and weaknesses of existing approaches”. In: *Environment International*. ISSN: 18736750. DOI: [10.1016/j.envint.2019.05.019](https://doi.org/10.1016/j.envint.2019.05.019).
- Thunis, P., Degraeuwe, B., Pisoni, E., Trombetti, M., Peduzzi, E., Belis, C., Wilson, J., Clappier, A., and Vignati, E. (Aug. 2018). “PM2.5 source allocation in European cities: A SHERPA modelling study”. In: *Atmospheric Environment* vol. 187, pp. 93–106. ISSN: 1352-2310. DOI: [10.1016/J.ATMOENV.2018.05.062](https://doi.org/10.1016/J.ATMOENV.2018.05.062). URL: <https://www.sciencedirect.com/science/article/pii/S1352231018303728?pes=vor>.
- Thürkow, M., Banzhaf, S., Butler, T., Pültz, J., and Schaap, M. (2023). “Source attribution of nitrogen oxides across Germany: Comparing the labelling approach and brute force technique with LOTOS-EUROS”. In: *Atmospheric Environment* vol. 292, p. 119412. ISSN: 1352-2310. DOI: <https://doi.org/10.1016/j.atmosenv.2022.119412>. URL: <https://www.sciencedirect.com/science/article/pii/S1352231022004770>.
- Thürkow, M., Kirchner, I., Kranenburg, R., Timmermans, R., and Schaap, M. (2021). “A multi-meteorological comparison for episodes of PM10 concentrations in the Berlin agglomeration area in Germany with the LOTOS-EUROS CTM”. In: *Atmospheric Environment* vol. 244, p. 117946. ISSN: 1352-2310. DOI: <https://doi.org/10.1016/j.atmosenv.2020.117946>. URL: <https://www.sciencedirect.com/science/article/pii/S1352231020306804>.
- Timmermans, R., Kranenburg, R., Hendriks, C., Thürkow, M., Kirchner, I., Pinxteren, D. van, and Schaap, M. (2020). *Establishing the Origin of Particulate Matter in Eastern Germany Using an Improved Regional Modelling Framework*. DOI: [10.1007/978-3-030-22055-6_1](https://doi.org/10.1007/978-3-030-22055-6_1).

-
- Timmermans, R., Kranenburg, R., Manders, A., Hendriks, C., Segers, A., Dammers, E., Gon, H. D. van der, Schaap, M., Dammers, E., Zeng, L., Wang, L., and Liu, Z. (2017). “Source apportionment of PM_{2.5} across China using LOTOS-EUROS”. In: *Atmospheric Environment*. ISSN: 18732844. DOI: 10.1016/j.atmosenv.2017.06.003.
- Timmermans, R., Pinxteren, D. van, Kranenburg, R., Hendriks, C., Fomba, K., Herrmann, H., and Schaap, M. (Apr. 2022). “Evaluation of modelled LOTOS-EUROS with observational based PM₁₀ source attribution”. In: *Atmospheric Environment: X* vol. 14, p. 100173. ISSN: 25901621. DOI: 10.1016/j.aeaoa.2022.100173.
- Timmermans, R., Denier van der Gon, H., Kuenen, J., Segers, A., Honoré, C., Perrussel, O., Builtjes, P., and Schaap, M. (2013). “Quantification of the urban air pollution increment and its dependency on the use of down-scaled and bottom-up city emission inventories”. In: *Urban Climate* vol. 6, pp. 44–62. ISSN: 2212-0955. DOI: <https://doi.org/10.1016/j.uclim.2013.10.004>. URL: <https://www.sciencedirect.com/science/article/pii/S2212095513000527>.
- Tsyro, S., Aas, W., Soares, J., Sofiev, M., Berge, H., and Spindler, G. (Oct. 2011). “Modelling of sea salt concentrations over Europe: key uncertainties and comparison with observations”. In: *Atmospheric Chemistry and Physics* vol. 11 (20), pp. 10367–10388. ISSN: 1680-7324. DOI: 10.5194/acp-11-10367-2011.
- Twigg, M. V. (Apr. 2011). “Catalytic control of emissions from cars”. In: *Catalysis Today* vol. 163 (1), pp. 33–41. ISSN: 09205861. DOI: 10.1016/j.cattod.2010.12.044.
- UBA (2019). *Luftqualität 2018*, p. 28. URL: www.umweltbundesamt.de/publikationen/.
- Valotto, G., Zannoni, D., Guerriero, P., Rampazzo, G., and Visin, F. (2019). “Characterization of road dust and resuspended particles close to a busy road of Venice mainland (Italy)”. In: *International Journal of Environmental Science and Technology* vol. 16 (11), pp. 6513–6526. ISSN: 17352630. DOI: 10.1007/s13762-019-02246-1. URL: <https://doi.org/10.1007/s13762-019-02246-1>.
- van der Gon, H. A. C., Bergström, R., Fountoukis, C., Johansson, C., Pandis, S. N., Simpson, D., and Visschedijk, A. J. H. (2015). “Particulate emissions from residential wood combustion in Europe – revised estimates and an evaluation”. In: *Atmospheric Chemistry and Physics* vol. 15 (11), pp. 6503–6519. DOI: 10.5194/acp-15-6503-2015. URL: <https://www.atmos-chem-phys.net/15/6503/2015/>.
- van der Gon, H. D., Hulskotte, J., Jozwicka, M., Kranenburg, R., Kuenen, J., and Visschedijk, A. (2018). “European Emission Inventories and Projections for Road Transport Non-Exhaust Emissions”. In: Elsevier. DOI: 10.1016/B978-0-12-811770-5.00005-4.
- van Pinxteren, D., Mothes, F., Spindler, G., Fomba, K. W., and Herrmann, H. (2017). *Auswertung der gravimetrischen PM₁₀- Messungen in Sachsen, Brandenburg, Mecklenburg-Vorpommern und Berlin zur Identifikation des Anteils verschiedener Quellen an der Feinstaubbelastung anhand der In-*

- haltsstoffe und anhand von Rezeptormodellierungen (PM-OST)*. URL: https://www.berlin.de/senuvk/umwelt/luftqualitaet/de/luftreinhalteplan_projekte/pm10_ursachenanalyse.shtml.
- van Pinxteren, D., Mothes, F., Spindler, G., Fomba, K. W., and Herrmann, H. (Mar. 2019). “Trans-boundary PM10: Quantifying impact and sources during winter 2016/17 in eastern Germany”. In: *Atmospheric Environment* vol. 200, pp. 119–130. ISSN: 13522310. DOI: [10.1016/j.atmosenv.2018.11.061](https://doi.org/10.1016/j.atmosenv.2018.11.061). URL: <http://www.sciencedirect.com/science/article/pii/S1352231018308446> <https://linkinghub.elsevier.com/retrieve/pii/S1352231018308446>.
- Van Zanten, M. C., Sauter, F. J., Kruit, R. J. W., Jaarsveld, J. A. V., and Pul, W. A. J. V. (2010). *Description of the DEPAC module: Dry deposition modelling with DEPAC_GCN2010 ; Report 680180001/2010*. RIVM (National Institute for Public Health and the Environment). URL: <https://www.rivm.nl/bibliotheek/rapporten/680180001.pdf>.
- Vautard, R., Builtjes, P., Thunis, P., Cuvelier, C., Bedogni, M., Bessagnet, B., Honoré, C., Moussiopoulos, N., Pirovano, G., and Schaap, M. (Jan. 2007). “Evaluation and intercomparison of Ozone and PM10 simulations by several chemistry transport models over four European cities within the CityDelta project”. In: *Atmospheric Environment* vol. 41 (1), pp. 173–188. ISSN: 13522310. DOI: [10.1016/j.atmosenv.2006.07.039](https://doi.org/10.1016/j.atmosenv.2006.07.039).
- Vautard, R., Moran, M. D., Solazzo, E., Gilliam, R. C., Matthias, V., Bianconi, R., Chemel, C., Ferreira, J., Geyer, B., Hansen, A. B., Jericevic, A., Prank, M., Segers, A., Silver, J. D., Werhahn, J., Wolke, R., Rao, S. T., and Galmarini, S. (2012). “Evaluation of the meteorological forcing used for the Air Quality Model Evaluation International Initiative (AQMEII) air quality simulations”. In: *Atmospheric Environment*. ISSN: 13522310. DOI: [10.1016/j.atmosenv.2011.10.065](https://doi.org/10.1016/j.atmosenv.2011.10.065).
- Ventriglio, A., Bellomo, A., Gioia, I. di, Di Sabatino, D., Favale, D., De Berardis, D., and Cianconi, P. (2021). “Environmental pollution and mental health: a narrative review of literature”. In: *CNS Spectrums* vol. 26, no. 1, pp. 51–61. DOI: [10.1017/S1092852920001303](https://doi.org/10.1017/S1092852920001303).
- Verstraeten, W. W., Boersma, K. F., Douros, J., Williams, J. E., Eskes, H., Liu, F., Beirle, S., and Delcloo, A. (2018). “Top-down NO_x emissions of european cities based on the downwind plume of modelled and space-borne tropospheric NO₂ columns”. In: *Sensors (Switzerland)* vol. 18 (9), pp. 1–15. ISSN: 14248220. DOI: [10.3390/s18092893](https://doi.org/10.3390/s18092893).
- Vestreng, V., Myhre, G., Fagerli, H., Reis, S., and Tarrasón, L. (July 2007). “Twenty-five years of continuous sulphur dioxide emission reduction in Europe”. In: *Atmospheric Chemistry and Physics* vol. 7 (13), pp. 3663–3681. ISSN: 1680-7324. DOI: [10.5194/acp-7-3663-2007](https://doi.org/10.5194/acp-7-3663-2007).
- Vestreng, V., Ntziachristos, L., Semb, A., Reis, S., Isaksen, I. S. A., and Tarrasón, L. (Feb. 2009). “Evolution of NO_x emissions in Europe with focus on road transport control measures”. In: *Atmospheric Chemistry and Physics* vol. 9 (4), pp. 1503–1520. ISSN: 1680-7324. DOI: [10.5194/acp-9-1503-2009](https://doi.org/10.5194/acp-9-1503-2009). URL: <https://acp.copernicus.org/articles/9/1503/2009/>.

-
- Viana, M., Kuhlbusch, T., Querol, X., Alastuey, A., Harrison, R., Hopke, P., Winiwarter, W., Vallius, M., Szidat, S., Prévôt, A., Hueglin, C., Bloemen, H., Wählin, P., Vecchi, R., Miranda, A., Kasper-Giebl, A., Maenhaut, W., and Hitzenberger, R. (2008). “Source apportionment of particulate matter in Europe: A review of methods and results”. In: *Journal of Aerosol Science* vol. 39, no. 10, pp. 827–849. ISSN: 0021-8502. DOI: <https://doi.org/10.1016/j.jaerosci.2008.05.007>. URL: <https://www.sciencedirect.com/science/article/pii/S0021850208001018>.
- Viana, M., Leeuw, F. de, Bartonova, A., Castell, N., Ozturk, E., and Ortiz, A. G. (Oct. 2020). “Air quality mitigation in European cities: Status and challenges ahead”. In: *Environment International* vol. 143, p. 105907. ISSN: 01604120. DOI: [10.1016/j.envint.2020.105907](https://doi.org/10.1016/j.envint.2020.105907).
- Vogelezang, D. H. P. and Holtslag, A. A. M. (1996). “Evaluation and model impacts of alternative boundary-layer height formulations”. In: *Boundary-Layer Meteorology* vol. 81 (3), pp. 245–269. ISSN: 1573-1472. DOI: [10.1007/BF02430331](https://doi.org/10.1007/BF02430331). URL: <https://doi.org/10.1007/BF02430331>.
- Wagner, S., Angenendt, E., Beletskaya, O., and Zeddies, J. (Oct. 2017). “Assessing ammonia emission abatement measures in agriculture: Farmers’ costs and society’s benefits – A case study for Lower Saxony, Germany”. In: *Agricultural Systems* vol. 157, pp. 70–80. ISSN: 0308521X. DOI: [10.1016/j.agsy.2017.06.008](https://doi.org/10.1016/j.agsy.2017.06.008).
- Wagstrom, K. M., Pandis, S. N., Yarwood, G., Wilson, G. M., and Morris, R. E. (July 2008). “Development and application of a computationally efficient particulate matter apportionment algorithm in a three-dimensional chemical transport model”. In: *Atmospheric Environment* vol. 42 (22), pp. 5650–5659. ISSN: 13522310. DOI: [10.1016/j.atmosenv.2008.03.012](https://doi.org/10.1016/j.atmosenv.2008.03.012).
- Walcek, C. J. (2000). “Minor flux adjustment near mixing ratio extremes for simplified yet highly accurate monotonic calculation of tracer advection”. In: *Journal of Geophysical Research: Atmospheres* vol. 105 (D7), pp. 9335–9348. DOI: [10.1029/1999JD901142](https://doi.org/10.1029/1999JD901142). URL: <https://agupubs.onlinelibrary.wiley.com/doi/abs/10.1029/1999JD901142>.
- Wang, Z. S., Chien, C.-J., and Tonnesen, G. S. (Nov. 2009). “Development of a tagged species source apportionment algorithm to characterize three-dimensional transport and transformation of precursors and secondary pollutants”. In: *Journal of Geophysical Research* vol. 114 (D21), p. D21206. ISSN: 0148-0227. DOI: [10.1029/2008JD010846](https://doi.org/10.1029/2008JD010846). URL: <http://doi.wiley.com/10.1029/2008JD010846>.
- Weger, M., Heinold, B., Engler, C., Schumann, U., Seifert, A., Föbög, R., Voigt, C., Baars, H., Blahak, U., Borrmann, S., Hoose, C., Kaufmann, S., Krämer, M., Seifert, P., Senf, F., Schneider, J., and Tegen, I. (Dec. 2018). “The impact of mineral dust on cloud formation during the Saharan dust event in April 2014 over Europe”. In: *Atmospheric Chemistry and Physics* vol. 18 (23), pp. 17545–17572. ISSN: 1680-7324. DOI: [10.5194/acp-18-17545-2018](https://doi.org/10.5194/acp-18-17545-2018).
- Weijers, E. P., Sahan, E., Ten Brink, H. M., Otjes, R. P., Schaap, M., Matthijsen, J., and Van Arkel, F. (Oct. 2010). *Contribution of secondary inorganic*

References

- aerosols to PM10 and PM2.5 in the Netherlands. Measurement and modelling results.*
- Wesely, M. (1989). “Parameterization of surface resistances to gaseous dry deposition in regional-scale numerical models”. In: *Atmospheric Environment (1967)* vol. 23, no. 6, pp. 1293–1304. ISSN: 0004-6981. DOI: [https://doi.org/10.1016/0004-6981\(89\)90153-4](https://doi.org/10.1016/0004-6981(89)90153-4). URL: <https://www.sciencedirect.com/science/article/pii/0004698189901534>.
- Wetzel, P. J. (1982). “Toward Parameterization of the Stable Boundary Layer”. In: *Journal of Applied Meteorology* vol. 21 (1), pp. 7–13. DOI: [10.1175/1520-0450\(1982\)021<0007:TPOTSB>2.0.CO;2](https://doi.org/10.1175/1520-0450(1982)021<0007:TPOTSB>2.0.CO;2). URL: [https://doi.org/10.1175/1520-0450\(1982\)021%3C0007:TPOTSB%3E2.0.CO;2](https://doi.org/10.1175/1520-0450(1982)021%3C0007:TPOTSB%3E2.0.CO;2).
- Whitten, G. Z., Hogo, H., and Killus, J. P. (1980). “The carbon-bond mechanism: a condensed kinetic mechanism for photochemical smog”. In: *Environ. Sci. Technol.* vol. 14 (6). doi: [10.1021/es60166a008](https://doi.org/10.1021/es60166a008), pp. 690–700. ISSN: 0013-936X. DOI: [10.1021/es60166a008](https://doi.org/10.1021/es60166a008). URL: <https://doi.org/10.1021/es60166a008>.
- WHO (2005). *WHO Air quality guidelines for particulate matter, ozone, nitrogen dioxide and sulfur dioxide: Global update 2005*, pp. 1–21. DOI: [10.1016/0004-6981\(88\)90109-6](https://doi.org/10.1016/0004-6981(88)90109-6). URL: <http://www.euro.who.int/en/health-topics/environment-and-health/Housing-and-health/publications/pre-2009/air-quality-guidelines.-global-update-2005.-particulate-matter,-ozone,-nitrogen-dioxide-and-sulfur-dioxide>.
- (2015). *World Health Organization Regional Office for Europe, 2015. Economic cost of the health impact of air pollution in Europe Clean air, health and wealth*. URL: <http://www.euro.who.int/pubrequest>.
- Wiedinmyer, C., Akagi, S. K., Yokelson, R. J., Emmons, L. K., Al-Saadi, J. A., Orlando, J. J., and Soja, A. J. (July 2011). “The Fire INventory from NCAR (FINN): a high resolution global model to estimate the emissions from open burning”. In: *Geoscientific Model Development* vol. 4 (3), pp. 625–641. ISSN: 1991-9603. DOI: [10.5194/gmd-4-625-2011](https://doi.org/10.5194/gmd-4-625-2011).
- Wiedinmyer, C., Yokelson, R. J., and Gullett, B. K. (Aug. 2014). “Global Emissions of Trace Gases, Particulate Matter, and Hazardous Air Pollutants from Open Burning of Domestic Waste”. In: *Environmental Science & Technology* vol. 48 (16), pp. 9523–9530. ISSN: 0013-936X. DOI: [10.1021/es502250z](https://doi.org/10.1021/es502250z).
- Wilkins, E. T. (Apr. 1954). “Air pollution aspects of the London fog of December 1952”. In: *Quarterly Journal of the Royal Meteorological Society* vol. 80 (344), pp. 267–271. ISSN: 00359009. DOI: [10.1002/qj.49708034420](https://doi.org/10.1002/qj.49708034420).
- Wintjen, P., Schrader, F., Schaap, M., Beudert, B., and Brümmer, C. (2022). “Forest–atmosphere exchange of reactive nitrogen in a remote region – Part I: Measuring temporal dynamics”. In: *Biogeosciences* vol. 19, no. 2, pp. 389–413. DOI: [10.5194/bg-19-389-2022](https://doi.org/10.5194/bg-19-389-2022). URL: <https://bg.copernicus.org/articles/19/389/2022/>.
- Wolke, R. and Knoth, O. (2000). “Implicit–explicit Runge–Kutta methods applied to atmospheric chemistry-transport modelling”. In: *Environmental Modelling & Software* vol. 15, no. 6. Air pollution modelling and simulation, pp. 711–719.

-
- ISSN: 1364-8152. DOI: [https://doi.org/10.1016/S1364-8152\(00\)00034-7](https://doi.org/10.1016/S1364-8152(00)00034-7). URL: <https://www.sciencedirect.com/science/article/pii/S1364815200000347>.
- Wolke, R., Schröder, W., Schrödner, R., and Renner, E. (2012). "Influence of grid resolution and meteorological forcing on simulated European air quality: A sensitivity study with the modeling system COSMO–MUSCAT". In: *Atmospheric Environment* vol. 53. AQMEII: An International Initiative for the Evaluation of Regional-Scale Air Quality Models - Phase 1, pp. 110–130. ISSN: 1352-2310. DOI: <https://doi.org/10.1016/j.atmosenv.2012.02.085>. URL: <https://www.sciencedirect.com/science/article/pii/S1352231012002233>.
- Yamartino, R. J. (2003). "Refined 3-d Transport and Horizontal Diffusion for the REM/CALGRID Air Quality Model". In: *Freie Universität Berlin, Institut für Meteorologie*. Ed. by Reaktorsicherheit des Bundesministeriums für Umwelt Naturschutz, B. und. URL: <http://www.umweltbundesamt.de/publikationen>.
- Yilmaz, N. and Atmanli, A. (Dec. 2017). "Sustainable alternative fuels in aviation". In: *Energy* vol. 140, pp. 1378–1386. ISSN: 03605442. DOI: [10.1016/j.energy.2017.07.077](https://doi.org/10.1016/j.energy.2017.07.077).
- Young, P. J., Naik, V., Fiore, A. M., Gaudel, A., Guo, J., Lin, M. Y., Neu, J. L., Parrish, D. D., Rieder, H. E., Schnell, J. L., Tilmes, S., Wild, O., Zhang, L., Ziemke, J., Brandt, J., Delcloo, A., Doherty, R. M., Geels, C., Hegglin, M. I., Hu, L., Im, U., Kumar, R., Luhar, A., Murray, L., Plummer, D., Rodriguez, J., Saiz-Lopez, A., Schultz, M. G., Woodhouse, M. T., and Zeng, G. (Jan. 2018). "Tropospheric Ozone Assessment Report: Assessment of global-scale model performance for global and regional ozone distributions, variability, and trends". In: *Elementa: Science of the Anthropocene* vol. 6. 10. ISSN: 2325-1026. DOI: [10.1525/elementa.265](https://doi.org/10.1525/elementa.265). eprint: <https://online.ucpress.edu/elementa/article-pdf/doi/10.1525/elementa.265/471141/265-4586-2-pb.pdf>. URL: <https://doi.org/10.1525/elementa.265>.
- Yusuf, A. A. and Inambao, F. L. (Sept. 2019). "Effect of cold start emissions from gasoline-fueled engines of light-duty vehicles at low and high ambient temperatures: Recent trends". In: *Case Studies in Thermal Engineering* vol. 14, p. 100417. ISSN: 2214157X. DOI: [10.1016/j.csite.2019.100417](https://doi.org/10.1016/j.csite.2019.100417).
- Zhan, Y., Luo, Y., Deng, X., Zhang, K., Zhang, M., Grieneisen, M. L., and Di, B. (Apr. 2018). "Satellite-Based Estimates of Daily NO₂ Exposure in China Using Hybrid Random Forest and Spatiotemporal Kriging Model". In: *Environmental Science & Technology* vol. 52 (7). ISSN: 0013-936X. DOI: [10.1021/acs.est.7b05669](https://doi.org/10.1021/acs.est.7b05669).
- Zhang, H., Wang, Y., Hu, J., Ying, Q., and Hu, X. M. (July 2015). "Relationships between meteorological parameters and criteria air pollutants in three megacities in China". In: *Environmental Research* vol. 140, pp. 242–254. ISSN: 10960953. DOI: [10.1016/j.envres.2015.04.004](https://doi.org/10.1016/j.envres.2015.04.004).
- Zhang, L., Gong, S., Padro, J., and Barrie, L. (2001). "A size-segregated particle dry deposition scheme for an atmospheric aerosol module". In: *Atmospheric Environment* vol. 35 (3), pp. 549–560. ISSN: 1352-2310. DOI: [https://doi.org/10.1016/S1352-2310\(00\)00326-5](https://doi.org/10.1016/S1352-2310(00)00326-5). URL: <http://www.sciencedirect.com/science/article/pii/S1352231000003265>.

References

- Zhang, R., Duhl, T., Salam, M. T., House, J. M., Flagan, R. C., Avol, E. L., Gilliland, F. D., Guenther, A., Chung, S. H., Lamb, B. K., and VanReken, T. M. (Mar. 2014). “Development of a regional-scale pollen emission and transport modeling framework for investigating the impact of climate change on allergic airway disease”. In: *Biogeosciences* vol. 11 (6), pp. 1461–1478. ISSN: 1726-4189. DOI: [10.5194/bg-11-1461-2014](https://doi.org/10.5194/bg-11-1461-2014).
- Zhang, W., Capps, S. L., Hu, Y., Nenes, A., Napelenok, S. L., and Russell, A. G. (2012). “Development of the high-order decoupled direct method in three dimensions for particulate matter: enabling advanced sensitivity analysis in air quality models”. In: *Geoscientific Model Development* vol. 5, no. 2, pp. 355–368. DOI: [10.5194/gmd-5-355-2012](https://doi.org/10.5194/gmd-5-355-2012). URL: <https://gmd.copernicus.org/articles/5/355/2012/>.
- Zimmermann, F., Lux, H., Maenhaut, W., Matschullat, J., Plessow, K., Reuter, F., and Wienhaus, O. (Feb. 2003). “A review of air pollution and atmospheric deposition dynamics in southern Saxony, Germany, Central Europe”. In: *Atmospheric Environment* vol. 37 (5), pp. 671–691. ISSN: 13522310. DOI: [10.1016/S1352-2310\(02\)00829-4](https://doi.org/10.1016/S1352-2310(02)00829-4).

Curriculum vitae

The curriculum vitae is not part of the online version for privacy regulations.

Danksagung

An dieser Stelle möchte ich mich bei all denjenigen bedanken, die mich während der Anfertigung meiner Doktorarbeit unterstützt, begleitet und motiviert haben.

Zuerst möchte ich mich bei Prof. Dr. Martijn Schaap und Prof. Dr. Tim Butler für die Betreuung und die Unterstützung, die ihr beide, Martijn und Tim, mir während der letzten Jahre entgegengebracht habt bedanken.

Du, Martijn, standest mir zu jeder Zeit mit hilfreichen und konstruktiven Diskussionen und Ratschlägen zur Seite. Auf deine Unterstützung konnte ich mich verlassen, auch wenn du im stressigen Arbeitsalltag eingebunden warst. Sogar während deiner wohlverdienten Elternzeit hast du dir Zeit für mich genommen! Auch für die Hilfe bei der Erstellung und Umsetzung der einzelnen Veröffentlichungen, insbesondere meiner Ersten, möchte ich mich bei dir bedanken. Deine Art und Weise bei der Hilfestellung und Motivation ist beispiellos. Die vielen Arbeitsstunden, die du mir hast zukommen lassen, haben den Grundstein gelegt und mich erst dazu bewogen, dass ich mich an einer Doktorarbeit versucht und diese am Ende tatsächlich auch abgeschlossen habe. Dir, Martijn, dafür noch einmal vielen Dank!


Dir, Tim, gebührt ein besonderer Dank. Deine konstruktiven Kritiken und Anregungen an den einzelnen Veröffentlichungen haben mich immer wieder dazu bewogen, diese zu verbessern. Unsere Zusammenarbeit hat mir insbesondere geholfen, meinen wissenschaftlichen Hintergrund zu erweitern. Du konntest mir helfen, meine Stärken und Schwächen aufzuzeigen. Meine Stärken weiß ich dank dir nun in Zukunft besser und gewinnbringend einzusetzen. An meinen Schwächen bin ich jetzt in der Lage, differenzierter und zielgerichtet zu arbeiten. Auch dir, Danke.

Ebenfalls möchte ich mich bei meinen Kollegen der AG TrUmF, Sabine Banzhaf, Ilona Jäkel und Joscha Pültz, bedanken, die meiner Arbeit mit viel Interesse gefolgt sind und mir auch in schwierigen Zeiten zur Seite standen. Ich danke auch allen Mitarbeitern des IfM für die angenehme Arbeitsatmosphäre und ständige Hilfsbereitschaft. Insbesondere bedanke ich mich hier bei Thomas Bergmann, der die IT an unserem Institut so stabil und einfach gestaltet und bei Ingo Kirchner, der mir die Möglichkeit gegeben hat, wieder an das IfM zurückzukehren. Auch bei meinen zahlreichen Projektpartnern außerhalb der FUB möchte ich mich für die vielen interessanten Debatten und Ideen, die maßgeblich dazu beigetragen haben, dass diese Doktorarbeit in dieser Form vorliegt, bedanken. Hervorzuheben ist die Zusammenarbeit mit den Kollegen des TNO. Beispielhaft ist die stetige Hilfsbereitschaft von Richard Kranenburg mit seinem unnachgiebigen technischen Support bei der Beantwortung jeglicher Fragen mit dem Umgang von LOTOS-EUROS und der Anwendung von Emissionsdatensätzen.

Einen nicht zu vernachlässigenden Anteil trägt auch ihr, meine Jungs von der SG Rot Weiss Neuenhagen, zu dieser Arbeit bei. Ihr habt mir die notwendige Ablenkung und eine fantastische neue Freizeitbeschäftigung geschenkt, die ich auch in Zukunft nicht mehr missen möchte.

Der größte Dank gebührt jedoch meiner Familie. Ohne meine Familie wäre diese Doktorarbeit nicht möglich gewesen, wenn auch der Großteil leider nicht, noch nicht oder nicht mehr im Stande ist diese Arbeit zu lesen. Insbesondere dir Hanna sowie euch, Madita und Marlon, die ihr mich die ganze Zeit über begleitet und leitet, gilt ein ganz besonderer Dank. Ihr seid mir ein stetiger Antrieb und schenkt meinem Leben täglich Freude. Ich möchte auch meinen Eltern und Großeltern danken, dass sie mir die Möglichkeit geebnet haben eine solch differenzierte Ausbildung, in Form eines Studiums, zu begehnen. Einen besonderen Dank möchte ich an alle richten, die leider nicht mehr bei uns sein können, mich aber auf dem Ausbildungsweg lange unterstützt und begleitet haben. Insbesondere dir, Papa, danke ich für die schönen Jahre, die wir gemeinsam verbringen durften und dass du mir die Inspiration für den Studiengang Meteorologie gegeben hast.

»If you do not believe you can do it then you have no chance at all.«

 A. Wenger

Selbstständigkeitserklärung

Hiermit erkläre ich an Eides Statt, dass ich die vorliegende Arbeit selbstständig und ohne fremde Hilfe angefertigt, keine anderen als die angegebenen Quellen und Hilfsmittel benutzt und die den benutzten Quellen wörtlich oder inhaltlich entnommenen Stellen als solche kenntlich gemacht habe.

Diese Arbeit hat in gleicher oder ähnlicher Form noch keiner Prüfungsbehörde vorgelegen.

Markus Thürkow

Berlin, 2024